

# Innovative cost estimation methods for building production

**Jana Smetanková, Peter Mésároš, Katarína Krajníková**

Technical University of Košice, Slovakia  
Civil Engineering Faculty, Institute of Technology, Economics and Management in Construction  
e-mail: jana.smetankova@tuke.sk, peter.mesaros@tuke.sk, katarina.krajnikova@tuke.sk

## Abstract

Technological progress is reflected in all industries. Obsolete project manuals in the construction industry are being replaced by digitized automated controls that monitor the project in real-time. One of the main trends is the introduction of technologies based on data analytics. Effective use of technology to collect and analyse data is key to improving a building's planning and management across its life cycle. Building information models, which process digital content related to the entire life cycle of a building, are becoming an effective tool. The main goal of the paper is to design and identify the structure of the developed database, which, based on the acquired knowledge, contains graphical models that have selected non-graphical information.

**Key words:** innovative methods, cost estimating, building production, database, structure

## 1 Introduction

Construction production and its requirements for support and use of information systems have its specifics. The use of standard and proven construction practices leads to the idea that construction does not need to use special, sophisticated management tools. It is becoming increasingly common that the implementation of construction works is often drifted by a stream of events and uncoordinated solutions. The result is often an exceeded budget, missing or overburdened resources, non-compliance with deadlines, low profit, or low quality of construction [1].

For this purpose, production automation and control are supported in the construction industry. Automation brings several benefits, such as:

- increase quality and accuracy,
- automation of the production process - replacement of human work in physically demanding, monotonous and dangerous work,
- simplification of tasks,

- increase efficiency and productivity to reduce costs,
- improving economic results,
- improving the working environment [2].

## 2 Cost estimating for building production

Cost estimating and creating a construction budget is one of the most critical parts of the project life cycle. The purpose of the valuation is to determine the price of the construction work, including the profit. The success of any construction company depends on the ability to determine the amount of costs so that the company covers its costs and, at the same time, achieves the highest possible profit. When choosing a construction company, the customer considers several criteria, such as:

- Offer price,
- Own previous experience with the construction company,
- Recommendation from own contacts,
- Previous realization by the construction company -references,
- Delivery date,
- Insurance guarantee
- Company size,
- Advertising [3].



Figure 1: The key criteria according to which the customer decides when choosing a construction company [4]

The basis for the correct and high-quality processing of the construction budget is project documentation and valuation tools. Based on the above documents, a price calculation is processed. The term calculation represents purpose-oriented calculations, which are a set of procedures by which the costs necessary to achieve the final construction work are determined and calculated. The structure of costs for construction works and supplies can be divided into

costs for direct materials, costs of direct wages of the contractor, costs of machines, other direct costs of the contractor, production overheads, administrative overheads, and profit [5].

The system of valuing construction output varies from country to country. The most used tools for valuing construction production include BIMestiMate, Cubit Buildsoft, iTWO costX, Nevaris, Vico Cost Planner, ConEst, ProEst NetPricer, Vision InfoSoft and others.

BIMestiMate software is the first Polish 5D BIM tool. The system allows project planning in terms of costs. Cost estimation can be done either in the traditional way or using BIM technology. The system allows you to work with BIM models (in IFC format), present virtual models (compositions, floors, element types, etc.), calculate volumes, areas, element lengths or element groups, detect discrepancies in different versions of the same file, compare offers and create quantity take-offs and cost estimates. The process of performing a quantitative take-off is automatic, easy, accurate and intuitive. The system eliminates errors caused by calculations [6].

Another application used for estimating construction projects is the Cubit Estimating Buildsoft application. Cubit Estimating is a tool for estimating construction output with a high number of functionalities - for example, automated take-off creation, cost estimation, change notification, reporting and analysis, IFC model import, import of own price databases, cost management, coding and scanning of drawings, BIM reader, creation of 3D visualizations and others. These functionalities support profit maximization, save time and increase the accuracy of planning and management of construction production [7].

iTWOcostX software is a tool to support intelligent collaboration and project management. It is possible to import 2D and 3D models in the application and thus create accurate take-offs and cost estimates. Take-offs are created directly from 3D models. The application has sufficient functions, such as advanced display tools, defining model and structure specifications, automated model update, change notification, determining construction costs, importing price list databases directly from suppliers, comparing prices, creating manuals and flowcharts and more [8].

Nemetschek Allplan is one of the leaders in software tools. Nevaris is a tool for effective planning and management of construction processes. Nevaris has a number of modular platforms, such as Nevaris Build (construction planning) and Nevaris Finance (company finance management - accounting, controlling, etc.). Nevaris Build is a unified, integrated software tool for designers, architects, contractors, and developers. Within the program, it is possible to perform a comprehensive AVA analysis (selection, valuation, and accounting control), which is supplemented by project account and cost calculation modules. Nevaris Build enables the creation of automated take-offs, cost estimation, management and planning of subcontractors, constructions, and structures. The solution includes the procurement process - planning, management and control of construction projects from bid processing to final invoices [9][10].

The ConEst application is a tool for the complete planning and management of construction projects. ConEst focuses primarily on the planning of electrical, low-voltage and safety installations and fire protection systems. In the application, it is possible to create an accurate

list of materials, working hours, costs, centrally manage all aspects of the project (tracking orders, changes) and create work reports. Within the database, it is possible to import items directly from the ElectricSmarts online catalogue into the InteliBid database [11][12].

ProEst NetPricer is an online material pricing service. NetPricer allows you to integrate items directly from the ElectricSmarts online catalogue into the ProEst database. The application is an innovative tool for estimating construction prices. The user has access to electronic catalogues that have certified product data - specifications, prices and so on [13].

Selected software applications enable the valuation of construction production, by assigning the total costs for the implementation of the selected construction detail. The mentioned elements do not have detailed information about the production technology and prices of materials and works necessary for the realization of the selected construction detail.

In the Slovak construction industry, software applications Cenkros, Kalkulus and Odis are mostly used for cost estimating construction production. These software applications contain individual price lists of works and materials. The result of the work in the mentioned software applications is the total budget for the construction work. The user obtains information on the costs of the construction work, concretely labour costs (wages), materials, machine costs, other direct costs and determines the amount of costs for production and administrative overheads.

### **3 Innovative method for cost estimating for building production**

Software applications for cost estimating construction production are currently being developed. In Slovakia, the applications Cenkros, Kalkulus and Odis are still preferred. These applications work with classifiers and classification systems of construction production. Construction output is valued based on indicative tools of construction works, technical and economic indicators, composite book of indicative prices of materials, composite book of machine-hours rates and composite book objectified ancillary budget costs.

The Faculty of Civil Engineering of the Technical University of Košice supports efforts to create new innovative methods of valuing and evaluating buildings. Various projects are implemented at the faculty, such as the project APVV-17-0549 "Research of knowledge-based and virtual technologies for intelligent designing and realization of building projects with an emphasis on economic efficiency and sustainability", which aims to create innovative and interactive tool enabling the valuation of construction production and the evaluation of the building from selected points of view. Based on the project's goals a knowledge database is being developed.

#### **3.1 Innovative tool for valuation and evaluation of buildings -structure design**

The main aim of the project APVV-17-0549 "Research of knowledge-based and virtual technologies for intelligent designing and realization of building projects with an emphasis on economic efficiency and sustainability" is to design a knowledge database of elements. The individual elements will be information models that will contain graphical and non-graphical

information. Based on the market analysis and the possibility of problems (loss of information, model parameters) in the transfer of data in IFC format between software applications, the goal was to design a database that would combine selected parameters into one environment, i.e., database of compatible IFC component models. This database is a standard tool for BIM software applications. The method of realization, the choice of the type of construction elements and the construction technology differs for various types of constructions. The database is designed primarily for the planning and management of residential buildings, specifically family houses. The expected benefit of this database will be a tool that will help the user to choose the technical, technological, and material solutions of selected details and constructions. The user defines which parameters and criteria are decisive aspects of the selection. At the same time, the system evaluates the defined criteria and subsequently, through the Machine Learning tool, will predict the selection to the user or search for the optimal solution based on the user-defined parameters and criteria. The parameters contained in the database and individual predictions will be determined based on a survey among individual participants in construction production.

The structure of the database of structural elements considers the technological and structural solution, selected economic (financial) and time parameters, parameters of the service life of the elements and specifies selected environmental aspects, i.e., the sustainability of the elements. The elements contain information about:

- realization costs,
- time-consuming implementation,
- operating costs - administration and maintenance costs,
- economic expression of durability,
- disposal costs,
- time-consuming liquidation,
- environmental parameters - Primary energy intensity (PEI), Global Warming Potential (GWP), Acidification Potential (AP).

### **3.2 Design and working in the proposed database of structural elements – a demonstration of the economic evaluation of a selected construction detail**

The first step in the design and creation of the database was dividing the building into functional parts. When dividing a building in terms of design and technical parameters, it was necessary to consider the function of the element, the method of construction and consider the technological aspect of construction. The technological aspect of the construction process is the division of the construction into phase and partial processes. It was important to assign all their types and kinds to individual structural elements. The building is divided into these 15 functional elements, parts (see Figure 2 Division of the construction into functional parts):



Figure 2: Division of the construction into functional parts

### 3.2.1 Design and technical parameters

The proposed database of construction elements enables the creation of construction details. As part of the work in this environment, the user will gain important information about selected economic parameters across the life cycle of the construction detail. The work in the proposed database consists of three steps:

1. definition of priority properties - defining the range and weight of individual parameters,
2. creation of construction detail,
3. automatic assignment of selected economic parameters.

The first step of work in the proposed database of structural elements is the definition of priority properties or parameters. The user will define the range and weight for each parameter. The user defines the category (intervals), ranges by individual parameters, the costs in every phase of the project (maximum cost) - design phase, implementation phase, operational phase (maintenance and construction management costs) and liquidation phase, interval (range) or category required service life of construction detail (maximum value of economic expression of service life), time required (implementation phase, operational phase, liquidation phase) and interval (range) of selected environmental aspects - LCA assessments - bound primary energy (PEI), CO<sub>2</sub> and SO<sub>2</sub> emissions. The user defines the weight, the order of individual categories of parameters - costs, time, the life of elements, environmental aspects and defines the weight of individual types of costs and environmental parameters, too. For example, if the user selects realization costs as a priority type, the user will be notified when selecting individual elements of the construction detail and exceeding the specified interval of the amount of realization costs. After the alert, the user will be able to retroactively change the way of solving the construction detail or accept the amount of costs and continue designing other parts of the structure.

The next step is to create a construction detail. For example, when designing a structural detail of a pitched roof, the user must follow flowchart (see Figure 3 Flowchart – creating a pitched roof detail).



Figure 3: Flowchart – creating a pitched roof detail

This is how the user configures the construction detail. The result of the configuration in the database will be an information model of the detail - a 3D model showing the composition of the construction detail with an accurate description of materials (see Figure 4 Example of a structural element – pitched roof- description and specification).

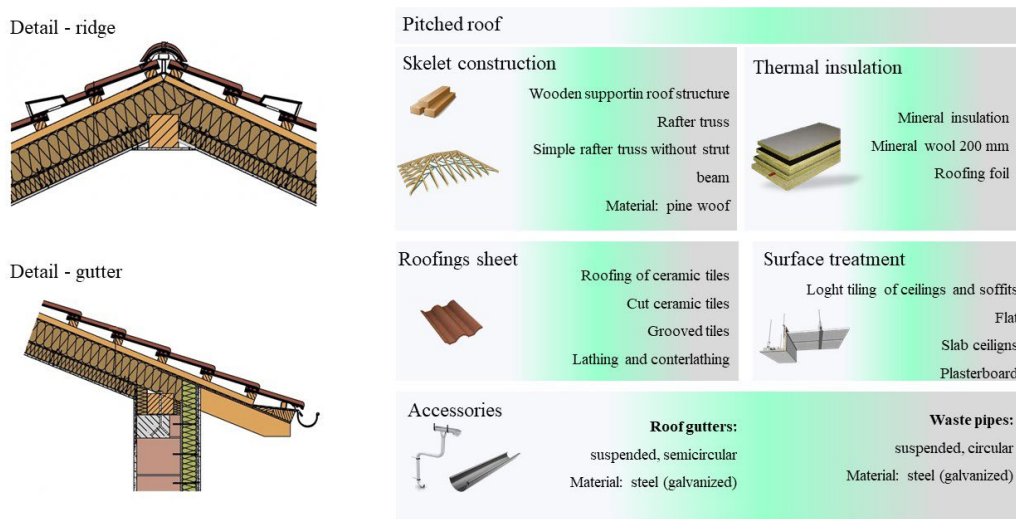


Figure 4: Example of a structural element – pitched roof- description and specification

### 3.2.2 Economic and time parameters – realization phase

Individual building elements and structures have information on costs throughout the life cycle of the building. Calculations, cost determination and technological analysis across the life cycle (implementation, operation, and liquidation phase) were determined based on the Classification of Building Structures and Works and the CENEKON database. The mentioned databases contain information on indicative price prices of materials, goods, services, works and information on the time required of the implementing of selected works and structures (standard hours, technological breaks, and others). Acquisition costs are divided based on a calculation formula into direct material, direct wages, costs of machinery and equipment, other direct costs, production and administrative overheads, profit, and risk. The complete

construction budget for the implementation of the selected roof structure is shown in see Figure 5 Cost estimating- realization phase. The element also has information on the time required for realization (Figure 6 Technological analysis – realization phase) [5].

Realization phase			
ECONOMIC PARAMETERS	Process	Unit of measure (UM)	Unit price (€)
	Installation of ceramic roofing Tondach, inclination from 35° to 60 °	m2	14,06
	Ceramic roofing Tondach Twist basic	ks	1,40
	Ceramic roofing TONDACH TWIST half	ks	1,63
	TONDACH TWIST ventilation ceramic roofing	ks	4,95
	TONDACH TWIST anti-snow ceramic roofing	ks	2,80
	TONDACH Tuning Twin Power roofing foil over 35 °, for rafters	m2	8,16
	Base strip made of galvanized sheet metal, 200 mm	m	7,96
	Installation of bonded roof truss structures made of lumber with an average area of 120-224 cm2	m	7,16
	Pine blanks - prisms quality	m3	197,86
	Installation of battens of simple roofs for finishing up to 60 °	m	0,73
	Prisms of pine unworked angled quality About (140,160,200 mm)	m3	219,86
	Assembly of contractile for inclination above 35 °	m	1,66
	Installation of thermal insulation of sloping roofs attached by nailing and tying to battens between and under the rafters hr. over 10 cm	m2	9,50
	ISOVER DOMO PLUS 20 strip, 200x1200x8400 mm, glass wool insulation suitable for sloping roofs, attics, ceilings and light floors	m2	8,58
	Installation of thermal insulation of sloping roofs attached by nailing and tying to battens between and under the rafters	m2	12,55
	ISOVER DOMO PLUS 10 strip, 100x1200x8400 mm, glass wool insulation suitable for sloping roofs, attics, ceilings and light floors	m2	4,29
	Attic SDK Rigips RB 12.5 mm, on R-CD construction and rafter hinges without TI	m2	25,34
	TONDACH corner, using aluminum ventilation strip, inclination from 38 ° to 60 °	m2	57,79
	Gutters made of galvanized PZ sheet, semi-drip semicircular 250 mm	m	21,50
Conical kettle made of galvanized PZ sheet, for pipes with a diameter of up to 100 mm	ks	22,88	
Base strip made of galvanized PZ sheet, 200 mm	m	7,96	
Downpipes made of galvanized PZ sheet, round diameter 100 mm	m	19,13	
<b>Total price €</b>			<b>657,75</b>

Figure 5: Cost estimating- realization phase

Realization phase				
Time parameters	Process	measure (UM)	elaboratenes (Nh)	
	Installation of ceramic roofing Tondach, inclination from 35° to 60 °	m2	0,733	
	TONDACH Tuning Twin Power roofing foil over 35 °, for rafters	m2	0,116	
	Base strip made of galvanized sheet metal, 200 mm	m	0,394	
	Installation of bonded roof truss structures made of lumber with an average area of 120-224 cm2	m	0,307	
	Installation of battens of simple roofs for finishing up to 60 °	m	0,046	
	Assembly of contractile for inclination above 35 °	m	0,104	
	Installation of thermal insulation of sloping roofs attached by nailing and tying to battens between and under the rafters hr. over 10 cm	m2	0,330	
	Installation of thermal insulation of sloping roofs attached by nailing and tying to battens between and under the rafters	m2	0,301	
	Attic SDK Rigips RB 12.5 mm, on R-CD construction and rafter hinges without TI	m2	1,162	
	TONDACH corner, using aluminum ventilation strip, inclination from 38 ° to 60 °	m2	0,905	
	Gutters made of galvanized PZ sheet, semi-drip semicircular 250 mm	m	0,906	
	Conical kettle made of galvanized PZ sheet, for pipes with a diameter of up to 100 mm	ks	1,239	
	Base strip made of galvanized PZ sheet, 200 mm	m	0,394	
	Downpipes made of galvanized PZ sheet, round diameter 100 mm	m	0,662	
	<b>Total elaboratenes - hour</b>			<b>8,59</b>
	<b>Total elaboratenes - days</b>			<b>1</b>
<b>Technological breaks - days</b>			<b>0</b>	
<b>Total elaboratenes (work+breaks) - days</b>			<b>1</b>	

Figure 6: Technological analysis – realization phase



The service life, management and maintenance of individual structural elements and details are characterized by several specifics that the user must take into account when using structures and buildings. With the specific construction detail - sloping roof made of ceramic tile, insulated with mineral insulation and surface treatment - plasterboard ceilings, it is necessary to clean the roof gutters and waste pipes twice a year from leaves and dirt and at least once every 15 years is it is necessary to carry out a treatment of the structure with paint (see Figure 7 Operational phase – maintenance of gutters and waste pipes).

### Operational phase – gutters and waste pipes

Process		Interval	Unit of measure (UM)	Unit price (€)	Unit elaboratenes (Nh)	
Washing	Cleaning from leaves and dirt	twice a years (spring, autumn)	hour	12,85	1,060	
					<b>Total price €/ m2</b>	<b>12,85</b>
					<b>Total elaboratenes hours/m2</b>	<b>1,060</b>
	<b>Declared service life of the element from the manufacturer</b>					<b>50</b>
	<b>Number of cleanings during the declared service life</b>					<b>100</b>
	<b>Total price (cleaning costs over the declared lifetime) €/m2</b>					<b>1285</b>
	<b>Total labor (labor expended on cleaning during the declared service life) hours/m2</b>					<b>53</b>
Process		Interval	Unit of measure (UM)	Unit price (€)	Unit elaboratenes (Nh)	
Construction treatment	surface degreasing	as needed (once in 15 years)	m2	7,290	0,181	
	surface cleaning – sanding, scraping		m2	1,660	0,056	
	application of anti-corrosion coating		m2	40,340	0,013	
	toapcoat application (2 coats) - hydrophobic coating					
	<b>Total price €/ m2</b>					<b>49,290</b>
	<b>Total elaboratenes hours/m2</b>					<b>0,25</b>
	<b>Declared service life of the element from the manufacturer</b>					<b>50</b>
<b>Number of cleanings during the declared service life</b>					<b>3</b>	
<b>Total price (cleaning costs over the declared lifetime) €/m2</b>					<b>147,87</b>	
<b>Total labor (labor expended on cleaning during the declared service life) hours/m2</b>					<b>0,75</b>	

Figure 7: Operational phase – maintenance of gutters and waste pipes

In addition to the protection and maintenance of roof gutters, it is crucial to treat and clean the roofing, more detailed specifications (cost and time per 1 m<sup>2</sup>) see Figure 8 Operational phase - maintenance of ceramic tiles.

Operational phase – ceramic tiles

Process		Interval	Unit of measure (UM)	Unit price (€)	Unit elaboratenes (Nh)
Washing - cleaning from dust and dirt	cleaning	Once a year (in the interval of 10-15 years)	m2	1,740	0,100
		<b>Total price €/ m2</b>			
	<b>Total elaboratenes hours/m2</b>				<b>0,1</b>
	<b>Declared service life of the element from the manufacturer</b>				<b>80</b>
	<b>Number of cleanings during the declared service life</b>				<b>6</b>
	<b>Total price (cleaning costs over the declared lifetime) €/m2</b>				<b>10,44</b>
	<b>Total labor (labor expended on cleaning during the declared service life) hours/m2</b>				<b>0,6</b>
Process		Interval	Unit of measure (UM)	Unit price (€)	Unit elaboratenes (Nh)
Construction treatment	cleaning from moss, lichens, soot dust and grease	as needed (once every 15 years)	m2	1,740	0,100
	inspection of roofing (cracks, fissures, scratches)		hour	5,750	0,935
	penetrating coating (need for 6 hours of technological break)		m2	0,235	0,013
	application of acrylic paint (brush, roller, airless machine)		m2	4,579	0,270
	<b>Total price €/ m2</b>				<b>12,304</b>
	<b>Total elaboratenes hours/m2</b>				<b>1,318</b>
	<b>Technological break (TB) hours</b>				<b>6</b>
	<b>Total elaboratenes hours/m2</b>				<b>7,318</b>
	<b>Declared service life of the element from the manufacturer</b>				<b>80</b>
	<b>Number of cleanings during the declared service life</b>				<b>5</b>
	<b>Total price (cleaning costs over the declared lifetime) €/m2</b>				<b>61,52</b>
<b>Total labor (labor expended on cleaning during the declared service life) hours/m2</b>				<b>36,59 + TB</b>	

Figure 8: Operational phase -maintenance of ceramic tiles

It is also important to determine the cost of the liquidation phase of the structure. A detailed description of the dismantling processes of the mentioned roof structure (their time and financial demands of implementation) is shown in Figure 9: Liquidation phase – technological and cost analysis. The disposal price of 1 m<sup>2</sup> of ceramic roofing is about 275,43 € and the total workload is about 2 days.


Liquidation phase		Process - description	Unit of measure (UM)	Unit price (€)	Unit elaboratenes (Nh)
 <p>Disassembly Technological and cost analysis</p>	Removal of thermal insulation - mineral wool	m2	1,01	0,066	
	Mass transfer-dismantling- thermal insulation -mineral wool	t	39,93	2,155	
	Disassembly of carpentry structures - truss	m2	1,6	0,097	
	Disassembly of carpentry structures - battens, counter battens	m2	0,67	0,047	
	Material transfer - disassembly - carpentry structures	t	49,31	1,82	
	Disassembly of plasterboard ceiling with load-bearing structure	m2	4,41	0,311	
	Material transfer-disassembly-plasterboard ceiling	t	67,37	4,046	
	Dismantling of gutters	m	0,67	0,047	
	Disassembly of plating	m	1,07	0,075	
	Material transfer - disassembly - plumbing constructions	t	65,65	4,679	
	Disassembly of ceramic roofing - inclination up to 60 °	m2	2,97	0,218	
	Material transfer - disassembly - ceramic roofing	t	40,77	2,419	
	<b>Total price €/ m2</b>				<b>275,43</b>
	<b>Total elaboratenes hours/m2</b>				<b>15,982</b>
<b>Total elaboratenes days</b>				<b>2 days</b>	

Figure 9: Liquidation phase – technological and cost analysis

### 3.2.3 Element durability and facility management

In addition to information on the method of protection and maintenance of the mentioned construction detail, information on the service life of individual structural elements is also important. With the selected construction detail, the service life of the individual construction elements is as follows:

- ceramic tiles - declared service life of 80 years,
- wooden structure - declared service life 50-100 years,
- thermal insulation from mineral wool - declared service life of 50 years,
- elements made of galvanized sheet metal - roof gutters and waste pipes - declared service life of 50 years,
- Rigips RB ceiling - declared service life of 50-70 years [14].

The service life of the elements is an important factor that significantly influences the user's decision-making process. Service life affects the economic parameters of the building. The longer the life of the elements and the lower the resource required to manage and maintain the elements, the more economical advantageous the element could be. In the construction detail of a sloping roof made of ceramic tile, insulation made with mineral wool, waste pipes and gutters made of galvanized sheet metal and interior finish made of plasterboard ceilings, the most stressed part of the detail is the roof covering made of ceramic tile, which is affected by external influences. Based on the above fact, we can consider the ceramic tile as a decisive or determining element of the life of the structural detail. In the event of damage to the said layer, other structural parts may be degraded - the load-bearing structure, thermal insulation, and plasterboard ceiling. Based on this fact, we can define the service life of the construction detail to 80 years. It is therefore important to express the economic life of the construction detail. For this purpose, it is possible to quantify the total costs across the life cycle (costs of implementation, administration, maintenance, and disposal of the structural detail) during the declared lifetime of the structural detail, in this case, for 80 years.

The economic expression of longevity can be found through the proposed relationship:

$$L_{\epsilon} = \frac{C_r + C_o + C_d}{DS_1} \text{ [€ / year]} \quad (1)$$

Legend of abbreviations:

$L_{\epsilon}$  - economic expression of the lifetime of the detail,

$C_r$  - costs of realization of construction detail,

$C_o$  - costs of operation of the construction detail (during the declared service life of the construction detail),

$C_d$  - costs of disposal of construction detail,

$DS_i$  - number of years of declared service life of the construction detail.

This relationship determines the economic expression of the lifetime of the details for one year during the life cycle in the declared lifetime of the details of the building.

With the mentioned specific construction detail - a sloping roof made of ceramic tile, insulated with mineral insulation and a surface treatment made of plasterboard ceilings, it is possible to economically express the service life at 38,97 €/year. The economic expression of longevity is determined based on the above relationship (detailed description see Figure 10 Economic expression of lifetime - ceramic roofing):

$$L_{\text{€}} = \frac{c_r + c_o + c_d}{DS_i} = \frac{464,40 + 2377,61 + 275,43}{80} = 38,97 \text{ [€/year]} \quad (2)$$

$C_r$  - costs of realization of construction detail = 464,40 €/m<sup>2</sup>,

$C_o$  - costs of operation of the construction detail (during the declared service life of the construction detail) = 2377,61 €/m<sup>2</sup>,

$C_d$  - costs of disposal of construction detail = 275,43 €/m<sup>2</sup>,

$DS_i$  - number of years of declared service life of the construction detail = 80 years.

Type of detail (decisive element)	ceramic tiles		
Declared service life of the construction detail	80		
Type of costs	Cost of realization €/m2		
		464,40	
	Operating costs €/m2	cleaning of the roof structure - during a service life of 80 years - 6 times	10,44
		treatment of the roof structure - during a service life of 80 years - 5 times	61,52
		gutter cleaning (ATTENTION - lower declared service life of the element (50 years) as a construction detail, therefore it is necessary to replace the structural element after the declared service life of the element) - costs determined based on the need to perform the task (80 times) + replacement of the element (realization costs)	2059,20
		gutter treatment (ATTENTION - lower declared service life of the element (50 years) as a construction detail, therefore it is necessary to replace the structural element after the declared service life of the element) - costs determined based on the need to perform the task (5 times) - no replacement (included in the previous item)	246,45
	Total operating costs €/m2		2377,61
Disposal costs €/m2		275,43	
Total costs	Total costs across the life cycle € / m2		
	3117,44		
	Total costs € / year (per year during the declared service life of the construction detail)		
	38,97		

Figure 10: Economic expression of lifetime - ceramic roofing

### 3.2.4 Environmental aspect, sustainability feature

In addition to economic, technological parameters and information on facility management and durability, important considerations of the life cycle of elements are also information considering the environmental aspects of individual elements. Construction elements can have different impacts on the environment and therefore, it is important to consider their impacts on the environment, respectively the use of resources, the quality of the internal environment and the like.

Increasingly, the construction life cycle assessment - LCA - is being implemented in the construction industry. LCA is a life cycle analysis in terms of sustainability. Every part of the product life cycle can impact the environment. There are many types of LCA and LCA-related assessments, such as environmental product declarations (EPDs), studies per the product or sector-specific standards, problem analyses (carbon or water footprint, social LCA) and long-term monitoring studies [15].

The evaluation of LCA consists of four main phases, namely the definition of objective and scope, investment analysis, impact assessment and interpretation. We know three commonly

used LCA assessment methods, namely the ecological scarcity (ECO) method, the environmental theme (ET) method, the environmental priority strategies in the product design (EPS) method [16].

The ecological scarcity (ECO) method is a term related to the relationship between supply and demand. The term defines the ecological deficiency between the critical load of pollutants and the actual load of anthropogenic emissions of this pollutant. The critical load can be defined as either environmental critical load (sustainable load) or politically maximum acceptable limits (policy objectives). Since different regions have different sensitivities to pollutants and different levels of pollution, it is necessary to adjust the calculation by a coefficient that takes into account regional differences [16].

The environmental theme (ET) method is a method developed by McKinsey & Company Inc., The Center for Environmental Science in Leiden (CML) and The Dutch National Institute for Health and Environment (RIVM). The total calculation is performed through 3 steps[16],:

1. Environmental load of the product - the product is assigned information on the degree of environmental pollution based on a thorough analysis of the product into individual components, respectively into individual related equivalent pollutants.
2. Sum - the calculation of the equivalent environmental burden of the selected product is determined by the sum of the individual equivalent values corresponding to the individual components of the product,
3. Determination of impact fractions - it is possible to summarize the total impact after using mass factors (WI) and consider the relative severity of a different environment.
4. The ET method provides some leeway in the choice of topics and how weighting factors are assigned.

The environmental priority strategies in product design (EPS) method are developed by The Swedish Federation of Industries and Volvo Car Corporation. There are two types of load indices: source indices and emission indices [16].

One pollutant can have many effects on the environment, health, society. Pollutant emissions can be considered as the beginning of a chain of change, where the first change is called the primary effect. The primary effect is defined as changes, often of a chemical or physical nature. Biological changes occur as higher-order effects (for example 34). The difference between the methods lies in where and what is the evaluation of the interconnected chains of pollutants, for example the evaluation of the emitted substance (e.g. CO), the evaluation of the physic-chemical change of the environment (e.g. global warming due to radiation exposure), or evaluation of the effect of the change on human life (e.g. assessment of lost land due to increased sea levels, headaches and other effects [16].

The ECO and ET methods allow some flexibility in the choice of standards relevant for the purpose of the calculation. The critical load can be defined as an environmentally sustainable load. Both methods make it possible to meet political and environmental goals. Data quality and accuracy may vary slightly. This is due to possible differences in the statistics, depending on the sources from which the data were obtained. Based on the above, the methods just mentioned will be used in determining the parameters of the environmental load of the elements [16].

In the database, selected environmental aspects are assigned to individual elements, such as PEI – primary energy intensity, GWP- global warming potential, AD – acidification potential (see Figure 11 Environmental assessment of elements - PEI, GWP, AP parameters) [17][18].



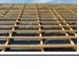
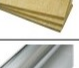




 ELEMENT, CONSTRUCTION	Primary energy intensity- PEI	Emissions CO <sub>2</sub> ekv. - Global Warming Potential-GWP	Emissions SO <sub>2</sub> ekv.- Acidification Potential-AP
 Ceramic roofing Tondach	159,950 unit of measure tom <sup>2</sup>	7,000	0,002
 Laths, counterlaths	18,370 unit of measure tom <sup>3</sup>	-1,270	0,000
 Thermal insulation of roofing strip mineral wool	3386,400 unit of measure to m <sup>3</sup>	153,680	1,090
 Safety under-roof vapor-permeable foil	162,720 unit of measure to m <sup>2</sup>	4,780	0,030
 Gutters and plating of galvanized sheet metal	202,020 unit of measure to m	8,900	0,060
 Attic SDK Rigips RB 12.5 mm for R-CD construction and rafter hinges without TI	3255,000 unit of measure to m <sup>3</sup>	152,250	0,500
 Truss-load-bearing structure - building timber from spruce	1020,600 unit of measure to m <sup>3</sup>	-760,860	0,670
$\Sigma$	<b>8505,06 unit of measure</b>	<b>-435,52</b>	<b>2,352</b>

Figure 11: Environmental assessment of elements - PEI, GWP, AP parameters

## 4 Conclusion

Developments in the field of construction are changing the way construction production is implemented and managed. Construction production is characterized by a working environment that is unstructured and faces unpredictable and uncontrollable situations. Construction process management requires a wealth of information that needs to be effectively managed and administered. Based on the complexity of construction production, new methods are being developed to support efficient, economic and optimal management of construction production. The article deals with the design of a new knowledge database. The individual elements of the database contain graphical and non-graphical information. The elements have information on the design and technical solution, the need for costs and time of realisation (realisation and operation phase), the durability of the element, information of facility management and information on the impact of the elements on the selected environmental parameters.

The tools and applications available so far enable the evaluation of selected elements from various points of view or enable the analysis of selected properties and specifications - costs, time planning, environmental impacts, and the like. However, the market still does not have a tool or a unified environment to evaluate and analyse selected elements based on several

crucial parameters and user preferences. Progress in this area is constantly advancing, individual applications allow data transfer in a compatible format, such as IFC, but there is still a significant loss of data, or incompatibility of tools and methods of analysis of selected structures and elements. The database creates a structure and determines the method of evaluation and creation based on user preferences. Individual parameters were determined based on market analysis and requirements of individual users within the phases of the life cycle of buildings - preparation, planning, management, and use.

Due to the constant development of new innovative materials and technologies, it will be necessary to update the parameters contained in the database at least once a year. The implementation of new materials and technologies, although in the initial phase may represent an increase in costs and time, in the end, new technologies and materials will result in increased profits for construction companies. Thanks to the optimization of all phases of the project, from design to liquidation, the efficiency and effectiveness of financial, time and environmental management of construction processes will increase.

The initial start-up costs and funding sources of the target customer base, marketing strategy and review of the competition and the projection of revenues and expenses will be covered from the resources of the scientific research project of the Faculty of Civil Engineering TUKE APVV-17-0549 "Research of knowledge-based and virtual technologies for intelligent designing and realisation of building projects with an emphasis on economic efficiency and sustainability". The next goal will be to obtain a trademark or patent for the proposed tool, the structure of the database. Following the acquisition of the trademark, efforts will be made to establish cooperation with existing software companies and to obtain sponsors for the future development and advancement of the proposed database.

## Acknowledgements

The paper presents partial research results of project "Use of building information model in planning the life cycle of buildings" and of project APVV-17-0549 "Research of knowledge-based and virtual technologies for intelligent designing and realization of building projects with emphasis on economic efficiency and sustainability".

## References

- [1] Systematic. (2013). *Construction production schedule in cloud (Harmonogram stavebnej výroby v cloude*. 12.05.2021, [https://www.systematic.sk/web/index.php?option=com\\_content&view=article&id=129%3Aharmonogram-v-prostredi-cloudu&catid=24%3Akalkulus-blog&itemid=14](https://www.systematic.sk/web/index.php?option=com_content&view=article&id=129%3Aharmonogram-v-prostredi-cloudu&catid=24%3Akalkulus-blog&itemid=14)
- [2] Tejankar. (2019). *The Use of Automation in Construction Industry*. 12.05.2021, <https://www.engineeringcivil.com/the-use-of-automation-in-construction-industry.html>
- [3] Kros. (2017). *How to correctly and objectively evaluate a construction contract (Ako správne a objektívne oceniť stavebnú zákazku)*. 11.05.2020, <https://www.kros.sk/blog/ako-spravne-a-objektivne-oceniť-stavebnu-zakazku/>
- [4] Kros. (2017). *The key criteria according to which the customer decides when choosing a construction company* 11.05.2021, <https://new.kros.sk/wp-content/uploads/2019/04/0000121326.png>
- [5] Nagy. (2013). *Prices in construction – basic carrier on information about the scope of construction activities*. 11.05.2021, <https://stavebnictvo.sk/profiles/blogs/cena-v-stavebn-ctve-z-kladn-nosite-ka-inform-cie-o-rozsahu>
- [6] BIMestiMate. (2021). *About*. 18.09.2021, <https://bimestimate.eu/en/bimestimate-about/>



- [7] Buildsoft. (2021). *TakeOff & Price Lists*. 15.09.2021, <https://www.buildsoft.com.au/cubit-estimating>
- [8] ITWOCostX. (2021). *Products*. 15.08.2021, <https://www.itwocostx.com/costx/products/>
- [9] Nevaris. (2021). *Nevaris Build*. 15.08.2021, <https://www.nevaris.com/produkte/nevaris-build/>
- [10] Nevaris. (2021). *Nevaris Finance* 15.08.2021, <https://www.nevaris.com/produkte/nevaris-finance/>
- [11] ElectricSmarts' Network. (2021). *ConEst Software systems*. 14.08.2021, <https://www.electricsmarts.com/netpak-featuring-netpricer-service/works-with/conest-intellibid>
- [12] Conest Software Systems. (2021). *Electrical Estimating & Project Management Software*. 15.09.2021, <https://www.conest.com/products/>
- [13] ElectricSmarts' Network. (2021). *NetPak's NetPrices works with you software*. 15.09.2021, <https://www.electricsmarts.com/netpak-featuring-netpricer-service/works-with/proest-estimating>
- [14] Vyparina. (2011) Specifics of determining the general value of real estate and buildings (Špecifiká stanovenia všeobecnej hodnoty nehnuteľností a stavieb), Proceedings of seminar lectures University of Tülin at EDIS, 2011 (44-45). Tülin. ISBN 978-80-554-0334-2.
- [15] Pre-sustainability. (2020). *Life Cycle Assessment (LCA) explained*. 15.09.2021, <https://pre-sustainability.com/articles/life-cycle-assessment-lca-basics/>
- [16] Baumann, Rydberg. (1994). Life cycle assessment – A comparison of three methods for impact analysis and evaluation. *Journal of Cleaner Production*. Volume 2 (Issue 1), p.13-20. DOI 10.1016/0959-6526(94)90020-5
- [17] Zeleňáková, Purcz, Ondrejka Harbuláková and Oravcová. (2016). Determination of pollutant concentrations in the Krasny Brod River profile based on the Buckingham theorem. *Desalination and Water Treatment*. Volume 57 (Issue 6), 2693-2701. <https://doi.org/10.1080/19443994.2015.1031709>.
- [18] Harbulakova, Zelenakova and Sugarekova. (2018). Preparation status of the municipalities on dealing with the foold protection in the Presov region, Slovakia. *SGEM 2018. 1.5. Science and technologies in geology, oil and gas exploration, water resources, forest ecosystems : oil and gas exploration, hydrology and water resources forest ecosystems*. Volume 18, 391-398. DOI 10.5593/sgem2018V/1.5/S02.049

## Exploring the impact of balconies on cooling energy demand in an arid climate zone

Soufiane Boukarta<sup>1,2\*</sup>

<sup>1</sup> Institut d'Architecture et d'Urbanisme (IAU), University of Blida 1. Algeria  
<sup>2</sup> Ecole polytechnique d'Architecture et d'Urbanisme (EPAU), Laboratoire Ville, Urbanisme et Développement Durable (VUDD). Algiers, Algeria.

\*e-mail: boukarta.soufiane@univ-blida.dz

### Abstract

This paper explores the impact of balconies on the energy demand required for cooling in the arid climate zone of the city of Adrar, in Algeria. For the purpose to assess several situations of the balconies, we have chosen a parametric method based on a campaign of thermal simulations. The open and eliminated balcony type were selected and characterized by four parameters: the balcony to room ratio, the orientation, the window type, and the balcony position. A set of 100 simulations was selected randomly based on the Monte-Carlo probability technique. The final sample was corrected based on Cook's distance which gave 85 simulations as a final sample size. A generalized regression model was performed to identify the impact of each parameter. The accuracy of the model is above 97% and the sensitivity analysis shows that the most important factor is the balcony to room ratio which could reduce the energy demand up to 26% followed by the window type (24%), the orientation (8%) and the balcony position (5%). This conclusion stresses the idea of considering the balcony as a passive solution to reduce the cooling energy demand.

**Key words:** Adrar, arid climate zone, balcony, parametric analysis, cooling energy demand.

## 1 Introduction

The residential sector consumes more than 40% of the final energy consumption [1, 2], and several orientations are prepared across the world to reduce the use of fossil energy. To do so, several papers discuss the passive and the active ways to reduce the energy demand in the residential sector. Within the higher densities proposed and stressed by the sustainable development goals, the balconies constitute a real substitute for the courtyard [3]. The balcony also represents an important parameter in explaining the satisfaction of inhabitants regarding the cities' liveability [4, 5].

Ribeiro et al. in their review show that most of the studies considering the impact of balconies on the energy demand come from western and Asian cities [3]. For this purpose, the present

paper explores the idea stressing the **passive role** of balconies in reducing the energy demand in an arid climate zone [3]. We have selected the city of Adrar because its climate is typical and represents a large zone of Algeria's south Saharan.

In the second section of this paper, a literature review is presented aiming to highlight the balconies' type, and the methods used to carry out their effect on the cooling energy demand. The third section presents our method to identify the correlation between energy demand and the characteristics of balconies. The fourth section presents and discusses our results with a comparison with the results obtained from the literature review. Finally, in the fifth section, the conclusion highlights the results and limits of our approach and proposes some tracks for further research.

## 2 Literature review

The papers reviewed consider the balcony as an architectural solution to improve the Indoor Environment Quality (IEQ). Mainly, three objectives are targeted by researchers: (1) the impact of the balconies on the interior comfort, for heating and cooling demand [6], (2) airflow patterns and ventilation quality [7, 8] with and without balconies, and (3) the balcony as an acoustic shielding [9, 10]. Our paper fits in the first set of studies and aims to highlight the impact of balconies on the cooling energy demand.

The literature highlights several types of balconies. Three types are considered based on the opening criterion: (1) Open Balconies (OB), which are characterized by their direct opening to the outside. This type of balcony is stressed for the warm climate zones because of its shading potential [11, 12]. (2) Glazed Balconies (GB) reduce the contact between the balcony and the outdoor [13]. This type could be proposed by architects and is mainly recommended for the cold climates for their heat potential, or it could be also the case of a transformed balcony and this case is very widespread in the developing countries like Algeria, Tunisia, or Morocco [2]. (3) The third type of balcony is the Eliminated Balcony (EB) [14]. This case is also widespread in developing countries, and it aims to enlarge the indoor surface. In our case and as a response to the harsh side of our climate zone, we have selected the Open Balcony with some situations of Eliminated Balconies to be able to assess the importance of balconies in reducing the cooling energy demand.

To assess the importance of the impact of the balconies on the cooling energy demand, two main approaches exist: (1) A simulation [15, 16] and (2) in-situ-based approaches [17, 12]. Some papers consider the in-situ measurements as a technique of calibration to verify the quality of the simulations and to test new improvement techniques [22]. Because of its high flexibility in representing a high number of situations, the simulation-based approach is considered to predict the impact of the balcony on energy demand.

The results regarding the impact of the balcony on the cooling energy demand show a positive impact and reduce the energy consumption by up to 12% in Hong Kong [18]. The authors explain this reduction by the shading potential of the overhang which decreases the amount of solar radiation. Authors also claim the positive technology effect of windows on the energy

cooling demand, i.e., the solar transmittance and the reflective or absorptive glazing.

In the same track, Raeissi and Taheri (1998) have also obtained almost the same results for the city of Shiraz in Iran [19]. The overhang shading potential could reduce up to 12.7% of the energy demand of cooling in the summer. Authors have considered the horizontal depth of balconies and they claim that it would be more profitable to consider the balcony geometry (depth) to reach a trade-off between the optimization of the energy demand required for cooling and lighting according to the fourth geographical orientations. In China, and for the same purpose, Yu et al. (2008) found a reduction of almost 8% in electricity energy demand achieved through the balcony overhang shading effect. A combined strategy (thermal insulation of exterior walls, the solar radiation absorptance of the exterior wall, window to wall ratio, window categories and the length of the overhang) could result in electricity saving potential of up to 21.08 and 34.77 % for cooling and heating respectively [20]. In the present paper, we aim to explore the impact of different balcony situations on the energy demand by varying several parameters. The next section explains the method adopted.

### 3 Method

The method adopted follows the steps below:

#### A. Conceiving the design of experiments:

The first step consists in conceiving an archetype on which several parametric variations could be applied. For this purpose, we have sketched a single room space of 18 m<sup>2</sup> as a reference design, and we have added a 2.1 m<sup>2</sup> of French window (1x2.1 m) and its dimensions remain fixed for all the other situations. See Figure 1 below.

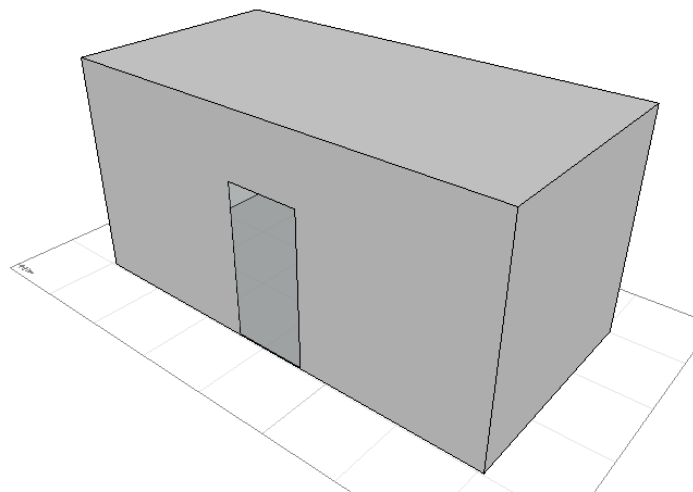


Figure 1: The base line design (no balcony situation)

#### B. Parametric variation:

To assess the impact of the balcony on the energy demand, we have selected four main parameters usually used by architects when designing balconies. (1) The balcony/room ratio. This parameter highlights the area of the balcony regarding the room area. And it could be obtained with overhang situation and by hollowed-out balconies (See Figure 2 below). We

have considered a range of ratios with several values: 0 (no balcony), 0.16, 0.2, and 0.5. (2) The second parameter considered is the position of the balcony, whether in the centre, left, or on the right of the room. (3) The orientation is the third parameter considered for this study. We have directly selected the four geographic orientations, north, west, east, and south. (4) The last parameter considered is the glazing type of the French window. We have considered two parameters for this purpose, the thermal transmittance (U-value) and solar heat gain (SHG) coefficient. Four cases were selected: (a) a simple glazing window (U value = 5.1 W/m<sup>2</sup>.K and SHG = 0.94); (b) a double glazing window (U-value = 2.26 W/m<sup>2</sup>.K and SHG = 0.75); (c) a double glazing window (U-value = 1.8 W/m<sup>2</sup>.K and SHG = 0.60); and (d) the high performance high glazing window (U-value = 1.25 W/m<sup>2</sup>.K and SHG = 0.45). All these window types exist already in the Algerian market. See Table 2.

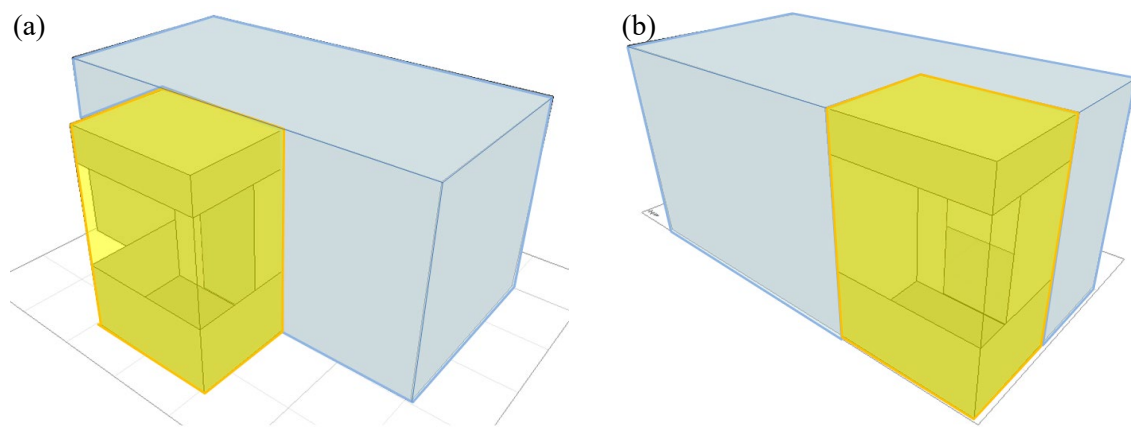


Figure 2: Balcony geometry and position. (a) Overhanging balcony, (b) Hollowed-out balcony

Other thermal characteristics of the room are fixed, and their values are considered as for the standards proposed by the regulatory document (DTR). See Table 1 below.

Table 1: Thermal characteristics of design elements

Building element	U-value
100 mm thick concrete slab on ground.	0.88 W/m <sup>2</sup> .K
Ceiling (insulated pot floor, 200 mm)	0.36 W/m <sup>2</sup> .K
Exterior walls (double brick cavity render, 150mm; 50 mm air gap; and 100 mm brick)	1.34 W/m <sup>2</sup> .K

### C. Sampling

A first random sample size of 100 simulations was considered based on the Monte-Carlo technique which is based on random sampling in the possible interval variation of each variable. The importance of this method is more felt when the interval is wide and when there is no linearity between the dependant and independent variables. Also, this method was used because it does limit the number of possible situations and cover a large range of parameter variation [21]. To perform an accurate model, we have corrected the sample by using Cook's distance. We have eliminated all the cases with a value higher than 0.2. A total of 85 simulations is the sample size considered to perform the model, see Appendices, Tables A-1

and A-2.

Table 2: Frequency of the parameters considered in the model

Parameters	Values	N (frequency)
Balcony/room ratio	no balcony	23
	0.16	27
	0.2	26
	0.5	9
Balcony position	Right	31
	Centre	24
	Left	30
Window type (U-value)	0.94	18
	0.75	26
	0.60	20
	0.45	21
Orientation	South	20
	East	18
	West	24
	North	23

A generalised regression model is performed based on the 85 simulations and the results are presented in the next section.

#### 4 Results and discussion

The generalised regression model does allow considering all the parameters variation and permits to carry out the importance of each variation. The variance inflation factor (VIF) was checked to identify the multicollinearity of the variables introduced in the model. The VIF values of the entire variables are less than 3 and the tolerance values are larger than 0.2, which indicates that there is no multicollinearity, and all the variables are independent of each other [23], see Table 3 below. We have introduced the interaction between the window type and the façade orientation in the model. The accuracy of the model performed is above 97%, as indicated in Table 4 below.

Table 3: Multicollinearity test

	Tolerance	VIF
Balcony/room ratio	0.998	1.002
Balcony position	0.998	1.002
Window type	0.992	1.008
orientation	0.990	1.010

Table 4 : The generalised regression model

Source	The sum of squared type III	df*	Squared mean	f**	Significance
Corrected model	15759.900a	20	787.995	102.011	0.000
Constant	351794.959	1	351794.95	45542.008	0.000
Window type * Façade orientation	195.211	9	21.690	2.808	0.008
Bal/room ratio	3821.629	3	1273.876	164.911	0.000
Balcony position	102.819	2	51.409	6.655	0.002
Window type	5677.584	3	1892.528	244.999	0.000
Façade orientation	582.050	3	194.017	25.117	0.000
Error	494.376	64	7.725		
Total	557306.759	85			
Corrected total	16254.276	84			

R<sup>2</sup> = .970 (R<sup>2</sup> adjusted = .960)

\*df : degree of freedom

\*\*f : f-statistics. All f-statistics values of the variables are greater than zero which means that the null hypothesis is rejected, and the model is good for predicting.

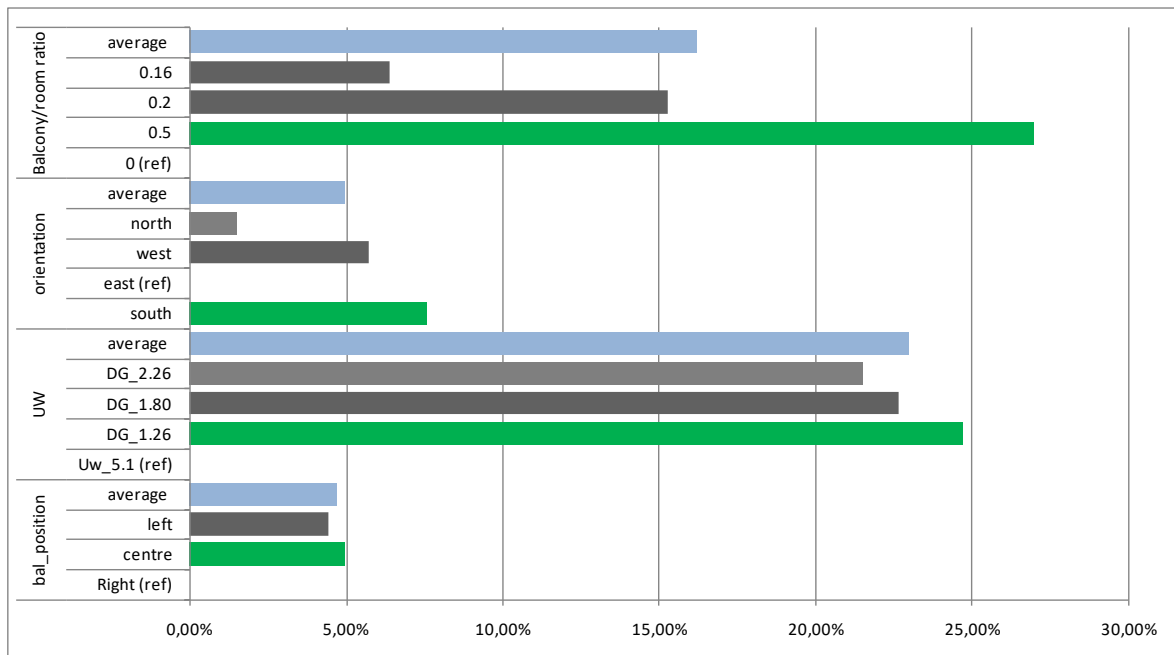


Figure 3: Energy saving for all the parameters

Figure 3 shows clearly that the balcony to room ratio plays an important role in reducing the cooling energy demand of up to 27 % for the ratio of 0.5. In the second position comes the window quality characterized in this paper by the solar heat gain (SHG) and the U-value of the window. The high-performance double-glazed window with an SHG of 0.45 and a U-value of 1.26 could reduce the cooling energy demand up to 24.70%. Also, it is worth to highlighting that the variation of the energy saving is almost the same for all the double

glazed windows which means that there is no need to enhance the insulation or the solar heat gain up to 1.26 W/m<sup>2</sup>.K and 0.45 respectively. A double glazed with a U-value of 2.26 and SHG of 0.75 W/m<sup>2</sup>.K could reduce the cooling energy demand up to 21.51%. The impact of the orientation in reducing the cooling energy demand is observed for the south orientation of the facade because the south orientation has the maximum sun hours and the highest solar altitude which means that a deep balcony will reduce the solar incidence and create higher shading areas. Also, our results show a weak impact of the balcony position, with a small impact of 5% for a central position. The overhang effect could explain this impact.

A negative linearity behaviour is observed using a bivariate correlation between the cooling energy demand, the window type (-0.674), and the balcony to room ratio (-0.37). The cooling demand decreases with the increasing quality of the window and the depth of the balcony especially with hollowed-out balcony because it allows more shading potential.

Considering the construction cost, all the balcony strategies remain interesting and reduce the cooling energy demand, but the utility area is more important with overhanging balcony type. The highest energy saving potential is observed for hollowed-out balconies. Regarding the average value for each parameter, the window type gets the first position with an average value of 23%, followed by the balcony to room ratio with a 16.22% average value. The orientation and balcony position have approximately the same average impact of almost 5%.

## 5 Conclusion

In this paper, we have performed a sensitivity analysis based on a generalized regression model to assess the impact of the balcony characteristics on reducing the cooling energy demand for a room in Adrar, situated in an arid climate zone. Our results highlight the importance of the balconies as a passive solution to reduce the cooling energy demand. The balcony to room ratio which also could be interpreted as a balcony depth has an important shading potential, and its impact could reduce the cooling energy demand by more than 25% and more efficiently than a high-performance double-glazed window. The idea of stressing the balcony as a passive solution is verified in this climate zone. In this paper, we have considered only the impact of the balcony on the cooling energy demand based on the Open Balcony type. For further purpose and research, the glazed balcony or glazed and open balcony could be considered and analysed for both cooling and heating energy demand.

## References

- [1] Boukarta, S., & Berezowska, E. (2017). Exploring the Energy Implication of Urban Density in Residential Buildings. *Journal of Applied Engineering Sciences*, 7(1).
- [2] Boukarta, S., & Berezowska-Azzag, E. (2018). Energy demand of occupant's spatial modification in residential buildings. Case study of Médéa, Algeria. *Selected Scientific Papers-Journal of Civil Engineering*, 13(s1),15-28.
- [3] Ribeiro, C., Ramos, N. M., & Flores-Colen, I. (2020). A review of balcony impacts on the indoor environmental quality of dwellings. *Sustainability*, 12(16), 6453.
- [4] Kotulla, T., Denstadli, J. M., Oust, A., & Beusker, E. (2019). What Does It Take to Make the Compact City Liveable for Wider Groups? Identifying Key Neighbourhood and Dwelling Features. *Sustainability*, 11(12), 3480.



- [5] Omrani, S., Garcia-Hansen, V., Capra, B. R., & Drogemuller, R. (2017). On the effect of provision of balconies on natural ventilation and thermal comfort in high-rise residential buildings. *Building and Environment*, 123, 504-516.
- [6] Hastings, S. R. (2004). Breaking the “heating barrier”: Learning from the first houses without conventional heating. *Energy and Buildings*, 36(4), 373-380.
- [7] Chand, I., Bhargava, P. K., & Krishak, N. L. V. (1998). Effect of balconies on ventilation inducing aeromotive force on low-rise buildings. *Building and environment*, 33(6), 385-396.
- [8] Kahsay, M.T.; Bitsuamlak, G.T.; Tariku, F. CFD simulation of external CHTC on a high-rise building with and without façade appurtenances. *Build. Environ.* 2019, 165.
- [9] Kropp, W., & Bérillon, J. (1998). A theoretical model to investigate the acoustic performance of building facades in the low and middle frequency range. *Acta Acustica united with Acustica*, 84(4), 681-688.
- [10] Wang, X.; Mao, D.; Yu, W.; Jiang, Z. Acoustic performance of balconies having inhomogeneous ceiling surfaces on a roadside building facade. *Build. Environ.* 2015, 93, 1–8.
- [11] Giovannini, L., Verso, V. R. L., Karamata, B., & Andersen, M. (2015). Lighting and energy performance of an adaptive shading and daylighting system for arid climates. *Energy Procedia*, 78, 370-375.
- [12] Saleh, P. H. (2015). Thermal performance of glazed balconies within heavy weight/thermal mass buildings in Beirut, Lebanon's hot climate. *Energy and Buildings*, 108, 291-303.
- [13] Mihalakakou, G. (2002). On the use of sunspace for space heating/cooling in Europe. *Renewable Energy*, 26(3), 415-429.
- [14] Kim, G., & Kim, J. T. (2010). Healthy-daylighting design for the living environment in apartments in Korea. *Building and Environment*, 45(2), 287-294.
- [15] Foged, I. W. (2019). Thermal responsive performances of a Spanish balcony-based vernacular envelope. *Buildings*, 9(4), 80.
- [16] Nowak-Dzieszko, K., & Rojewska-Warchał, M. (2015). Influence of the balcony glazing construction on thermal comfort of apartments in retrofitted large panel buildings. *Procedia Engineering*, 108, 481-487.
- [17] Dahlan, N.D.; Jones, P.J.; Alexander, D.K.; Salleh, E.; Alias, J. Evidence base prioritisation of indoor comfort perceptions in Malaysian typical multi-storey hostels. *Build. Environ.* 2009, 44, 2158–2165.
- [18] Chan, A. L. S., & Chow, T. T. (2010). Investigation on energy performance and energy payback period of application of balcony for residential apartment in Hong Kong. *Energy and Buildings*, 42(12), 2400-2405.
- [19] Raeissi, S., & Taheri, M. (1998). Optimum overhang dimensions for energy saving. *Building and Environment*, 33(5), 293-302.
- [20] Yu, J., Yang, C., & Tian, L. (2008). Low-energy envelope design of residential building in hot summer and cold winter zone in China. *Energy and Buildings*, 40(8), 1536-1546.
- [21] Kaoula, D., & Bouchair, A. (2019). The pinpointing of the most prominent parameters on the energy performance for optimal passive strategies in ecological buildings based on bioclimatic, sensitivity and uncertainty analyses. *International Journal of Ambient Energy*, 1-28.
- [22] Babae, F.; Fayaz, R.; Sarshar, M. The optimum design of sunspaces in apartment blocks in cold climate. *Archit. Sci. Rev.* 2016, 59, 239–253.
- [23] Li, C., Li, J., & Wu, J. (2018). What drives urban growth in China? A multi-scale comparative analysis. *Applied Geography*, 98, 43-51.

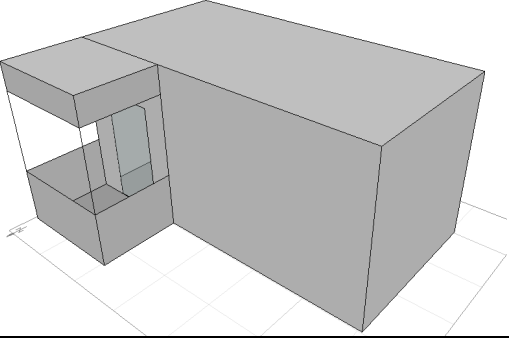
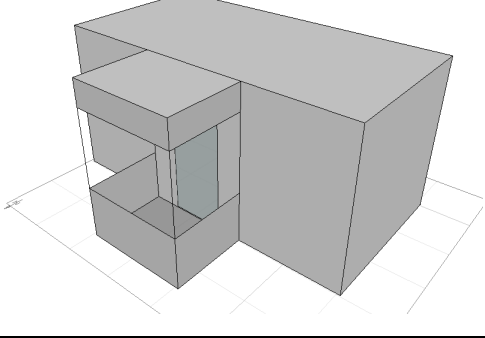
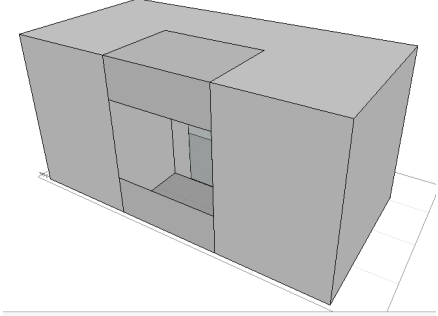
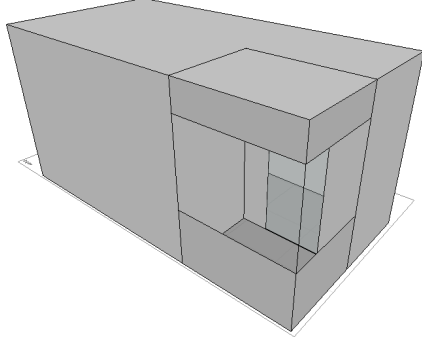
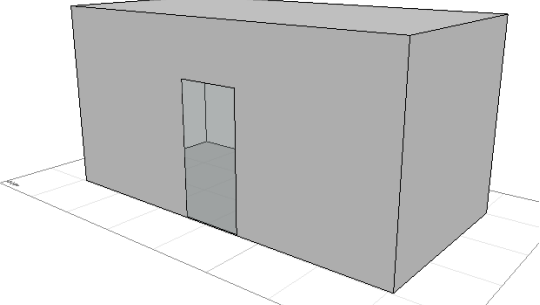
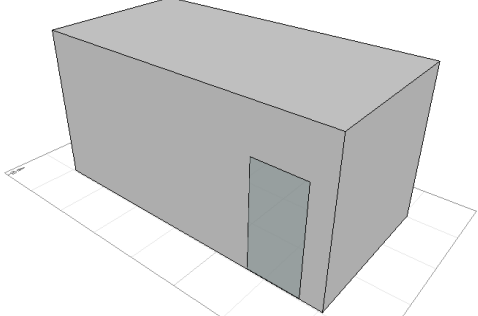
**Appendices:**

Table A- 1: The parametric variation

Cases	Bal_ratio	Bal_pos	Solar heat gain	Faç_orien	Cooling_demand
1.	0.16	Left	DG 0.75	east	73,92
2.	0.16	Centre	SG 0.94	north	83,24
3.	0.2	Left	DG 0.75	east	85,09
4.	0.16	Centre	DG HE 0.45	west	69,26
5.	0.2	Right	SG 0.94	west	102,48
6.	No balcony	Centre	DG 0.65	north	80,11
7.	No balcony	Right	DG HE 0.45	south	79,72
8.	No balcony	Right	SG 0.94	south	104,03
9.	0.2	Left	SG 0.94	west	108,24
10.	0.16	Right	DG 0.75	east	74,87
11.	0.2	Right	DG HE 0.45	west	76,68
12.	0.16	Centre	DG HE 0.45	north	66,52
13.	No balcony	Right	DG HE 0.45	east	83,25
14.	No balcony	Left	DG 0.65	east	83,64
15.	No balcony	Centre	DG HE 0.45	east	83,25
16.	No balcony	Centre	SG 0.94	north	100,10
17.	No balcony	Centre	DG 0.65	east	83,64
18.	0.5	Right	DG 0.65	north	55,77
19.	0.16	Right	DG 0.65	south	68,80
20.	0.16	Left	DG HE 0.45	east	70,56
21.	0.2	Right	DG 0.75	south	78,73
22.	0.16	Centre	SG 0.94	west	92,00
23.	0.16	Right	DG 0.75	south	72,03
24.	0.2	Left	DG 0.75	north	83,05
25.	0.5	Left	DG HE 0.45	south	66,60
26.	0.5	Left	DG 0.75	east	68,25
27.	0.2	Right	DG HE 0.45	south	74,63
28.	0.16	Left	DG 0.75	west	72,69
29.	0.5	Left	DG HE 0.45	west	62,37
30.	0.16	Centre	DG 0.65	north	70,15
31.	0.2	Left	DG 0.75	south	81,88
32.	No balcony	Centre	DG HE 0.45	north	78,57
33.	0.16	Left	DG HE 0.45	north	66,52
34.	0.2	Centre	DG 0.65	north	67,99
35.	0.2	Centre	DG 0.75	south	71,48
36.	0.16	Left	DG HE 0.45	west	69,26
37.	0.2	Centre	DG 0.75	west	73,53
38.	0.16	Left	SG 0.94	east	95,68
39.	0.2	Right	DG HE 0.45	north	73,50
40.	0.16	Centre	SG 0.94	east	95,67
41.	0.2	Left	SG 0.94	west	108,24
42.	0.16	Left	DG HE 0.45	south	67,52
43.	No balcony	Left	DG 0.65	north	80,11
44.	0.16	Right	DG 0.65	north	67,81

45.	0.2	Right	SG 0.94	west	102,48
46.	0.16	Centre	DG HE 0.45	east	70,55
47.	No balcony	Left	DG HE 0.45	south	79,73
48.	No balcony	Left	DG 0.75	south	83,77
49.	0.2	Left	DG 0.65	south	79,79
50.	0	Centre	DG 0.65	west	82,52
51.	0.5	Right	DG 0.75	north	55,79
52.	0.2	Left	DG 0.75	west	85,86
53.	0.16	Centre	DG 0.75	north	70,02
54.	0.2	Right	DG 0.75	south	78,73
55.	No balcony	Centre	DG 0.75	west	85,72
56.	No balcony	Right	DG 0.75	west	85,72
57.	0.2	Left	DG 0.65	east	82,24
58.	No balcony	Centre	DG 0.65	south	80,98
59.	0.2	Right	DG 0.75	east	82,05
60.	0.16	Centre	DG 0.65	south	68,82
61.	No balcony	Right	SG 0.94	west	110,31
62.	0.2	Right	DG 0.75	north	77,63
63.	No balcony	Right	DG 0.65	north	80,11
64.	0.2	Right	SG 0.94	west	102,48
65.	0.16	Right	SG 0.94	north	83,23
66.	0.16	Right	DG 0.75	east	74,87
67.	No balcony	Left	SG 0.94	north	100,10
68.	0.2	Right	DG 0.75	east	82,08
69.	0.5	Left	DG 0.65	west	64,38
70.	0.5	Right	DG 0.65	west	55,84
71.	0.5	Right	DG HE 0.45	south	55,71
72.	No balcony	Centre	DG HE 0.45	south	79,73
73.	No balcony	Left	DG 0.75	north	82,64
74.	0.16	Centre	DG 0.75	west	72,69
75.	No balcony	Right	SG 0.94	east	114,59
76.	No balcony	Centre	SG 0.94	east	114,59
77.	0.2	Left	SG 0.94	south	95,44
78.	0.2	Right	DG 0.65	west	77,80
79.	0.16	Right	DG HE 0.45	west	69,91
80.	0.16	Left	DG 0.65	north	68,08
81.	0.2	Left	SG 0.94	west	108,24
82.	0.5	Right	DG 0.65	south	55,68
83.	0.16	Left	DG 0.75	west	72,69
84.	0.2	Left	DG 0.75	north	70,02
85.	0.16	Centre	DG HE 0.45	north	66,52

Table A- 2: Geometry of some modelled cases (the thickness of the overhang was not considered)

<b>Overhanging balconies with 0.16 balcony to room ratio</b>	
	
Left position and north orientation	Central position and north orientation
<b>Hollowed-out balconies with 0.2 balcony to room ratio</b>	
	
Central position and west orientation	Right position and west orientation
<b>No balcony</b>	
	
Central position and East orientation	Central position and south orientation

## Use of Biopolymers in the Stabilization of Clay Soils

Idoui Imane<sup>1</sup>, Rehab Bekkouche Souhila<sup>2</sup>, Benzaid Riad<sup>3</sup>, Berdi Inas<sup>4</sup>

<sup>1, 3, 4</sup> Geological Engineering Laboratory (LGG), Jijel University, Algeria.

<sup>2</sup> Civil Engineering Department, LMGHU Laboratory, Skikda University, Algeria.  
e-mail: solrehab@yahoo.fr

### Abstract

The treatment and stabilization of soils make it possible to recycle materials on construction sites in preparation for the installation of a final covering or the construction of a road network. In road geotechnics, various materials such as lime, cement, and pozzolans were used as additions to stabilize clay soils. In recent years, biopolymers and bacteria are of increasing interest to researchers in the field of stabilization and improvement of the physico-mechanical and chemical characteristics of clay soils. Currently, in place of traditional clay treatment techniques and to minimize environmental problems, natural fibrous waste is being used increasingly and spectacularly. Several studies on biotechnological engineering applications already exist, such as the use of vegetation, algae, bacteria, enzymes, and biopolymers. The northern Algerian region where the urban tissue does not stop expanding contains significant potential in terms of wheat straw, which represents a very present agricultural waste. So, there is a local interest in the sustainable development of several regions known to produce wheat. This study is interested in investigating the effect of wheat straw on the stabilization of swelling clay soil. In order to improve the physico-mechanical characteristics of clay soils, a series of laboratory tests (Atterberg limit, Proctor test, direct shear test, Oedometer test, and unconfined compressive strength test) were carried out on reconstituted clay soil with defined initial properties through numerous analyses (e.g., XRD and XRF) and then treated with different vegetable fiber content. The results indicate that there is an improvement in the compressibility characteristics of the treated soil, a remarkable decrease in the swelling index and the compressibility index respectively with increasing percentages of wheat straw.

**Keywords:** biopolymer, soil improvement, treatment, clay, wheat straw.

## 1 Introduction

Jijel province in northern Algeria knows a significant expansion of urban fabric due to the demographic growth in the last years (103.6 habitants per km<sup>2</sup>) [1]. This expansion stretches and extends over virgin terrains in the vicinity of the major cities. As the geology of Jijel and its climatology know a serious complexity, the targeted terrains are mainly argillaceous terrains that often show lower geotechnical characteristics like consistency limits, particle size, compaction, consolidation, permeability, and shear strength and their interactions [2]. These characteristics differ over the different regions of the province. Subsequently, the

construction sites and urban infrastructures face numerous engineering and geotechnical problems (settlement, collapse, and land-sliding). Soil stabilization is the ultimate solution to improve the geotechnical properties of these soils, where numerous technics are being employed like using lime and cement to the soils [3, 4] which offer practical and economical solutions, other researchers have studied the influence of the addition of polymers on the improvement of the geotechnical properties of clays, they have confirmed the favorable effect of these materials [5- 8].

Even though these traditional technics are efficient in strengthening the soils and bettering their technical properties, serious environmental problems are encountered, especially ecological ones like greenhouse gases emission, pollutant leakage to groundwaters, recycling of concrete and cements wastes, plus their expansive costs [9]. [10] Have studied the immediate and long-term effects of lime and wheat straw on consistency characteristics of clayey soil, the study has shown that the shrinkage and swelling of clayey soils may adequately be managed through mixing an appropriate amount of lime and wheat straw as soil stabilizing agents for both immediate and long-term effects. The current study deals with soil stabilization using eco-friendly biopolymer "Wheat Straw". The use of this biopolymer in soil stabilization is not brand new, where it has been used in the last years in different countries China [11], India [12, 13], and Algeria [14]. In conjunction with plentiful biopolymers, mainly extracted from vegetable fibers such as rice husk [15, 16], fiber jute [17], bagasse fiber [18], coconut fiber [19], sisal fiber [20], and wheat husk [21]. These materials showed decent improvement on the characteristics of the treated soil [22], principally in shear resistance, dry density, and plasticity parameters. Yet, the use of these materials in the Jijel area is still limited or not even used. Also, the actual knowledge about their efficiency and the exact impact of using them on these soils' characterization is not well constrained. Hence, we offer in the actual work a detailed study on the impact of using Wheat Straw in enhancing geotechnical properties of a reconstituted soil from the Herraten region, in Jijel province. The idea of using a reconstituted soil in this study is to obtain a swelling soil with well-defined properties that can be used further as a reference, then to see the effect of wheat straw on its geotechnical properties.

## 2 Data and Methodology

Cost The studied soil was extracted from a potential construction site in the new city of Herraten, nearby Jijel town in northern Algeria (Figure 1A). The studied area and generally Jijel region are characterized by a humid climate, significant precipitation, and an important hydrographic network. The geological studies indicate that the studied area is located in the Jijel basin. This basin is mainly filled by Neogene and quaternary sedimentary deposits. Herraten is situated on the Hill of Herraten where the outcrops are basically post-nappes deposits (Figure 1.B). These deposits are identified as blue grayish clays with mediocre geotechnical properties. The technics used so far in the studied area to enhance these parameters are the aforementioned classic techniques (lime and cement).

### 2.1. Soil

The soil samples were taken from approximately 3.5 to 4m of depth. The initial properties and

measurements of the raw soil were taken in the first place, then, it was mixed with the Bentonite powder, a commercial product with clayey characteristics that will boost the swelling properties in order to fit with study purposes. The resulting reconstituted soil will be the initial sample of the work that will receive additives, or as referred to soil 0% in all further analysis, tests, and experiences in this study. Using reconstituted soil is also crucial in eliminating the inconsistency of specimens during the tests and ensuring the repeatability and sufficient samples with exact known parameters [23]. These factors are imperative for any comparative studies with additive content [24].

The bentonite used comes from the M'sila Sidi-Ali region, Mostaganem province. It was provided by BENTAL Company. The detailed geotechnical properties of the raw soil, bentonite powder, and the resulting reconstituted soil are described below.

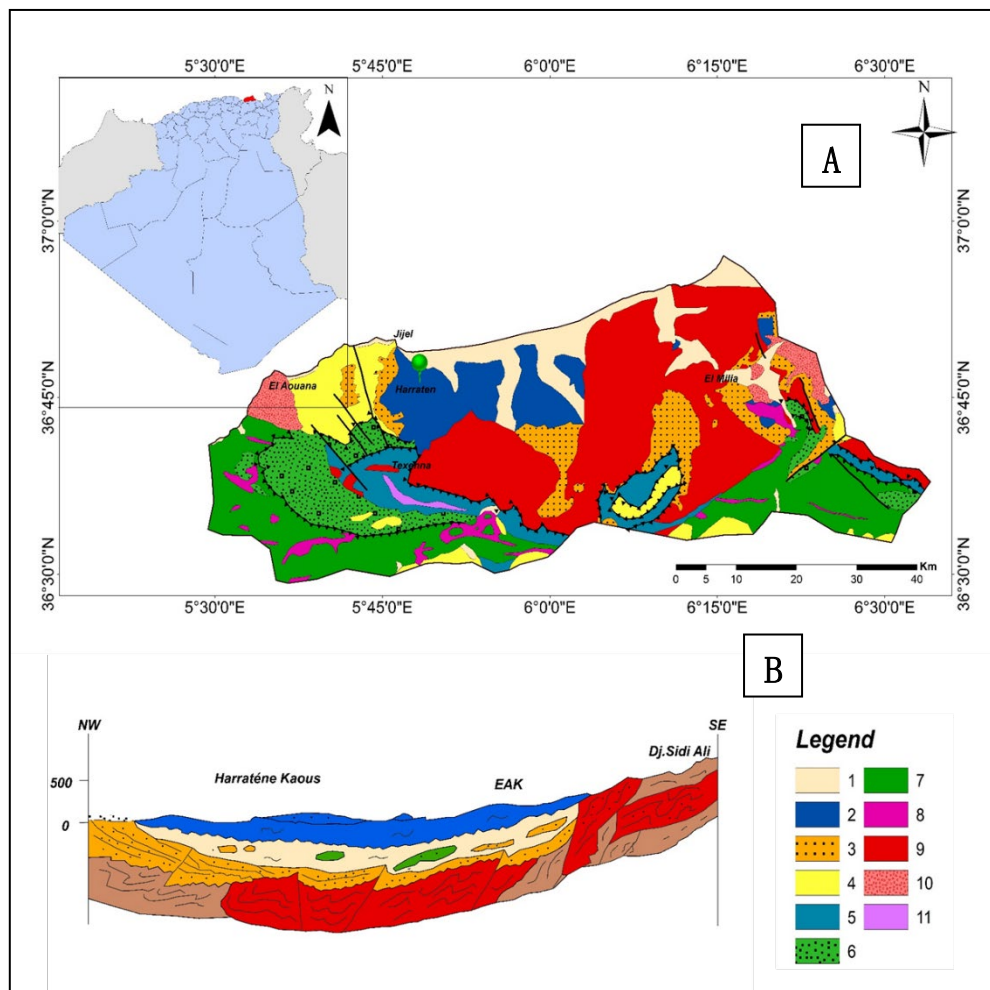


Figure 1: Simplified geological map of the Jijel region and the localization of the study area.

Legend: 1. Quaternary 2. Postnappe 3. Oligo Miocène Kabyle 4. Numidian series 5. Tellian 6. Massylien flysch 7. Mauritanien Flysch 8. Triassic Rocks 9. kabyle basement 10. Magmatic rocks 11. Volcano sedimentary unit [25]

### 2.1.1. Natural Soil characterization

Even there were previous studies that dealt with soil samples from the region of Herraten, different chemical, mechanical and physical measurements, and analyses were carried out on the natural soil samples to define its exact characteristics. The most important parameters of the soil are resumed below. Table 1 displays the physical properties of the soil where the dry density, optimum moisture content, Atterberg limits, and the blue methylene value were calculated. These measurements indicate that the soil has low plasticity and low swelling properties. The results of the chemical analysis (XRF) are shown in Table 4.

Table1: Physical Properties of the natural soil

Maximum dry density(t/m <sup>3</sup> )	Water content (%)	Liquid limit (%)	Plastic limit (%)	Plastic index (%)	Methylene Blue
1.75	16.14	45.63	20.36	20.27	3.8

Figure 2 shows the grain size distribution of the studied soil. 98% of the soil grains have less than 100µm in diameter and 65% of the grain are smaller than 10µm. After the GTR classification, the soil is considered as clay soil Class A2.

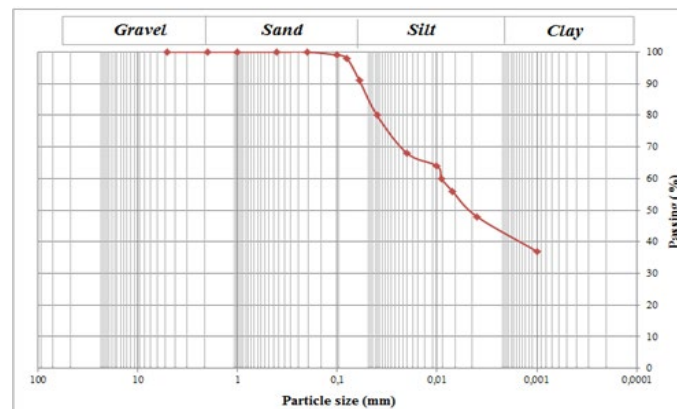


Figure 2: Grain size distribution of base soil

### 2.1.2. Bentonite

The Bentonite powder is a commercial product derived from a sedimentary rock that has the same name and is mainly used in the ceramic industry. It is characterized by high adsorption properties and ionic exchange. As mentioned before, it is employed in the ongoing study to augment the swelling properties of the soil. Table 4 shows the results of the chemical analysis (XRF) of bentonite which are related to its mineralogical origin. These chemical properties show that bentonite is composed of a high percentage of SiO<sub>2</sub>, Al<sub>2</sub>O<sub>3</sub> and CaO. the value of the SiO<sub>2</sub> / Al<sub>2</sub>O<sub>3</sub> ratio is 4.53. This value is the index of a montmorillonite [26]. The bentonite is classified in the calcic type given the preponderance of the percentage of calcium over sodium [27]. Table 2 shows the initial physical properties of the bentonite which are critical in constraining the reconstituted soil parameters in further steps of this study.



Table 2: Physical properties of the bentonite

Maximum dry density( $t/m^3$ )	Water content (%)	Liquid limit (%)	Plastic limit (%)	Plastic index (%)	Methylene Blue
1.75	16.14	175	30	145	25.21

### 2.1.3. Reconstituted soil

The soil 0% adopted in our study is a mixture of 60% natural soil and 40% bentonite (Figure 3) [6, 27]. Enhance mineralogical analyzes on the reconstructed soil were carried out by X-ray diffraction (XRD). The obtained detailed mineralogical composition of the reference soil and which has a direct influence on the geotechnical characteristics of the soil mainly the porosity, permeability, and swelling is displayed in Figure 4. As this soil is continued by the mixture of the two given components, it's mainly constituted by tectosilicates, phyllosilicates, inosilicates, and carbonates.

The diffractogram (XRD) presented in Figure 4, presents characteristic peaks that correspond to crystalline phases formed mainly by Quartz, calcite, and Montmorillonite. Other minerals also are present but minor. The chemical analysis on the reconstituted soil was performed by an X-ray fluorescence spectrometer (XRF).

The results of this analysis are shown also in Table 4. And reveal the abundance of silica  $SiO_2$ , aluminum oxide  $Al_2O_3$  and calcium oxide  $CaO$  with almost 55%, 14,3%, and 17,4% respectively; The  $K_2O$ ,  $MgO$ ,  $Na_2$ , and  $TiO$  are present in form of traces. The geotechnical characteristics of the reference soil are resumed in Table 3.



Figure 3: a) Natural soil; b) Bentonite; c) Reconstituted soil (60% natural soil +40% bentonite); d) Wheat straw

Table 3: Geotechnical properties of reconstituted soil (60 % Natural soil + 40% Bentonite)

Physical and chemical characteristics	Values
Liquid limit $LL$ (%)	68.72
Plastic limit $PL$ (%)	25.3
Plasticity Index $IP$ (%)	43.42
Optimum water content $W_{opt}$ (%)	23.12
Maximum dry density $\gamma_{dmax}$ ( $t/m^3$ )	1.64
Cohesion $C$ (kPa)	0.28
Internal friction angle $\varphi$ ( $^\circ$ )	4
Methylene blue value	8.33

Table 4: Chemical composition of Bentonite, Natural soil, Reconstituted soil, and Wheat straw. X-Ray Fluorescence results

	SiO <sub>2</sub>	CaO	Al <sub>2</sub> O <sub>3</sub>	Fe <sub>2</sub> O <sub>3</sub>	K <sub>2</sub> O	MgO	Na <sub>2</sub> O	TiO	Cl	SO <sub>3</sub>	P <sub>2</sub> O <sub>5</sub>
Natural Soil	47.2	25.4	14.1	6.8	2.37	1.95	0.339	0.59	/	0.119	0.276
Reconstituted soil	55	17.4	14.3	5.44	2.54	2.36	1.43	1.06	/	0.215	0.225
wheat straw	34.8	19.8	8.15	8.42	10.4	1.46	4.08	0.92	5.66	3.99	1.74
Bentonite	65.8	6.36	14.5	3.5	2.65	2.87	3.04	0.34	0.14	0.47	/

## 2.2. Wheat straw (WS)

Wheat straw is a natural biopolymer with the ion-exchange property. Wheat straw, a by-product obtained after harvesting wheat grains, with an annual world global production of 529 million tons [28]. The composition of these residues contains about 32.7% of cellulose and 24.5% of hemicelluloses [29]. Cellulose fibrils and lignin confer mechanical strength properties [30]. WS is an abundant and eco-friendly material.

In the current study, the wheat straw used for soil treatment is obtained from agricultural wheat fields from Mila province in Algeria. Before using it in further steps, the wheat straw was subjected to initial pretreatment: first, it was air-dried to remove moisture, then was carefully sieved using a 5mm caliber sieve. The diameter of the resulting straws ranges from (0.5 to 5 mm) and have a length of (10 mm to 50 mm), Figure 3. Properties of wheat straw of the reference soil are resumed in Table 5.

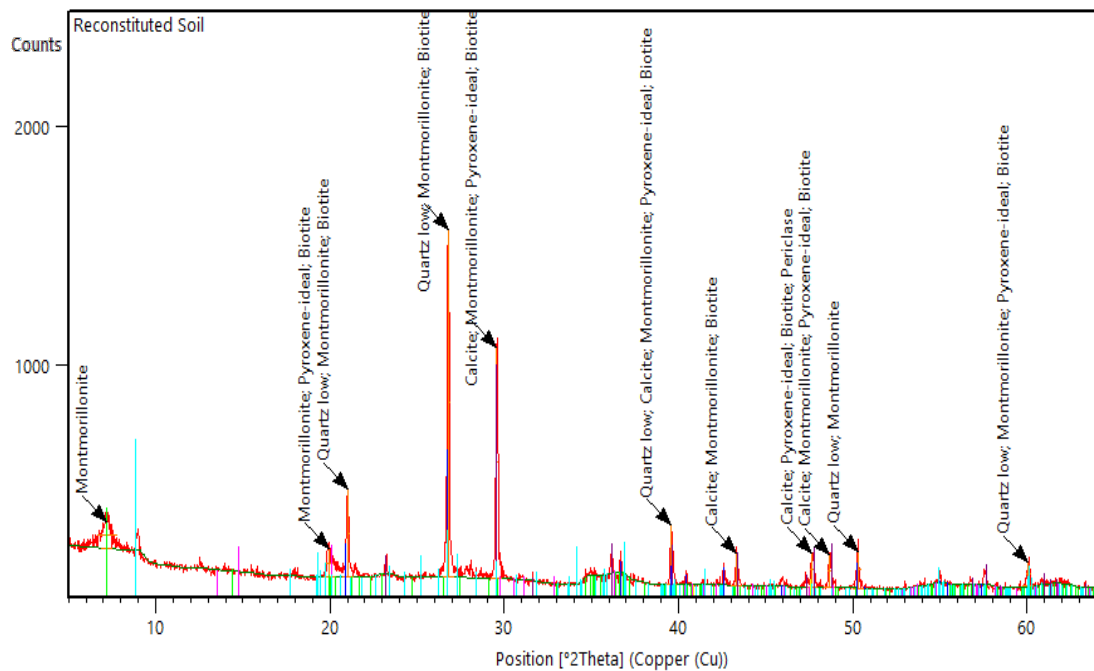


Figure 4: X-ray diffraction pattern of reconstituted soil for mineralogical composition

Table 5: Properties of wheat straw

Color	pH	Specific gravity $G_s$
Straw yellow	7.7	0.19

Once we have reconstituted the soil with the desirable geotechnical characteristics, four pretreated WS proportions were added. These proportions are 1%, 3%, 6%, and 9% relative to the weight of the used soil.

### 2.3. Test procedure

To evaluate and determine the influence of wheat straw on the physic mechanical properties of the mixture (Reconstituted soil - wheat straw), we performed an experimental program on both untreated and wheat straw treated samples. This program includes the determination of the specific gravity ( $G_s$ ), the effect of WS on the pH, plasticity tests to evaluate the Atterberg limits, Proctor analysis, direct shear test, the unconfined compression strength analysis to determine resistance (UCS). Finally, two different types of tests to determine the swelling: the odometer test and free swelling index.

Table 6: Engineering test with standard code

Name of the test	Description of the test	Test code
specific gravity ( $G_s$ )	ratio of the weight of a given volume of the material to the weight of an equal volume of distilled water, using water pycnometer method determine the specific gravity of a soil composed of particles.	BS 1377-2 (1990)
pH analysis	Evaluate the impact of wheat straw on the pH of the soil.	NF ISO 10390-1994
Atterberg limits	determine soil liquid limit, plastic limit and plasticity index in compliance with the conditions stipulated in the standard test methods	NF P94-052-1
Proctor standard compaction test	Determine the maximum dry density (MDD) and the optimum moisture content (OMC).	NF P94-093
Direct shear strength	Study the influence of the treatment of wheat straw on the resistance parameters using the casagrande box using the wet mix method (under consolidated drained conditions).	NF P94-071-1
Free swelling index test (FSI)	Determine the free-soil swelling index. Free swell is the raise in the volume of a soil when immersed or soaked in water or other solvent, without any external constraint.	with IS 2720 (Part-40)-1977
Unconfined compressive strength	A compression test is carried out to determine the compressive strength of treated and untreated soil. The test pieces were assayed in varying proportions wheat straw and crushed	NF P94 -077

### 3 Results and discussion

#### 3.1 Effect of wheat straw on the specific gravity

Table 7 presents the measured specific gravity of solid grains ( $G_s$ ) of the used materials. The first  $G_s$  value (WS) represents the specific gravity of the wheat straw only, whereas the second value (0%) represents the specific gravity of the untreated soil. The remaining values represent the value of the specific gravity of each treated soil sample.

Table 7: Variations of the specific gravity of soil with the addition of the WS

WS content (%)	WS	0%	1%	3%	6%	9%
Specific gravity ( $G_s$ )	0.19	2.31	2.14	1.64	2.29	2.31

The behavior of the specific gravity of the soil can be described as follow; first, with adding 1% of WS the  $G_s$  decreased significantly compared to its initial value of 2.31 (untreated soil). This behavior was also observed when adding 3% of WS. A gentle decrease of the  $G_s$  is observed on the soil treated with 6% of WS. The value of the  $G_s$  remains unchangeable with the addition of 9% of WS.

Note that 3% marks the decreasing threshold of  $G_s$  that may be due to the fact that WS replaces a large part of the voids in the soil, thus making the soil much denser. Previous studies have reported a decrease in the specific gravity of the soil depending on the addition of wheat straw [10].

### 3.2 Effect of wheat straw on soil pH meters

The variation of the pH value in function of the proportions of added wheat straw is illustrated in Table 8. An additional proportion of WS 12% was used to confirm the obtained threshold in this test.

Table 8: The effect of wheat straw content on pH value of soil

pH value	0%	1%	3%	6%	9%	12%
Additive content (%)	10.33	10.22	9.98	9.60	9.59	9.59

The value from the table shows that when Wheat Straw is applied to the soil with a 1, 3, and 6%, ratio, the pH reached 10.22, 9.98, and 9.60 respectively while no change in the pH value was observed when using 9% or more of the WS.

The slight decrease in the pH value of the treated soil is probably due to the mineralogical composition of the soil used. The optimum wheat straw content corresponds to a pH value of 9.59 at which the amount of WS added is sufficient for chemical reactions to take place.

### 3.3 Effect of adding Wheat straw on Atterberg limits

We performed Atterberg limit tests on soil treated with different percentages of wheat straw (WS). The obtained results are summarized in the following Table:

Table 9: Atterberg limits test results

WS content (%)	Atterberg limits		
	Liquid limit (%)	Plastic limit (%)	Plasticity Index (%)
0%	76.86	22.66	54.2
1%	89.58	40.48	49.10
3%	91.36	42.71	48.65
6%	89.42	43.96	45.46
9%	87.09	49.2	37.89

In the beginning, we observed an increase in the liquidity limits until the addition of 3% of wheat straw, followed by a decrease beyond this percentage (Table 9).

Table 7 shows a decrease in the plasticity index value has decreased from 54.2% to 37.89% with 9% WS additive.

Adding the powder to the clay soil causes the Atterberg limit values to change slightly. The results indicate that as the percentage of wheat straw increases, the liquidity limit ( $LL$ ) and plasticity limit ( $PL$ ) also increase, however, the plasticity index ( $PI$ ) decreases.

The increase in the liquidity limits is due to the reaction of the wheat straw with clay particles. The decrease in the plasticity index indicates an improvement in the workability of the soil, these results are similar to those found in the literature [12, 13].

### 3.4 Effect of wheat straw on Compaction Characteristics

The results of the compaction test of the treated soils in comparison with reference soil are shown in Figure 5, They show an increase in the optimal moisture content (OMD) of the soil from 16% to 20% parallelly to the decrease of the maximum dry density (MDD) from 1.65 to 1.32 g/cm<sup>3</sup>, depending on the increasing proportions of the added wheat straw (0% to 6%). The behavior of the soils treated with 9% is different from the other treated soils, where the OMD remains stable compared to the non-treated soil, the dry density goes down to 1.29 g/cm<sup>3</sup>.

These results indicate that the optimum of the proctor curve of the treated soils shifts right and downward compared to the optimum of the reference soil (Figure 5) for the soils treated with 1% to 6%. Whereas the optimum of the soil treated with 9% shifts only downward compared to the curve of reference.

The rise in moisture content is explained as the amount of water required to moisten the added WS's that is characterized by a wide surface area and its ability to absorb water. On the other hand, the use of wheat straw leads to a reduction in dry density progressively. This reduction indicates that the soil is less compacted, in other words, it contains more voids. This variation is of course due to the low density of the wheat straw compared to the soil.

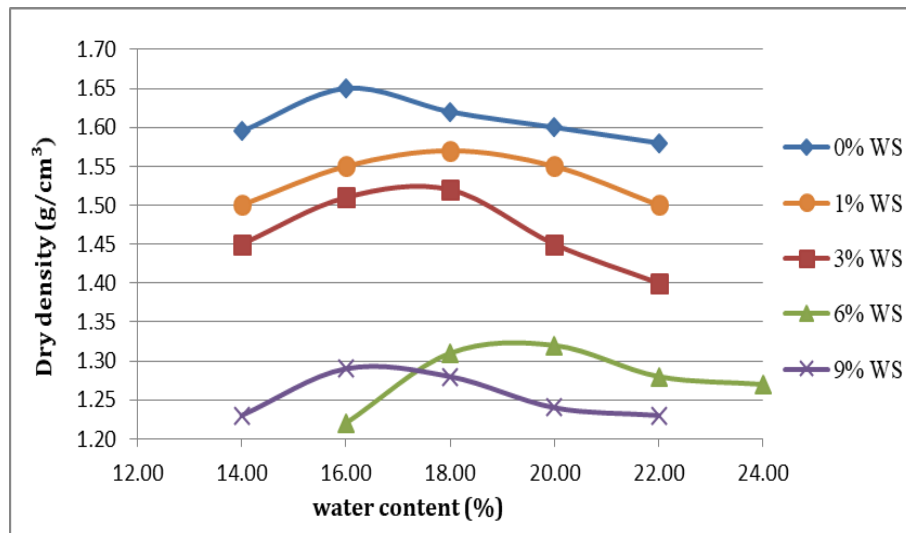


Figure 5: Compaction curves of soil with different percentages of wheat straw

These effects on the maximum dry unit weight are similar to that on the specific gravity of the wheat straw stabilized soil and could have resulted from the variation of the specific gravity of the stabilized soil with the wheat straw content, these results are confirmed by those found in previous studies [12].

### 3.5 Effect of wheat straw on Shear Strength Parameters (Direct Shear Test)

The shear strength tests of the untreated soil and treated soil with different percentages of wheat straw were performed as per NF P 94-071-1. The results of the influence of the different percentages of wheat straw on the cohesion and the friction angle are shown in Table 10.

In general words, we note that the increase in the concentration of wheat straw leads to a higher friction angle ( $\phi$ ) and a decrease in cohesion ( $C$ ). According to Table 10 below, the friction angle varied from  $6^\circ$  to  $16.17^\circ$  for an addition ranging from 1% to 9% meanwhile the initial friction angle of the untreated soils was  $4^\circ$ . A higher value of the cohesion was observed on the results of the soil treated with 1% in comparison to the untreated soil. This increase was followed by a progressive decrease from 0.36 bar to 0.04 bar upon the percentages of the added wheat straw.

Table 10: Friction angles and cohesion of wheat straw-treated clay

Wheat straw concentration (%)	Cohesion $C$ (bars)	Friction angle $\phi$ ( $^\circ$ )
0	0.3	4
1	0.36	6
3	0.2	8
6	0.17	10.75
9	0.04	16.17

From the results of the tests, it can be concluded that the shear characteristics after the addition of different proportions of straw were improved considerably compared to the untreated soil. The improvement is explained by the resulting composition of the granular matrix of the treated soil which gives it a solid character.

### 3.6 Effect of wheat straw on soil compressibility

The compressibility tests of the untreated soil and treated soil with different percentages of wheat straw were performed as per NF P94- 068.

Figure 6, Figure 7, and Figure 8 show the results of the effect of wheat straw on the variation of the soil compressibility for different percentages of wheat straw fiber. The results include the consolidation pressure index, the coefficient of compressibility, and swelling.

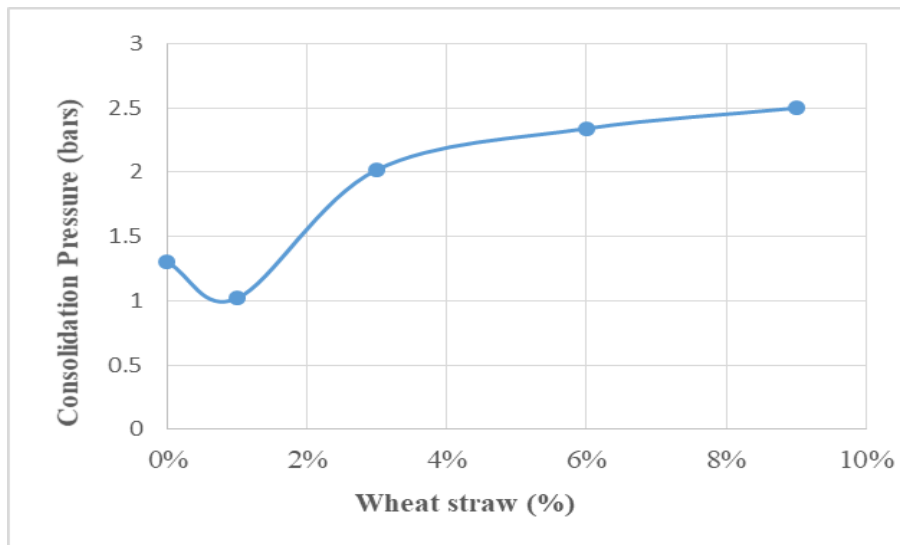


Figure 6: Consolidation Pressure Variation as a function of % wheat straw

The compressibility index as a function of the percentage of wheat straw presents a disproportional behavior where it decreases in response to the increase of the WS. It is worthy to mention that the decreasing was more important with the adding of 1% till 3%, after that, only a gentle decrease is observed.

The swelling index curve displays a different behavior from the previous one. When adding 1% almost no change is observed. Then it is followed by a significant decrease of the SC from 12 to almost 6% with the adding of 3%. The addition of 6% of WS seems doesn't have a significant effect where no change of the SC is observed, however, the addition of 9% is marked by another significant decrease of the SC down to 4%.

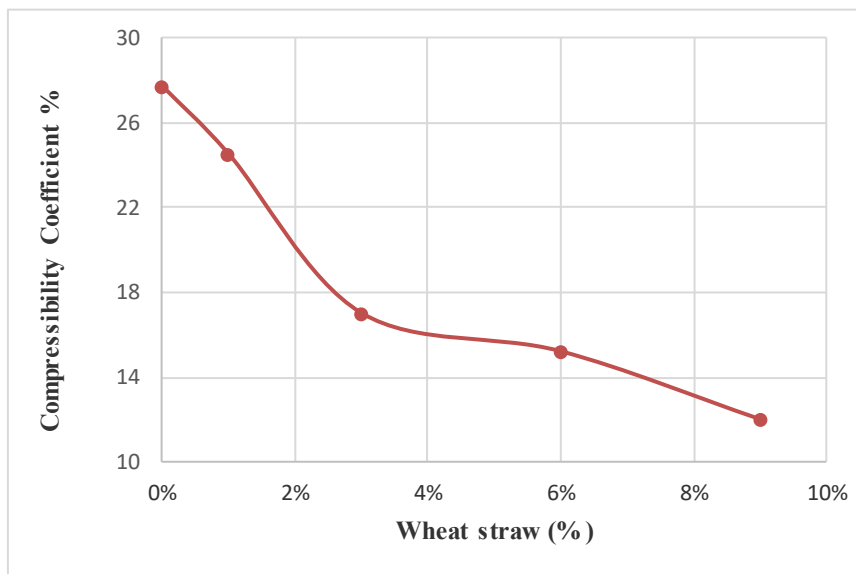


Figure 7: Compressibility Coefficient Variation as a function of % wheat straw



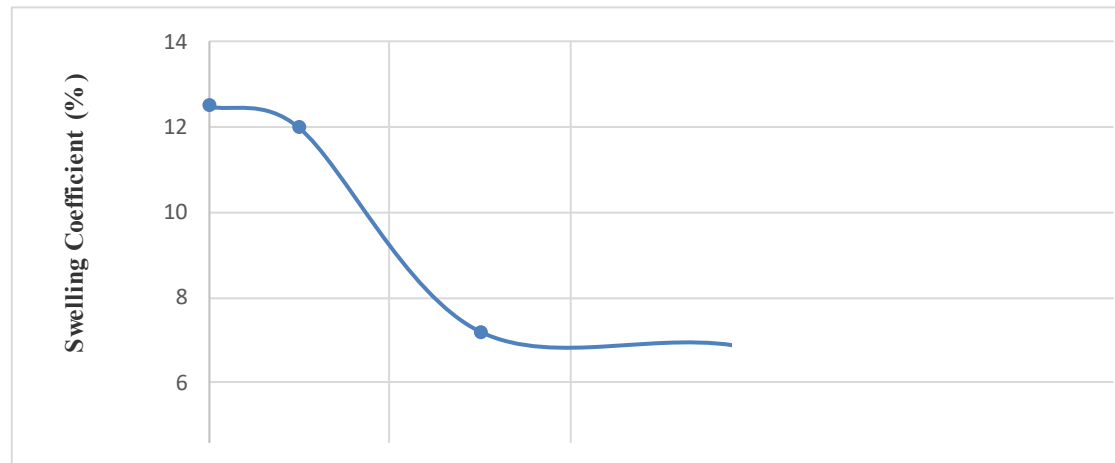


Figure 8: Swelling Coefficient Variation as a function of % wheat straw

We note that the consolidation pressure decreases until the addition of 1% wheat straw, once exceeding this proportion, the consolidation pressure increases in function of the adding proportions where the soil seems to reach the threshold of 9%.

We found that there is an improvement in the compressibility characteristics of the treated soil, a remarkable decrease in the swelling, and the compressibility indexes respectively with increasing percentages of wheat straw.

The decrease in the compressibility index is probably due to the decrease in porosity of the soil and subsequently the decrease in permeability. The reduction in permeability prevents water from flowing inside the soil, thus reducing the efficiency of the dissolution of biopolymer particles (wheat straw) inside the treated samples. This effect was described in numerous studies [31].

### 3.7 Effect of wheat straw on the free swelling index test (FSI)

The free swelling index (FSI) of the clay treated with the addition of 1, 3, 6, and 9% are shown in Table 11.

Table 11: Effect of WS on Free Swell Index behavior of soil

Additive content (%)	0%	1%	3%	6%	9%
Value FSI (%)	86	33.33	27.27	23.07	15.78

From Table 11, it can be concluded that increasing the percentage of WS in soil from 0% to 9%, led to a significant reduction of FSI. When the WS content reached 9%, the value of the Free Swell Index was reduced from 86% to 15.78%. The decrease in the FSI values can be reached even with small percentages of WS as is proved in the results of the test using 1%.

It can be concluded that even with a very low rate of wheat straw, the value of FSI can considerably reduce this reduction indicates that the addition of WSB reduces the swelling of the clay soil.

### 3.8 Effect of wheat straw on the unconfined compressive strength (UCS) test

The test pieces were assayed in varying proportions wheat straw and crushed after 24 hours (Figure 9).

Figure 10 shows the variation in stress-strain of the samples of the untreated reconstituted soil and the reconstituted soil treated with different content of wheat straw after 24 hours of curing.

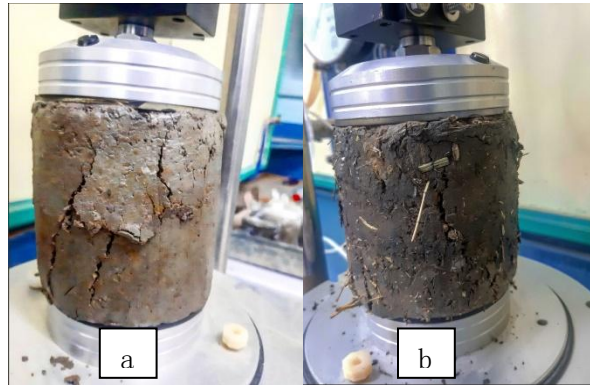


Figure 9: Specimen deformation: (a) untreated soils, and (b) Soil stabilized with 6 % WS

The plot displays the results of the axial stress and the rupture threshold in the function of the axial strain (deformation). A clear differential behavior is observed on the curves of the different proportions with almost a linear proportional aspect. Both the duration and resistance to the compression are expanded parallelly to the adding of the WS. The untreated soil needed only 200 kPa to reach the rupture point whereas the 9% of soil required almost 500 kPa to reach the rupture threshold.

Figure 11 shows the variation of wheat straw on the unconfined compressive strength (UCS) of soil reconstituted alone and treated with different proportions of WS. The value of the unconfined compressive strength increased significantly from 197.95 kN/m<sup>2</sup> at 0% addition to 494.51 kN/m<sup>2</sup> at 9% wheat straw. It is clear that if we increase the wheat straw content the peak of the value of the UCS increases.

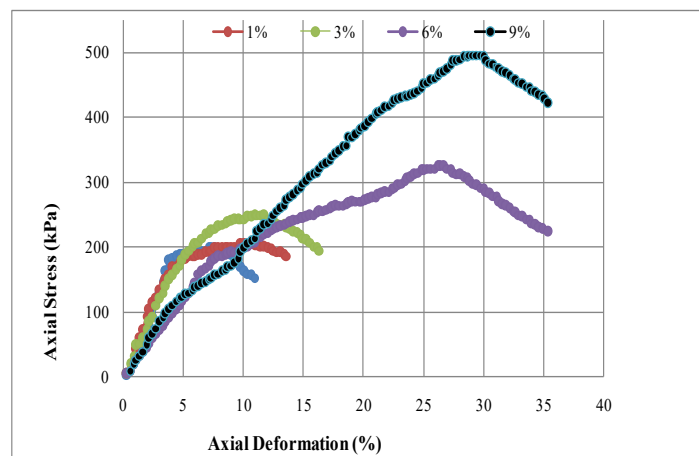


Figure 10: Stress - strain curves for Stress - strain curves for specimens containing different amounts of

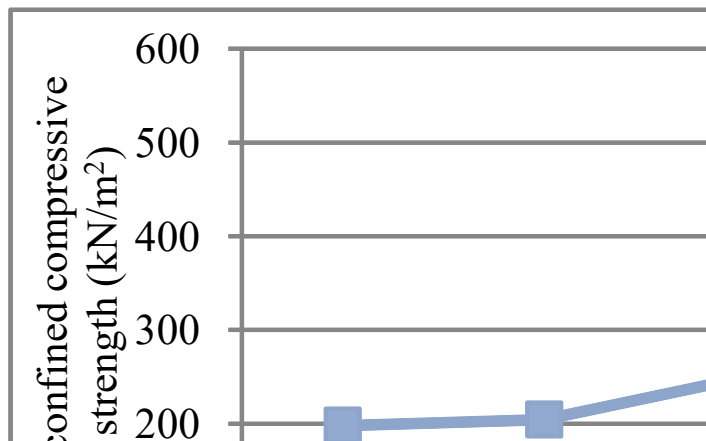


Figure 11: Influence of wheat straw on the unconfined compressive strength

This increase in compressive strength is attributed to the reaction of wheat straw with clay soil particles which results in the formation of a straw binder that enhances the cohesivity of the soil particles, these results are confirmed by those found in previous studies [12, 22].

#### 4 Conclusions

Clay soil changes volume depending on its humidity. It swells with moisture and tightens with drought, causing vertical and horizontal piles and cracking of the soil. The present work was carried out in order to improve the geotechnical characteristics of a reconstituted soil (Soil-bentonite) from the Harraten region in the Jijel province using eco-friendly biopolymer “wheat straw”. Different proportions of wheat straw; 1%, 3%, 6%, and 9% were used to depict the behavior of the soil in the function of these added materials. In the light of this study, numerous tests were performed (specific gravity, Atterberg Limits, Proctor standard compaction, Unconfident compressive strength, free swelling index, Direct Shear Test, and odometer test). According to the obtained results, significant changes in the physico-mechanical parameters were observed by the addition of wheat straw, these changes are related to the quantity of the WS. The information that can be derived from these results can be resumed as follow:

- In function, if its specific gravity, the soil became much denser by the adding of WS where it replaces a large part of the voids in the soil. Where the 3% marks the decreasing threshold of  $G_s$ .
- The optimum wheat straw content corresponds to a pH value of 9.59 at which the amount of WS added is sufficient for chemical reactions to take place.
- Adding the powder to the clayey soil caused a slight change in the Atterberg limit values. The results indicate that as the percentage of wheat straw increases, the liquidity limit ( $LL$ ) and plasticity limit ( $PL$ ) also increase, meanwhile the plasticity index ( $PI$ ) decreases.
- The results of the compaction test of the treated soils in comparison with reference soil

show an increase in the optimal moisture content (OMD) of the soil from 16% to 20% parallelly to the decrease of the maximum dry density (MDD) from 1.65 to 1.32 g/cm<sup>3</sup>.

- In general words, we note that the increase in the concentration of wheat straw leads to a higher friction angle ( $\varphi$ ) and a decrease in cohesion ( $C$ ) From the results, it can be concluded that the shear characteristics after the addition of different proportions of straw were improved considerably compared to the untreated soil.
- We found that there is an improvement in the compressibility characteristics of the treated soil, a remarkable decrease in the swelling index and the compressibility index respectively with increasing percentages of wheat straw.
- From the results, it can be concluded that increasing the percentage of Wheat Straw in soil from 0% to 9%, led to a significant reduction of FSI, and adding WS to the soil improved the values of unconfined compressive strength.

The study of the effect of wheat straw on the mechanical behavior of swelling clays has shown that the shrinkage and swelling of clay soils which can cause several problems in civil engineering infrastructure can be adequately managed and solved by mixing an appropriate amount of wheat straw as a soil stabilizer.

## References

- [1] State of the population (2008). ONS in collections statistiques n° 163: Armature Urbaine, Exploitation exhaustive du recensement général de la population et de l'habitat (RGPH).
- [2] Roy, S., & Bhalla, S. K. (2017). Role of geotechnical properties of soil on civil engineering structures. *Resources and Environment*, vol. 7, no 4, p. 103-109.
- [3] Zouhair, A., Dekayir, A., Doss, M., & Kamal, E. (2014). Stabilisation des sols argileux par la chaux. *Journées Nationales de Géotechnique et de Géologie de l'Ingénieur JNGG2014 – Beauvais 8-10 juillet 2014*.
- [4] Koliass, S., Kasselouri-Rigopoulou, V., & Karahalios, A. (2005). Stabilization of clayey soils with high calcium fly ash and cement. *Cement and Concrete Composites*, vol. 27, no 2, p. 301-313.
- [5] Belouahem, Saida, Bekkouche, Souhila Rehab, Nouaouria, Mohamed Salah, Messast, Salah and Idoui, Imane. (2021). Experimental Study on the Sol-Bentonite mixture stabilized by different types of Polymers, *Selected Scientific Papers - Journal of Civil Engineering*, vol.16, no.1, pp.45-55. <https://doi.org/10.1515/sspjce-2021-0004>.
- [6] Rehab, Bekkouche, S; and Boukhatem, G. (2016). Experimental Characterization of Clay Soils behavior stabilized by polymers. *J. Fundam. Appl. Sci.*, 8(3), 1193-1205.
- [7] Souhila, Adjabi and Salah, Nouaouria Mohamed. (2021). Behaviour of cemented and compacted clayey sand reinforced with two types of fibers, *Selected Scientific Papers - Journal of Civil Engineering*, vol.16, no.1, pp.87-103. <https://doi.org/10.1515/sspjce-2021-0007>.
- [8] Rehab, Bekkouche, Souhila; Boukhatem, Ghania; Mendjel Djenette. (2018). Mechanical Behavior of Clay Reinforced by Layers of Polymer, *International Invention of Scientific Journal*, [S.l.], v. 2, n. 04, p. 130-133.
- [9] Chang, I., & Cho, G. C. (2012). Strengthening of Korean residual soil with  $\beta$ -1, 3/1, 6-glucan biopolymer. *Construction and Building Materials*.
- [10] Muhammad, G., & Marri, A. (2018). Immediate and long-term effects of lime and wheat straw on consistency characteristics of clayey soil. *Geomechanics and Engineering*, 16(3), 217–231. <https://doi.org/10.12989/GAE.2018.16.3.217>
- [11] Li, M., Chai, S. X., Zhang, H. Y., Du, H. P., & Wei, L. (2012). Feasibility of saline soil reinforced with

- treated wheat straw and lime. *Soils and foundations*.vol. 52, no 2, p. 228-238.
- [12] Kumar,N., Gautam,N., Chaturvedi, D. (2018). Soil Stabilisation by Wheat Straw Ash and Cement. *International Journal of Research in Engineering, IT and Social Sciences*, Vol.8, p. 210-216.
- [13] Sunil, Kumar, Meena; Raghvendra, Sahu; & Ramanathan, Ayothiraman. (2021) Utilization of Waste Wheat Straw Fibers for Improving the Strength Characteristics of Clay, *Journal of Natural Fibers*, 18:10, 1404-1418, DOI: 10.1080/15440478.2019.1691116.
- [14] Benhaoua, W., Grine, K; & Kenai, S. (2020). Performance of Stabilized Earth with Wheat Straw and Slag. *MRS Advances* 5, 1285–1294. <https://doi.org/10.1557/adv.2020.174>.
- [15] Muntohar, A. S; and Hantoro, G. (2000). Influence of Rice Husk Ash and Lime on Engineering Properties of a Clayey Subgrade, *Electronic Journal of Geotechnical Engineering*, vol. 5, p. 1-9.
- [16] Basha, E. A., Hashim, Roslan; Mahmud, H. B., et al. (2005). Stabilization of residual soil with rice husk ash and cement. *Construction and building materials*, vol. 19, no 6, p. 448-453.
- [17] Zafar, Iqbal, Ahanger; and Abhishek, Bawa. (2018). Utilization of Jute Fibre as Soil Reinforcement. *International Journal of Civil Engineering and Technology*, 9(8), pp. 1320-1326.
- [18] Dang, L, C., Khabbaz, H., Fatahi, B. (2017). An experimental study on engineering behaviour of lime and bagasse fibre reinforced expansive soils. In : *ICSMGE 2017-19th International Conference on Soil Mechanics and Geotechnical Engineering*, Seoul.
- [19] Jagwani, D., & Jaiswal, A. (2019). Expansive Soil Stabilization by Cinder of Coconut Husk. Available at SSRN 3353634.
- [20] Prabakara, J., and Sridhar, R. (2002). Effect of random inclusion of sisal fiber on strength behavior of soil. *Construction and Building Materials*, vol. 16, no 2, p. 123-131.
- [21] Attom, M., and Shatnawi, M. (2005). Stabilization of Clayey Soils using Hay Materials, *Journal of Solid Waste Technology and Management*, vol. 31, no 2, p. 84-92.
- [22] Saini, H., Khatti, J., & Acharya, B. (2019). Stabilization of black cotton soil by using sugarcane bagasse ash. *International Journal of Scientific Research and Review*, Vol. 07, Issue 01, p. 128-132.
- [23] Samira, Z. (2018). Amélioration des propriétés géotechniques des argiles par l'utilisation de sous-produits industriels (Doctoral dissertation, Université Badji Mokhtar-Annaba).
- [24] Soltani, A., Taheri, A., Khatibi, M., & Estabragh, A. R. (2017). Swelling potential of a stabilized expansive soil: A comparative experimental study. *Geotechnical and Geological Engineering*, vol. 35, no 4, p. 1717-1744.
- [25] Villa. J. M, (1980). La chaîne Alpine d'Algérie orientale et des confins Algero-Tunisiens. Thèse de Docteur ES Science Paris 3T. 665 pages.
- [26] Grim, R. and Guven, N. (1978). *Bentonite: Geology, Clay Mineralogy Properties and Users*. Elsevier Science Publishing, New York.
- [27] Debieche, M., and Kaoua F. (2019). Experimental study of the hydraulic performance of a soil reconstituted in a compact state (sand-bentonite).
- [28] Kapoor, M., Panwar, D., & Kaira, G. S. (2016). Bioprocesses for enzyme production using agro-industrial wastes: technical challenges and commercialization potential. In *Agro-Industrial Wastes as Feedstock for Enzyme Production* .p. 61-93.
- [29] Batzias, F. A., Sidoras, D. K., Siontorou, C. G., Bountri, A. N., Politi, D. V., Kopsidas, O. N., & Zervopoulou, S. P. (2014). Experimental design for estimating parameter-values of modelling crude oil adsorption on thermo-chemically modified lignocellulosic biomass. *International Journal of Arts & Sciences*, vol. 7, no 3, p. 205.
- [30] Calabi, Floody, M., Medina, J., Rumpel, C., Condron, L. M., Hernandez, M., Dumont, M., & de la Luz Mora, M. (2018). Smart fertilizers as a strategy for sustainable agriculture. *Advances in agronomy*, vol. 147, p. 119-157.
- [31] Ayeldeen, M., Negm, A., El-Sawwaf, M., & Kitazume, M. (2017). Enhancing mechanical behaviors of collapsible soil using two biopolymers. *Journal of Rock Mechanics and Geotechnical Engineering*, vol. 9, no 2, p. 329-339.

## Investigation of the mechanical and thermal characteristics of an eco-insulating material made of plaster and date palm fibers

Mokhtar Rachedi<sup>1,2\*</sup>, Abdelouahed Kriker<sup>1,2</sup>

<sup>1</sup> Departement of Civil Engineering, University Kasdi Merbah, Ouargla, Algeria.

<sup>2</sup> Laboratory of Exploitation and Valorization of Natural Resources in Arid Zone, University Kasdi Merbah, Ouargla, Algeria.  
e-mail: mokedi@hotmail.fr

### Abstract

The negative impact of the production and use of building materials on the environment has become evident, so in recent decades, to find more sustainable, eco-friendly, and low-cost materials, the last research tends to reconsider the use of natural fibers and traditional building materials. This paper aims to develop a bio-composite based on the southern Algerian region's local materials consisting mainly of plaster and waste from date palm trees. Many properties were examined experimentally through previous research of our team (physical, mechanical, and microstructure characteristics) [1, 2] to characterize these materials. Several samples of bio-composite of plaster configurations with short length (20mm) and eight-weight ratios (0.5% - 4%) of palm fibers were prepared for mechanical, thermal, and physical characterizations. In addition, tested all previous properties on the specimens after 28 days of curing in normal conditions. The results show a clear improvement in the bio-composites mechanical performance (an increase in the bending strength with achieving compressive strength) and their thermal properties, which have been well developed (density, thermal conductivity, and specific heat capacity). To enhance the resistance of palm fibers to chemical degradation in the plaster's alkaline environment and improve the adhesion between them, these fibers were treated with a NaOH solution of 1% concentration. The plaster's composites reinforced with date palm fibers can be qualified as eco-friendly and thermal insulation building materials.

**Keywords:** plaster, date palm fibers, thermal conductivity, specific heat, density, bending strength, compressive strength

## 1 Introduction

All activities related to the construction sector, whether manufacturing building materials, constructing buildings, building operation, or even demolition of buildings. In fact, directly or indirectly affect the environment according to the United Nations Environment Program, these activities consume about 40% of the total global energy, 25% of the total water, and 40% of the total resources [3]. To *reduce* these adverse effects, researchers carry out considerable efforts to develop new methods to produce current building materials and

turning to eco-friendly building materials with good thermo-mechanical properties is the best option in the framework of improving energy efficiency in the construction sector [4]. In this context, several studies have been conducted to investigate the possibility of reverting to the use of traditional building materials such as gypsum, plaster, clay, etc. Due to its peculiar properties and eco-friendly nature. In order to enhance the mechanical, physical, and thermal properties of these materials, they were mixed with natural fibers. Indeed, these new composites are natural, renewable products with interesting thermo-physical and acoustic properties for developing effective building materials.

The southern region of Algeria is rich in natural resources that can be directly exploited as building materials. There are unlimited thick deposit layers of gypsum in this region, which has been used since ancient times as a building material, but its greater use is limited in decoration works due to its fragility and weak mechanical properties. This is a desert area, so the date palm trees are widely spread, the latter being a valuable treasure of natural fibers with promising physical and mechanical properties [5]. This research aims to study the possibility of valuing these eco-friendly materials by developing a new composite made of plaster reinforced with date palm fiber. In this regard, some works have already been reported that dealt with characterizing various properties of the composites of the plaster reinforced with natural fibers; we can summarize below:

The use of cellulose fibers has been investigated to improve the mechanical properties of plaster. Khanfer et al. [6] blend different concentrations of cellulose fibers with plaster; all the composites' physico-mechanical parameters improve significantly as fibers' concentration is increased. Ioculano et al. [7] researched the interaction between the plaster matrix and chemical-treated abaca fibers and found that the various composites obtained have good mechanical properties. The addition of low percentages of abaca fibers to plaster leads to enhanced toughness, flexural strength, and even compressive strength. To improve the plaster composite's thermal and mechanical performance, Maaloufa et al. [8] compared the effect of adding alpha fibers and cork granules to plaster mixtures. Thermal conductivity is improved considerably; the alpha fiber increases mechanical properties; however, the cork granules make the composite more brittle. Alcaraz et al. [9] studied the mechanical characteristics of plaster reinforced with jute fabric. Ultimately jute fabric can be used as an environmentally cost-effective and to increase the mechanical properties of plaster. Gallala et al. [10] produce a plaster composite containing palm fibers (DPFW) after carrying out several tests, it is observed that the addition of 17% of DPFW with a length of 20 mm, produced a composite with good thermal properties ( $\lambda = 0.52 \text{ Wm}^{-1}\text{K}^{-1}$ ). Mechanical properties had better results than non-fiber-reinforced samples. Based on these results, the authors recommend that the studied biocomposite can be used as an eco-friendly insulation material. The thermal diffusivity and conductivity of plaster reinforced with palm fibers were investigated experimentally by Boulaoued et al. [11] to evaluate the possibility of using this new material as an insulating material to reduce energy consumption in buildings. The obtained results have shown a remarkable improvement in the thermal properties of plaster reinforced with palm fibers. Almusawi et al. [12], in their studies, demonstrated the importance of reinforcing the plaster by palm fiber in improving mechanical performance. Naiiri et al. [13] evaluated the effect of doum palm fibers on the properties of plaster mortar. This study confirmed the improvement in mechanical, thermal properties, and a damage reduction of the fiber-

reinforced plasters, achieved when adding doum palm fibers to plaster mortar. Djoudi et al. [14] explored palm fibers' influence on the mixed plaster and gravel's thermal characteristics. The obtained results clearly show that the thermal conductivity, specific heat, and thermal diffusion are considerably improved.

In all the studies reviewed, it appears evident that there is a global trend towards expanding the use of eco-friendly building materials, especially those reinforced with natural fibers this is due to the encouraging results obtained. This work is a continuation of the research of E.V.N.R.A.Z.<sup>1</sup> The laboratory mainly aims to develop local building materials (plaster, clay, etc.) reinforced with palm fiber. For these reasons, our goal is to discuss the plaster's mechanical, physical, and thermal properties by adding palm fibers. More specifically, this work's main objective is to improve the insulating aspect of plaster reinforced with palm fiber for use as an energy-saving building material in southern Algeria, which is characterized by temperature fluctuations during winter and summer.

## 2 Description of the materials used

### 2.1 Plaster

The plaster used in this study is semi-hydrated local gypsum (calcination process at a temperature of 120-150 °C.) extracted from the quarries of Ghardaia in southern Algeria by the OASIS company. This plaster possesses as characteristics presented in Table 1 (according to the standard NF B12-401). The following equation represents the solidification and hydration of sulfate of calcium Hemi hydrated:

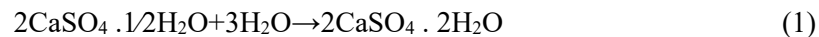


Table 1: Characteristics of plaster

<b>Apparent density [kg/m<sup>3</sup>]</b>	840-915	
<b>Absolute density [kg/m<sup>3</sup>]</b>	1100-1300	
<b>Particle retained by the sieve of 800 μm</b>	2.60%	
<b>Particle retained by the sieve of 200 μm</b>	14.20%	
<b>Fineness modulus [cm<sup>2</sup>/g]</b>	1500-8000	
<b>Setting time (W/P = 0.6)</b>	Beginning (min)	7
	End (min)	15

### 2.2 Fibers

Palm trees are prevalent in southern Algeria. Significant amounts of fiber from these trees are eliminated annually throughout the harvest season. To reduce the waste of this natural and renewable material, opted to use these fibers with plaster to obtain a new eco-material using local materials. Palm fibers were obtained from the surface of the trunks of the male palm tree from the oases of Ouargla (Southern Algeria). First, the collected fibers were washed with tap

<sup>1</sup> Laboratory of Exploitation and Valorization of Natural Resources in Arid Zones



water, so any dust or impurities were removed. Then, manually dismantled into bundles of fibers. The fibers were left in the laboratory for 24 h before being cut to the desired lengths, finally collected in bags for later use. In previous studies, the E.V.N.R.A.Z Laboratory research team investigated the physical and mechanical properties of palm fibers [5]. Table 2 summarizes it.

Table 2: Physical and mechanical properties of the fibers

<b>Apparent density [kg/m<sup>3</sup>]</b>	512.21 - 1088.81		
<b>Absolute density [kg/m<sup>3</sup>]</b>	1300 - 1450		
<b>Tensile strength [MPa]</b>	<i>L</i> = 100 mm	<i>L</i> = 60 mm	<i>L</i> = 20 mm
	170 ±40	240 ±30	290±20
<b>Failure deformation</b>	<i>d</i> = 0.232 (diameter of fibers 8 mm)		
<b>Humidity ratio</b>	<i>w</i> = 9.5 - 10.5 %		
<b>Absorption rate (after 24 h)</b>	<i>TA</i> = 96.83 - 202.64 %		
<b>Diameter (fibers used)</b>	<i>D</i> = from 0.2 to 1 mm		

### 2.3 Lime

Aerial lime with a 6% mass fraction was used as a retardant of plaster setting time by decreasing its solubility. This addition does not affect the mechanical properties of the composites but somewhat improves stabilizes the alkaline environment of the plaster.

### 2.4 Mixing water

In this work, according to NF EN 1008 standard, ordinary tap water of the university lab was used to prepare various plaster mixes and all necessary curing.

## 3 Samples preparation

### 3.1 Pre-treatment and preparation of fibers

To remove the weak layers of palm fiber, such as lignin and hemicellulose, which are not resistant to plaster's alkaline environment, chemical treatment has been used. This treatment improves the mechanical properties of the fibers and adjusts the adhesion strength of the fiber-matrix interface. The conditions for the treatment of fibers are based on the results of recent studies [15,16]. Firstly, the pre-prepared clean fibers were soaked in 1% concentration NaOH solution at 100°C for 1 h and then washed with water to remove the excess of NaOH sticking to the surface of the fibers, after that it bleached with sodium chloride, finally the fibers were washed again thoroughly with water and dried in the room temperature for 24 h before use.

### 3.2 Composite preparation

To assess the effect of date palm fiber addition on the performance of plaster. The composites are prepared with different fiber contents: 0, 0.5, 1, 1.5, 2, 2.5, 3, 3.5 and 4%, and a fixed

length of 20 mm. The formulation of plaster composites was prepared by Standard NF EN 13279-1. The composite design optimization was developed in two steps. In the first one, the optimization of the plaster mix was detailed as follows: the water–plaster ratio was equal to 0.60. In the second step, the fibers are incorporated in the plaster matrix percentages varying from 0.5 to 4%. A control sample was elaborated for comparison. Prismatic molds of dimensions 40 mm x 40 mm x 160 mm were used for mechanical tests while parallelepiped molds with dimensions of 40 mm x 80 mm x 160 mm were used for thermo-physical measurements.

To get homogeneous composites prepared manually, the recommendations of Kriker et al. [5] were respected, which consisted of: (1) First, immersing the treated fibers in water for five minutes before use. (2) Second, mixing in dry fiber with the plaster. (3) Finally, adding the lime and water solution in the proportions stated above. After demolding operation, all molds were cured under laboratory conditions:  $T = 25 \pm 2$  °C and relative humidity  $RH = 60 \pm 2\%$ , for 28 days.

For each composite, three manufactured samples were tested to determine the average values of physical, thermal, and mechanical properties.

## 4 Testing procedures and equipment

### 4.1 Physical properties

The density of the samples was determined from the weight and volumetric measurements.

### 4.2 Mechanical properties

The mechanical tests were performed in accordance with the European Standard EN 13279-2. Measurements were made using a 50 kN capacity press, with speed loading fixed at  $0.5 \pm 0.1$  mm/min and  $3.00 \pm 0.2$  mm/min for flexural and compressive strengths, respectively.

The method of measuring flexural strength is presented in Figure 1(a). The load is applied to the transversal section of the sample. The flexural strength was calculated using the following equation:

$$R_f = \frac{1,5F_f \times L}{b^3} \text{ [MPa]} \quad (2)$$

The compressive test is determined on half of the specimens retained from the flexural test, as shown in Figure1(b). The compressive strength was calculated using the following equation:

$$R_c = \frac{F_c}{b^2} \text{ [MPa]} \quad (3)$$

With:  $F_f$  and  $F_c$ : maximum load in N  
 $L$ : the distance between support ( $L = 100$  mm).  
 $b$ : the width of specimen ( $b = 40$  mm).

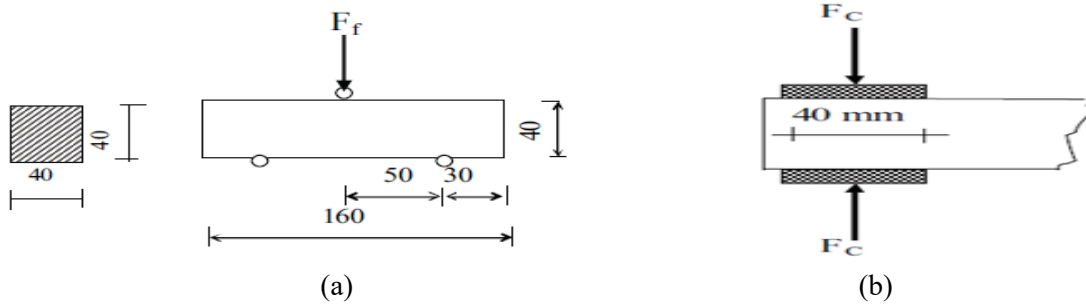


Figure 1: Scheme illustrative of the mechanical tests: (a). The flexural strength (b). The compressive strength

### 4.3 Thermal properties

To access the effect of palm fibers' presence on plasters' thermal behavior, their thermal conductivity  $\lambda$  (W/mK) and specific heat capacity  $C_v$  (J/m<sup>3</sup>K) were measured according to NFE993-15, using the hot wire method. The experiment was carried out as shown in Figure 2.

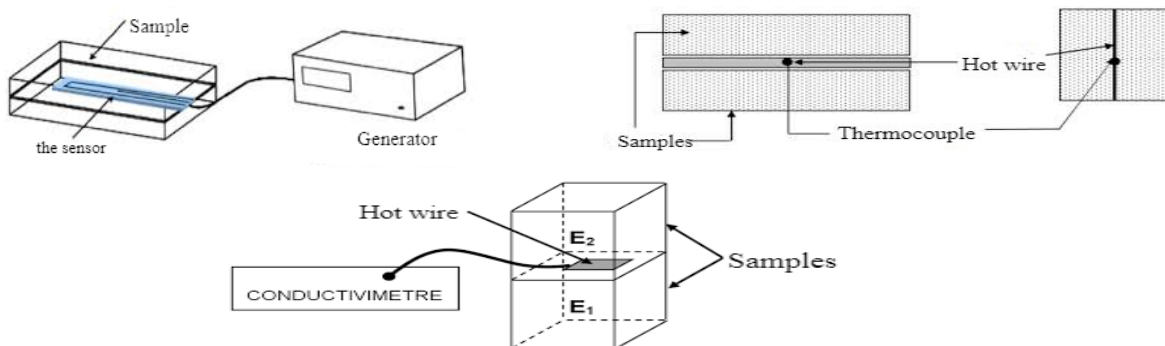


Figure 2: Experimental setup for the measuring of thermo-physical properties

## 5 Results and discussion

Any new building material, such as plaster reinforced with palm fiber, must achieve specific mechanical and physical properties to be usable. The following are the characterizations of some essential properties of an insulating material composed of plaster and palm fiber summarized in Table 3.

Table 3: Physical, mechanical, and thermal properties of plaster composites

Fiber ratio (in the composites) (%)	Density (kg/m <sup>3</sup> )	Compressive strength (MPa)	Flexural strength (MPa)	Thermal conductivity (W/mK)	Specific heat (J/kgK)
0	1240.13± 0.87	11.68±1.34	4.11± 1.02	0.67± 0.13	1471.00± 3.31
0.5	1116.12± 1.01	11.45± 0.91	4.60± 0.33	0.56± 0.10	1691.65± 2.42
1	1029.31± 1.04	11.10± 1.87	4.97± 1.01	0.52± 0.07	1838.75± 4.01
1.5	930.10± 1.2	10.63± 0.20	5.26± 1.10	0.49± 0.01	1971.14± 2.22
2	868.09± 0.91	10.40± 0.73	5.43± 0.21	0.46± 0.09	2074.11± 3.83
2.5	806.08± 0.22	10.16± 0.22	5.47± 0.21	0.44± 0.11	2147.66± 2.11
3	768.88± 0.34	9.93± 0.68	5.34± 0.56	0.43± 0.08	2221.21± 1.91
3.5	719.28± 1.03	9.46± 0.66	5.18± 0.41	0.42± 0.07	2294.76± 3.07
4	694.47± 0.92	9.23± 0.57	4.73± 0.22	0.42± 0.09	2353.60± 2.84

### 5.1 Physical properties

Figure 3 shows the variation of the density according to the percentage of fibers. It has been noticed that the addition of fiber to the plaster leads to a significant decrease in its density. It is observed that the progressive incorporation of an increasing percentage of fibers (from 0 to 4%) into a plaster involves a density reduction between 10% and 44% (1116.12 and 694.47 kg/m<sup>3</sup>); this decrease in density is because palm fibers are low in density compared to plaster. The addition of these fibers leads to increased voids in the resulting compounds due to poor cohesion between the fibers and the plaster paste, the latter due to the random distribution of the fibers and insufficient compaction. This decrease in density can be considered the first positive characteristic of natural fibers, as lightweight building materials are greatly encouraged in modern engineering. This phenomenon is always taking place on composite with plaster and vegetable fibers according to several works such as Laoubi et al. [17], and Ochang et al. [18].

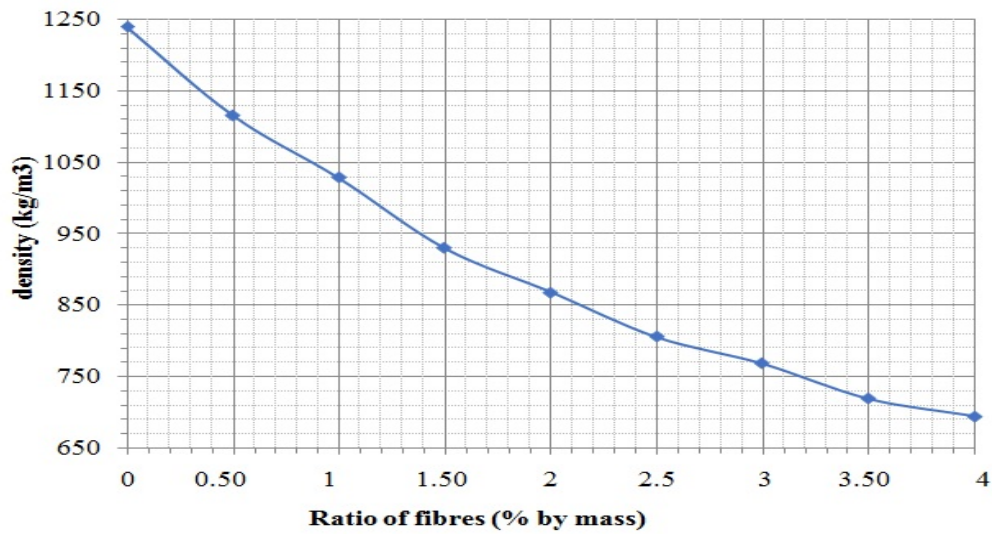


Figure 3: The density of the composites as a function of the ratio of date palm fibers

### 5.2 Mechanical properties

The variations in the plaster composites' compressive strength as a function of the fiber content, illustrated in Figure 4(a). The results indicated slight stability in the compressive strength of the samples with a content of 0.5% to 1 % of the fiber compared to the reference samples; This is due to the uniform distribution of the short fibers corresponding to these proportions and the excellent adhesion between the fibers and the plaster matrix. As for the plaster composites in which the fiber content exceeds 1%, the compressive strength decreases significantly, as the relative decrease is about 22% for samples with 4% fiber content. This behavior is due to the loss of workability and many voids and pores due to the poor distribution of the fibers in the matrix, and this leads to disrupts the mineral skeleton of the composites. These results agree with previous research, such as [9,14].

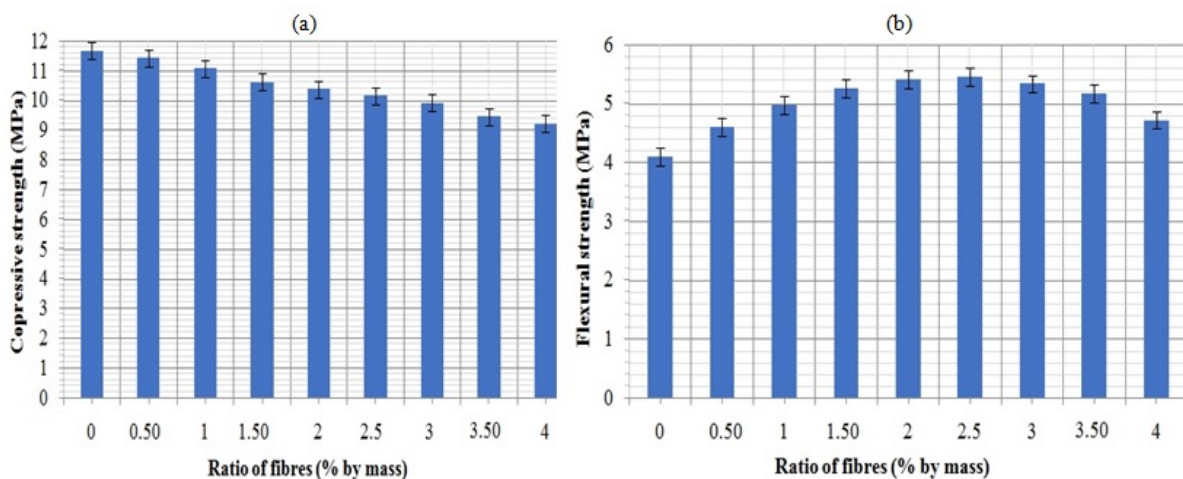


Figure 4: The composites' mechanical properties as a function of the ratio of date palm fibers: (a) Compressive strength (b) Flexural strength

Concerning the flexural strength of composites, Figure 4(b) shows its evolution as a fiber content function. At first, the samples show a significant increase in the flexural strength compared to the reference samples; an improvement of 30 and 35% was observed in samples with a fiber content between 2 and 2.5%; this behavior can be related to the role played by the fiber in composites by reducing the propagation and progression of the cracks, and an excellent superficial interlocking between the matrix and the fibers contributes to this. As for the samples with high fiber content, they showed a sharp decrease in flexural resistance. The worst bending resistance was recorded for samples with 2.5% fiber content. This is due to the poor distribution of the fibers, which causes an increase in these samples' porosity. This performance was reported by Benaniba et al. [19], Kenai et al. [20], and Boumhaout et al. [21] considered plaster and mineral paste reinforced with natural fibers.

### 5.3 Thermal properties

Thermal properties are one of the most important properties that must be defined for building materials before use. Among these properties are thermal conductivity and specific heat, which depend on the morphology, composition, and homogeneity of the material considered.

Figure 5(a) presents the influence of the date palm fibers content on the composite material's thermal conductivity. As can be seen, an increase in the content of palm fiber reduces the thermal conductivity of the composites, thus providing a new material with superior thermal behavior, as a decrease in the thermal conductivity was recorded from 0.67 to 0.42  $\text{W m}^{-1}\text{K}^{-1}$  when the ratio of fibers is changed from 0 to 4%, which represented a loss of 39%, as compared to the reference composite. These results can be explained, on the one hand, by the fact that the palm fibers had lower thermal conductivity than plaster. In this sense, several researchers have used this argument to explain the decrease in thermal conductivity of the plaster reinforced with natural fibers [17]. Moreover, on the other hand, other researchers have also attributed this behavior to the voids entrapped between the palm fibers and the plaster, due to the weak adhesion between the fibers and the matrix and to poor samples preparation, which creates closed porosity zones, thus increasing the insulation aspect of the material. These observations agree with the results of most researchers who were interested in improving the thermal properties of plaster through adding natural fibers [1,2,14,21].

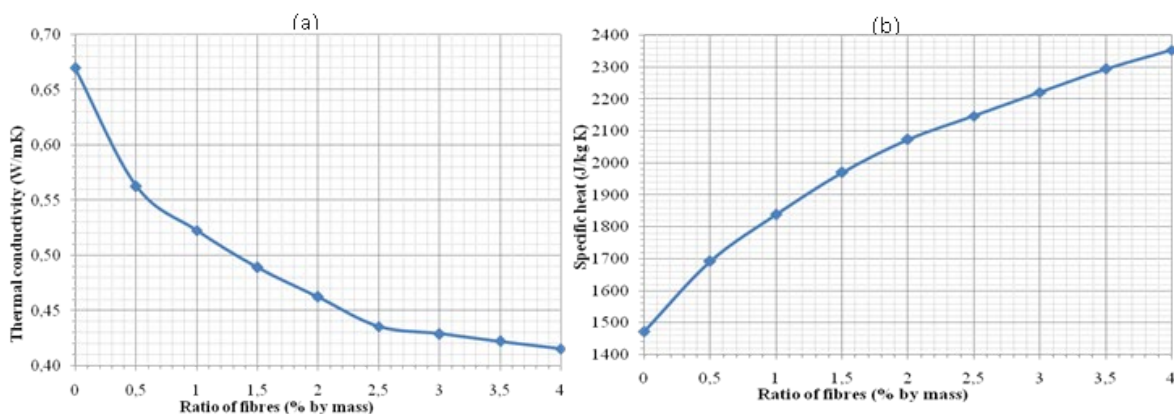


Figure 5: The composites' thermal properties as a function of the ratio of date palm fibers: (a) Thermal conductivity (b) Specific heat

Specific heat capacity is a measure of the energy required to raise 1 kg of material by 1°C, and it is an important parameter to estimate their potential use in the building. The specific heat is presented in Figure 5(b). The addition of palm fiber decreases the specific heat of plaster composites. The results obtained show that increasing the fiber content in compounds from 0% to 4% leads to an increase in the specific heat from 1471.00 J/kgK to 2353.60J/kgK, which increases 60%. This was followed by more or less stability.

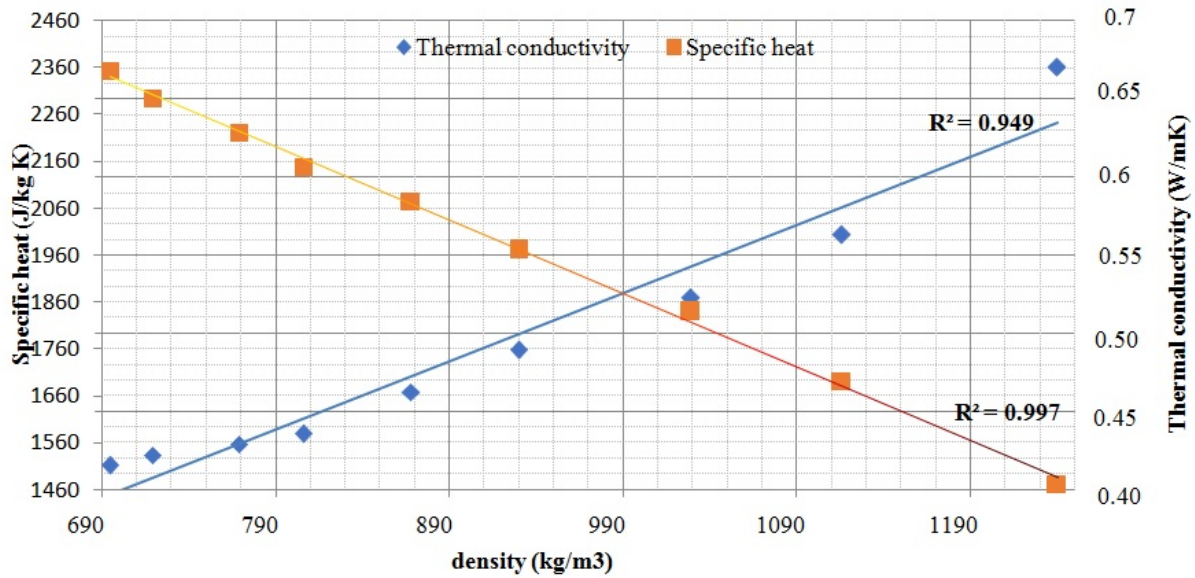


Figure 6: Relationship between density and thermal properties of the composites of plaster reinforced with palm fibers.

These results can be explained by the fact that the incorporation of the natural palm fibers, which are characterized by higher specific heat than pure plaster, and that the presence of the fibers increases the ratio and size of the voids that allow the trapping of air that has a significant specific heat equal to 1005 J/kgK. All this tends to improve the thermal insulation of the composites. The obtained results are following those in the literature. They reported that adding natural fibers to mineral mixtures increases their specific heat [1,14,18].

It was evident from previous results that the plaster's thermal properties are significantly improved when palm fibers are added, and their presence leads to obtaining lightweight plaster composites because the increase in the fibers leads to the production of more voids. Figure 6 represents the direct relationship between the plaster's density and thermal properties reinforced with date palm fibers. From these results, it is clear that the thermal properties were significantly enhanced with decreased density. These results are comparable to several researchers reported, such as Naiiri et al. [13] and Benaniba et al. [19]. A relationship between density and thermal properties was obtained with good dispersion and a correlation coefficient  $R^2=0.94$  for thermal conductivity and  $R^2=0.99$  for specific heat. These characteristics open a promising future for these new composites.

## 6 Conclusions

This study is part of a project that aims to introduce new insulation materials based on abundant and eco-friendly local materials. In this study, the physical, thermal, and mechanical properties of insulating composites consisting of plaster and date palm fibers were described, which are two materials broadly available in southern Algeria. Where the importance of thermal insulation comes in this region due to the high temperature in summer, as it approaches 50°C. The various properties were measured by varying the palm fibers' ratio (With a length of 20 cm) from 0% to 4% in the mass of the plaster composites. The most obvious results of this study can be summarized as follows:

- The new composites' physical properties revealed a 20% decrease in the density of up to 22% when 4% of palm fiber is added to the plaster mix. This is what qualifies this product according to ACI 213R-87 to be a lightweight material.
- In general, a significant improvement was recorded in the mechanical performance of the new composites. An increase in bending strength of 35% was observed when going from control samples to those containing 2.5% of the fibers. Moreover, using short palm fibers leads to a slight decrease in compressive strength estimated at 22% compared to the control samples. Therefore, according to the results of the mechanical properties obtained, these new composites can be used in buildings for non-structural elements which do not require high strength.
- The new composites' thermal insulation performance has been confirmed because the inclusion of palm fibers in the plaster mixes gets to a decrease in the thermal conductivity of the samples by 39% and an increase in the specific heat by 60%, compared to the control samples. These good properties make the plaster's composites with palm fibers beneficial for preventing heat transfer and saving energy in buildings.
- Finally, improving the fibers' surface through chemical treatment plays a significant role in the previous results, even making the new composites more durable and resistant to external factors.
- On a larger scale, there is an immediate demand to continue efforts to make the product more sustainable and eco-friendlier, notably in a desert environment such as southern Algeria, where the problem of water scarcity is exacerbated. It is at the core of sustainable development and is critical for socio-economic development. Therefore, the authors suggest conducting future studies to reduce water use in processing raw materials. One suggestion might be to use process water but must be subject to regular checks, following the FN EN 1008 standard.

In conclusion, we can note that the new materials obtained have competitive physical, thermal, and mechanical properties and the advantage of being environmentally friendly local materials, harmless, and less expensive. According to the Algerian standard DTR C3.2, this composite can be used to produce pre-cast plaster panels for walls, ceiling tiles, and hollow-core surface finishes.

This will be a fruitful area for further work. Future work in this field should be directed to improving the various characteristics and subjecting the composites to various potential factors to confirm, improve and develop the results.



## References

- [1] M. Rachedi, A.Kriker. Thermal properties of plaster reinforced with date palm fibers. *Civil and Environmental Engineering*. 2020;16,2: 259-266.
- [2] F. Hafsi, A.Kriker, S.Abani. Contribution Study to the Thermal Insulation of the Builders in the Desert Regions of Exploiting Gypsum Fiber Reinforced Palm. *AIP Conference Proceedings*. 2017; 1814,1: 020029.
- [3] United Nation Environment Programme, Environment for development, available at <http://www.unep.org/sbci/AboutSBCI/Background.asp>.
- [4] A. Braiek, M. Karkri, et All. Estimation of the thermophysical properties of date palm fibers/gypsum composite for use as insulating materials in building. *Energy and Buildings*. 2017;140: 268–279.
- [5] Kriker A, Debicki G, Bali A, Khenfer MM, Chabannet M. Mechanical properties of date palm fibres and reinforced date palm fibres concrete in hot-dry climate. *Cement Concrete Comp*. 2005;27: 554–564.
- [6] M. M. Khenfer, P.P. Morlier. Cellulose fibres reinforced plaster. *Materials and Structures*.1999; 32:52-58.
- [7] Iucolano F, Caputo D, Leboffe F, Liguori B. Mechanical behavior of plaster reinforced with abaca fibers. *Constr Build Mater*. 2015; 99:184–91.
- [8] A. KHABBAZI, J. Kettar. Thermal Thermal and Mechanical Behavior of the Plaster Reinforced by Fiber Alpha or Granular Cork. *International Journal of Civil Engineering and Technology*. 2017; 8,7: 1026–1040.
- [9] J.S.Alcaraz, I.M. Belda, et Al. Mechanical properties of plaster reinforced with yute fabrics. *Composites Part B*. 2019;178: 107390.
- [10] W. GALLALA, H.M.M. KHATER, et Al. production of low-cost biocomposite made of palm fibers waste and gypsum plaster. *Int. Contam. Ambie*. 2020; 36,2: 475-483.
- [11] I.Boulaoued, I.Amara, A.Mhimid. Experimental Determination of Thermal Conductivity and Diffusivity of New Building Insulating Materials. *journal of heat and technology*.2016; 34,2: 325-331.
- [12] A.M. ALmusawi, T.S. Hussein, M.A. Shallal. Effect of Temperature and Sisal Fiber Content on the Properties of Plaster of Paris. *International Journal of Engineering & Technology*. 2018;7: 205-208.
- [13] F.Naiiri , L.Allegue, M.Salem, R.Zitoune, M.Zidi. The effect of doum palm fibers on the mechanical and thermal properties of gypsum mortar. *Journal of Composite Materials*. 2019:1–19.
- [14] A.Djoudi, M.M.Khenfer, A.Bali , T.Bouziani. Effect of the addition of date palm fibers on thermal properties of plaster concrete: experimental study and modeling. *Adhesion Science and Technology*.2014; 28,20: 2100-2111.
- [15] M. Rachedi, A.Kriker. Optimal composition of plaster mortar reinforced with palm fibers. *J Civil Eng Environ Sci*. 2018; 4: 44–49.
- [16] A.Achour, F.Ghomari, N.Belayachi. Properties of cementitious mortars reinforced with natural fibers. *J of Adhesion Science and Technology*. 2017; 10: 1–25.
- [17] H. Laoubi, M. Bederina, et Al. Study of a New Plaster Composite Based on Dune Sand and Expanded Polystyrene as Aggregates. *The Open Civil Engineering Journal*. 2018; 12: 401-412.
- [18] M.B. Ochang, P.R. Jubu, et Al. Investigation of Thermal Properties of Fabricated Plaster of Paris -Rice Husk Ash Composite with Varying Matrix-Filler Volume Fractions for Thermal Insulation Applications. *American Journal of Engineering Research*.2018; 7,6: 215-222.
- [19] S. Benaniba, Z. Driss, et All. Thermo-mechanical characterization of a bio-composite mortar reinforced with date palm fiber. *Journal of Engineered Fibers and Fabrics*. 2020; 15:1–9.
- [20] A. Kenai, M. Rezagui, et All. Performance of Repair Mortar with Natural Fibers. *MRS Advances*.2020; 5,17: 1295– 1304.
- [21] M. Boumhaout, L. Boukhattem, et Al. Thermomechanical characterization of a bio-composite building material: Mortar reinforced with date palm fibers mesh. *Construction and Building Materials*. 2017; 135: 241–250.

## Predicting energy demand of residential buildings: A linear regression-based approach for a small sample size

Soufiane Boukarta<sup>1,2</sup>

<sup>1</sup>Institute of Architecture et Urbanism (IAU), university of Blida 1

<sup>2</sup>VUDD laboratory (EPAU)

e-mail: boukarta.soufiane@univ-blida.dz

### Abstract

The key design strategies that reduce the energy demand of buildings are not present in most thermal codes in many countries. Therefore, modeling techniques offer an alternative to combine the architects' modus operandi with the energy efficiency in the early stages of architectural design and with higher speed and precision. However, a review of the scientific literature using modeling techniques shows that most researchers use a relatively large sample of thermal simulations. This paper proposes a simplified method based on the linear regression modeling technique and considers a relatively smaller sample of thermal simulations. A total of 6 key building design strategies were identified, related to the urban context, building envelope, and shape factor. A simulation protocol containing 60 possible combinations was designed by random selection. In the present study, the Pleiades software was used to estimate the annual energy demand for heating and cooling for a typical dwelling in a humid climate zone. A parametric study and sensitivity analysis to identify the most efficient parameters was performed in SPSS 21. The resulting model predicts the annual energy demand with an accuracy of 93.7%, a root mean square error (RMSE) of 5.88, and a scatter index (SI) of 8.59%. The models performed could efficiently and quickly assist architects while designing the buildings in the architectural practice.

**Key words:** linear regression, small sample size, design of experiment, sensitivity analysis, energy demand, humid climate zone structure

## 1 Introduction

The issue of buildings' energy efficiency has returned to the forefront of many countries' political agendas because of the high cost of energy and even more so because of the climate change that the world is facing, and which is likely to be exacerbated if no action is taken to mitigate it. Energy consumption in residential buildings is significant worldwide and represents more than 43% of final energy consumption in Algeria [1]. The energy demand of the residential sector grew by 8.3% per year in the last decade (2007-2017), driven by population and economic growth. The residential sector emits more than 34 million tonnes of CO<sub>2</sub> or 36% of the total greenhouse gas (GHG) emissions [1]. Because of this relatively large share of a country's energy consumption and resulting GHG emissions, any increase in energy

efficiency in residential buildings would result in significant energy savings and emissions reductions.

In the usual architectural design process, the architectural project is based on several guidelines to satisfy the main design requirements, namely, integration with the site, aesthetics, functionality of the project, and energy efficiency. The latter is partly overlooked by architects because the key design strategies are not accompanied by their importance in explaining energy demand. Therefore, it is at this stage that the designer should consider design alternatives to reduce the energy demand of his building.

In several countries across the world, there is a thermal code that proceeds by static calculation, but this method is not adapted to the architect's modus operandi when designing the project and which, to sum up, is mainly based on drawings developed based on sketches, such as the glazing rate, orientation, prospect and building shape factor. Therefore, modeling techniques predicting the energy performance of buildings could play a role as a tool to support the design and analysis of energy-efficient buildings. These models simulate the effect of different design parameters that architects tend to use without knowing their impact on energy demand [2].

Linear regression is one of the most common methods used to model the energy demand in buildings [2, 3, 4, 38]. It combines the speed of a simple method and the precision of a dynamic thermal simulation [2]. Several studies used the regression technique for several purposes. Semahi et al. [4] used linear regression to assess the correlation between the bioclimatic potential for cooling and heating with the energy demand obtained from dynamic thermal simulation and have found a correlation of  $R^2$  values of 0.88 and 0.7 respectively. Carlo and Lamberts [5] developed a model based on linear regression to assess the electricity demand in regards of the quality of the commercial building envelope in Brazil. In the same track, Bansal and Bhattacharya [6] performed a model to predict the annual energy demand based on the variation of climatic conditions in India. A strong correlation between weather conditions and the energy demand for both cooling and heating was observed ( $R^2$  0.9). Also, Li et al. [7] developed regression models to predict the energy performance on several types of building envelopes and daylighting controls. Regression models could also be used to predict the monthly energy consumption. Catalina et al. [8] have performed in France a regression model based on the variation of 3 key factors, the thermal transmittance value of the building envelope, window to wall ratio, and the building shape factor.

The sample size used is in general relatively high, with 2000 possible combinations for Bouyer [3], 30000 for Amiri et al. [2], 270 for Catalina et al. [8]. In general, the number of possible simulations depends on the number of variables introduced in the study. For example, if we have 6 variables and a range of 6 variations per variable, the possible combination is 66 which gives 46656 possible combinations which represents a heavy campaign of dynamic simulations. Therefore, authors limit the number of possible combinations by choosing a random number of possibilities, but the number of possibilities in several studies remains important. In this paper, we test how well would the models perform within a relatively small sample size.

## 2 Literature review

The review of the scientific literature on the main driving factors reducing the energy demand in buildings led to classifying the most influential parameters according to 4 registers [9-12].

### 2.1 The occupant behavior

The occupant behavior is considered as the main source of uncertainty when we should perform thermal and dynamic simulation. Several researchers [13-18] showed that the occupants' behavior could explain a variation of the energy demand by up to 50 to 200% [19]. Hong and Lin [20] classify the occupant behavior according to their impact on the energy demand into three classes: an austerity class, standard or normal, and wasteful class. The occupant impact on the energy demand is still the object of research and its effect is difficult to predict. Some authors prefer studying the variation of the energy demand based on one occupant in a single space [20]. The approaches based on thermal simulations still use simplified schedule occupancy to be able to predict the energy demand more closely to real cases [4]. Abuimara et al. [21] and in a standard commercial building with a floor area of 1728 m<sup>2</sup>, tested 75 occupants' distribution scenarios with an average density of 0.05 person/m<sup>2</sup>, which remained unchanged for the entire building. A variation in occupancy density varied from 0 to 0.21 person/m<sup>2</sup>. The authors found only 9% as a major impact of the variation of the occupancy density on energy demand. To reduce the rate of discomfort due to occupant density, the authors concluded that it would be necessary to deploy adaptive technologies as a function of occupancy density to the HVAC systems.

### 2.2 The design factors

The design factors are usually studied within two approaches: (i) The engineering approach which is based on the determinist algorithm used via thermal simulation software [22, 9, 23, 3, 24]. The occupancy schedule is usually simplified [4] and considered as unchanged to be able to assess the design factors' impact in explaining the energy demand; (ii) A statistical approach, also called historicist approach [19]. This approach is based on the final energy consumption of the building stock and a set of indicators to perform models of forecasting and monitoring of energy use. This approach could be used within a top-down method to assess the variation of the energy demand of a city for a long time. The factors mainly used within this approach are socio-economic data, climate conditions, and energy cost. In a contrast, the bottom-up approach considers building stock based on a set of building categories and then generalizes the results to the whole building stock based on the similitude between buildings categories. This approach allows considering the design and/or the socio-economic factors to explain the energy performance [12, 24, 25, 10].

### 2.3 Urban context

Urban context is a relatively new field of research for energy efficiency studies [9, 11, 12]. The impact of the urban context is mediated by solar admittance, ventilation, lighting, and transportation. It could explain the variation of the energy demand by up to 10% [9] and 50% [11] if we consider both buildings and transportation.

## 2.4 Building energy systems

Building energy systems consider the quality and the technology of the HVAC systems. Dascalaki et al. [10] introduced this register within a statistical approach and Abuimara et al. [21] suggested improving the adaptability of the HVAC technology according to the buildings' occupancy.

The number of variables selected varies relatively from one study to another, 17 for Amiri et al. [2], 6 for Ali-Toudert and Weidhaus [26] and 7 for Bouyer [3], and 3 for Catalina et al. [8]. It is possible to classify the most important variables in the three main components: (i) The environment context. Several studies introduce the climatic conditions, height to width ratio (prospect), vegetal density, the solar orientation, built density, and the amplitude of air temperature which is an interesting variable when we are interested in a comparison between two climate zones; (ii) The design factors. The most important factor representing the design is its building shape factor which is equal to the area to the volume ratio. It's commonly intended that the smaller value of the building shape factor helps to reduce energy demand. In other studies, we find the passive volume which represents the depth of 2 times the ceiling height which is usually equal to 6 meters. This band of 6 meters of depth is naturally lighted, sunny, and ventilated, so its energy demand is smaller than the other spaces of the building considered [9, 11]; (iii) The third component is the quality of the insulation envelope regarding the climatic conditions. In several studies, we found glazing ratio, the thermal transmittance of windows, the thermal resistance of walls, floors, and ceilings, and the thermal mass of materials. The thermal inertia of a material is its ability to provide a temperature phase shift in the heat transfer between the exterior and a building's interior. It is a recommended quality in climates with important thermal amplitude; (iv) Occupancy schedule. The variation of this variable could impact the energy demand from 50% to 200% [19]. In several studies, the occupancy schedule appears as an important variable. Shakouri et al. [17] have found that calibrating the occupancy schedule is more important than the structural approach (reduction of the cooling/heating volume and an increase of the glazed area) with 71% and 33% respectively of impact.

To perform a successful regression model, several parameters have to be fitted. All the data must satisfy all the assumptions of the linear regression; the normality distribution, independence of independent variables, linearity, and homoscedasticity of residuals which is also known as the homogeneity of the variance [27]. To ensure that the data are normally distributed, a variable with a value larger than 1 for Skewness or out of the range of 2, -2 for the Kurtosis test must be transformed before performing the linear regression [28]. In linear regression, variables considered for the model must be independent without similarity between them. To this end, the variance inflation factor (VIF) larger than 5 and minimum tolerance lesser than 0.2 [27] indicate that there is multicollinearity, and the independent variable has to be removed from the model.

To validate a linear regression model, we must check its  $P$ -value which has to be less than 0.05 to be considered a significant model with a 95% confidence interval. Then, the homoscedasticity of the standardized residual must also be checked. To do so, the  $P$ -value of the Kolmogorov-Smirnova and Shapiro-Wilk should be larger than 0.05 to ensure that the model has a homogeneous variance [28].

The quality of the performed linear regression model is checked based on the coefficient of determination  $R^2$ , RMSE, and the Scatter Index (SI). The Root Mean Squared Error (RMSE)

has to be closer to zero, and the Scatter Index indicates the percentage error. The SI is the RMSE divided by the mean of the observations and multiplied by 100 [29]. RMSE is calculated based on the formula (1).

$$\text{RMSE} = \sqrt{\frac{1}{n} \sum_{i=1}^n (S_i - O_i)^2} \quad (1)$$

where  $n$  is the number of the observations,  $S_i$  is the simulated cases and  $O_i$  is the observed cases.

The formula of the linear regression model is as follows:

$$Y = C + \beta_1(X_1) + \beta_2(X_2) + \beta_3(X_3) + \beta_4(X_4) + \dots + \beta_i(X_i) \quad (2)$$

with  $Y$  as the dependent variable (cooling, heating, or total energy demand),  $C$  is constant,  $\beta$  is the coefficient of regression and  $X_i$  is the independent variable. To find the best regression model that predicts accurately the energy consumption, stepwise regression [30] is usually performed especially when the number of explanatory variables is large.

In this paper, the engineering approach is chosen, and we focus our attention on the energy efficiency of buildings in humid climate zone, the urban context and building parameters are the main registers considered in this paper.

### 3 Methods

The method adopted is based on 6 steps as follows (see Figure 1):

- (1) Identification of the potential variables from the literature review that could explain the energy demand variation. We have identified six variables: (i) Environmental variables with the building height to street width ratio also called prospect ( $H/W$ ); (ii) the solar orientation ( $OR$ ); (iii) The envelope insulation, with the thermal resistance of exterior walls ( $Re$ ); (iv) the thermal transmittance of windows ( $U_w$ ); (v) glazing ratio which is the ratio of window to room area ( $Gr$ ). We have not selected the ceiling insulation because the actual thermal code considers already a high thermal resistance; (vi) and the building shape factor ( $A/V$ ) which is calculated by the ratio of the area of contact with the exterior air and the volume of the dwelling. The lower is the building shape factor, the lesser is the energy demand for cooling and heating because the area of thermal loss is lesser.
- (2) The second step is to prepare a protocol of simulation containing all the range of variation for each variable (see Table 1). The occupancy schedule is unchangeable for all the cases to be able to assess the main effect of the 6 variables selected for this paper, see appendix A1. We have set a variation that includes at least a minimum, an average, and a maximum value for each variable so that the possibilities can always be represented within this range of variation. This approach reduces the number of simulations and widens the predictive potential of the models.

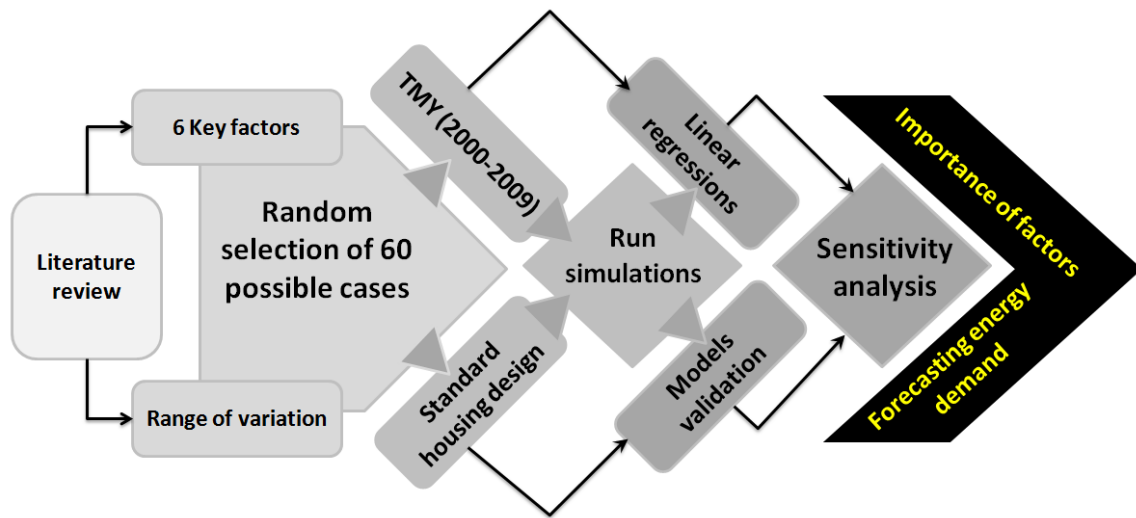


Figure 1: Method framework

- (3) The third step is to conceive a simulation plan with a random selection of variables. A set of 60 simulations was prepared.
- (4) The fourth step is to conceive a typical dwelling to be considered as a baseline model (see Figure 2).
- (5) The fifth step is running the 60 simulations under Pleiades software to obtain the heating and cooling energy demand (kWh/m<sup>2</sup>.y). This software has been validated by the CNERIB (the National Centre for Studies and Research in the Building Industry) which is the authority to issue certificates of conformity in Algeria. The typical Meteorological Year (TMY) used covers the period of ten years (2000-2009). This data is obtained from Meteonorm [31] based on the data of the station of Dar Elbeida (Algiers).
- (6) The sixth step is the modeling stage. A total of three regression models are performed for cooling, heating, and total energy demand.

Table 1: Variables range variation

Variables*	Variable's name	Range of variation
H/W	prospect	1, 2, 3, 4, 5, 6
OR	orientation	0, 45, 90, 135, 180, 225, 270, 315
$Re$ (m <sup>2</sup> .K/W)	thermal resistance	Conventional $Re$ (0.63), optimized $Re$ (2.67, 1.75, 3.95)
$U_w$ (W/m <sup>2</sup> .K)	thermal transmittance	(simple glazing) 5, (double glazing) 3.8, 2.79, 1.70, (triple glazing) 0.72
Gr	glazing ratio	10%, 20%, 30%
A/V	shape factor	0.31, 0.6, 0.66, 0.7
TMY	typical meteorological year	2000-2009

\* Schedule occupancy (see Appendix A1), Thermal characteristics of the materials used in the simulations (see appendix A2)

Space	Area (m <sup>2</sup> )
1-Living room	19.25
2-Bedroom 1	15.75
3-Bedroom 2	12.25
4-wc	1.75
5-Bathroom	4.5
6-Kitchen	8.75
7-Hall	7.75
Total	70 m <sup>2</sup>



Figure 2: Left. Areas of the spaces. Right. Shape of the typical dwelling

## 4 Results

### 4.1 Algiers Climate zone

This section presents a short climate analysis of the city of Algiers which belongs to the A climate zone, which is characterized by a humid climate according to the classification of the thermal code C3-2. The humid climate is globally characterized by a hot and humid climate in summer and mild, rainy, and humid winters. According to a comfort range of 20-27 °C [32] the heating (HDD<sub>20</sub>) and cooling (CDD<sub>27</sub>) degree days are respectively 1524 and 124 in the city of Algiers. The average monthly temperature in winter is about 10.5 °C with a daily minimum of -0.4 °C. The average monthly temperature in summer is about 25.5 °C with a maximum of 38°C. The Monthly mean data (2000-2009) are presented in Table 2 and give an overview of the climate background.

Table 2: Variables range variation

Month	$Ta^*$	$Ta_{min}$	$Ta_{max}$	$Rh$	$Gh$	$Sh$	$Dh$	$FF$	$Sd$	$RR$	$Tg$
Jan	9.94	5.24	15.74	81.30	65	28	37	2.39	166	77	10.34
Feb	10.99	6.00	16.86	77.24	85	43	42	2.50	170	51	10.16
Mar	13.54	8.15	19.50	75.71	127	67	60	2.69	200	55	13.6
Apr	15.49	9.89	21.22	75.33	161	88	73	2.99	223	39	15.76
May	19.06	13.60	24.53	73.34	196	112	84	2.99	280	46	19.72
Jun	22.90	17.08	28.59	68.95	204	118	86	3.09	300	2	23.98
Jul	26.08	20.63	31.51	67.94	227	144	83	3.10	330	3	26.68
Aug	26.27	20.77	31.87	68.67	193	112	81	2.90	300	10	27.23
Sep	22.99	17.85	28.50	73.14	153	93	60	2.80	241	31	23.7
Oct	20.13	15.00	26.00	74.42	107	53	54	2.29	209	40	19.6
Nov	14.47	9.88	20.04	77.09	71	35	36	2.50	172	98	13.69
Dec	11.80	7.46	17.22	78.04	65	33	32	2.59	161	95	10.94

\*  $Ta$ : Temp Avg Daily (°C),  $Rh$ : Rel Humidity (%),  $Sd$ : sunshine duration (hours),  $Ta_{min}$ : Temp Avg Daily low (°C),  $Gh, Sh, Dh$ : Glo Horiz Rad, direct, diffuse (Wh/m<sup>2</sup>),  $RR$ : precipitation (mm),  $Ta_{max}$ : Dry Bulb Temp, Avg Daily high (°C),  $FF$ : wind speed (m/s),  $Tg$ : Ground temperature (°C)



### 4.2 Bioclimatic potential of the humid climate zone

The bioclimatic potential is estimated based on Climate Consultant software analysis which is free didactical software developed by the UCLA energy design tools group [33]. Based on the air temperature and air humidity, the psychometric diagram shows how to improve the comfort zone based on 15 strategies. In this paper, we have used the ASHRAE 55-2010 Thermal comfort model which assumes that occupants adapt their clothing to thermal conditions (1.0 to 1.3 met). As output, this software contributes in terms of percentage and number of hours of thermal comfort gained for each proposed design strategy.

The psychometric diagram indicates that the climate of Algiers is 13.3% of the year thermally comfortable. With 33.1% (2897 hours), the internal heat gains represent the most important factor reducing the heating demand, and the passive solar gains and thermal mass could improve further the comfort up to 12.1% (1061 hours) and 2.7% (239 hours) respectively. Sun shading of windows and adaptive comfort ventilation contribute by up to 14.2% (1242 h) and 18.8% (1651 h) respectively in reducing cooling demand. Also, dehumidification is required and could improve the thermal comfort up to 13.2% (1159 h). All the passive design strategies cited above could provide thermal comfort for up to 53.9% per year. Active cooling and heating are required up to 8.3% (724 h) and 24.5% (2143 h) respectively (see Figure 3).

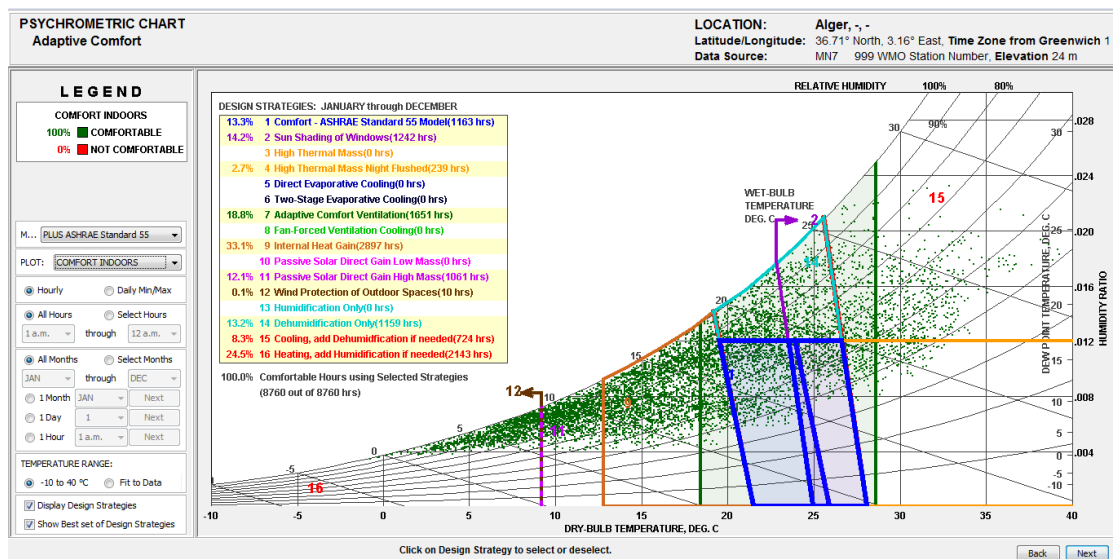


Figure 3: Psychrometric charts of the climate of Algiers

### 4.3 Regression models

A random combination between the six factors selected is presented in Figure 4. Each combination represents a simulation, a total of 60 simulations were performed under Pleiades software. Based on the first stage regression modeling, we have identified 4 cases as outliers and removed them from the final regression models. We have performed three regression models, for cooling, heating, and total energy demand.

SS

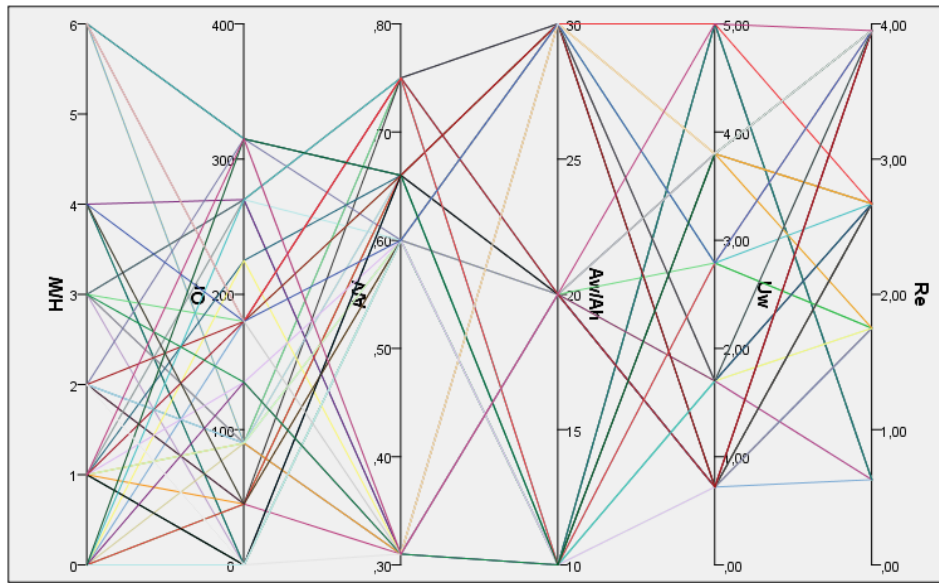


Figure 4: The random combination between variables

### 4.3.1 Multicollinearity test

The first test to check is the multicollinearity test which indicates that all the independent variables selected for the regression model are not similar. All the VIFs indicate a value closer to 1 and a tolerance value larger than 0.2 (see Table 3).

Table 2: Variables range variation

Variables*	Total energy demand		Heating energy demand		Cooling energy demand	
	Tolerance	VIF	Tolerance	VIF	Tolerance	VIF
<b>log10 <math>U_w</math></b>	.923	1.083	.861	1.162	.909	1.100
<b>log10 <math>Re</math></b>	.801	1.248	.760	1.316	.920	1.087
<b><math>Aw/Ah</math></b>	-	-	.851	1.175	.881	1.135
<b><math>H/W</math></b>	.971	1.030	-	-	.955	1.047
<b><math>A/V</math></b>	.956	1.046	.940	1.064	-	-
<b>OR</b>	.800	1.249	.766	1.306	-	-

\*  $U_w$ : Thermal transmittance of windows,  $Re$ : thermal resistance of exterior walls,  $Aw/Ah$ : glazing ratio,  $H/W$ : Prospect,  $A/V$ : shape factor, OR: orientation

### 4.3.2 Linearity test of the models

Based on the scatter plot of the standardized predictions and residuals values, it appears that the relationship is linear because the relationship between the results obtained from the simulations and those predicted by models is almost zero since the residuals are randomly scattered around zero [34] (see Figure 5).

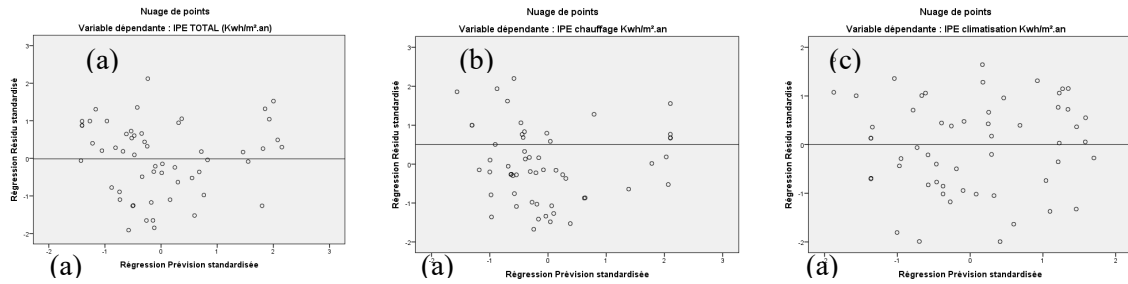


Figure 2: linearity test of residuals. (a) Total energy demand, (b) Heating and (c) Cooling energy demand

### 4.3.3 Normality test

The normality test is checked by the Skewness and Kurtosis test for both independent variables and for residuals. Tables 4 and 5 indicate clearly that the data fit the normality test.

Table 4: Normality test of the independent variables

	$A_w/A_h^*$	H/W	A/V	$U_w$	Or	Re
<b>Skewness</b>	.139	.846	-.597	.152	.226	-.102
<b>Kurtosis</b>	-1.612	-.092	-1.301	-1.425	-1.292	-1.153

\*  $U_w$ : Thermal transmittance of windows,  $Re$ : thermal resistance of exterior walls,  $A_w/A_h$ : glazing ratio, H/W: Prospect, A/V: shape factor, OR: orientation

Table 5: Normality test of residuals

	Total energy demand	Heating energy demand	Cooling energy demand
<b>Skewness</b>	-.210	.272	-.240
<b>Kurtosis</b>	-.640	-.501	-.777

Also, the Q-Q plots of standardized residuals show a linear distribution of quantiles which indicate that the models fit the normality assumption.

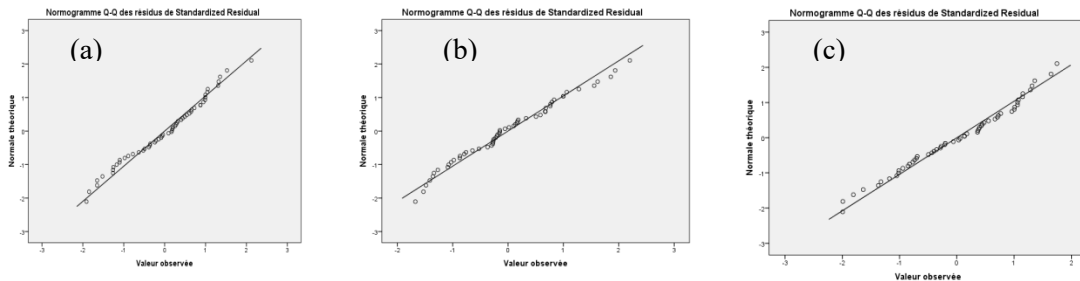


Figure 3: Q-Q plot of residuals. (a) Total energy demand, (b) Heating, and (c) Cooling energy demand

#### 4.3.4 Homoscedasticity test

The homoscedasticity test is satisfied when the error value doesn't vary considerably as the value of the predictor changes. Table 6 shows that residuals do satisfy both the Kolmogorov-Smirnov and the Shapiro-Wilk test, and the regression models performed could predict the energy demand for both heating and cooling.

Table 6: Homoscedasticity test

Models	Kolmogorov-Smirnov		Shapiro-Wilk	
	Statistic	Sig	Statistic	Sig
<b>Total energy demand</b>	.088	<b>,200*</b>	.977	<b>.353</b>
<b>Heating energy demand</b>	.079	<b>,200*</b>	.976	<b>.318</b>
<b>Cooling energy demand</b>	.092	<b>,200*</b>	.974	<b>.256</b>

\* Sig>0.05 means that the homoscedasticity test is satisfied

Based on the four tests presented above, the multicollinearity, linearity, normality, and the homoscedasticity tests, the three regression models performed could be considered as a valid model and its accuracy depends on the items presented in the next section.

#### 4.4 The accuracy of the regression models

The accuracy of a regression model is linked to three indices:

- (1) The coefficient of determination ( $R^2$ ) which represents the power of prediction of the models. The  $R^2$  is high for the three regression models performed, 0.937, 0.885, and 0.895 for the total energy demand, heating, and cooling energy demand respectively (see Figures 7 and 8).
- (2) The RMSE has the same unit as the energy demand which means that its value is relative to the average value of observed values. Within the three models performed, the RMSE calculated is 5.88, 5.49, and 3.14 (kWh/m<sup>2</sup>.y) for the total, heating and cooling energy demand respectively. These results indicate that the three models indicate quite well the energy demand.

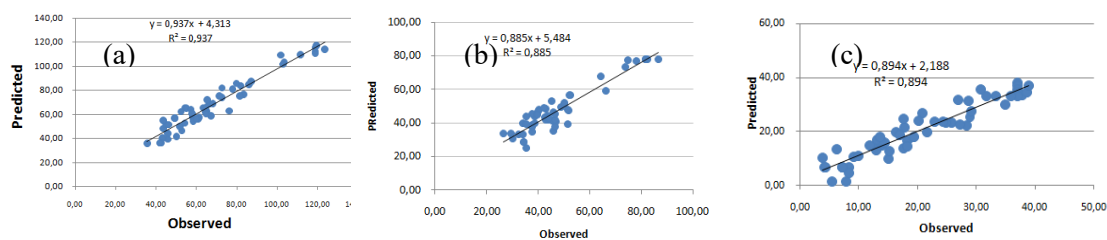


Figure 4: Coefficient of determination of: (a) Total, (b) Heating and (c) Cooling energy demand

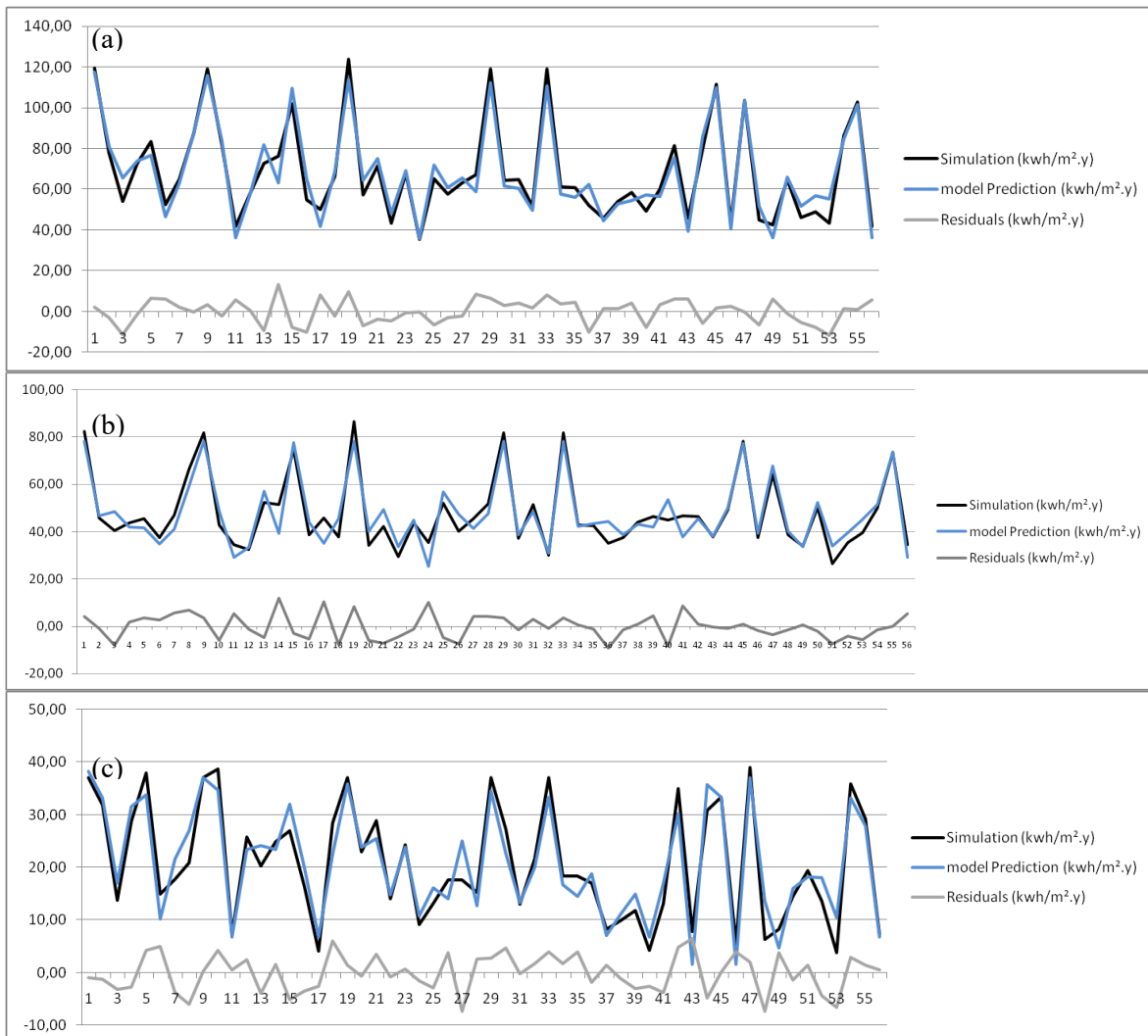


Figure 5: Total model predictions results vs. simulated energy demand. (a) Total, (b) Heating, and (c) Cooling energy demand

- (3) The Scatter Index (SI) precisely presents the importance of each model by reporting the RMSE to the average value of the observed one (simulation results). The SI of the three models is 8.49%, 10.74%, and 16.84% for the total, heating, and cooling energy demand (see Figure 9).  
 These results mean that the most accurate model obtained is the one for the total energy demand.

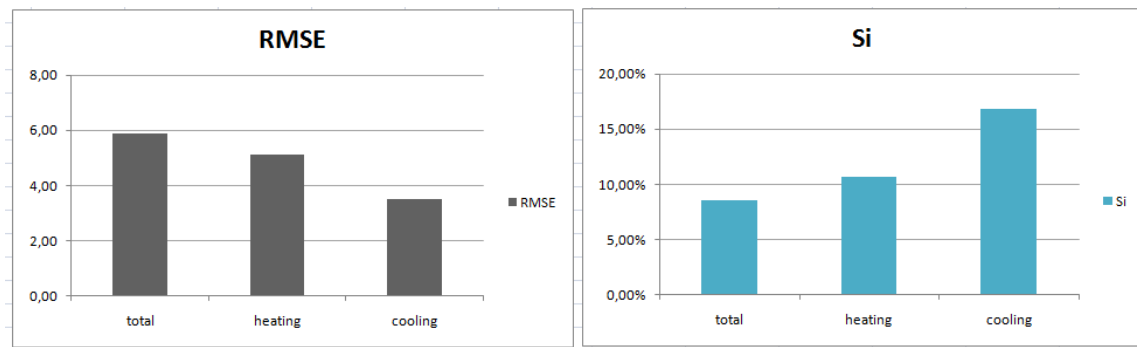


Figure 6: RMSE and SI of the three models

#### 4.5 Sensitivity analysis

The summary of the three regression models is presented in Table 7. All the variables fit the threshold of the  $P$ -value ( $<0.05$ ). It means that the variables selected explain well the variance of the energy demand. Also, the  $\beta$  value, which measures the total effect of the predictor variables, indicates that exterior walls' thermal resistance has the greatest impact on reducing energy demand. Indeed, the  $\log_{10}$  of the thermal resistance of exterior walls reduces energy consumption by up to  $-62 \text{ kWh/m}^2\cdot\text{y}$  for each standard deviation of the thermal resistance.

Table 7: Summary of the regression models

	Total		Heating		Cooling	
	$\beta$	$P$ -value	$\beta$	$P$ -value	$\beta$	$P$ -value
constant	93.775	.000	80.619	.000	14.464	.000
$\log_{10} U_w$	28.362	.000	7.634	.003	19.665	.000
$\log_{10} Re$	-62.009	.000	-37.905	.000	-23.754	.000
H/W	-1.716	.001	-	-	-1.224	.000
A/V	-13.962	.008	-16.960	.000	-	-
Or	-.024	.007	-.026	.001	-	-
Aw/Ah	-	-	-.524	.000	.524	.000
	<b><math>R^2=0.937</math></b>		<b><math>R^2=0.885</math></b>		<b><math>R^2=0.895</math></b>	

To assess the importance of each variable we have computed the ratio of  $\beta$  to standard deviation values and the results are presented in Figure 10. The most important factors are those related to the envelope of the buildings. For every  $+1 \text{ m}^2\cdot\text{K}\cdot\text{W}^{-1}$  in the thermal resistance of exterior walls,  $+0.2$  in the shape factor (A/V), and  $-1 \text{ W/m}^2\cdot\text{K}$  in the thermal transmittance of windows values, the energy demand could be reduced by up to  $-32.63$ ,  $-16.4$ , and  $-13.56 \text{ kWh/m}^2\cdot\text{y}$  respectively. Similar findings were found by Boukarta and Berzowska-Azzag [35]. The effect of the glazing ratio is weak, and it neutralizes itself because the energy demand reduced for the heating demand is required for the cooling demand. It is worth clarifying that the importance of the glazing ratio could be higher with higher  $U_w$  values because the thermal loss and the solar gains would be also higher. The impact of the orientation is also very weak, and it could be explained by the fact that the orientation loses its importance with the higher level of envelope insulation.

The same impact was found by Tahmasebi et al. [36]. The height to width ratio (H/W) reduces slightly the energy demand for cooling by increasing the area of sun shading.

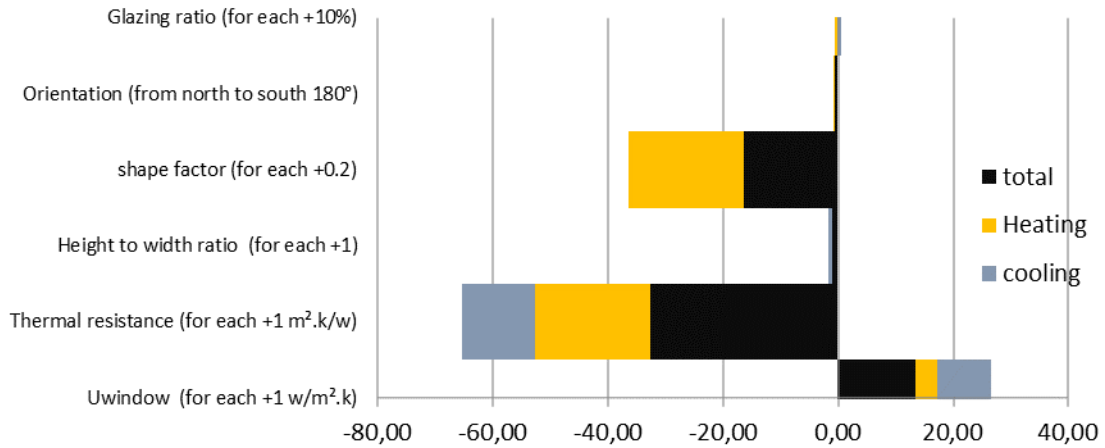


Figure 70: The importance of variables

The best case, observed in our sampling is the case combining the highest thermal resistance of exterior walls,  $U_w$ , and an average value of 0.66 for the shape factor (A/V ratio). Also, the best orientation is observed when the living room and room number 2 were oriented directly to the south ( $180^\circ$ ) and it is worth here to notify that the orientation is mainly depending on the occupancy schedule. The best glazing ratio is 30% because the HDD is higher than the CDD. And the best prospect ratio is observed with the value  $H/W=2$  because it ensures a profitable area of sun shading which could be beneficial for both cooling and heating demand (see Figure 11). Our results fit with the recommendations obtained from the psychometric diagram presented in Figure 5.

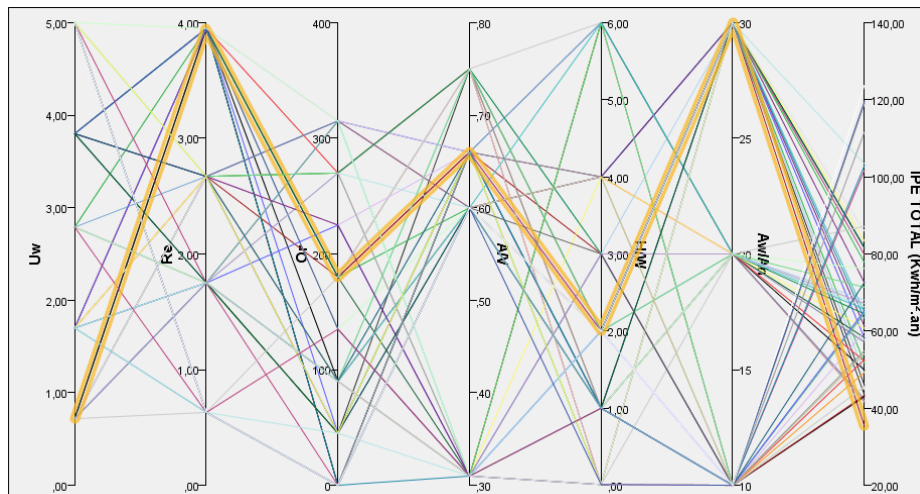


Figure 81: The best combination of the six variables

## 5 Conclusion

The purpose of this paper is to perform regression models to predict the energy demand of cooling and heating of a residential building in the humid climate zone of Algiers based on the variation of a set of 6 design variables largely used by architects in different stages of design. A small sample size of 60 thermal simulations was performed and used as data to perform regression models. 5 parameters were kept for the total energy demand, 5 also for the heating demand, and 4 for the cooling energy demand. The regression models were tested for the four assumptions to validate the regression models and we have also used the RMSE and Scatter Index (SI) to assess the accuracy of the models performed. The results obtained from the models' prediction show that the errors in the prediction of the annual energy demand compared to the simulated ones were acceptable and that the total energy demand regression model ( $R^2=0.937$  and  $SI=8.49\%$ ) is the best followed by the cooling and heating energy demand models. The sensitivity analysis performed shows that the parameters linked to the shape and the envelope insulation have the highest impact, while the glazing ratio, the height to width ratio, and the orientation of the building have a relatively weak impact on the energy demand. Also, the results obtained confirm that it is possible to utilize the predicting models based on a relatively small sample size.

The performed regression models could be used to predict the annual energy demand of residential buildings and could also be used as a baseline to thermal rehabilitation, and it could also test the different strategies to reduce the energy demand at a larger scale.

## References

- [1] APRUE. (2019), L'Agence Nationale pour la Promotion et la Rationalisation de l'Utilisation de l'Energie (2005), La situation énergétique nationale, chiffre 2017, édition 2019.
- [2] AMIRI, Shideh Shams, MOTTAHEDI, Mohammad, et ASADI, Somayeh. Using multiple regression analysis to develop energy consumption indicators for commercial buildings in the US. *Energy and Buildings*, 2015, vol. 109, p. 209-216.
- [3] BOUYER, Julien. Modélisation et simulation des microclimats urbains-Etude de l'impact de l'aménagement urbain sur les consommations énergétiques des bâtiments. 2009. PHD dissertation. Université de Nantes, France.
- [4] SEMAHI, Samir, ZEMMOURI, Noureddine, SINGH, Manoj Kumar, et al. Comparative bioclimatic approach for comfort and passive heating and cooling strategies in Algeria. *Building and Environment*, 2019, vol. 161, p. 106271.
- [5] CARLO, Joyce et LAMBERTS, Roberto. Development of envelope efficiency labels for commercial buildings: Effect of different variables on electricity consumption. *Energy and Buildings*, 2008, vol. 40, no 11, p. 2002-2008.
- [6] BANSAL, Naresh K. BHATTACHARYA, Amitabh. Parametric equations for energy and load estimations for buildings in India. *Applied thermal engineering*, 2009, vol. 29, no 17-18, p. 3710-3715.
- [7] LI, D. H. W., WONG, Sai Li, et CHEUNG, King Lok. Energy performance regression models for office buildings with daylighting controls. *Proceedings of the Institution of Mechanical Engineers, Part A: Journal of Power and Energy*, 2008, vol. 222, no 6, p. 557-568 568.
- [8] CATALINA, Tiberiu, VIRGONE, Joseph, et BLANCO, Eric. Development and validation of regression models to predict monthly heating demand for residential buildings. *Energy and buildings*, 2008, vol. 40, no 10, p. 1825-1832.
- [9] RATTI, Carlo, BAKER, Nick, et STEEMERS, Koen. Energy consumption and urban texture. *Energy and buildings*, 2005, vol. 37, no 7, p. 762-776.
- [10] DASCALAKI, Elena G., DROUTSA, Kaliopi, GAGLIA, Athina G., et al. Data collection and analysis of the building stock and its energy performance—An example for Hellenic buildings. *Energy and Buildings*, 2010, vol. 42, no 8, p. 1231-1237.



- [11] SALAT, Serge. Les villes et les formes urbaines: sur l'urbanisme durable. France, 2011.
- [12] BOUKARTA, Soufiane. BEREZOWSKA-AZZAG, Ewa. 'Urban island' as an energy assessment tool: The case of Mouzaia, Algeria. *Journal of Applied Engineering Science*, 2017, vol. 15, no 2, p. 128-139.
- [13] BARTIAUX, Françoise. A socio-anthropological approach to energy-related behaviours and innovations at the household level. ECEEE (European Council for Energy-Efficient Economy): ECEEE 2003 summer study proceedings—Time to turn down energy demand, 2003, p. 1239-1250.
- [14] SWAN, Lukas G. et UGURSAL, V. Ismet. Modeling of end-use energy consumption in the residential sector: A review of modeling techniques. *Renewable and sustainable energy reviews*, 2009, vol. 13, no 8, p. 1819-1835.
- [15] SUBRÉMON, H. Pour une anthropologie sensible de la consommation d'énergie. Université de Paris X-Nanterre. 2009. PHD dissertation, France.
- [16] YU, Zhun, FUNG, Benjamin CM, HAGHIGHAT, Fariborz, et al. A systematic procedure to study the influence of occupant behavior on building energy consumption. *Energy and buildings*, 2011, vol. 43, no 6, p. 1409-1417.
- [17] SHAKOURI, Mahmoud, BANIHASHEMI NAMINI, S. S., et JAVAHERI, Amin. Analysis and Comparison of Impacts of Design Optimization Approach with Occupant Behaviour on Energy Consumption Reduction in Residential Buildings. *International Journal of Engineering and Technology*, 2012.
- [18] OUYANG, Jinlong et HOKAO, Kazunori. Energy-saving potential by improving occupants' behavior in urban residential sector in Hangzhou City, China. *Energy and buildings*, 2009, vol. 41, no 7, p. 711-720.
- [19] DALL'O', Giuliano, Annalisa GALANTE, Marco TORRI, "A methodology for the energy performance classification of residential building stock on an urban scale". *Energy and Buildings* 48 (2012) 211–219.
- [20] HONG, Tianzhen et LIN, Hung-Wen. Occupant behavior: impact on energy use of private offices. Lawrence Berkeley National Lab.(LBNL), Berkeley, CA (United States), 2013.
- [21] ABUIMARA, Tareq, O'BRIEN, William, et GUNAY, Burak. Quantifying the impact of occupants' spatial distributions on office buildings energy and comfort performance. *Energy and Buildings*, 2021, vol. 233, p. 110695.
- [22] BOUKARTA, Soufiane. BEREZOWSKA-AZZAG, Ewa. Energy demand of occupant's spatial modification in residential buildings. Case study of Médéa, Algeria. *Selected Scientific Papers-Journal of Civil Engineering*, 2018, vol. 13, p. 15-28.
- [23] STEEMERS, Koen. Energy and the city: density, buildings and transport. *Energy and buildings*, 2003, vol. 35, no 1, p. 3-14.
- [24] MAÏZIA, Mindjid, SÈZE, Claire, BERGE, Sébastien, et al. Energy requirements of characteristic urban blocks. *Proc. of CISBAT 2009-Renewables in a changing climate-From Nano to urban scale*, 2009.
- [25] CAPUTO, Paola, COSTA, Gaia, et FERRARI, Simone. A supporting method for defining energy strategies in the building sector at urban scale. *Energy Policy*, 2013, vol. 55, p. 261-270.
- [26] ALI-TOUDERT, Fazia et WEIDHAUS, Juliane. Numerical assessment and optimization of a low-energy residential building for Mediterranean and Saharan climates using a pilot project in Algeria. *Renewable Energy*, 2017, vol. 101, p. 327-346.
- [27] LI, Cheng, LI, Junxiang, et WU, Jianguo. What drives urban growth in China? A multi-scale comparative analysis. *Applied geography*, 2018, vol. 98, p. 43-51.
- [28] KIM, Hae-Young. Statistical notes for clinical researchers: assessing normal distribution (2) using skewness and kurtosis. *Restorative dentistry & endodontics*, 2013, vol. 38, no 1, p. 52-54.
- [29] NEILL, Simon P. et HASHEMI, M. Reza. Ocean modelling for resource characterization. *Fundamentals of ocean renewable energy*, 2018, p. 193-235.
- [30] Hastie, T., Tibshirani, R., & Friedman, J. (2009). *Linear methods for regression*. In *The elements of statistical learning* (pp. 43-99). Springer, New York, NY.
- [31] METEOTEST, Software METEONORM 7, 2016. <https://meteonorm.com/en/>.
- [32] DTR C3.2, Règlement Thermique des Bâtiments d'Habitation - Règles de calcul des déperditions Calorifiques, Fascicule 1, Document Technique Réglementaire, Ministère de l'habitat et de l'urbanisme, CNERIB, Alger, 2004.
- [33] UCLA, Climate Consultant 6.0, 2017. [www.energy-design-tools.aud.ucla.edu/climate-consultant/](http://www.energy-design-tools.aud.ucla.edu/climate-consultant/).
- [34] SANTOS NOBRE, Juvêncio et DA MOTTA SINGER, Julio. Residual analysis for linear mixed

- models. *Biometrical Journal: Journal of Mathematical Methods in Biosciences*, 2007, vol. 49, no 6, p. 863-875.
- [35] BOUKARTA, Soufiane. Déterminants de la forme urbaine générant le potentiel de maîtrise de l'énergie en zone semi-aride. 2019. PHD dissertation. Ecole polytechnique d'architecture et d'urbanisme (EPAU).
- [36] TAHMASEBI, Mohammad Mahdi, BANIHASHEMI, Saeed, et HASSANABADI, Mahmoud Shakouri. Assessment of the variation impacts of window on energy consumption and carbon footprint. *Procedia engineering*, 2011, vol. 21, p. 820-828.

Appendix A1: Schedule occupancy

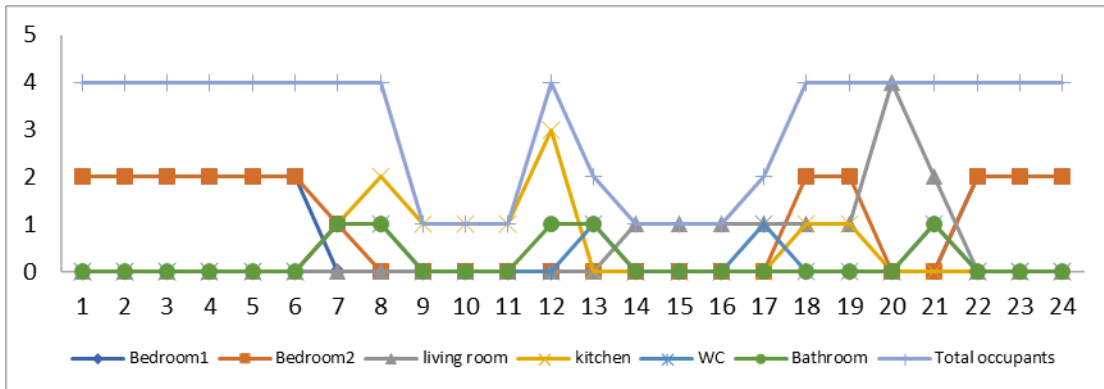


Figure A1- 1 : Schedule occupancy of weekdays

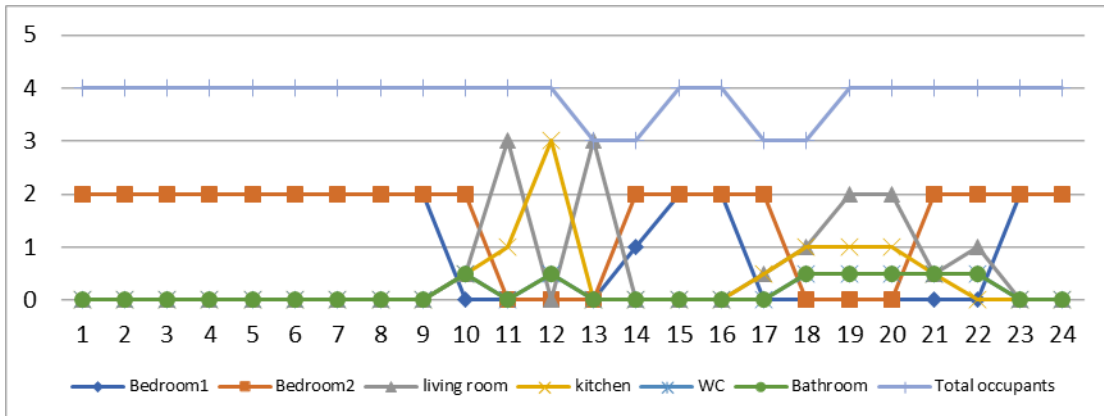


Figure A1- 2 : Schedule occupancy of Fridays

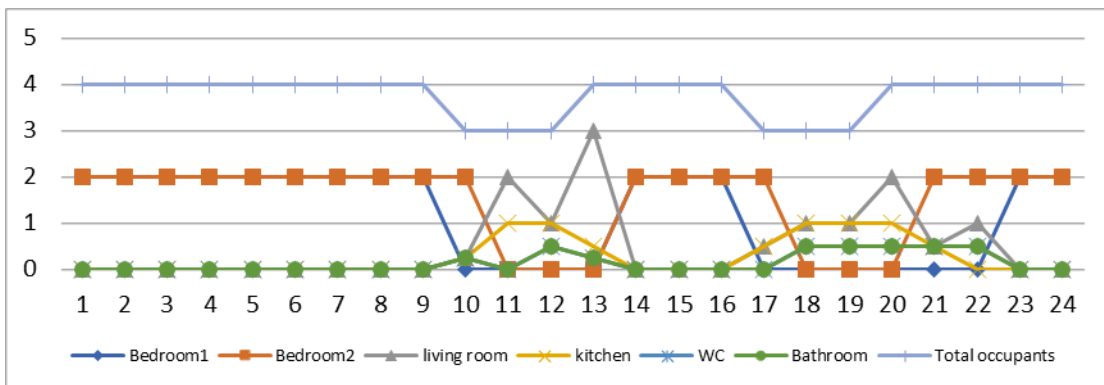


Figure A1- 3 : Schedule occupancy of Saturdays

**Appendix A2: Thermal characteristics of the materials used in the simulations**

Table A2-1: Thermal characteristics of the materials used in the simulations

<b>Envelope</b>			
<b>Exterior Walls</b>	<b>Composition</b>	<b>Thickness (cm)</b>	<b>Thermal Resistance (m<sup>2</sup>K/W)</b>
Double walls	Cement mortar	02.0	0.01
	Hollow brick	15.0	0.27
	Air gap	05.0	0.16
	hollow brick	10.0	0.18
	Cement mortar	02.0	0.01
			Total: 0.63
Double walls+insulation	Cement mortar	02.0	0.01
	Hollow brick	15.0	0.27
	Expanded polystyrene	05.0	1.28
	Hollow brick	10.0	0.18
	Cement mortar	02.0	0.01
			Total: 1.75
Mono Walls (certified)	Cement mortar	02.0	0.01
	Mono wall	30.0	2.65
	Cement mortar	02.0	0.01
			Total: 2.67
Mono Walls +insulation	Cement mortar	02.0	0.01
	Mono wall	30.0	2.65
	Expanded polystyrene	05.0	1.28
	Cement mortar	02.0	0.01
			Total: 3.95
<b>windows</b>	<b>Type</b>	<b>U<sub>w</sub> (W/m<sup>2</sup>.K)</b>	
	Single glazing	05.00	
	Double glazing A	03.80	
	Double glazing B	02.79	
	Double glazing C	01.70	
	Triple glazing	0.72	
<b>Exterior door</b>	Wooden door	05.00	
<b>Floor and ceiling</b>			
	<b>composition</b>	<b>Thickness (cm)</b>	<b>Thermal resistance (m<sup>2</sup>K/W)</b>
<b>Ceiling</b>	Cement mortar	02.00	0.01
	Slabs	16.00	0.13
	Heavy Concrete	04.00	0.02
	Expanded polystyrene	10.00	2.56
	Concrete slope	03.00	0.08
	Bituminous felt 36-S	03.00	0.13
	Gravel	03.00	0.08
			Total: 3.01
<b>Floor: Slab on ground</b>	Heavy concrete	20.00	0.11
	Expanded polystyrene	04.00	1.03
	Mortar	05.00	0.04
	Tiling	02.00	0.01
			Total: 1.19
<b>Interior</b>			
<b>Interior wall</b>	<b>Composition</b>	<b>Thickness (cm)</b>	<b>Thermal resistance (m<sup>2</sup>K/W)</b>
<b>Brick partition</b>	Plaster	02.00	0.06
	Hollow brick	05.00	0.10
	plaster	02.00	0.06
			Total: 0.22
<b>Interior door</b>	<b>material</b>	<b>U<sub>w</sub> (W/m<sup>2</sup>.K)</b>	
<b>Door</b>	Wooden door	05.00	

## A simplified 3D model for existing tunnel response to piles construction

**Bousbia Nawel, Messast Salah, Houssou Noura**

University of 20 Août 1955 - Skikda, Algeria  
Faculty of Technology, Department of Civil Engineering  
Laboratory LMGHU, University 20 Août 1955 - Skikda, Algeria  
e-mail: bousbia1101@yahoo.com

### Abstract

The construction and loading of deep foundations (piles) of high-rise buildings causes a considerable effect in terms of stresses and deformation and requires assessing their impact on the response of adjacent tunnels to deformations, particularly for pile foundations, which are often constructed in locations very close to existing tunnels. The execution process for piles structures generates displacements, stresses, and forces, which are transferred through the piles' soil surrounding a nearby existing tunnel. The research presented in this paper has led to a significantly improved understanding of pile-tunnel interaction problem. It is crucial for the analysis of the impact of the pile construction on an existing tunnel. The treated topic appears in a setting of an urban environment, where we construct numerous profound foundations, sometimes in contact or adjacent to a. In this paper, the response of the existing tunnel under constructed pile process is studied. Numerical modeling was carried out using Plaxis3D software in which the Mohr-Coulomb Model (MC) has been used for modeling, while the piles/ tunnels are modeled as a linear elastic material. Furthermore, a parametric study is conducted, and its cases are investigated. The displacements and the stresses generated on the tunnel lining decreases with the increase in relative distance between pile and tunnel (spacing), the location/length of the pile from the tunnel, the pile diameter, the number of piles. We have also identified two geometrical parameters of the tunnel: shape section and thickness lining which play a prominent role in the interaction between an existing tunnel and a new pile to excavate.

**Key words:** tunnel, piles, Mohr-Coulomb model, movements, finite element analyses

## 1 Introduction

Many big cities all over the world are using tunnels, either for transportation, storage, or telecommunication purposes. Due to the increase of using these tunnels and to augment the high-rise buildings constructed in the urban area, there is a significant interaction between these buildings and the adjacent tunnels, Therefore, it is important to study the interaction and effects between soil-tunnel-pile in the urban area.

This interaction is a complex problem in geotechnical engineering, where we find two main sorts of interaction problems.

- Tunnel traffic inevitably induces changes in stress and deformation in the ground, which could cause ultimate and serviceability problems to piles of structure. Hence, there is an effect of tunneling on nearby pile foundations.
- Bored piles inevitably induce changes in stress and deformation in the ground, which could cause ultimate and serviceability problems to an adjacent tunnel. Hence, there is an effect of pile foundations on the adjacent tunnel.

Several studies have been undertaken to understand the mechanisms of the soil–tunnel–pile interaction. Besides, many researchers presented an overview of the effect of tunnel excavation on existing nearby piles foundations [1-6]. However, a few studies have been performed on the reverse of the problem, i.e., the effect of piles foundations on an existing tunnel.

Deep foundations arrangement affects adjacent tunnels and becomes more significant when a tunnel is nearby the piles. This is because the piles are generally located in deep terrain levels, so they can be neighboring a tunnel. It is also important to study the influence of piles' operations on an adjacent tunnel in terms of additional forces/stresses and displacements of this tunnel to control the dangerous convergence of these tunnels.

When studying the effects of bored pile construction and pile loading on an existing tunnel using the Finite Element Method, there are many influential factors in the assessment process[7, 8, 9, 10].

Arunkumar et al. [11] investigated the effects of pile loading on existing tunnels embedded in cohesive soil using three-dimensional Finite Element Analysis carried out in ABAQUS.

This study aims to simulate numerically the interaction between new deep foundations (piles) and an existing tunnel in the urban area and to evaluate the effect of configuration/parameters of piles (location/depth) on the tunnel position. A 3D Finite Element Model with linear interface elements is modeled using the software Plaxis3D for the analysis of the response of the existing tunnel during the pile construction process.

## 2 Numerical model of the pile-tunnel interaction

Finite Element Analyses have been performed using the commercial Plaxis3D software. A tunnel has been designed specifically for the analysis of stress-strain behavior of the ground and structures around it. The program allows a three-dimensional finite element mesh to be generated, based on a repetitive geometrical cross-section. The cross-section was 100 m wide and 40 m deep and consisted of linear strain 15-node triangles. The groundwater level was set at the ground level.

In this study, we examined the stresses and displacements related to the changing geometrical pile parameter (the depth, the relative position, the spacing and the shape cross-section). It was assumed that tunnel is excavated and then the pile was constructed. The results were assessed to determine the effect of the construction of deep piles on an adjacent tunnel.

### 2.1 Numerical model definition

The grid size chosen to study the problem was 100 m×40 m. The tunnel is circular in cross-section with 10 m outer diameter  $D$  and 0.40 m thick concrete lining; the crown  $C$  of the tunnel was 13 m below the surface of the ground, i.e.,  $C/D=1,3$  (cover depth to tunnel diameter). The top 5 m of the grid were loam soil, and the rest was clay. A single pile, 28 m in

length with 1 m in diameter, was erected at a lateral distance of 8 m from the centerline of the tunnel (Figure1).

The displacement of the model was fixed in the x-direction in the walls and the y-direction at the bottom.

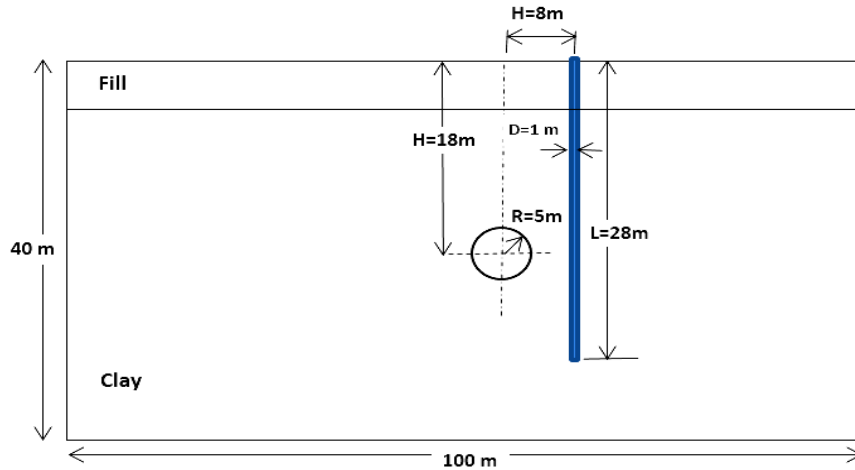


Figure 1: Single pile problem used in the numerical analysis in transversal section

## 2.2 Numerical model definition

The soil behavior was described by Mohr-Coulomb, through the elastic-plastic constitutive model and defined by the parameters listed in Table 1.

The tunnel (a circular section of diameter  $D = 10$  m) was modeled as a circular cavity. Full-face excavation of the pre-existing bored tunnel was considered with the lining supporting the tunnel immediately. The tunnel is planned to be constructed in homogeneous soil. The analysis is carried out using the linear elastic model for tunnel lining.

In this analysis, typical lining parameters of the tunnel were adopted. Table 2 summarizes the properties of tunnel lining. The behavior of the pile is assumed to be linear-elastic with Young's modulus  $E = 23\,500$  MPa and a Poisson's ratio  $\gamma = 0,25$ .

The length and width are equal to  $L_{pile} = 28$  m and  $d_{pile} = 100$  cm, respectively. The pile parameters are given in Table 3. Concrete piles and tunnels were used to simulate the same friction and behavior of concrete piles and tunnels in the field.

Table 1: Properties of the soil layers used in numerical simulations

Soil	Thickness $d$ (m)	Density $\rho$ (kN/m <sup>3</sup> )	Elastic Modulus $E$ (kN/m <sup>2</sup> )	Poisson Ratio $\gamma$ (-)	Cohesion (kPa)	Friction angle $\theta$ (°)
Loam	5	18	$1.5 e^4$	0.3	20	23
Clay	35	20	$2.6 e^4$	0.3	30	25

Table 2: Properties of lining tunnel's thickness (40 cm)

Material	Normal stiffness $EA$ (kN/m)	Elasticity modulus $EI$ (kN/m <sup>2</sup> )	$d$	$w$	$\gamma$
Lining	$1.4 e^7$	$1.867 e^5$	0.40	10	0.25

Table 3: Properties of piles (D = 100cm) used in numerical simulations

Material	Density $\rho$ (kN/m <sup>3</sup> )	Elastic Modulus $E$ (kN/m <sup>2</sup> )	$\gamma$
Pile's diameter (1 m)	25	$2,35 e^7$	0.25

### 3 Verification of tunnel-soil-pile interaction

A 3D numerical model is developed with Plaxis3D to predict the behavior of ground surface subjected to excavation simulation of the tunnel, and to envisage the behavior of tunnel lining induced by ground movement towards the excavation of the resulting deep foundations.

#### 3.1 Verification of tunnel soil interaction

The tunnel- induced vertical surface settlement is obtained by taking the difference between the surface settlement with the tunnel and without the tunnel [12, 13, 14].

The settlement of each tunnel is calculated according to Equation (1) and summed. The disturbance associated with tunnel construction changes the properties of the surrounding soil, and hence alters the effect of the subsequent tunneling operation through that zone of the soil. The surface settlements  $S$  above the single tunnel constructed in soft ground are usually assumed to follow an inverted Gaussian curve, i.e.:

$$S = S_{max} \exp(-x^2/2i^2) \quad (1)$$

Where  $S_{max}$  is the maximum settlement (over the tunnel axis),  $x$  is the orthogonal distance from the tunnel axis, and  $i$  is the width of the settlement trough [15].

The surface settlement is predicted with elastic-plastic approach and it is observed from the results, showing that the maximum surface settlement is 8.15 mm, as shown in Figure 2.

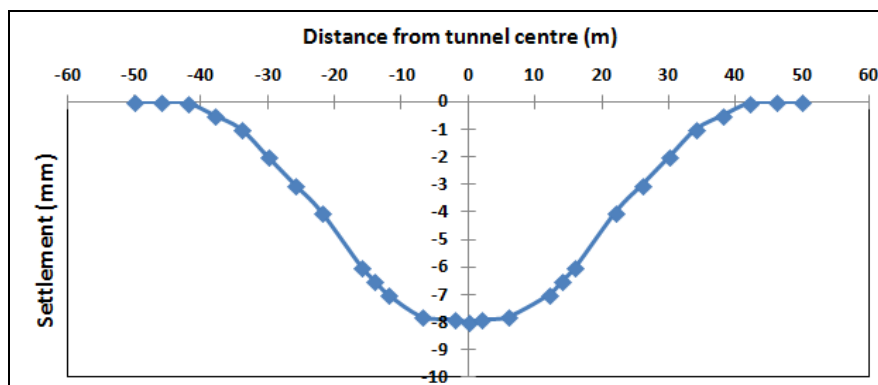


Figure 2: Surface settlement trough for the tunnel in the transverse section



The global displacements of the tunnel lining may be expressed as the movements of the tunnel crown. The crown moved downwards by approximately 37 mm and the invert moved upwards by approximately 58 mm. The diametrical tunnel distortions were less than 3.3 mm around the entire tunnel circumference, and the global movements were approximately 58.73 mm in the y-direction (vertical) and 3.3 mm in the x-direction.

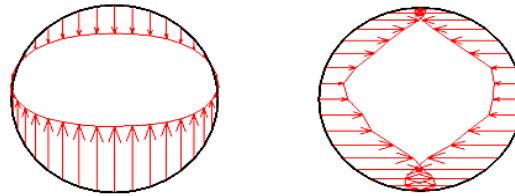


Figure 3: Displacements of the tunnel lining due to the tunnel excavation in the transverse section [Curves program screen from Plaxis3D]

Figure 3 gives the contours showing deformation of the circumference of the tunnel lining's section due to the excavation tunnel in the transverse section. These global displacements (vertical and horizontal) cause the diametrical shrinking of a tunnel section, so the global displacements were about 59 mm in the y-direction.

The internal efforts and stresses contours (forces, the bending moment, the torsion moment, and the shear stresses) induced in the lining tunnel due to tunnel's construction before interaction with the new pile, are shown in Table 4.

Table 4: The internal efforts and stresses induced in the lining tunnel before interaction with the new bored pile [Curves program screen from Plaxis3D].

Axial forces = -1.13 kN/m	Bending moments = 258.17 kN.m/m	Torsion moment = - 26.54 kN.m/m	Shear stresses = - 57.15 kN/m <sup>2</sup>

### 3.2 Verification of pile-soil interaction

A 3D numerical model is developed with Plaxis3D to predict the behavior and the response of soil during the drilling of a circular single pile, because the piles construction process can cause significant movements of the adjacent soil. Kahyaoglu et al. [16] analyzed numerically with the aid of the Finite Element Method, the piles subjected to lateral soil movement to evaluate the loads acting on the passive pile and to determine the behavior of soil around piles due to the soil mechanism. Figure 4 presents the deformation of the pile relative to pile head load. The secure load corresponding to the 12.6 mm settlement predicted by the analysis is 4500 kN.

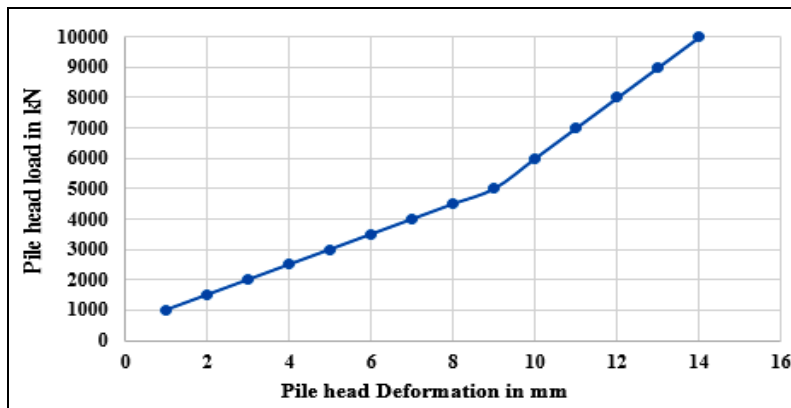


Figure 4: Deformation of the pile relative to the pile head load

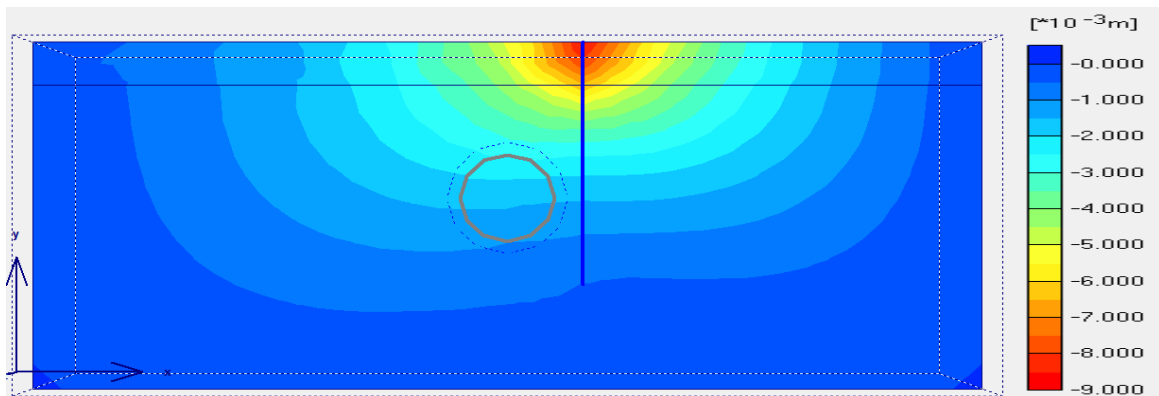


Figure 5: Deformation of the head pile-contours [Curves program screen from Plaxis3D].

Figure 5 shows the variation of the horizontal displacement vectors with depth in the piles at the interface element between the soil and pile zone. We remark that the maximum displacement deformation in soil occurs at the pile's top (about 9 mm).

#### 4 Modeling of tunnel-soil-pile interaction

The effect of the piles' construction on an existing tunnel lining is a common interaction problem in an urban area that can be solved using the Finite Element Method with Plaxis3D. The finite element analysis is performed in two stages. The first step concerns the construction of the tunnel, which exists before the construction of the pile foundations, modeled through the deactivation of soil elements situated in the excavated zone and activation of the lining elements. The second step concerns the construction of the single pile, which exists near the tunnel.

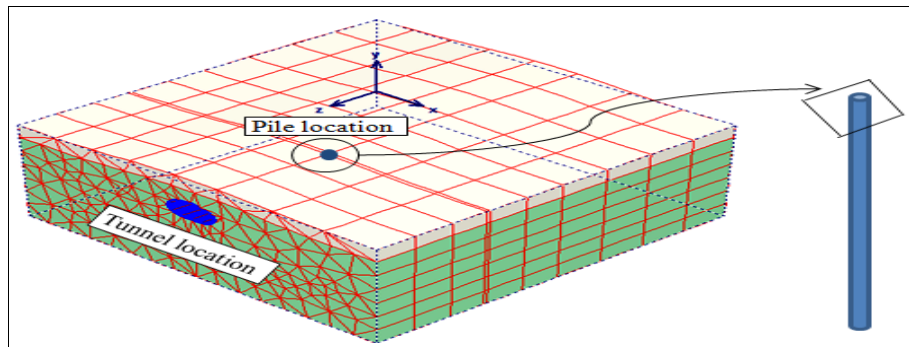


Figure 6: 3D view of the simulation model

Figure 6 shows the typical 3D model of the tunnel-soil-pile system. The problem associated with piles adjacent to the urban tunnel has been examined with a 3D model simulation using the Finite Element Method. The tunnel is circular in cross-section with a 10 m outer diameter; the crown of the tunnel is 13 m below the surface of the ground. A single pile, 28 m in length with 1 m in diameter, was erected at a lateral distance of 8 m from the centerline of the tunnel.

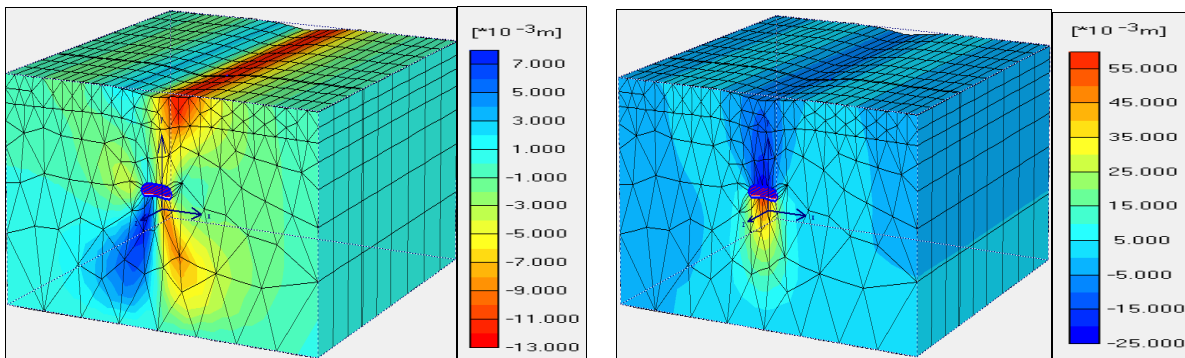


Figure 7: Horizontal and vertical displacement contours around the tunnel after the pile's construction [Curves program screen Plaxis3D].

The typical horizontal and vertical displacements fields from Plaxis 3D, obtained after pile loading in soil mass in x- and y- directions are shown in Figure 7. According to this figure, we determine the extreme horizontal displacements  $U_x$  due to the excavation in the free soil of adjacent tunnel, giving a value of 12 mm, and the extreme vertical displacements  $U_y$  with a value of 57 mm.

## 5 Analysis results

The effect of the pile-bored construction on an adjacent tunnel is assessed in terms of the global displacements and the internal forces that build up in the lining during the pile's excavation.

Various numerical analyses have been performed on the tunnel lining with a presence of a single nearby pile. Some conclusions can be made from the results as follows:

### 5.1 Effect of the position of piles concerning the tunnel

Piles of varying locations are investigated in the soil model [17]. In this model study, six different pile spacing configurations (locations)  $S$  ( $S1 = 6.5$  m;  $S2 = 7.5$  m;  $S3 = 8$  m;  $S4 = 10$  m;  $S5 = 12$  m and  $S6 = 20$  m) are shown in Figure 8.

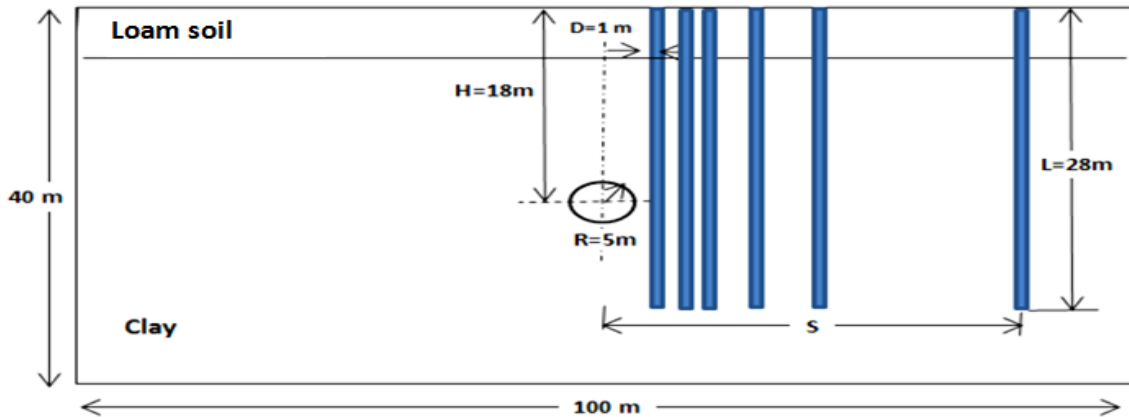


Figure 8: Different positions of a single pile relative to the axis of the tunnel

The effect of the relative position between tunnel and pile on an adjacent tunnel lining regarding the displacements and the internal forces (axial forces, the bending moment, the torsion moment, and the shear stresses) induced by single pile's excavation can be noticed in Figures 9 and 10.

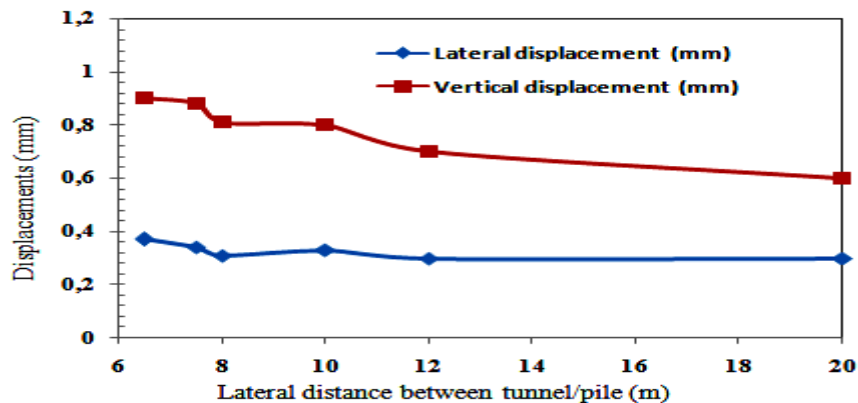


Figure 9: Lateral and vertical displacements relative to the distance between the tunnel and single pile

Figure 9 plots the lateral displacement in the x-direction and the vertical displacement in the y-direction due to pile excavation at the lining of the adjacent tunnel relative to the distance between the existing tunnel and the single pile following six configurations of pile bore. Results of this study show that pile spacing has some effect on the tunnel lining response (displacements). As expected, a high gradient of displacements in tunnel lining existed for distances of less than 10 m from the tunnel. The largest displacements occurred closest to the tunnel ( $S = 6.5$  m).

The horizontal displacement at the tunnel lining was between 0.3 mm and 0.37 mm whereas the vertical displacement at the tunnel lining was between 0.6 mm and 0.9 mm. Higgins et al. [18] predicted distortions of the tunnel due to pile construction of no more than 1 mm.

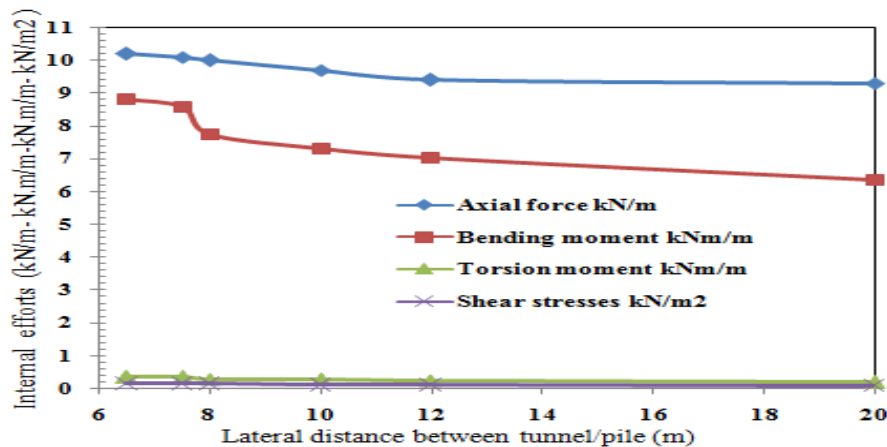


Figure 10: Internal efforts and stresses in the tunnel lining relative to the distance between tunnel and pile

The profiles of the internal efforts and the stresses induced in the tunnel lining due to the pile construction are given in Figure 10. The results of this study illustrate that the pile spacing has an insignificant effect on the tunnel lining response, especially, the torsion moment and the shear stresses. As expected, whereas there is some effect on the tunnel lining regarding the force and bending moment (Figure 10) a high gradient of the force and bending moment existed for distances from the tunnel of less than 10 m. The largest displacements occurred closest to the tunnel ( $S = 6.5$  m). When the distance between the tunnel and the pile increases, there is a decrease of the displacements and the internal efforts and the stresses induced in the lining of the existing tunnel. We studied the effect of the pile construction distance on the continuous lining of the tunnel. We can say that there are a few effects on an existing tunnel lining due to pile construction (insignificant effects due to the diminutive pile excavation comparable to the size of the tunnel). However, an interaction exists between the existing tunnel and the pile.

## 5.2 Influence of pile diameter

The pile diameter is an important parameter in transferring the load to the soil [19]. The cross-sectional dimension of the pile influences adjacent tunnel lining regarding the displacements and the internal efforts (forces, the bending moment, the torsion moment, and the shear stresses) induced by the single pile's construction (shown in Figures 11 and 12).

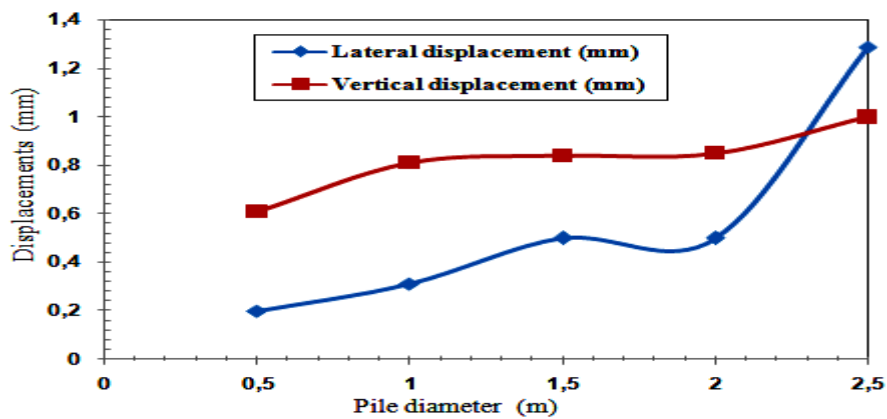


Figure 11: Lateral and vertical displacements in the tunnel lining relative to the pile diameter

Figure 11 shows the lateral and the vertical displacements induced in the tunnel lining due to the pile’s construction relative to the pile’s diameter. Five different pile diameters  $d$  were tested, ( $d = 0.5$  m;  $d = 1$  m;  $d = 1.5$  m;  $d = 2$  m and  $d = 2.5$  m). The results of this study show that the pile diameter has a significant effect on the tunnel lining response (displacements). The maximum value of displacements in the tunnel lining arises when the pile with a diameter of 2.5 m is excavated, while the minimum value was observed at the pile diameter equal to 0.5 m. We can conclude that the size of the drill significantly affects the exiting adjacent tunnel.

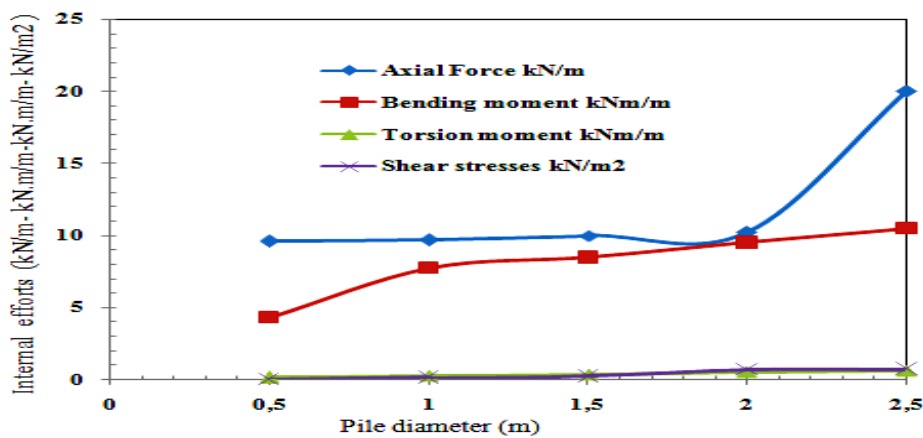


Figure 12: Internal efforts and stresses in the tunnel lining relative to the pile diameter

Figure 12 shows that the pile diameter (dimension) has significant effects on the tunnel lining response, regarding the axial force and the bending moment, whereas there is an insignificant effect on the tunnel lining regarding the torsion moment and shear stresses. It is very clear that the diameter of the bored pile plays a large role in the tunnel response in terms of axial force.

Generally, when the pile diameter increases, there is an increase of the lateral and vertical constraints in the space separating the tunnel and single pile and that is the reason for the increase of displacements and the internal efforts induced in the tunnel lining.

### 5.3 Effect of pile length

To study the effect of pile length on the tunnel response [20], six cases with different pile lengths varying from 13 to 38 m have been considered. In these cases, the pile lengths  $L$  ( $L = 13$  m;  $L = 18$  m;  $L = 23$  m;  $L = 28$  m;  $L = 33$  m and  $L = 38$  m) were analyzed. For the analysis presented throughout this part, we keep the lateral distance between the pile and the centerline of the tunnel ( $x = 8$  m) and the pile diameter  $d_{pile}$  of 1 m.

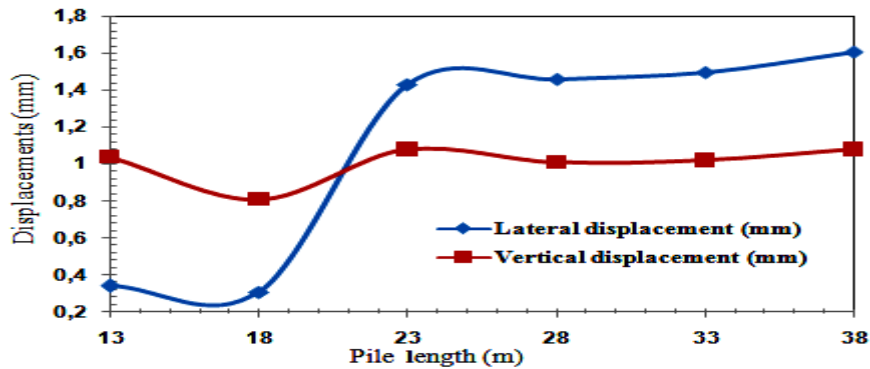


Figure 13: Lateral and vertical displacements in the tunnel lining relative to the length of the pile

The lining of the existing tunnel response in terms of the lateral and the vertical displacements depends on the pile length, as is shown in Figure 13.

According to this Figure, we remark that the most values of displacements at the tunnel lining are appearing when using the pile length of more than 18 m.

When the pile's excavation is 13 m in length, we reach the crown of the tunnel, where the global displacements surrounding the tunnel move downwards. Starting from 18 m and more, the displacements surrounding a tunnel move upwards, hence, there are more movements that affect the tunnel. The maximum values occur with the pile length equal to 38 m.

The largest displacements occurred for the pile length 38 m. The horizontal displacement at the tunnel lining was equal to 1.61 mm whereas the vertical displacement at the tunnel lining was equal to 1.08 mm.

The profiles of the internal efforts and the stresses induced in the tunnel lining due to the pile construction at different pile lengths are given in Figure 14.

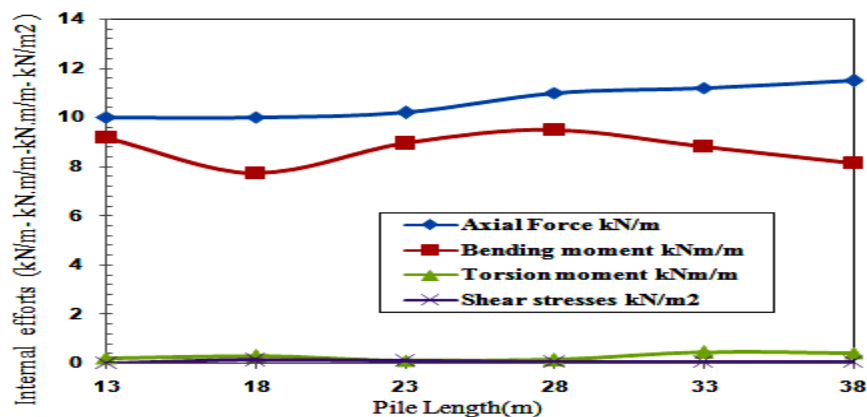


Figure 14: Internal efforts and stresses induced in the tunnel lining relative to the pile length

In Figure 14, we observe clearly that there is an insignificant interaction between tunnel and pile in terms of the torsion moment and the stresses induced in the tunnel lining. There is a significant interaction between tunnel and pile in terms of the axial force and the bending moment (Figure 14). The maximum values of internal efforts and the stresses appear when digging the pile with the length of 38 m.

In general, when the length of the pile increases, there is an increase of the lateral and vertical constraints in the space separating the tunnel and single pile and that is the reason for the increase of displacements and the internal efforts in the tunnel lining.

#### 5.4 Effect of the pile configurations (number of piles)

The effect of the number of piles on the stability of the existing tunnel lining has been investigated [21]. We are interested to examine the effects of piles number on lining of the existing tunnel and its response in terms of the displacements, the internal efforts, and the stresses. The results of this study are given in Figures 15 and 16.

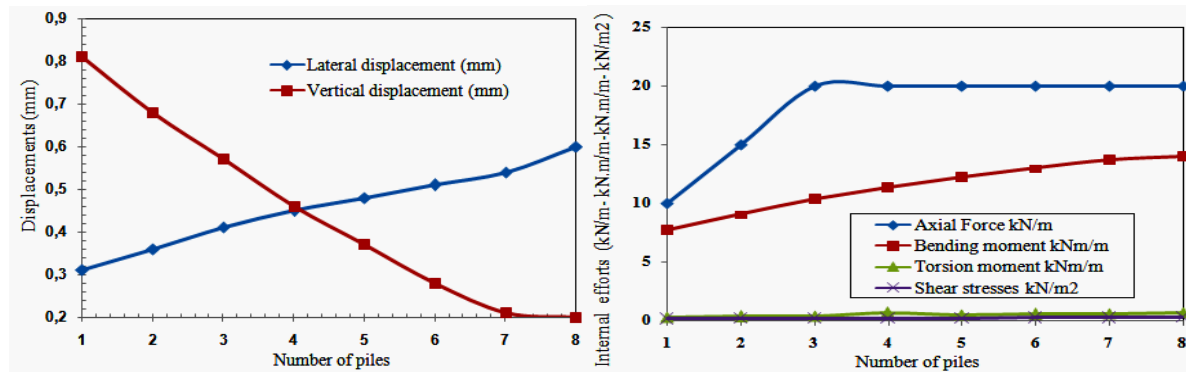


Figure 15: Displacements relative to piles number

Figure 16: Internal efforts relative to piles number

It can be seen from Figures 15 and 16 that the displacement profiles, the internal efforts, and the stresses induced in the lining of the existing tunnel due to the construction of one or more piles, calculated numerically, are significantly affected by the number of piles excavated. We note that the lateral displacement values are opposite to the vertical displacement values (Figure 15). Therefore, when the number of piles excavated increases, there is an increase of the lateral constraints and a reduction of the vertical constraints in the space separating the tunnel and piles and that is the reason for the increase of lateral displacements and the decreases of vertical displacements. For the internal efforts and shear stresses induced in the tunnel lining (Figure 16), we remark that an increase in the number of the piles, results to the increase of internal efforts and stresses.

In few words, more piles result in more movements, and a consequent instability of soil surrounding the existing nearby tunnel.



## 6 Tunnel cross-sectional and lining thickness effect

### 6.1 Tunnel cross-sectional effect on interaction between pile-tunnel

Concluding from the numerical analysis executed on the interaction between pile and tunnel, we judge that there is a significant effect of pile foundation construction on the tunnel lining; an interaction exists between the existing tunnel and the pile construction.

Hence, the question that imposes here is, does the geometry of the tunnel do have a role in this interaction? To answer this question, three different shapes of the tunnel are examined. The first tunnel is circular with a diameter of 10 m, the second is square with sides of the length of 9.10 m, and the last tunnel is elliptical (major axis,  $a = 11$  m, minor axis,  $b = 9$  m).

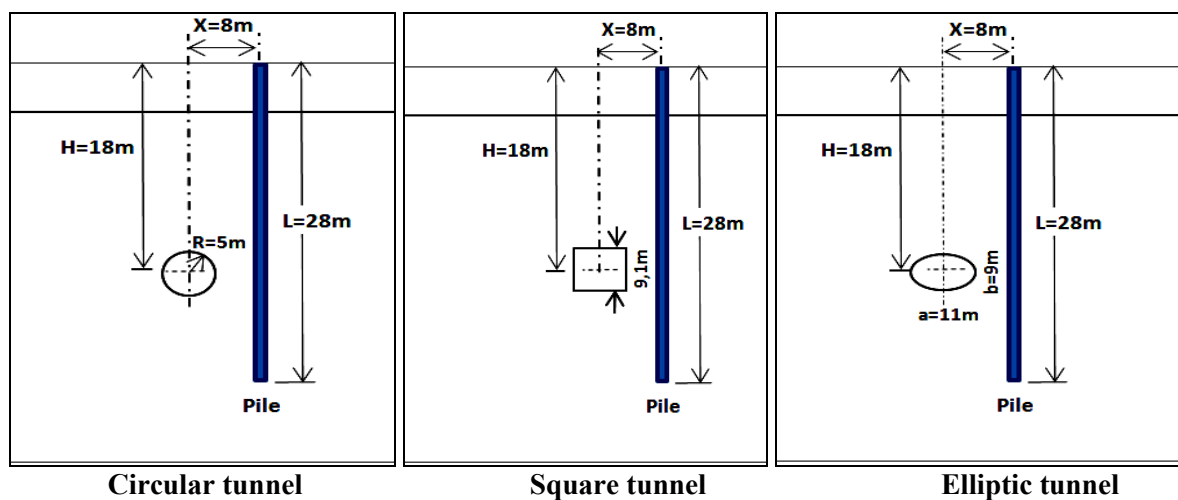


Figure 17: The general geometry of each tunnel case

It should be noted that the pile cross-sectional area is the same for all shapes of the tunnel. In the three cases, the displacements, and the internal efforts (axial force, bending moment, torsion moment) and stresses induced in the lining of tunnel case were studied, as is shown in Figure 18 and 19.

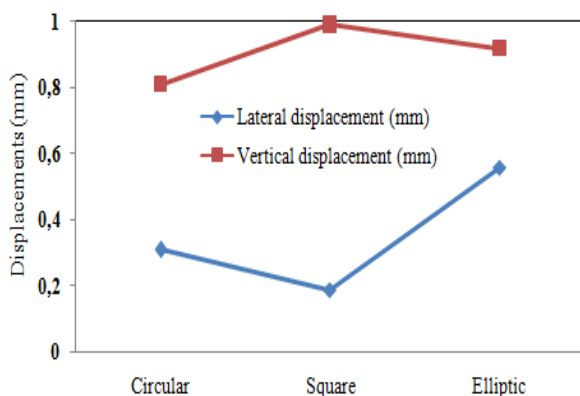


Figure18: Displacements in the lining relative to different shapes of the tunnel

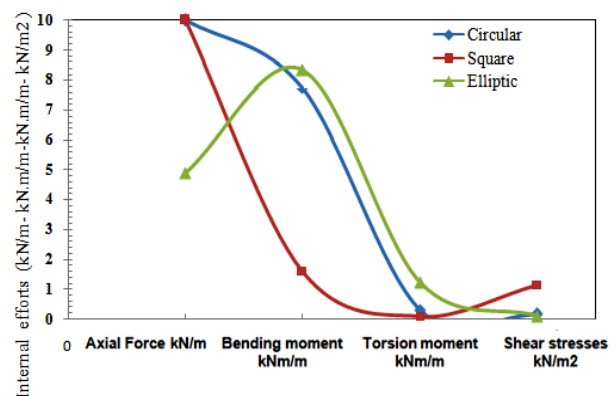


Figure19: Internal efforts and stresses in the lining relative to different shapes of the tunnel

In the case of the circular tunnel (reference case), the response of the tunnel lining to the pile construction is different from those in square and elliptic tunnels, either from displacements or from the internal efforts as shown in Figure 18 and 19. The results of the different cases of tunnel shapes show that the square tunnel suffers from high vertical displacement (1.0 mm) more than circular and elliptic shapes. The elliptic tunnel suffers from high lateral displacement (0.58mm) more than circular and square shapes (Figure 18). In the case of square shape, the response of the tunnel lining is identical to that of the circular shape in terms of axial force, which equals 10 kN/m, while in elliptic shape it is 5 kN/m (Figure 19). The maximum bending moment in elliptic shape is 8.5 kN.m; while in circular and square shapes are 7.74 kN.m and 1.62 kN.m, respectively. The same goes for the torsion moment, the maximum value appears when using the elliptic shape.

There is a significant effect on the lining of the existing tunnel in terms of the shear stresses due to the construction of a new pile, in the case of the square tunnel. Through this study, we confirm that the shapes of tunnels play a prominent role in the interaction between the pile and the existing tunnel. Generally, the elliptical tunnel may cause high movements of soil compared to the square and the circular tunnels, which were minimal in the circular tunnel. The elliptical tunnel has the maximum values of lateral displacement, bending moment, and torsion moment, while the square tunnel has the maximum values of vertical displacement and shear stresses. Finally, for less interaction between the pile and the existing tunnel, we recommend that the shape of the tunnel be circular.

## 6.2 Effect of lining thickness on the interaction between pile -tunnel

The lining flexibility of the existing tunnel plays an important role in the value of displacements and internal efforts after interaction [22, 23]. In this study, six values of lining thickness were adopted for the tunnel, i.e., 200 mm in thickness (represents very flexible lining), 300 mm and 400 mm (represent relatively stiff lining), 500 mm (represents stiff lining), 600 mm and 700 mm (represent very stiff lining). For each value of lining thickness of the tunnel, the lateral distance relative to the pile bored is fixed to 8 m. The influence of the lining thickness of the tunnel on the interaction between the pile and the adjacent tunnel is assessed in terms of the global displacements of the tunnel lining and the forces, moments, and stresses that build up in the lining during the pile's excavation. The results of this study are given in Figures 20 and 21.

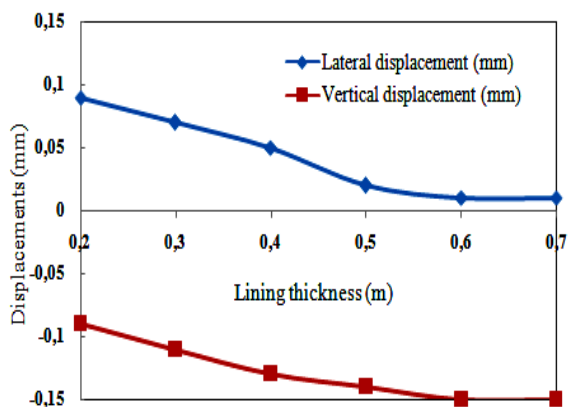


Fig 20: Displacements relative to the lining thickness

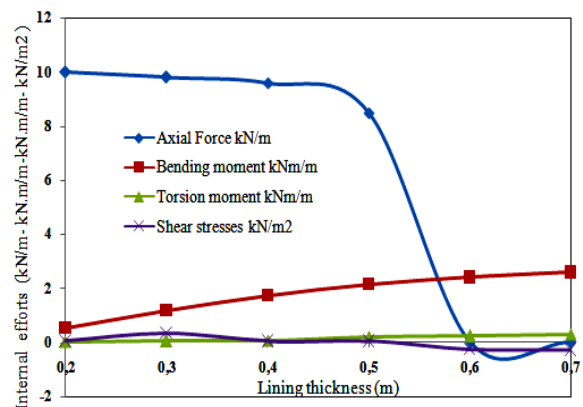


Fig 21: Internal efforts, stresses relative to the lining thickness

The first analysis shows that the lateral displacements induced in the tunnel lining and the internal efforts are increased after the bored pile construction. The vertical displacements are decreased after the pile construction. There is an interaction between the existing tunnel and the pile construction. It can be seen from Figure 20 that for the stiff and very stiff lining, the interaction between the pile and the adjacent tunnel is relatively negligible. The effect of pile construction on the tunnel lining is insignificant for the stiff and very stiff lining in terms of the lateral displacements (the increase is inconsiderable).

For the vertical displacements, there is a significant interaction between the pile and the existing tunnel for the stiff and very stiff lining (the decrease is considerable)

It can be seen from Figure 21 that for the stiff and very stiff lining, the interaction between the pile and the tunnel is relatively considerable. There is a significant effect of the pile construction on the tunnel lining for the stiff and very stiff lining in terms of the axial force and bending moment. On contrary, there is an insignificant interaction between the pile and the tunnel, whatever is the thickness of the tunnel lining. So, the thickness of the tunnel lining has an important role in the interaction between the pile and the existing tunnel.

## 7 Conclusion

The pile-tunnel interaction is a three-dimensional problem. In this research, Plaxis3D software has been used to predict the response of an existing tunnel under the effect of an individual bored pile in the urban area and to evaluate the variation of displacements, the internal efforts, and stresses induced in the lining of the existing tunnel due to the pile construction. A tunnel is located adjacent to the pile construction; a pile is installed around the tunnel at the separation distance of 8 m from the centerline of the tunnel. The influence of bored piles on existing tunnels is a common problem, and the study presented in this article has led to a significantly improved understanding of the interaction problem. It has been confirmed that there are many influential factors in the appraisal of the influence of pile construction on an adjacent tunnel lining. The following conclusions were drawn from this study:

- The construction process for the urban pile foundations, generates instability of the surrounding soil of the piles.
- A significant change in the forces, displacements, bending moments, and the stress build-up in the tunnel lining during the deep foundations' excavation on the side of the tunnel where the pile is located results in an interaction between the existing tunnel and the new pile.
- When the three geometrical parameters of piles (relative location, length, and diameter) increase, there is an increase of the lateral and vertical constraints in the space separating the tunnel and the single pile, resulting in the higher displacements, internal efforts, and stresses in the tunnel lining.
- Pile configuration: If the number of the excavated piles increases, there is an increase of the lateral displacements and a reduction of the vertical displacements. Also, the increase in the number of piles will cause an augmentation of the axial forces and bending moment induced in the tunnel lining.
- The two geometrical parameters of the tunnel (shape and thickness) play a prominent role in the interaction between the pile and the existing tunnel.

Elliptical tunnels may cause high movements in soil compared with square and circular

tunnels, with the minimum in circular tunnels. Therefore, for less interaction between the pile and the existing tunnel, we recommend that the shape of the tunnel be circular. Also, the thickness of the tunnel lining plays an important role in the interaction between the new pile and the existing tunnel. For a tunnel of stiff and very stiff lining, the interaction between the bored pile and the adjacent tunnel is relatively negligible.

The effects of piles closest to the tunnels, particularly in terms of internal efforts' changes and diametric deformations of the tunnels are considerable and remarkable.

## References

- [1] Chen, L. T., Poulos, H.G. and Loganathan, N. (1999). Pile response caused by tunneling. *Journal of Geotechnical and Geoenvironmental Engineering*. ASCE 125(3), 207-215.
- [2] Coutts, D. R. and Wang, J (2000). Monitoring of reinforced concrete piles under horizontal and vertical loads due to tunneling. *Tunnels and Underground Structures*. 514- 546.
- [3] Loganathan, N., Poulos, H.G. & Xu, K.J. (2001) Ground and pile-group responses due to tunnelling. *Soils and Foundations* 41(1), 57-67.
- [4] Lee, G.T.K. and Ng, W.W.C. (2005) Effects of advancing open face tunnelling on an existing loaded pile. *Journal of Geotechnical and Geoenvironmental Engineering*. 131(2), 193- 201.
- [5] Cheng, C. Y., Dasari, G.R., Chow, Y.K. and Leung, C.F (2007). Finite element analysis of tunnel-soil-pile interaction using displacement controlled model. *Tunnelling and Underground Space Technology* 22(4), 450- 466.
- [6] Surjadinata J, Hull T S, Carter J P, Poulos H G (2006). Combined finite- and boundary-element analysis of the effects of tunneling on single piles. *International Journal of Geomechanics* 6(5), 374–377.
- [7] Emilio Bilotta, Gianpiero Russo, Carlo Viggiani (2008). Numerical analysis of piles to reduce ground movements induced by shallow tunnelling. *Rivista Italiana di Geotecnica* 2, 24-30.
- [8] Nahla M. Salim, Sherine Jafaar Lafta (2017). The Impact of Driving and Loading Piles on Existing Tunnel. *Imperial Journal of Interdisciplinary Research (IJIR)*, 3(7), 262–270.
- [9] Nahla M. Salim, Sherine Jafaar Lafta (2020). Effect of a driven pile on an existing tunnel. *Journal of Engineering and Sustainable Development*. 24(1), 94–109.
- [10] Yao J, Taylor R N, Mc Namara M A, (2006). The effects of bored pile installation on existing tunnels. Proc of 6<sup>th</sup> International conference on Physical modelling in Geotechnics. Hong Kong
- [11] Arunkumar, S. Ayothiraman, R (2010). Effect of Vertically Loaded Pile on Existing Urban Tunnel in Clay. Indian Geotechnical Conference, 16–18.
- [12] Felix Christian Schroeder (2002). *The influence of bored piles on existing tunnels*. PhD thesis, Department of civil and Environmental Engineering, University of London.
- [13] Mroueh, M. & Shahrouh, I. (2002). Three-dimensional finite element analysis of the interaction between tunneling and pile foundations. *Int. J. Numer. Anal. Meth. Geomech.* 26, 217-230.
- [14] Loganathan, N. & Poulos, H.G. (1999) Tunnelling induced ground deformations and their effect on adjacent piles. Proc. 10 the Australian Tunnelling Conference, (241-250). Melbourne.
- [15] Barakat, M.A (1996). *Measurements of ground settlement and building deformations due to Tunnelling*. PhD. thesis, Imperial College, University of London.
- [16] Mehmet Rifat Kahyaoglu, Gökhan İmançlı, Okan Önal, and Arif S. Kayalar (2012). Numerical Analyses of Piles Subjected to Lateral Soil Movement. *KSCE Journal of Civil Engineering* 16(4), 562-570.
- [17] M. Wasif Naqvi, Mohd. Ahmadullah Farooqi (2018) Effect of Piled Structures on the Tunnel Stability for Different Pile-Tunnel Configurations. ISGTI 2018. 2018: Delhi, India.
- [18] Higgins, K.G., Chudleigh, I., StJohn, H.D. & Potts, D.M. (1999) An example of pile tunnel interaction problems. Proc. Int. Symp. on Geotechnical Aspects of Underground Construction in Soft Ground, (99-103). Balkema.
- [19] Mohammed Y. Fattah, Nahla M. Salim and Asaad M.B. Al-Gharrawi (2018). Effect of Pile Diameter on the Behavior of Fully Plugged Pipe Pile Group in Sandy Soil. 14th ASEC conference in Jordan. 2018 (12-15): Jordan University of Science & Technology.

- [20] Xu Huang, Helmut F. Schweiger and Hongwei Huang (2013). Influence of Deep Excavations on Nearby Existing Tunnels. *International Journal of Geomechanics ASCE* (13) 17-18.
- [21] Nahla M. Salim, Sherine Jafaar Lafta (2020). The Effect of Group of Piles on Existing Tunnel. IOP Conf. Series: Materials Science and Engineering 737. DOI:10.1088/1757-899X/737/1/012093.
- [22] Hefny, A.M., Chua, H.C. and Jhao, J. (2004) Parametric studies on the interaction between Existing and new bored tunnels. *Tunn. Undergr. Space Technol* 19, 4-5.
- [23] M. Karakuş, R.J. Fowell (2002). Effects of lining thickness on settlement and hoop stress for a tunnel driven in soft ground. The 6<sup>th</sup> Regional Rock Mechanics Symposium. (299-304).

## Experimental and numerical study of the behavior of a stone column subject to the loading effect

Haouam Houda<sup>1</sup>, Messast Salah<sup>1</sup>

<sup>1</sup>LMGHU University August 20, 1955 SKIKDA, LMGHU University August 20, 1955 SKIKDA  
e-mail: djeffalhouda802@gmail.com, msalah2007msalah@gmail.com

### Abstract

The realization of engineering structures in compressible sites, requires in-depth geotechnical reconnaissance, as well as a study of the mechanical behavior of the soil, in order to adapt suitable soil improvement solutions. This is the case with the Annaba viaduct in Algeria, where it was found during the site survey that the soil is poor and very compressible. The foundations in these soils eventually pose the problem of their low bearing capacity and significant settlement. This, therefore, leads to the choice of reinforcement techniques. Among the many methods of improving soils, we have selected the stone column technique. The object of our article is to study the behavior of these columns, in terms of settlement and, through the loading tests on real site, we have found out that the intermediate columns are stiffer and more confined than the bank columns and the percentage reduction in settlements of these two types is important. Then, this experimental study is validated by the Plaxis 2D software, where the configurations are studied to find the best model that approximates the real behavior of the reinforced soil.

**Key words:** stone column, mechanical behavior, loading, settlement, numerical modeling, reduction of settlements

## 1 Introduction

Several studies are done on the behavior of stone columns, but few researchers have studied their behavior in a real site, citing [1-8], etc. However, quite a few researchers who have studied the behavior of these inclusions using digital software, such as [9-14], have confirmed the effectiveness of stone columns. They consolidate the soil and contribute to reducing settlement. To confirm this, a real study is made on a new construction site. This is the case of the access ramps to the Annaba viaduct in Algeria, from where it was found that the soil is very compressible, so the reinforcement of the soil by the stone columns was the effective solution to enhance the properties of the soil. In our case, we are interested in the mechanical behavior of stone columns in terms of settlement due to the loading effect of the column head, using the in-situ test called the plate test or loading test. However, the digital component has been incorporated as well, using the Plaxis 2D V8 digital software, to validate the experimental results in order to approximate the reality as close as possible.

## 2 Experimental component

### 2.1 Location and geological and geotechnical survey of the structure

The structure is located at the southern exit of Annaba. It is located near a 468 meters-long viaduct and ends with two overpasses, generating two railway beams, to the North and the South. This structure is connected to the road, by two access ramps made of significant embankments of variable height (max height 6 m). The whole structure rests on mediocre soil which requires a specific geotechnical study.

This called for carrying out soundings, performing laboratory tests and in situ tests, namely the static and dynamic penetrometer, pressuremeter tests, the CPT, and laboratory tests on core samples taken during on-site soundings. We are focused in this study on the soundings carried out on the access ramp on the south side of the structure. These soundings allowed us to know the different layers of the soil, their nature and thickness (from top to bottom), as well as their physical and mechanical characteristics. The characteristics of the soil are the following:

Level 0. Embankments: This is the first layer, consisting of embankments, approximately 3 m thick.

Level a. Soft sandy clays: This layer consists of a plastic sandy clay of gray color, of very soft consistency, located under the embankments, with a thickness of 6 m.

Level b1. Loose clay sands: This is a level of clay sands, moderately loose compactness, 3 m thick).

Level b2. Compact clay sands: Under the previous layer, we find clay sands of moderately dense compactness, 11.5 m thick.

Level c. Gray plastic clays: This is a layer of greenish-gray clay, with higher or lower plasticity and a solid consistency, its thickness is 3.5 m. Table 1 summarizes the geotechnical parameters of the different soil levels.

Table 1: Summary of field parameters

Levels	Friction angle $\varphi$	Cohesion $C$ [kPa]	Wet density $\gamma$ [kN/m <sup>3</sup> ]	Dry density $\gamma_d$ [kN/m <sup>3</sup> ]	Young's modulus $E$ [MPa]
0	25°	0.0	17	15	1
a	25°	0.0	17	15	2
b1	30.5°	0.0	19	16	8
b2	32.5°	0.0	19	16	25
c	28°	5.0	20	17	10

Among the in-situ tests carried out, is the pressuremeter test, this test gave the following results (see Table 2):

Table 2: Results of pressuremeter tests

Coast (depth) [m]	Creep pressure $P_f$ [bar]	Limit pressure $P_l$ [bar]	Pressuremeter module $E_m$ [bar]	$E_m/P_l$ [-]	Soil type
2	4.2	8.4	88	10	Compressible soil
4	2.1	4.0	15	3	
6	2.2	4.4	24	5	
8	2.3	4.6	15	3	
10	3.5	7.1	35	4	
12	6.9	13.8	64	4	
14	6.6	12.0	48	3	
16	7.4	14.8	98	6	
18	10.3	20.6	151	7	
20	10.7	16.4	59	3	
22	11.8	23.8	159	6	
24	13.2	26.5	309	11	

According to fascicle No. 62, Title V [15], the findings confirm that we are in very compressible terrain, therefore, this soil requires a reinforcement technique to increase its lift and improve its characteristics. Among the solutions considered, the realization company chose the consolidation of the ground by stone columns, because of its economic side.

According to the analytical calculation method of Priebe [16], the company adopted the diameter of the columns of 0.80 m, their depth is 9 m, spaced from each other by 2 m, with a staggered distribution. The number of columns carried out under the access ramp on the south side is 2111. The columns are constructed in a wet way (Figure 1).



Figure 1: Realization of a wet stone column

To confirm the enhancement of the soil, tests must be carried out after the completion of the columns. Three loading tests were carried out, distributed as shown in Figure 2.

The loading test is composed of a hydraulic cylinder (see Figure 3), the diameter of the distribution plate is 0.80 m, the settlements are measured at 4 points of the plate using



comparators (precision indicators 100<sup>th</sup> of a millimeter). Each loading level is controlled employing a pressure gauge, the service load to be tested is  $Q_s = 9.79$  t, the maximum load is equal to 150% of  $Q_s$ , a constant load is ensured for each level. The load cycle and stages follow the control criteria of standard ASTM D1 143, section 5.6.

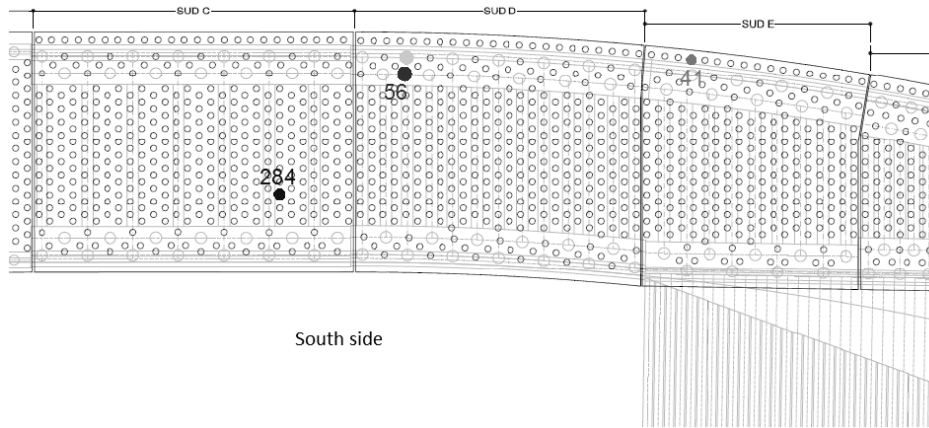


Figure 2: Distribution of loading tests (plan view)

Figure 3 shows the picture of the site loading test:



Figure 3: Loading test

## 2.2 Results and interpretation

The results found through the stone column loading test, allowed us to plot the evolution curves of the settlements as a function of the loading stages, as well as the reduction curve of the settlements of the middle column and the column adjoining the pile. This allowed us, to plot the reduction curve of the settlements of the middle column and the column adjoining the pile compared to the edge column, as a function of loading (Figures 4 and 5 successively).

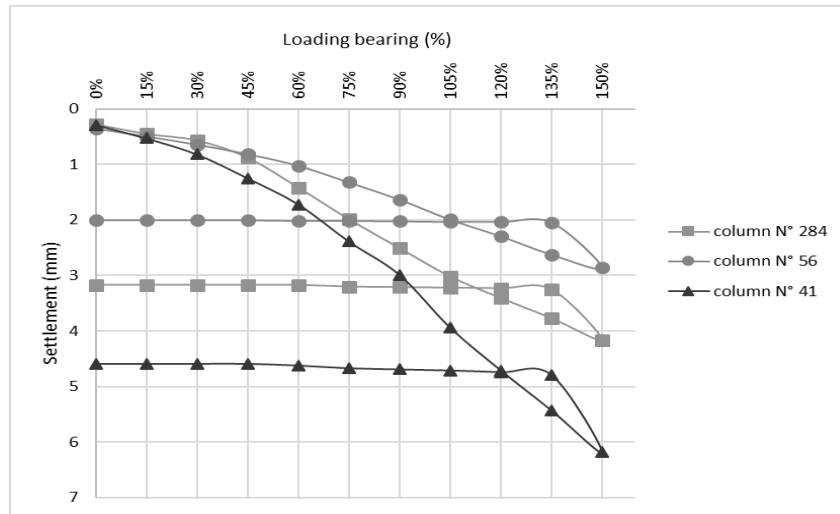


Figure 4: The evolution of settlements due to loading and unloading of columns

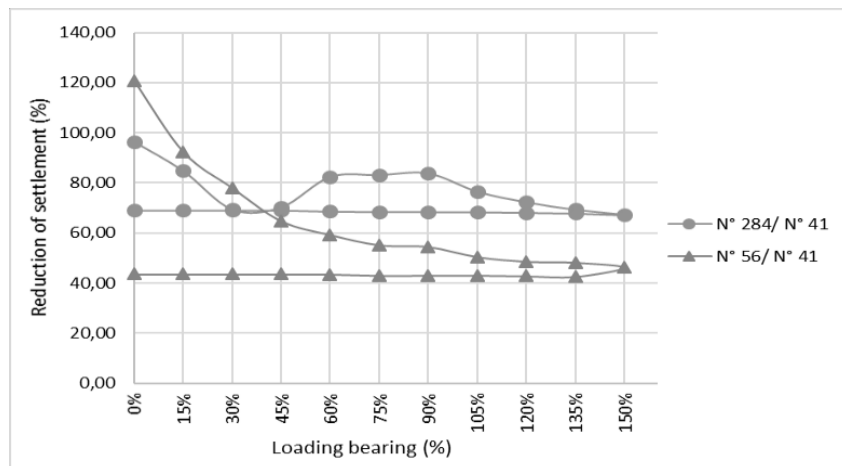


Figure 5: Reduction of settlements of the middle column and the column adjacent to the pile compared to the edge column

In Figure 4, we see that up to the level of 150% of the applied load, the curves are almost linear. On the other hand, in the unloading phase, the settlement decreases until the deformations stabilize, which explains that the columns, did not undergo rupture, which confirms the mode of elastoplastic deformation. Also, the settlements are more or less tight which confirms the good containment of the materials. To be precise, we see that the settlements for the edge columns are of the order of 6 mm, while the settlement for middle columns is of the order of 3.5 to 4 mm and the columns adjoining the piles are less than 3 mm. That is to say that the middle columns reduce the settlement more than the edge columns and the piles are another upgrade of soil consolidation.

Figure 5 shows the reduction in settlements of the middle column and the column adjacent to the pile with respect to the edge column. We noticed that the two curves look similar. For

loads between 30% and 105% of  $Q_s$ , the settlements observed on columns no. 284 and no. 56 are successively 60% and 80% lower than the settlements of the edge columns, beyond 120% of  $Q_s$  and for the unloading phase, these settlements decrease to 50% and 70% for columns no. 284 and 56. It can be observed that the middle columns are stiff and better compacted than the bank (edge) columns. Also, the combination of the two reinforcement techniques, namely stone column, and pile technique, gives us favorable results.

### 3 Numerical validation

To simulate the real behavior of stone columns in terms of settlement under the effect of loading, the validation of the experimental study is carried out using the Plaxis 2D software, in order to find the model as an approximation of the experimental results. Three configurations are studied. The first configuration proposed is the model of an isolated column. This device is widely used until today for the sizing of special foundations and stone columns. The second configuration is presented by the introduction of a wall with an interface, which represents the drill wall, then making the column by inserting the stone ballast in layers. The third configuration analyzes a model of the concentric rings equivalent to groups of stone columns which surround the column subjected to the effect of loading. Subsequently, these configurations are compared with a model without reinforcement.

The parameters introduced in the Plaxis software are summarized in Table 3:

Table 3: Geotechnical characteristics of the different soil layers

Noun	Type	Dry density $\gamma_d$ [kN/m <sup>3</sup> ]	Wet density $\gamma$ [kN/m <sup>3</sup> ]	Permeability $K_x$ [m/s]	Permeability $K_y$ [m/s]	Poisson' s ratio $\nu$ [-]	Young' s modulus $E$ [kN/m <sup>2</sup> ]	Cohesion $C$ [kN/m <sup>2</sup> ]	Friction angle $\phi$ [°]
Level 0	Drained	15	17	1E -6	1E-6	0.3	1000	1	25
Level a	Undrained	15	17	9.3E -8	9.3E -9	0.3	2000	1	25
Level b1	Drained	16	19	1E-6	1E-6	0.3	8000	1	30.5
Column	Drained	16	19	1E-6	1E-6	0.3	16000	1	33.5

Figure 6 shows the three configurations to be studied.

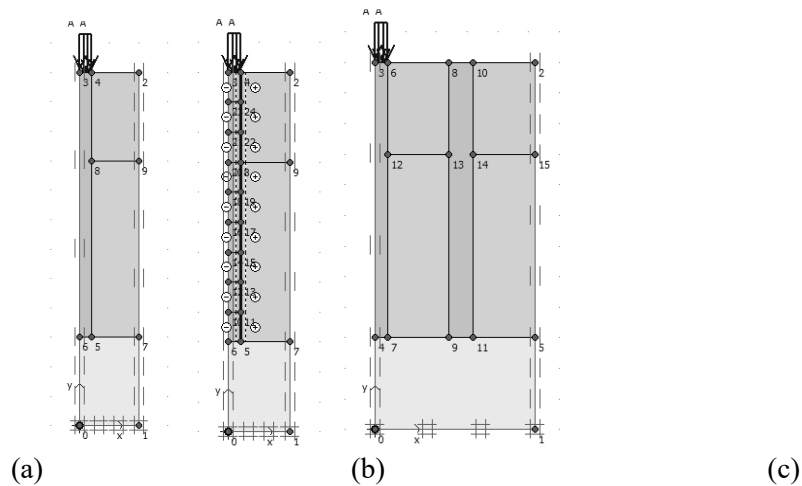


Figure 6: The three configurations to be studied: (a) Model of an isolated column; (b) Model of a column made per layer; (c) The model of a column surrounded by a concentric ring

### 3.1 Model of an isolated column

The modeling of an isolated ballasted column is carried out as axisymmetric, using 15 nodes. The dimensions used for this model are 12 m in height and 2 m in width, with a column 9 m deep and 0.8 m in diameter, buried in the different layers of soil as shown in Figure 6a.

The boundary conditions are the following:

- horizontal movements are blocked at the axis and at the lateral end of the model,
- horizontal and vertical movements are blocked at the base of the model.

A distributed load is applied to the top of the column representing the loading test.

The different calculation phases are the installation of the column, the consolidation of the soil for one day and application of the loading program as follows: (1.47 t / 2.94 t / 4.41 t / 5.87 t / 7.34 t / 8.81 t / 10.28 t / 11.75 t / 13.22 t / 14.69 t).

### 3.2 Model of a column made per layer

The second configuration is presented by the introduction of a wall with an interface, which represents the wall of the drilling machine (blocking by the wall then release expansion of the ballast by removing the wall as shown in Figure 6b). This wall is characterized by a normal stiffness  $EA = 7.5 \cdot 10^7 \text{ kN/m}$ , a bending stiffness  $EI = 106 \text{ kN.m}^2/\text{m}$  and the equivalent thickness  $d = 400 \text{ mm}$ . This device is modeled as axisymmetric with 15 nodes. The dimensions of the model adopted and the stone column, are the same as in the first configuration. The different phases of calculation are the installation of the wall, the installation of the column by a layer of 1m, the consolidation of the ground for one day, and application of the loading program as follows: (1.47 t / 2.94 t / 4.41 t / 5.87 t / 7.34 t / 8.81 t / 10.28 t / 11.75 t / 13.22 t / 14.69 t).

### 3.3 Model of a column surrounded by a concentric ring

The third configuration is presented by the model of a concentric ring, equivalent to the model of a group of stone columns which surround the central column (figure 7).

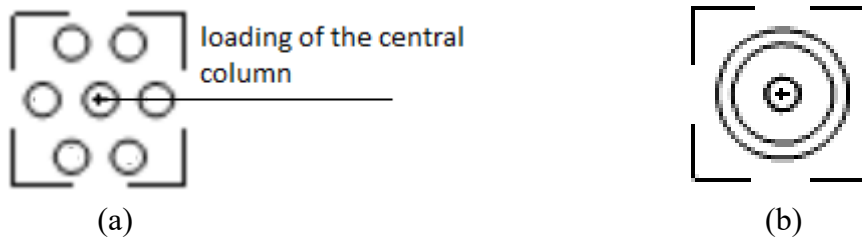


Figure 7: Geometric configuration: (a) Model of a group of columns; (b) Equivalent model of a concentric ring.

This model is carried out as axisymmetric with 15 nodes. The dimensions of the adopted model are 12 m in length and 5 m in width (Figure 6c). The different calculation phases are identical as in the first configuration.

### 3.4 Results and interpretation

The results obtained after the generation of the three models, allowed us to plot the settlement curves of the three configurations, as a function of the loading stages and compare them with the column settlement curves produced in the experiment and the settlement curve of the ground without reinforcement.

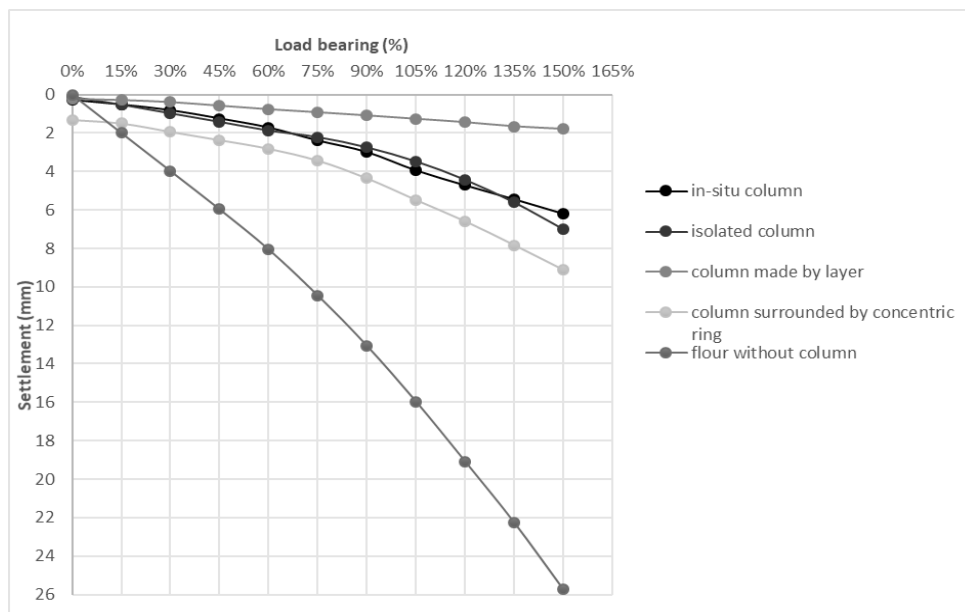


Figure 8: Comparison of settlements of unreinforced soil and reinforced soil with columns under the effect of loading from in-situ data and those obtained by Plaxis 2D

From the results obtained (Figure 8), it is very clear that the addition of a stone column improved the soil and reduced settlements in the three configurations solved in Plaxis 2D V8, compared with the soil settlement curve without column.

The configuration of the column carried out per layer gives us values of settlements that are low compared to the other configurations, while the settlements resulting from the configuration of the column surrounded by a concentric ring gives us relatively high values. On the other hand, the curve relating to the model of the isolated column is closer to the curve produced on-site than the two curves relating to the aforementioned models.

## 4 Conclusion

From this experimental study, confirmed by digital simulations, we can conclude that stone columns are one of the best techniques to reduce settlement in compressible soils. Middle columns perform better in reducing the colon-loaded settlements, in which, the reduction of the settlement concerning the edge cells is 60% in the lifting phase. On the other hand, it is of the order of 10% in the unloading phase, which confirms that the middle columns are steeper and more confined than the edge columns. That implies the columns work better in groups. The summarized results of the settlement curves show a good performance of the simple digital model of an isolated column, representing the real behavior of soil reinforced by stone columns. Moreover, the settlements resulting from the digital model of the isolated column are identical to those recorded on the site, therefore well-aligned with the site experiments.

## References

- [1] Greenwood, D.A., (1970). *Mechanical improvement of soils below ground surface*. In: Proceedings of Ground Improvement Conference. Institute of Civil Engineering, pp. 9-29.
- [2] Slocombe B.C., Moseley M.P. (1991). *The testing and instrumentation of stone columns*, Deep Foundation Improvements: Design, construction and testing ASTM STP 1089, p. 85-100.
- [3] Balaam N P., Booker J R (1985). Effect of stone column yield on settlement of rigid foundations in stabilized clay. International journal for numerical and analytical methods in geomechanics.vol. 9, pp.331-351.
- [4] Watts, K.S., Johnson, D., Wood, L.A., Saadi, A. (2000). An instrumented trial of vibro ground treatment supporting strip foundations in a variable fill, *Géotechnique*, 50, (6), p. 699-708.
- [5] Dhouib A, Soyey B, Wehr J, Priebe H.J. (2004). *Méthode de Priebe : origine, développement et applications*. Actes du Symposium International sur l'amélioration des sols en place (ASEP-GI 2004). Edition presses de l'ENPC-LCPC. Paris, Vol. 1 PP 131-146
- [6] Dhouib, A. et Blondeau, F., (2005). *Colonnes ballastées*. Edition Presses des Ponts et Chaussées. Paris.
- [7] Vincent Six, (2006). *Analyse du comportement des colonnes ballastées : influence des conditions initiales*, laboratoire de mécanique de Lille (UMR 8107)
- [8] Corneille S. (2007). *Amélioration des sols par inclusions semi-rigides*, Thèse de Doctorat INPL.
- [9] Deb, K., (2008). *Modeling of granular bed-stone column- improved soft soil*. Int. J. Numer. Anal. Methods Geomech. 32(10),1267–1288.
- [10] Almeida, M.S.S., Hosseinpour, I., Riccio, M., (2013). *Performance of a geosynthetic encased column (GEC) in soft ground: numerical and analytical studies*. Geosynth. Int. 20 (4), 252-262.
- [11] Castro, J, (2014). *Numerical modelling of stone columns beneath a rigid footing*. Group of Geotechnical Engineering, Department of Ground Engineering and Materials Science, University of Cantabria, Avda. de Los Castros, s/n, 39005 Santander, Spain.
- [12] Ng and Tan (2014). *Design and analyses of floating stone columns*, Soils and Foundations2014; 54(3):478–487
- [13] Geng, L, Tang, L, Cong, S.Y, Ling, X.Z, Lu, J, (2016). Three-dimensional analysis of geosynthetic-encased granular columns for liquefaction mitigation. Geosynth. Int. 24(1), 45–59.
- [14] Debnath, P., Dey, A.K., (2017). Bearing capacity of geogrid reinforced sand over encased stone columns in soft clay. Geotext. Geomembr. 45, 653–664.

- [15] Ministry of Equipment, lodgment and Transport (1993), « *Règles techniques de conception et de calcul des fondations des ouvrages de génie civil – Cahier des clauses techniques générales applicables aux marchés publics de travaux* », Fascicule 62 – Titre V.
- [16] Priebe, H. J. 1976. *Evaluation of the settlement reduction of a foundation improved by Vibro-Replacement*. Bautechnik, 2, 160-162.

## Behaviour of Self-Compacting Concrete incorporating Natural Perlite used as Part of Cement and as Aggregates

Sabria Malika Mansour<sup>1</sup>, Youcef Ghernouti<sup>1</sup>

<sup>1</sup> M'Hamed Bougara University, Algeria, Faculty of Technology, Civil Engineering Department, Research unit: Materials, Processes and Environment  
e-mail: s.mansour@univ-boumerdes.dz

### Abstract

Perlite, a natural glassy volcanic rock could be used as supplementary cementitious material to reduce environmental pollution and the consumption of precious natural resources in the concrete industries. The aim of this work is to assess natural perlite used as 50% aggregates substitution by volume (sand or gravel) and as 10%, 15%, 20% cement substitution in self-compacting concrete. Workability characteristics and mechanical properties were analysed. Results showed that replacing 50% of natural aggregates with 50% of perlite aggregates or substituting cement with 10% of perlite powder generated the best workability characteristics and improved compressive, flexural strength, and elastic modulus of concrete at 28 days. Moreover, the results were combined to develop correlations that prove to be good between mechanical properties of self-compacting. Using perlite as aggregates offers a new source of supply and saves natural aggregates. Also, perlite used as cement substitution helps to reduce PC consumption, cost, and CO<sub>2</sub> emission.

**Key words:** self-compacting concrete, perlite, fresh properties, mechanical strength, elastic modulus

## 1 Introduction

Self-Compacting Concrete (SCC) is considered as the most revolutionary development in the construction sector. Since this is based on the elimination of vibration [1, 2] the final product is of higher quality, with the additional benefit that the overall cost of casting is lower [3]. The use of SCC is increasing [4, 5]. Self-compacting concrete contains fine additions which allow it to flow easily and have good workability. Calcareous fillers are often used as additions. However, it is still possible to vary the nature of additions used in mixes of cement. Also, the type of aggregates can be replaced and save natural aggregates. The use of natural perlite as a component of SCC concrete can substantially affect its properties.

Perlite is a glassy volcanic rock that contains approximately 70–75% SiO<sub>2</sub> and 12–18% Al<sub>2</sub>O<sub>3</sub>. Its 2–6% chemically combined water causes it to expand and become a cellular material of extremely low bulk density when heated to a temperature of 900 °C. Thus, the



expanded perlite is used in various constructional, horticultural, and industrial applications [6, 7]. Due to its glassy structure and high  $\text{SiO}_2$  and  $\text{Al}_2\text{O}_3$  contents, perlite is a pozzolan. Although its pozzolanic characteristics have been mentioned in some limited numbers of technical papers.

Urhan [8] examined the alkali silica and pozzolanic reactions on expanded perlite aggregate concrete. It indicated that even under very unfavourable conditions, once the concrete is made from reactive aggregates or pozzolanic materials, there is always a small amount of alkali silicate gel produced which may cause a subsequent slight expansion of which the magnitude is a function of the mechanical strengths of the concrete. Erdem et al. [9] showed that the perlites possess sufficient pozzolanic characteristics to be used in the production of blended cement.

Terkman & Kantarci [10] investigate drying shrinkage of SCC concrete including mixtures of expanded perlite aggregate at different curing conditions and found that with increasing moisture content and unit quantity of perlite aggregate, drying shrinkage of concrete decreases. Yu et al. [11] indicate that perlite powder has a high pozzolanic effect and is an active mineral admixture (MA) for concrete. Also, Bhuvaneshwari et al. [12] found that for obtaining lightweight concrete, the optimum replacement percentage of sand by Perlite is 10%. The compressive, split tensile, and flexural strength was reduced if the replacement percentage of Perlite will be increased. In addition, using perlite as an aggregate in Portland cement and gypsum plasters for exterior applications and for the fire protection of beams and columns is also very efficient [13]. Johari et al. [14] found that using perlite as an admixture at a proper level of replacing with OPC, generally reduced porosity, mean pore size, and pore diameter of the microstructure of cement paste. Yu et al. [15] studied the influence of perlite powder as an admixture on the pore structure of cement pastes. Their study demonstrated that due to the pozzolanic reaction, it could diminish porosity and pores diameter in cement pastes.

In the work of Esfandiari & Loghmani [16], cement-lime binder was replaced by powder perlite PP at 0%, 5%, 10% 15%, and 20%. They found that the optimum percentage of PP was 6% on 28 and 90-day to obtain maximum compressive strength for SCC concrete. PP as a natural pozzolan is beneficial due to its low price and availability (depending on the region), as well as its ability to reduce the hydration heat and control the shrinkage of concrete mixtures. Nevertheless, its influence on the properties of concrete, including the reactivity (specifically in the early ages), strength, durability, and so on, is still a concern [17]. Sičáková et al. [18] analysed the time development of both compressive and flexural strength, including results of 2, 7, 28 and 90-day testing. They concluded that although perlite blended binders achieved lower strengths compared to conventional binders based on ground granulated blast furnace slag and fly ash, they have a promising potential. Flexural strength of 4.1–6.2 MPa and compressive strength of 18.8–38.5 MPa are sufficient for a number of practical applications and are expected to meet the required limits. Also, their improvement in the later period (90 days) was confirmed. Mansour [19] studied the effect of Algerian natural perlite used as fillers addition on the workability and physical-mechanical properties of steel fibre self-compacting concrete. They showed the beneficial effect of the use of perlite as fillers. Workability properties decreased slightly but an increase of mechanical strengths and elastic modulus was much more marked with the use of the steel hooked fibres. Moreover, El Mir and al. [20] evaluated the effect of waste perlite powder along with its combination with

limestone fillers, metakaolin, and silica fume on durability and long-term transport properties of self-consolidating concrete. They found that water permeability, carbonation, and chloride ion migration curtailed when perlite powder concentration reached 220 and 260 kg/m<sup>3</sup>. In contrast, the resistance against freeze/thaw remarkably improved. Mansour et al. [21] showed the performance of powder perlite use as cement substitution on workability, physical-mechanical properties of self-compacting concrete by destructive and non-destructive tests. They concluded that the association of 5% granite and 5% perlite has generated satisfactory workability and mechanical properties which approach those of the SCC reference concrete.

The objective of this work is to assess the natural perlite derived from the deposit of the company Bental located near Hamame Boughrara northwest of Tlemcen region (Algeria) when it is used as cement substitution varying from 10%, 15% to 20%, also used as aggregates (sand or gravel) in self-compacting concrete with a replacement rate of 50%. This can help solve the problem of lack of aggregates and in particular the use of alluvial aggregates. In this work, six formulations of self-compacting concrete were studied. Fresh properties such as slump flow, filling capacity, and resistance to segregation; also, hardened properties as specific gravity, compressive, flexural strength, and elastic modulus were determined. Moreover, obtained results were combined to develop correlations between mechanical properties of the destructive and non-destructive tests.

## 2 Materials and Methods

### 2.1 Materials

*Cement:* CPJ-CEM II/A 42.5 Portland cement from the M'sila cement plant is used. It is obtained by the finely ground mixture of clinker and additions (gypsum and limestone) according to Algerian standard NA 442. Its specific gravity is 3.1 g/cm<sup>3</sup> and its specific surface area Blaine SSB is 3900 cm<sup>2</sup>/g. Also, at 28 days, its compressive and flexural strength are 49 MPa and 8 MPa respectively. As an addition in the self-compacting concrete, a rate of 10% of limestone fillers is used. The limestone is characterized by high chemical purity and high whiteness. Its specific area Blaine is 7300 cm<sup>2</sup>/g, and its specific gravity is 2.66 g/cm<sup>3</sup>.

*Perlite:* The used perlite is of volcanic origin manually extracted from the deposit located in the northwest of Algeria. This grey-coloured perlite was extracted in the form of pieces of rock with diameters varying from 20 to 40 cm. The perlite rock was crushed and then steamed for 24 hours at a temperature of 80°C to remove any moisture, then crushed, grinded, and sieved at 80 μm when it was used as cement substitution. Perlite powder incorporating cement has a Blaine specific surface area of 5400 cm<sup>2</sup>/g and specific gravity of 2.38 g/cm<sup>3</sup>. The chemical compositions of cement, limestone, and powder perlite are shown in Table 1. Moreover, the X-ray diffraction pattern was established for the natural powder perlite (Figure 1).

Chemical composition shows that the rate of silica (64.44%) contained in perlite indicates the siliceous nature of perlite. In addition, the oxides rate [SiO<sub>2</sub>(%) + Al<sub>2</sub>O<sub>3</sub>(%) + Fe<sub>2</sub>O<sub>3</sub>(%)] is 80.89% corresponding to a value according to ASTM C 618 standard specification for natural pozzolans (min 70%) [22]. X-ray analysis of perlite shows a remarkable hump which signifies a high content of amorphous silica and peaks that characterize the crystalline phases such as

montmorillonite, quartz, albite, and muscovite (Figure 1). As a result, the chemical composition of the perlite shows the siliceous nature, their XRD pattern shows the amorphous structure, conformance of the perlite to the standard specification for natural pozzolans, ASTM C 618, and the previous studies [7, 23, 24] on the pozzolanic properties of the perlite prove from many aspects that perlite possesses certain pozzolanic characteristics and can be used as a cement replacement in concrete.

*Aggregates:* Used natural sand was a mixture of natural dune fine sand (DS) and river sand (RS). Different natural gravel types of class 3/8 mm, 8/15 mm were also used. Moreover, the perlite aggregates were obtained by crushing natural perlite rock to the desired dimensions of sand (0/4 mm) and gravel (3/8 mm, 8/15 mm) (Figure 2). The physical properties of natural aggregates and perlite aggregates are displayed in Table 2.

## 2.2 Methods

### 2.2.1 Concrete mixtures

Six SCC main groups of mixes were prepared with the binder dosage constant ( $430 \text{ kg/m}^3$ ) and 2% of superplasticiser (MEDAFLOW 30), having a density of 1.07 and chlorine content  $< 0.1 \text{ g/l}$ ; also, using 0.9 fixed gravel-to-sand ratio, 0.38 water to binder ratio and by using perlite rock as aggregates replacement (Perlite Sand PS or Perlite Gravel PG) and Perlite Powder PP as cement substitution at the rate of 10%, 15% to 20%. The SCC concretes are specified as PN0 (100% natural aggregates, 0% Perlite) which is the control SCC concrete, PS50 (50% RS(0/4 mm) natural river sand +50% PS(0/4 mm) Perlite sand), PG50 [50% (NG3/8) Natural Gravel+50% (NG8/15) Natural Gravel + 50% (PG3/8) Perlite Gravel + 50% (PG8/15) Perlite Gravel], PP10 (90% cement PC+10% Perlite Powder), PP15 (85% cement PC+15% Perlite Powder), PP20 (80% cement PC+20% Perlite Powder). The substitution of natural sand RS 0/4 mm and natural gravel NG3/8 or NG8/15 was carried out by volume because the densities of (3/8 and 8/15) perlite gravel and (0/4 mm) perlite sand are different from (3/8 and 8/15) natural gravel and (0/4 mm) natural sand (Table 2). Therefore, the weights of perlite aggregates and natural aggregates are different. Mix proportions of SCC mixtures are presented in Table 3.

### 2.2.2 Procedure

The bulk density  $\rho_f$  and  $\rho_h$  is measured in the fresh and the hardened states respectively according to the standard NF EN 12350-6 [30] and NF EN 12350-7 [31] respectively, for different SCC formulations. The fresh properties of performed SCC were evaluated from several tests such as slump flow test (NF EN 12350-8) [25], L-Box test (NF EN 12350-10) [26], and sieve stability test (NF EN 12350-11) [27] by determining the slump flow, filling rate, and segregation resistance respectively, whose values must be in accordance with the recommendations given by the European Federation of National Trade Associations EFNARC [28]. Otherwise, for mechanical tests and for each mixture, three prismatic SCC concrete samples (70x70x280 mm) and three cylindrical samples (110x220 mm) were manufactured according to standard NF EN 12390-2 [29]. After 24 hours, the samples were stored in water at  $20 \text{ }^\circ\text{C} \pm 2 \text{ }^\circ\text{C}$ . SCC was then tested in compression (NF P18-406) [30] and flexural (NF P18-407) [31] at maturities 7 and 28 days. An ultrasonic non – destructive

testing was used to detect cracks and other discontinuities in SCC concrete [32, 33]. The ultrasonic non-destructive testing technique (NFP 18-418) [34] is typically based on the measurement of the ultrasonic velocity passing through cylindrical samples. This velocity is closely related to mechanical properties and, more directly, to the modulus of elasticity. By using velocity, the elastic modulus of SCC concrete can be calculated with the Equation (1) given by Gupta et al. [35]:

$$E_d = (\rho \cdot V_{us}^2 / g) \cdot 10^{-2} \quad (1)$$

Where  $E_d$  is the dynamic modulus of elasticity (GPa),  $V_{us}$  is the ultrasonic pulse velocity (km/s),  $\rho$  is the specific density ( $\text{kg/m}^3$ ), and  $g$  the gravitational acceleration ( $9.81 \text{ m/s}^2$ ).

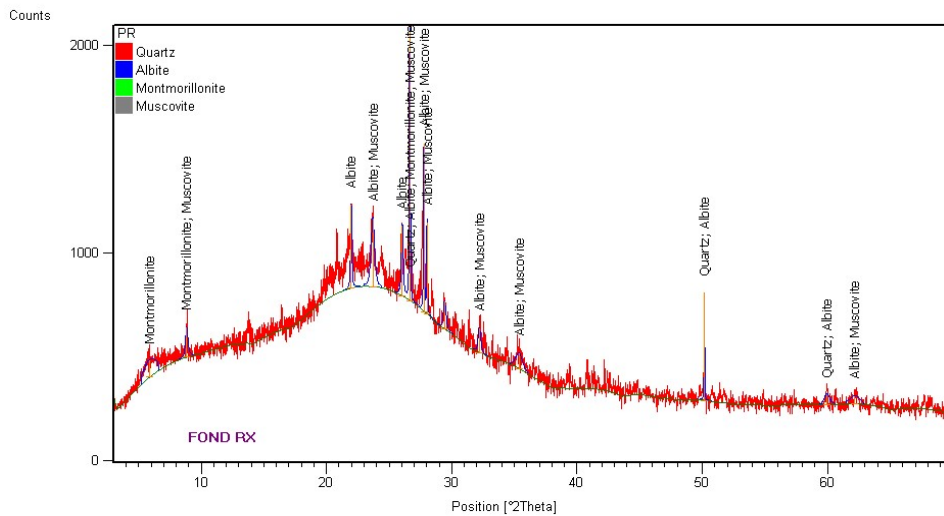


Figure 1: X-ray diffraction of the perlite (Cu  $\alpha$  filter Ni)

Table 1: Chemical composition of cement PC, perlite, and limestone (%)

Oxides	Cement PC	Perlite	Limestone
SiO <sub>2</sub>	16.96	64.44	4.83
Al <sub>2</sub> O <sub>3</sub>	4.68	14.94	1.04
Fe <sub>2</sub> O <sub>3</sub>	2.98	1.51	0.37
CaO	60.19	5.79	51.73
MgO	1.84	1.33	0.46
K <sub>2</sub> O	0.61	3.40	0.14
Na <sub>2</sub> O	0.093	1.87	0.08
SO <sub>3</sub>	1.65	0.88	0.08
Cl-	0.017	0.41	0.03
LOI	9.87	-	41.17



Figure 2: Stages of rock perlite recycling

Table 2: Physical properties of natural aggregates and perlite aggregates

Aggregate	DS	RS	NG3/8	NG8/15	PS0/4	PG3/8	PG8/15
Absolute density g/cm <sup>3</sup>	2,61	2,66	2,63	2,66	2,43	2,44	2,46
Apparent density g/cm <sup>3</sup>	1,31	1,53	1,42	1,42	1,28	1,41	1,43
Water content %	4.75	3.85	0.40	0.40	0.85	0.35	0.35
Sand equivalent %	69	72	-	-	76	-	-
Los Angeles coefficient %	-	-	24.3	24.3	-	27.2	27.2
Micro Deval coefficient %	-	-	26.8	26.8	-	29.3	29.3
Water Absorption %	0.96	0,95	0,64	0,60	0,75	0,66	0,67
Porosity %	2.46	2.36	1.74	1.62	1.98	1.73	1.73

Table 3: Mix proportions of SCC mixtures (kg/m<sup>3</sup>)

Constituents	PN0	PS50	PG50	PP10	PP15	PP20
Cement	430	430	430	387	365.5	344
Limestone fillers	43	43	43	43	43	43
Perlite	-	-		43	64.5	86
DS (fine sand)	348.43	348.43	348.43	348.43	348.43	348.43
RS (0/4mm)	574.48	287.24	574.48	574.48	574.48	574.48
PS (0/4mm)	-	262.41	-	-	-	-
NG 3/8	275.72	275.72	137.86	275.72	275.72	275.72
NG 8/15	557.77	557.77	278.88	557.77	557.77	557.77
PG 3/8	-	-	127.91	-	-	-
PG 8/15	-	-	257.92	-	-	-
Efficient Water	174,49	174,49	174,49	174,49	174,49	174,49
Superplasticizer	7,51	7,51	7,51	7,51	7,51	7,51
$\rho_h$ (kg/m <sup>3</sup> )	2254	2226	2228	2235	2233	2232

Table 4: Workability characteristics of SCC concrete

Constituents	PN0	PS50	PG50	PP10	PP15	PP20
$\rho_f$ (kg/m <sup>3</sup> )	2373	2322	2332	2365	2359	2354
Slump flow (cm)	71	69	68	70	62	60
Passing ability	0.9	0.85	0.82	0.84	0.81	0.80
Milt- Sieve stability (%)	4	4.2	4.1	5	6.2	7.1

### 3 Results and discussion

#### 3.1 Apparent bulk density of SCC concretes

Results in Table 3 and Table 4 show that the densities of SCC concrete are slightly less than that of the control SCC. For example, a low reduction of 2% was noted for the fresh SCC and 1.2% for the hardened SCC containing 50% sand, this is due to the fact that the quantity of sand (natural and perlite) in PS50 is with near 25 kg less than in PN0 because of the density of perlite sand which is lower than that of natural sand (Table 2).

### 3.2 Fresh properties of SCC

From the results of fresh properties, slump flow values are between 60 cm and 70 cm for all SCC containing perlite (Table 4), and no segregation was observed visually. These values are in agreement with the recommendations suggested by EFNARC for self-compacting concrete [28]. All SCCs are classified as SF2 except PP15 and PP20 which are classified as SF1. It is noted that the introduction of perlite as aggregates (sand or gravel) or as cement substitution decreased the slump flow of SCC. The slump flow of the control SCC and SCC with 10% of perlite are almost the same. But, beyond 10% of perlite, a remarkable slump flow decrease was obtained because the mix cement matrix absorbed more water. This decrease can be up to 15% for a cement substitution of 20% perlite. The reduction in slump flow is probably due to the high fineness of perlite compared to that of cement, which can absorb the water and consequently decreases SCC flowability. Moreover, perlite used as aggregates slightly decreases the slump flow and the fluidity of PS50 and PG50. The reduction was 3% and 4% respectively. In conclusion, the replacement of half of the natural aggregates by perlite aggregates, even better substituted the cement with 10% of natural powder perlite and generates good fluidity of SCC which aligns with those of the control SCC.

The L-box test is operated through the passing ability (ratio  $H_2/H_1$ ) which must be greater than 0.8 [28]. The obtained values were in conformity with EFNARC requirements for all SCCs, therefore their mobility in a confined environment is assured. This allows them to flow through the reinforcements correctly. L-Box test results  $\geq 0.80$  come under PA1 classes with 2 rebars and the test results  $\geq 0.80$  come under PA2 classes with 3 rebars. This means that the risk of blockage is avoided. All SCCs were classified as PL2. Compared to SCC control, the passing ability of PP15 and PP20 decreased more than for the other SCC variants. The reduction was 9% and 10%.

Concerning the segregation of SCCs, the sieve stability test is the essential point to be verified. This test is used to measure the milt corresponding to the ability of self-compacting concrete to segregation resistance. Obtained values ranging from 4% to 7.1% are acceptable ( $<15\%$ ) according to EFNARC requirements of self-compacting concrete [28]. This means that all SCCs are homogeneous stable and classified as SR2. The concrete PN0 is characterized by high stability (lower limit = 4%) and consequently a high resistance to segregation and to bleeding. It seems that using perlite as aggregates did not affect the stability of SCC. When the perlite is used as cement substitution, PP10, PP15, and PP20 are homogeneous but less stable than PN0. This is due to the increase of the amount of perlite fines in SCC which facilitates the passage through the sieve and increases the milt weight [38].

Moreover, the introduction of the perlite decreases the specific gravity  $\rho_f$  of fresh SCCs. This is due to fact that the specific gravity of perlite used as aggregates or as cement substitution is smaller than that of natural aggregates or cement respectively. The smallest reduction is obtained for SCC containing 10% of powder perlite.

### 3.3 Compressive strength of SCC concretes

Results of compressive strength of SCCs at different maturities are illustrated in (Figure 3). The compressive strength of all SCCs increases over time; also, it decreases when 50% of natural aggregates (sand or gravel) were replaced by 50% of perlite aggregates.

The reduction is not significant, at 28 days; it is limited at 6.6% and 4.2% for the SCC containing 50% of perlite sand and 50% of perlite gravel respectively. It is probably due to the fragility of the aggregates of perlite rock compared to natural aggregates. On the other hand, the introduction of perlite as cement substitution increases and exceeds that of control SCC. Indeed, at 28 days, a gain of strength of 8.7% and 2% was obtained when the cement was substituted by 10% and 15% of perlite powder respectively.

The increase of compressive strengths is due to the filling effect and pozzolanic reaction [39]. But, for the SCC containing 20% of perlite powder, a reduction of compressive strength of 7.5% was noticed. This can be explained by the lower cement PC content in PP20 SCC concrete. In the other words, this is due to the decrease of the main tricalcium silicate  $C_3S$  and bicalcium silicate  $C_2S$  cement minerals which are the first responsible for the development of the mechanical strengths. Also, the water destined to cement wetting was mobilized by the perlite due to its high fineness, which delayed the hydration process, therefore a decrease in strength has been recorded. A similar result was found in the study of Yu et al. [11].

### 3.4 Flexural strength of SCCs

Figure 4 shows the flexural strength of SCCs. It increases at maturities of 7d and 28d for all SCCs. The rate of 50% perlite sand or 50% perlite gravel affects the flexural strength of SCC with a loss of 14% and 6.3% respectively at 28 days. Furthermore, 10% of perlite rate substituting the cement increases flexural strengths which exceed those of SCC control. A gain of 3.3% is obtained at 28 days. These results confirm those of compressive strengths.

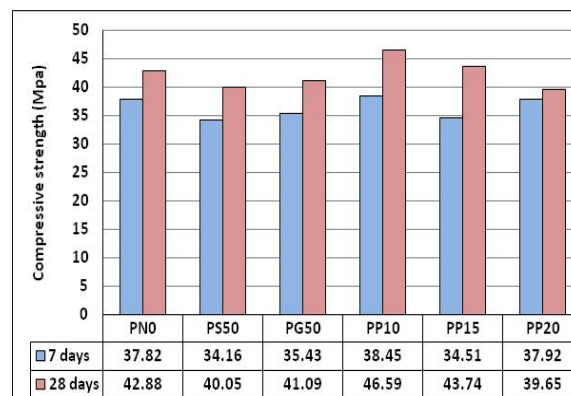


Figure 3: Experimental compressive strength of SCCs



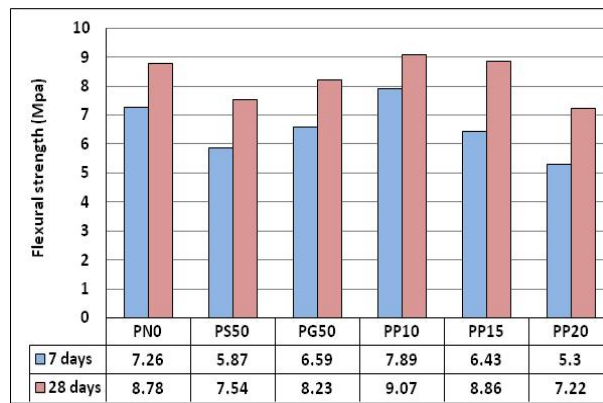


Figure 4: Flexural strength of SCCs

### 3.5 Ultrasonic pulse velocity of SCCs

The value of the ultrasonic velocity ( $V_{us}$ ) is another relevant indicator for the microstructure. This velocity is highly influenced by the presence of voids within the material. The results of the ultrasonic velocity of SCC specimens at 28 days are given in Table 5. It is shown that the replacement of 50% of natural gravel by perlite gravel did not affect the velocity. But the velocity increases to 7% when cement is replaced by 10% of perlite powder. This is due to the fineness and reactivity of the perlite powder with the porthlandite released during hydration of the cement, to produce hydrated calcium silicates C-H-S which densify the cement matrix. While the compactness and the density of concrete increased, the ultrasonic wave velocity and strength of concrete increased together [40, 41, 42]. Moreover, the quality of all SCCs was considered as generally good. Indeed, the ultrasonic wave velocity of a good quality concrete should be between 4100 m/s and 4700 m/s [41].

A relationship between experimental compressive strength  $R_{c(exp)}$  at 28 days of all SCCs and ultrasonic velocity  $V_{us}$  was obtained (Figure 5). It is in the exponential form with a coefficient  $R^2 = 0.7319$ . This relation is expressed by Equation (2):

$$R_{c(exp)} = 0.8356e^{0.0009V_{us}} \quad (2)$$

The model of this correlation is in the form  $R_c = a.e^{b.V_{us}}$ , where the compressive strength  $R_c$  can be directly determined from the ultrasonic velocity  $V_{us}$ . The form of this model is in agreement with the theoretical formula Rilem standards.

Table 5: Ultrasonic velocity and dynamic modulus of SCCs at 28 days.

SCC concrete	PNO	PS50	PG50	PP10	PP15	PP20
Ultrasonic velocity $V_{us}$ (m/s)	4330	4250	4340	4370	4350	4230
Dynamic modulus $E_d$ (MPa)	42260	40210	41960	42690	42262	39940

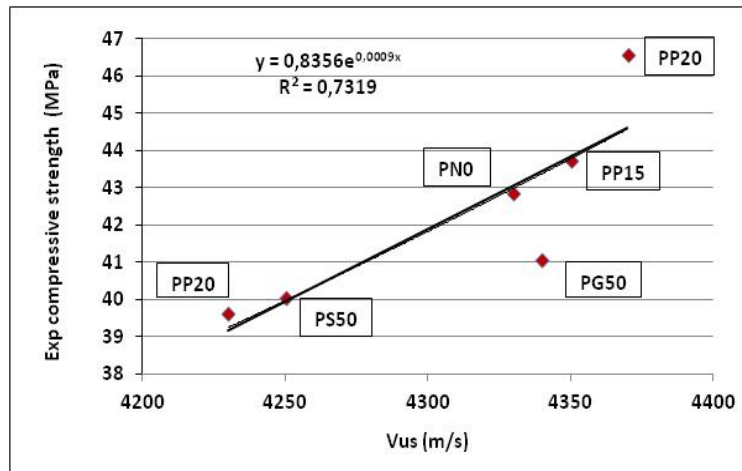


Figure 5: Relationship between experimental compressive strength and ultrasonic velocity

Moreover, the velocity can be used to calculate the compressive strength  $R_c(US)$  at 28 days using Equation (3):

$$R_c(US) = 0.08177e^{0.00147V_{us}} \quad (3)$$

In this study, compressive strength obtained experimentally by compressive test at 28 days and by using the ultrasonic velocity according to equation (3), are compared as shown in Figure 6. The two strengths evolve similarly and are mostly aligned especially at 28 days. They are in agreement. Indeed, a good polynomial relationship between  $R_{c(exp)}$  and  $R_{c(US)}$  was obtained with coefficient  $R^2 = 0.8751$  as shown in Figure 7 and expressed by Equation (4).

$$R_{c(exp)} = 0.131R_{c(US)}^2 - 11.379R_{c(US)} + 285.37 \quad (4)$$

Moreover, by comparing the two expressions of the strength as a function as the ultrasonic velocity given by equation (2) obtained by destructive test and the theoretical equation (3), a relative variation of the strength was obtained by the two equations ranging from 8% to 15%. This leaves us to conclude that equation (2) can be used to determine the compressive strength of SCC.

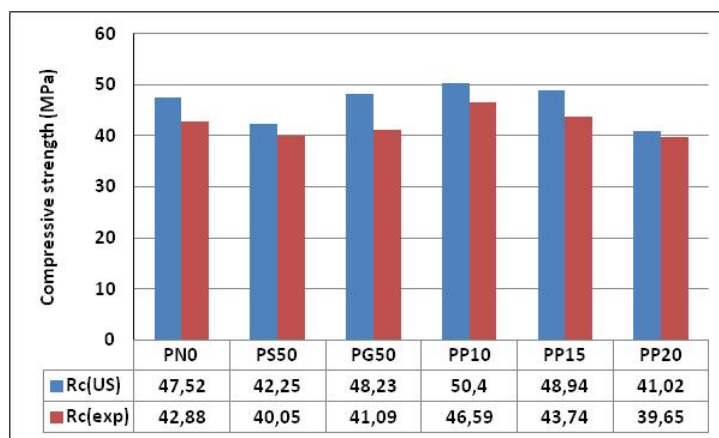


Figure 6: Ultrasonic and experimental compressive strength at 28 days of SCCs

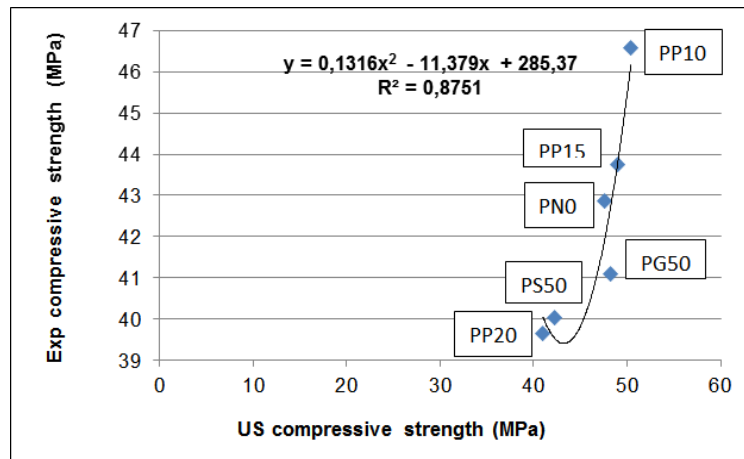


Figure 7: Relationship between experimental and ultrasonic compressive strength

### 3.6 Elastic modulus of SCC

Ultrasonic velocity depends strongly on the mechanical properties of the material, especially elastic modulus. From the values of ultrasonic velocity, the dynamic modulus of elasticity  $E_d$  was determined using Equation (1). On the other hand, the elastic modulus was also calculated by Equation (5) according to BAEL1991 standards [43]:

$$E_{(BAEL91)} = 11000 (R_{cj})^{1/3} \quad (5)$$

$R_{cj}$ : compressive strength at j day's old concrete.

$E_{(BAEL)}$  elastic modulus was determined for all SCCs at 28 days and compared to dynamic modulus  $E_d$ . The results illustrated in Figure 8 showed that for the two elastic moduli, incorporation of the rate of 10% and 15% of perlite powder used as cement substitution increases slightly (1%) elastic modulus of the SCC. Otherwise, the replacement of natural aggregates by 50% of perlite aggregates did not significantly affect the modulus of elasticity. In fact, a slight decrease of 1% and 5% were obtained for SCC containing perlite sand and perlite gravel respectively. This means that the perlite aggregates are of good quality with high elastic modulus and present a good adhesion with the cement matrix.

In addition,  $E_{(BAEL)}$  modulus varied similarly as the  $E_d$  but remained smaller than the latter. Compared to  $E_d$ ,  $E_{(BAEL91)}$  modulus is underestimated.

A relationship between the two elastic modulus of elasticity of all SCCs was obtained (Figure 9). The value of coefficient ( $R^2$ ) which is 0.9588 indicates a very good polynomial relationship between the elastic modulus  $E_{(BAEL91)}$  and the dynamic modulus  $E_d$  described by Equation (6).

$$E_{(BAEL91)} = 0.0007E_d^2 - 53.137E_d + 1e^6 \quad (6)$$

This relationship is interesting since it is possible to determine the  $E_{(BAEL91)}$  modulus from the dynamic elastic  $E_d$  modulus.

Another relationship can be obtained by connecting  $E_{(BAEL91)}$  and the ultrasonic velocity of SCCs. Figure 10 illustrates this relation which showed a good correlation between these parameters with coefficient  $R^2 = 0.868$ . It is described by Equation (7):

$$E_{(BAEL91)} = 0.1804V_{us}^2 - 1538.5V_{us} + 3e^6 \quad (7)$$

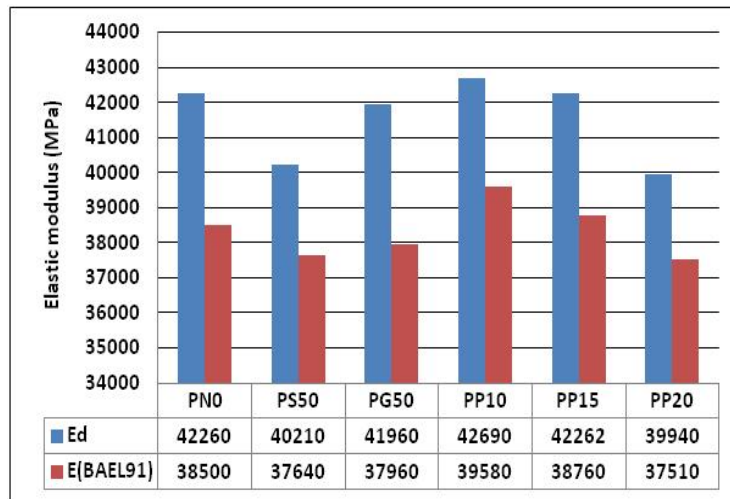


Figure 8: Dynamic and BAEL91 elastic modulus of SCCs

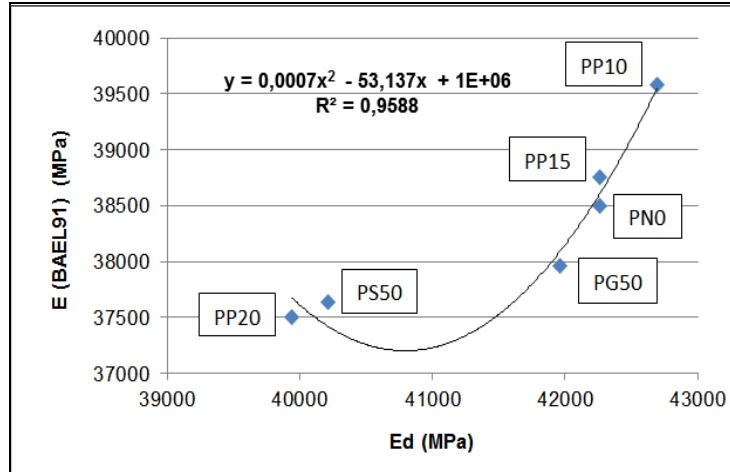


Figure 9: Relationship between  $E_{(BAEL91)}$  and  $E_d$  modulus

This relationship has a polynomial form which is in adequacy with the shape of the expression of the dynamic modulus  $E_d$  (1). From these results, it is possible to calculate the modulus  $E_{(BAEL91)}$  from the value of the ultrasonic velocity determined by a non-destructive test.

On the one hand, a relationship between the compressive strength determined by the ultrasonic velocity of the non-destructive test and the elastic modulus ( $E_d$ ,  $E_{(BAEL91)}$ ) was

established and illustrated in Figure 11. On the other hand, a relationship between the experimental compressive strength determined by the destructive test and elastic modulus ( $E_d$ ,  $E_{(BAEL91)}$ ) is illustrated in Figure 12.

Good polynomial correlations were obtained between the elastic modulus  $E_d$  or  $E_{(BAEL91)}$  and the ultrasonic compressive strength or experimental compressive strength respectively with coefficient  $R^2$  ranging from 0.875 to 1 as expressed by Equations (8, 9, 10, 11).

$$E_d = -89.6 R^2_{c(exp)} + 8092.4 R_{c(exp)} - 1398 \quad (8)$$

$$E_{(BAEL91)} = -2.34 R^2_{c(exp)} + 500 R_{c(exp)} + 2137 \quad (9)$$

$$E_d = -10.03 R^2_{c(us)} + 1214.3 R_{c(us)} + 6932.8 \quad (10)$$

$$E_{(BAEL91)} = 37.8 R^2_{c(us)} - 3265.7 R_{c(us)} + 107884 \quad (11)$$

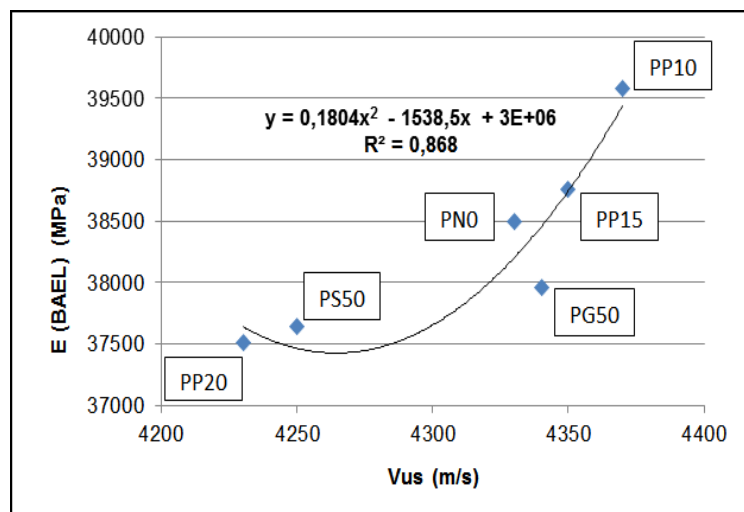


Figure 10: Relationship between  $E_{(BAEL)}$  modulus and ultrasonic velocity

From the correlations found in this study, it is worth noting that it is interesting to combine results of destructive and non-destructive tests to determine the mechanical properties of SCCs. For example,  $E_{(BAEL91)}$  modulus can be determined from dynamic modulus at 95.88% and from the ultrasonic velocity  $V_{(us)}$  at 86.8%. In addition, the experimental compressive strength value can be estimated from the strength calculated with the ultrasonic velocity at 87.5%.

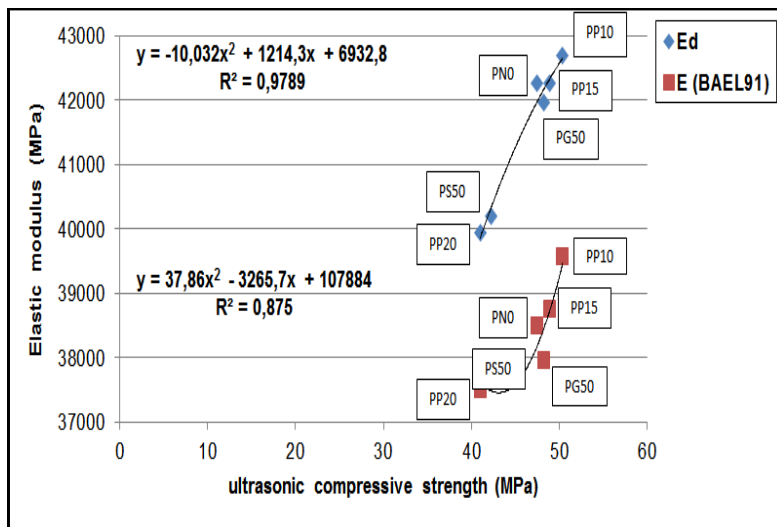


Figure 11: Relationship between elastic modulus  $E_d$ ,  $E_{(BAEL91)}$  and ultrasonic compressive strength

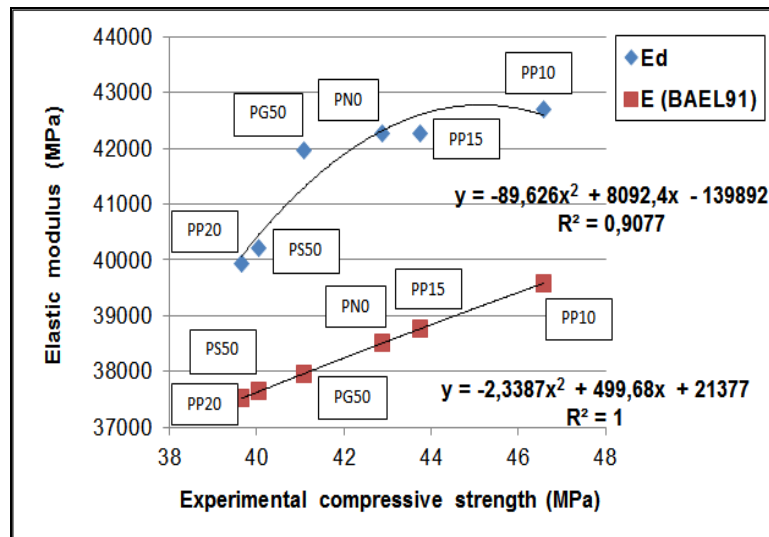


Figure 12: Relationship between elastic modulus  $E_d$ ,  $E_{(BAEL91)}$  and experimental compressive strength.

## 4 Conclusion

This study focused on the valorisation of natural volcanic rock, the perlite from western Algeria used as a component of the self-compacting concrete such as cement substitution and as aggregates. Based on obtained results, the following conclusions can be drawn:

- Investigated natural perlite has a specific area greater than that of cement, contains a high rate of silica, and has an amorphous structure. Therefore, it possesses sufficient pozzolanic characteristics to be used in cement and concrete.
- Values of fresh properties of performed SCCs are in agreement with the requirements of EFNARC for self-compacting concrete.
- Replacement of 50% of natural sand by 50% of perlite sand or substitution of cement by

10% of perlite powder improves the fresh properties.

- A gain of compressive and flexural strength of 8.7% and 3.3% respectively were obtained when the cement is substituted by 10% of perlite powder at 28 days.
- Concerning the non-destructive test, the ultrasonic velocity increases to 7% when the cement is replaced by 10% of perlite powder.
- From the ultrasonic velocity values, the quality of perlite SCC concretes can be considered as generally good.
- Replacement of natural aggregates by 50% of the perlite aggregates (sand or gravel) in self-compacting concrete can offer a new source of supply and save natural aggregates, especially with the problem of depletion of natural resources that meets the aggregates market.
- In addition, the use of 10% of perlite as the substitution in blended cement can be beneficial and help to reduce the PC consumption, therefore, cost and CO<sub>2</sub> emission especially for countries that produce considerable amounts of cement.
- A model of correlation in exponential form is obtained between the experimental compressive strength and ultrasonic velocity ( $R_{c(exp)} = 0.8356e^{0.0009V_{us}}$ ) with a coefficient  $R^2 = 0.7319$ . The form of this model is in agreement with the theoretical formula given by Rilem standards.
- A good polynomial relationship between experimental compressive strength  $R_{c(exp)}$  and strength determined using ultrasonic velocity  $R_{c(US)}$  is obtained with a coefficient  $R^2 = 0.8751$ . Indeed, the two strengths evolve similarly and are mostly aligned especially at 28 days. So, it is interesting to determine the compressive strength of concrete with an ultrasound test.
- The dynamic elastic modulus  $E_d$  can be directly determined from the experimental compressive strength  $R_{c(exp)}$  or ultrasonic strength  $R_{c(US)}$ . Good polynomial relationships were obtained with a coefficient  $R^2$  of 0.9077 for the relation between  $E_d$  and  $R_{c(exp)}$ , also 0.9789 for  $E_d$  and  $R_{c(US)}$ .
- Modulus of elasticity  $E_{(BAEL91)}$  can be directly determined respectively from the experimental compressive strength  $R_{c(Exp)}$  and ultrasonic strength  $R_{c(us)}$  with a correlation coefficient  $R^2 = 1$  and 0.875 respectively.
- $E_{(BAEL91)}$  modulus can be determined from the dynamic modulus with coefficient  $R^2 = 0.9588$  and from the ultrasonic velocity  $V_{us}$  with  $R^2 = 0.868$ . In addition, the compressive strength value can be estimated from the strength calculated with the ultrasonic velocity at 87.5%.
- Based on study results, ultrasonic velocity can be considered potentially useful in predicting the compressive strength and the elastic modulus of the SCC.

The use of these correlation curves allows a better estimate of the actual strength of SCC concrete as well as its modulus of elasticity compared to the usual curves recommended by the manufacturers of the devices or those established by other authors. Therefore, the establishment of a correlation between two parameters must be based on conditions appropriate to the study.

## References

- [1] Okamura, H. (1997). Self-compacting high performance concrete. *Concr.Int.* 19(7), 50–54.
- [2] Okamura, H. & Ouchi, M. (2003). Self-compacting concrete. *J. Adv. Concr, Technol*, 15.
- [3] Silva, P. R. & Brito, J. (2015). Experimental study of the porosity and microstructure of self-compacting concrete (SCC) with binary and ternary mixes of fly ash and limestone filler. *Construction and Building Materials*. 86, 101-112. <http://dx.doi.org/10.1016/j.conbuildmat.2015.03.110>.

- [4] Youjun, X., Baoju, L., Jian, Y. & Shiqiong, Z. (2002). Optimum mix parameters of high-strength self-compacting concrete with ultrapulverized fly ash. *Cem. Concr. Res.* 32, 477.
- [5] Ivanauskas, E., Rudzionis, Z., Navickas, A. A. & Dauksys, M. (2008). Investigation of shale ashes influences on the self-compacting concrete properties. *Mater. Sci. (Medziagotyra)*. 14(3), 247–253.
- [6] Chandra, S. & Berntsson, L. (2002). Lightweight aggregate concrete. *Science, technology, and applications NY*, William Andrew Publishing, Noyes.
- [7] Demirboga, R., O'ru'ng, I. R. & Gu'l, I. (2001). Effects of expanded perlite aggregate and mineral admixtures on the compressive strength of low-density concretes, *Cem Concr Res.* 31 (11), 1627–1632.
- [8] Urhan, S. (1987). Alkali silica and pozzolanic reactions in concrete Part 2: Observations on expanded perlite aggregate concretes. *Cem Concr Res.* 17(3), 465–77.
- [9] Erdem, T. K., Meral, C., Tokyay, M. & Erdogan, T. Y. (2007). Use of perlite as a pozzolanic addition in producing blended cements. *Cement & Concrete Composites.* 29, 13–21. DOI: 10.1016/j.cemconcomp.2006.07.018
- [10] Terkman, I. & Kantarci, A. (2006). Effect of expanded perlite aggregate and different conditions curing of the drying shrinkage of self-compacting concrete. *Indian journal of engineering & Materials sciences.* 13(6), 247-252.
- [11] Yu, L. H., Ou, H. & Lee, L. L. (2003). Investigation on pozzolanic effect of perlite powder in concrete. *Cement and Concrete Research.* 33(1), 73–76.
- [12] Bhuvaneshwari, K., Dhanalakshmi, G. & Kaleeswari, G. (2017). Experimental study on lightweight concrete using perlite. *International Research Journal of Engineering and Technology.* 4(4), 2451-2455.
- [13] Gunning, D. F., Eng, P., McNeal & Associates Consultants Ltd. (1994). *Perlite Market Study for British Columbia.*
- [14] Johari, M. A. M., Brooks, J. J., Kabira, S. & Rivard, P. (2011). Influence of supplementary cementitious materials on engineering properties of high strength concrete. *Construction and Building Materials*, 25(5), 2639-2648. <https://doi.org/10.1016/j.conbuildmat.2010.12.013>.
- [15] Yu, L. H., Ou, H. & Zhou, S. X. (2010). Influence of Perlite Admixture on Pore Structure of Cement Paste. *Advanced Materials Research.* 97, 552-555.
- [16] Esfandiari, J. & Loghmani, P. (2019). Effect of perlite powder and silica fume on the compressive strength and microstructural characterization of self-compacting concrete with lime-cement binder. *Measurement.* 147, 106846.
- [17] Karein, S., Motahari, M. et al. (2018). Effects of the mechanical milling method on transport properties of self-compacting concrete containing perlite powder as a supplementary cementitious material. *Construction and Building Materials.* 172, 677-684.
- [18] Sičáková, A., Figmigová, E. & Špak, M. (2020). Comparison of the strength development of binary and ternary cements containing perlite powder. *SSP – Journal of Civil Engineering.* 15(1), 47-57. DOI: 10.1515/sspjce-2020-0006.
- [19] Mansour, S.M. (2020). Physical-mechanical properties of steel fibre-reinforced self-compacting concrete containing natural perlite addition, *International Journal of Microstructure and Materials Properties.* 15 (2), 122-140. <https://doi/abs/10.1504/IJMMP.2020.106923>
- [20] El Mir, A., Nehme, S.G. & Assaad, J.J. (2020). Durability of self-consolidating concrete containing natural waste perlite powders, *Heliyon.* 6. <https://doi.org/10.1016/j.heliyon.2020.e03165>
- [21] Mansour, S.M., Haddadou, N. & Chaid, R. (2021). Valorization of powder of volcanic rocks used as cement substitution in self-compacting concrete, *European Journal of Environmental and Civil Engineering*, DOI: 10.1080/19648189.2021.1916782
- [22] Annual Book of ASTM Standards, ASTM C 618-01. (2002). Standard specification for coal fly ash and raw or calcined natural pozzolan for use as a mineral admixture in concrete. American Society for Testing and Materials, PA.
- [23] Wasserman, R. & Bentur, A. (1996). Interfacial inter-actions in lightweight aggregate concretes and their influence on the concrete strength. *Cem Concr Compos.* 18(1), 67–76.
- [24] Zhang, M. H. & Gjorv, O. E. (1990). Pozzolanic reactivity of lightweight aggregates. *Cem Concr Res.* 20(6), 884–90.
- [25] NF EN 12350-8. (2010). Essai pour béton frais – partie 8: béton autoplaçant– Essai d'étalement au cône d'Abrams.
- [26] NF EN 12350-10. (2010). Essai pour béton frais – partie 10: béton autoplaçant– Essai à la boîte en L.



- [27] NF EN 12350-11. (2010). Essai pour béton frais – partie 1: béton autoplaçant– Essai de stabilité au tamis.
- [28] EFNARC. (2005). European guidelines for self-compacting concrete: specification, production and use. Self-compacting concrete European project group.
- [29] NF EN 12390-2. (2001). Essais pour béton durci – Partie 2: confection et conservation des éprouvettes pour essais de résistance.
- [30] NF EN 12390-3. (2001). Essais pour béton durci - Partie 3: résistance à la compression des éprouvettes.
- [31] NF EN 12390-5. (2001). Essais pour béton durci - Partie 5: résistance à la flexion sur éprouvettes.
- [32] Krautkramer, J. H. (1977). Ultrasonic Testing of Materials. *Springer-Verlag*, Berlin.
- [33] Markham, M. F. (1957). Measurement of elastic constants by the ultrasonic pulse method. *British Journal of Applied Physics*. 8(6), 56-63.
- [34] NFP18- 418. (1989). Béton - Auscultation sonique- Mesure du temps de propagation d'ondes soniques dans le béton.
- [35] Gupta, T., Chaudhary, S. & Sharma, R. K. (2016). Mechanical and durability properties of waste rubber fiber concrete with and without silica fume. *J. Clean. Prod.* 112, 702-711. <https://doi.org/10.1016/j.jclepro.2015.07.081>
- [36] NF EN 12350-6. (2012). Essais pour béton frais - Partie 6: masse volumique.
- [37] NF EN 12350-7. (2012). Essais pour béton durci - Partie 7: masse volumique.
- [38] Mansour, S.M. (2020). Behavior of self- compacting concrete incorporating calcined pyrophyllite as supplementary cementitious material. *J. Build. Mater. Struct.* 7 (2), 119-129. <https://doi.org/10.5281/zenodo.4005645>
- [39] Wild, S., Khatib, J. M. & Jones, A. (1996). Relative strength, pozzolanic activity and cement hydration in superplasticised metakaolin concrete. *Cem Concr Res.* 26(10), 1537–44. [https://doi.org/10.1016/0008-8846\(96\)00148-2](https://doi.org/10.1016/0008-8846(96)00148-2)
- [40] Neville, A. M. & Brooks, J. J. (1987). *Concrete technology*. USA, Longman Group UK Limited.
- [41] Whitehurst, E. A. (1951). Soniscope tests concrete structures, Research and development laboratories of the portland cement association. *J Am Concr Inst.* 47, 433–44.
- [42] Jones, R. & Gatfield, E. N.(1955). *Testing concrete by an ultrasonic pulse technique*. London, H.M. Stationery Office.
- [43] Fascicule 62, CCTG, DTU P 18-702. (2000). Règles techniques de conception et de calcul des ouvrages et constructions en béton armé suivant la méthode des états limites, Règles BAEL 91.

## Asphalt mixture and its time delay of stress after strain at change of temperature and frequency

Ján Mandula, Jakub Bokomlaško

Technical University of Košice, Slovakia  
Faculty of Civil Engineering, Institute of Structural engineering, Department of Geotechnics and Transportation Engineering  
e-mail: jan.mandula@tuke.com, jakub.bokomlasko@tuke.sk

### Abstract

Materials in pavement construction are used due to their material properties. Asphalt mixtures, which are today most used during building pavement construction, have a significant place. Asphalt mixtures are classified as viscoelastic materials due to their material properties. This article focuses on the time delay of the stress behind the strain, which is a specific property for viscoelastic materials. It is particularly focused on one type of asphalt mixture, which is used in the binder course and in the upper base layer. The selected asphalt mixture was tested on a four-bending machine and the samples had a beam shape. The sample was tested at four temperatures and seven frequencies. In the discussion, the article focuses on the comparison of the time delay of the stress  $\Delta t$  behind the strain during the change of temperature and frequency. It is clear from the results that the selected asphalt mixture is significantly affected by the change in temperature as well as the change in frequency. The conclusion is devoted to a summary of the acquired knowledge and observation, which is focused on examples in practice.

**Key words:** asphalt mixture, frequency, time, load, stress

## 1 Introduction

Asphalt mixture is today the most widely used material in the construction and reconstruction of the upper layers of pavement. This material won the position due to the fast laying, price, availability, and material properties. It is these material properties that make it specific and give it many advantages as well as disadvantages. Material advantages include easy processability, recyclability, self-regeneration, and so on. Disadvantages include, in particular, sensitivity to changes in temperature and load frequency, where at different temperatures or frequencies the asphalt mixture achieves different stiffness modulus. It is precisely because of this specific property that it is classified as a viscoelastic material. The main phenomenon in viscoelastic materials under dynamic loading is the delay of strain under stress if the test is controlled by constant stress. In a constant displacement-controlled test, the

stress lags behind the strain. This delay is described by a phase angle, the value of which ranges from  $0^\circ$  to  $90^\circ$ . When the theory states that a material with a phase angle of  $0^\circ$  exhibits elastic properties and a material with a phase angle of  $90^\circ$  exhibits viscous properties [1,3]. The imaginary limit when the material is more elastic or viscous is a phase angle of  $45^\circ$  [1,3]. Figure 1 schematically shows on the sinusoid the delay of the resulting stress behind the strain. When the time delay is during one period of  $T$ .

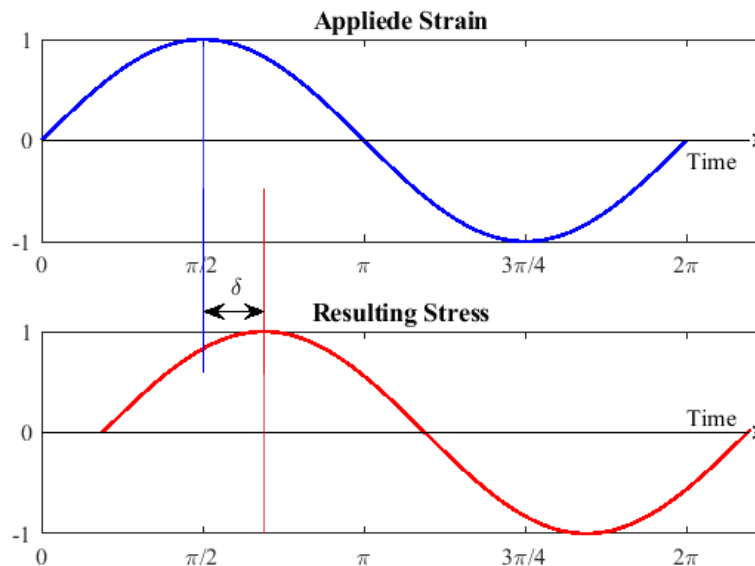


Figure 1: Viscoelastic properties  $0^\circ < \delta < 90^\circ$

## 2 Experiment

### 2.1 Material

The asphalt mixture marked AC 16 50/70 was mixed under laboratory conditions with a precisely determined composition. The composition of the asphalt mixture is given in Tab. 1.

Table 1: Composition of asphalt mixture AC 16 50/ 70

Components of the asphalt mixture	Percent [%]
Aggregate 8/16 mm	34.14
Aggregate 4/8 mm	19.18
Aggregate 0/4 mm	37.2
Stone flour	4.57
Asphalt binder	4.9
Filler WetFix BE	0.01
<b>Sum</b>	<b>100</b>

Granodiorite aggregate was used as a filler, which is characterized by suitable properties required for use in asphalt mixtures. Granodiorite is a type of aggregate classified as a deep igneous rock with a significant amount of quartz. It is close to granite, from which it is difficult to distinguish macroscopically. Granodiorites are usually light grey. Their construction is regular in all directions and mostly evenly grained. Granodiorite contains mainly quartz, plagioclase, and potassium feldspar. Of the other minerals, biotite and amphibole are often present [10]. From a mechanical point of view, it is a quality aggregate. The binder used was a 50/70 bituminous binder having a softening point of 50.5 °C and a penetration test of 58. In the penetration test, the time required for the needle to enter the sample at 25 °C is measured. It is bituminous that is often used in the production of asphalt mixtures. WetFix BE was also added to the mixture to improve the adhesion of the aggregate to the asphalt mixture. It is an additive which is a thermally stable viscous liquid of brown colour, and the main component is aliphatic amines and their derivatives, which are alkaline in nature.

## 2.2 Measurement method

The phase angle measurement was performed on a four-bending machine. When a beam shaped sample measuring 60 x 55 x 400 mm is mounted in the jaws at the edges of the device. The loading is provided by two jaws in the middle, which displacement in the vertical direction. The scheme of test equipment can be seen in Figure 2. The whole test equipment is placed in a climatic chamber, where the sample was loaded at different temperatures and frequencies.

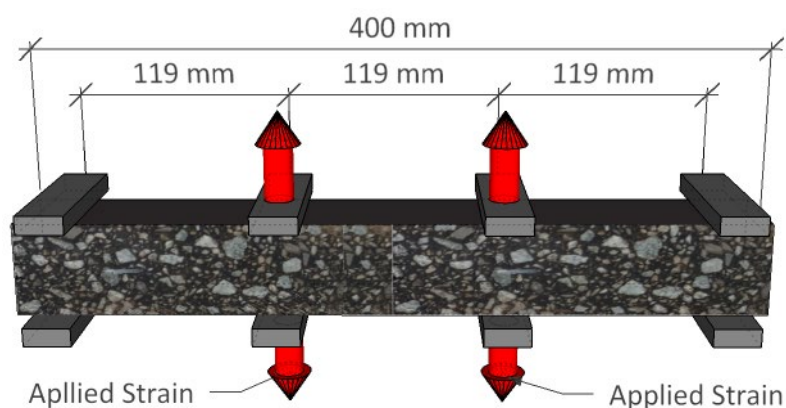


Figure 2: Scheme of test equipment

## 2.3 Phase angle measurement

The phase angle measurement was performed on a four-point bending device. The phase angle was taken as the average of the values from 100 cycles. The test was performed at temperatures of 27 °C, 11 °C, and 0 °C, on which the Slovak design methodology for the design of the pavement structure is based. The measurement was also performed at a temperature of 40 °C because this temperature is already detected in Slovakia in the summer on a pavement. The selected frequency range was 1, 5, 8, 10, 15, 20, 30 Hz. The range of

selected frequencies resulted from European standards and from research carried out on the given material. The stress on the beam was controlled by the strain, which was chosen according to STN EN 12697-26 so that during the test there is no decrease in the stiffness of the beam. The strain value was  $50 \mu\epsilon$ . The resulting phase angle values are shown in Figure 3. Where the x-axis plots the range of selected frequencies, and the y-axis shows the phase angle values.

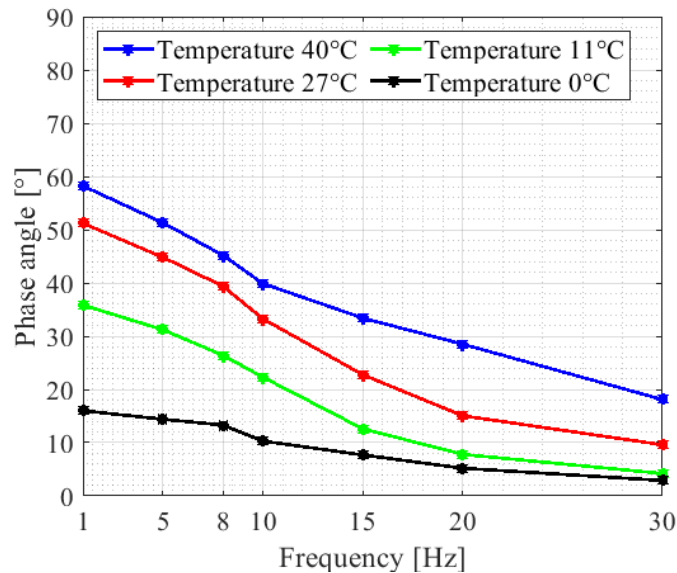


Figure 3: Dependence of phase angle [°] on frequency

As can be seen in Figure 3, as the frequency increases, the phase angle also decreases and the decrease has a rather linear course. When at a temperature of  $40 \text{ }^\circ\text{C}$  and a frequency of 1 Hz, a phase angle of  $58.2 \text{ }^\circ$  was recorded, which indicates that the beam already shows more viscous than elastic behaviour at a given stress and temperature. On the contrary, at a frequency of 30 Hz and the same temperature, the phase angle is only  $18.1 \text{ }^\circ$  and thus shows a more elastic behaviour. In contrast, at  $0 \text{ }^\circ\text{C}$ , the phase angle is lower. Where at a frequency of 1 Hz it has a value of  $16 \text{ }^\circ$  but at a frequency of 30 Hz the phase angle is only  $2.9 \text{ }^\circ$ . At such a low phase angle, it can already be said that the asphalt mixture has elastic properties [4].

#### 2.4 Calculation of time delay $\Delta t$

Subsequently, based on the obtained phase angle, the time  $\Delta t$  [s] (2) was calculated, which shows the time delay of the stress behind the strain. This phenomenon is typical for materials with viscoelastic behaviour [2,3].

$$\delta = 360 \cdot \frac{\Delta t}{T} \tag{1}$$

after adjustment

$$\Delta t = \frac{\delta \cdot T}{360} \tag{2}$$

Where :

$\delta$  - phase angle [°],

$\Delta t$ - time delay stress behind deformation [s],

$T$  - period [s].

The resulting  $\Delta t$  is shown in Figure 4. The selected range of selected frequencies is plotted on the x-axis. The value of  $\Delta t$  is plotted on the y-axis.

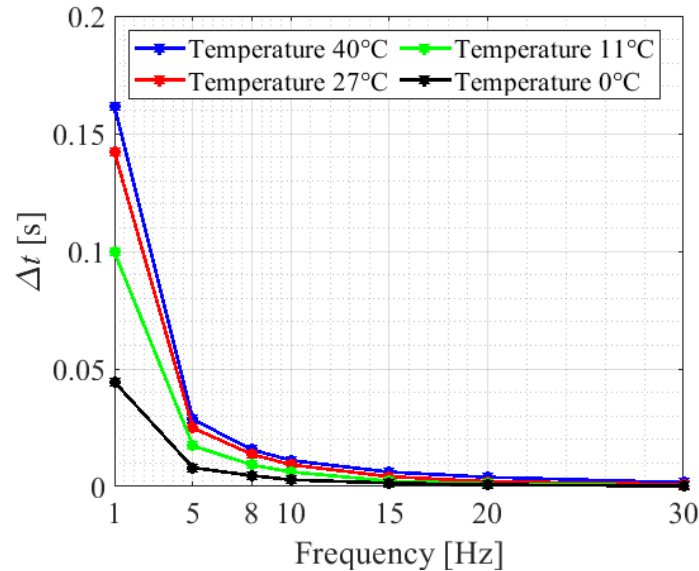


Figure 4: Dependence of  $\Delta t$  [s] on frequency

As can be seen in Figure 4, the curves at the selected temperatures have a decreasing tendency. When at the beginning a sharp decrease is recorded and with increasing frequency the curve stabilizes with a gradual decrease of the value of  $\Delta t$ . At a temperature of 40 °C and a frequency of 1 Hz, a time delay of 0.162 s was recorded. At the same temperature but at a frequency of 30 Hz, the time delay was only 0.00168 s. At the lowest selected temperature of 0 °C, the time delays were among the lowest values. For example, at a frequency of 1 Hz, the time delay was 0.0444 s, but at a frequency of 30 Hz, the time delay was only 0.000269 s. For better illustration, a graph was plotted to compare the phase angle and  $\Delta t$  for the selected values of frequency and constant temperature (Figure 5).

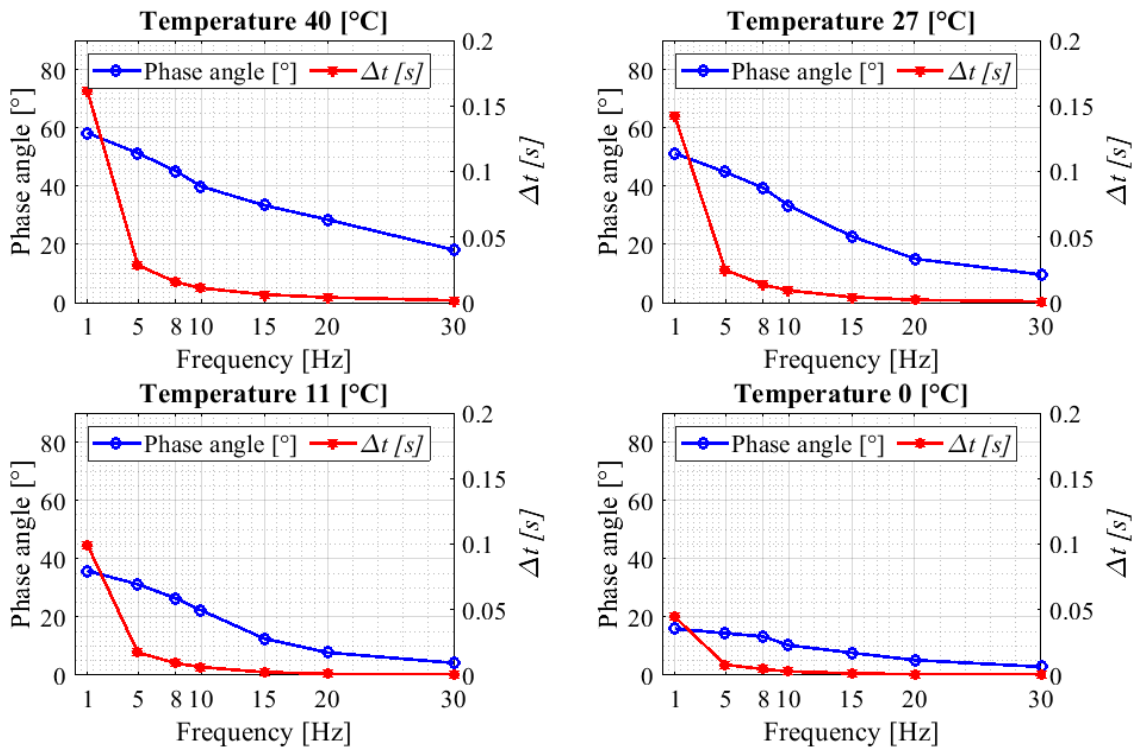


Figure 5: Dependence of phase angle [°] and  $\Delta t$  [s] on frequency

Figure 5a to 5d shows the dependence of  $\Delta t$  on the selected frequency range at the four monitored temperatures. Where the frequency range is plotted on the x-axis. The dependence of the phase angle at a constant temperature and a changing frequency is plotted on the left axis. The value of  $\Delta t$  depending on the changing frequency and constant temperature is plotted on the right y-axis. As can be seen from the graphs, as the frequency changes, both the phase angle and  $\Delta t$  decrease at all selected temperatures. The descent curve at the phase angle has a rather linear shape, but the curve  $\Delta t$  has a rather power shape. When at a frequency of 1 Hz, the largest value of  $\Delta t$  is detected, followed by a sharp decrease in values.

### 3 Evolution

For a better illustration of the difference between the individual temperatures and frequencies compared to the period, the individual values of the time delay  $\Delta t$  were converted to percentages. Where 100 %, the value of the period corresponding to the frequency was taken. The resulting comparison is shown in the bar graph in Figure 6. The graph shows the temperatures on the x-axis. Frequencies of 1, 10, 20, and 30 Hz were chosen for illustration.

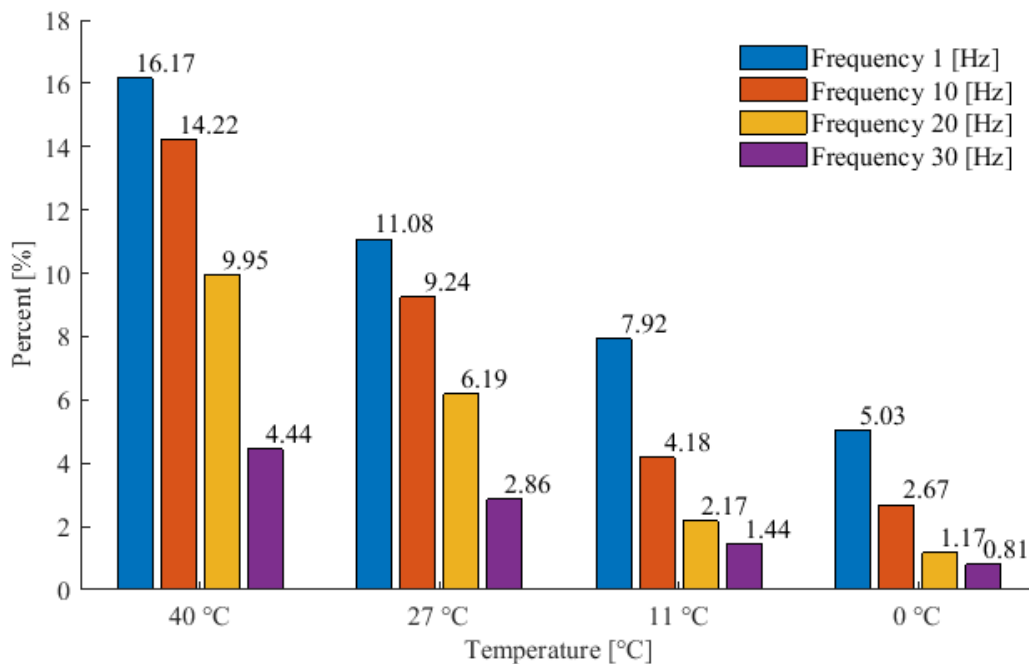


Figure 6: Percentage difference between the period and  $\Delta t$  [s] depending on the observed frequency

As can be seen from the graph, the percentage of time delay  $\Delta t$  has a decreasing tendency. Where with decreasing temperature and increasing frequency the time delay  $\Delta t$  decreases. In this case, for example, the percentage of time delay at 40 °C and 1 Hz is up to 16.17 %, but at a temperature of 0 °C, the percentage is only 5.03 %. In contrast, at a temperature of 40 °C and a frequency of 30 Hz, the percentage  $\Delta t$  is only 4.44 %, while at the same frequency and temperature of 0 °C, the percentage  $\Delta t$  is only 0.81 %. In such a case, the time delay of the stress behind the deformation is less than 1 %, and thus it can be assumed that the asphalt mixture will show more elastic properties and viscoelastic behaviour will be less influential. This fact is also supported by the value of the phase angle, which is only 2.3 ° at a temperature of 0 °C and a frequency of 30 Hz.

#### 4 Conclusion

From the results obtained from the selected test and the subsequent evaluation, a conclusion can be drawn. As the temperature rises, so does the phase angle and thus the time delay of the stress behind the strain. In contrast, the decreasing frequency of the load also increases the phase angle as well as the time delay  $\Delta t$ . This observed phenomenon corresponds to a typical material that exhibits different material properties and, in this case, different phase angles, as well as time, delays  $\Delta t$  when the temperature and frequency change. Such a significant effect of viscoelastic behaviour is caused by the chosen asphalt mixture. In the given asphalt mixture, a bituminium of the 50/70-type is used, which has a softening point of 50 °C on average. For this reason, higher viscoelastic characteristics were recorded at higher temperatures. Also, the frequency of loading affects the material properties, where at a frequency of, for example, 10 Hz, a higher time delay  $\Delta t$  was detected compared to a frequency of 20 Hz. The frequency of 10 Hz corresponds to an average speed of 50 km/h for



truck and the frequency of 20 Hz corresponds to an average speed of 80 km/h [2]. Therefore, if we look at it from a practical point of view, a road with a higher speed for truck, for example, 90 km/h, will show less damage than the same road at a lower speed, for example, 50 km/h due to different load frequencies [2].

## Acknowledgments

This work was supported by the Agency for the Support of Research and Development on the basis of Contract no.APVV-15-0777.

This work was supported by the Scientific Grant Agency of the Ministry of Education of Slovak Republic and the Slovak Academy of Sciences under project VEGA 1/0796/21.

## References

- [1] Komba J., Maina J.W., Anochie-Boateng J.K., O'connell J.. 2012. Analytical modelling of visco-elastic behaviour of hot-mix asphalt. Abstracts of the 31st Southern African Transport Conference, Proceedings ISBN Number: 978-1-920017-53-8.
- [2] Mollenhauer K., Wistuba M., Rabe R.. 2009. Loading Frequency and Fatigue: In situ conditions & Impact on Test Results. 2nd Workshop on Four Point Bending, Pais (ed.). University of Minho. ISBN 978-972-8692-42-1.
- [3] Manolis S., Eng P.. 2014. Engineering properties of asphalt cement binders and their relation to pavement performance. Presentation to Thirdyear Civil Engineering. Royal Military College of Canada.
- [4] Zhang R., Wang H., Gao J., You Z.. 2017. High temperature performance of SBS modified bio-asphalt. Construction and Building Materials 144:99-105, DOI: 10.1016/j.conbuildmat.2017.03.103.
- [5] Zbiciaka A., Michalczyk R., Brzeziński K.. 2016. Evaluation of fatigue strength of pavement structure considering the effects of load velocity and temperature variations. XXV Polish – Russian – Slovak Seminar “Theoretical Foundation of Civil Engineering”, Procedia Engineering 153 ( 2016 ) 895 – 902.
- [6] 2nd Workshop on Four Point Bending, Pais (ed.), © 2009. University of Minho. ISBN 978-972-8692-42-1.
- [7] Chabot A., Chupin O., Deloffre L., Duhamel D.. 2009. Viscoroute 2.0: a tool for the simulation of moving load effects on asphalt pavement. Road Materials and Pavements Design. Volume X – No X/2009,
- [8] Al-Qadi I.L., Fini E.H., Masson J.F., McGhee K.M.. 2008. Effect of Bituminous Material Rheology on Adhesion. Transportation Research Record: Journal of the Transportation Research Board, No. 2044, Washington, D.C., pp. 96–104. DOI: 10.3141/2044-11.
- [9] Xu Q., Solaimanian M.. 2009. Modelling linear viscoelastic properties of asphalt concrete by the Huet – Sayegh model. ISSN 1029-8436 print /ISSN 1477-268X online. Taylor & Francis, DOI: 10.1080/10298430802524784.
- [10] Wu H., Huang B., Shu X.. 2012. Characterizing viscoelastic properties of asphalt mixture utilizing loaded wheel tester (LWT). Road Materials and Pavement Design, Vol. 13, No. S1. 38–55, ISSN 1468-0629 print/ISSN 2164-7402 online, 2012 Taylor&Francis.
- [11] Biligiria K.B., Kaloush K., Uzan J.. 2010. Evaluation of asphalt mixtures' viscoelastic properties using phase angle relationships. International Journal of Pavement Engineering, Vol. 11, No. 2. 143–152. ISSN 1029-8436 print/ISSN 1477-268X online.

## Revenue House - architectural typology to be valorised

BoumazaOuafa<sup>1</sup>, Bordjiba Abdelhak<sup>1</sup>

<sup>1</sup>Department of Architecture, Badji Moukhtar University, Annaba, Algeria  
e-mail: boumazaouafa23@gmail.com

### Abstract

This research was carried out on the state of degradation of the historic core of Annaba city, Algeria. This degradation is caused by multiple factors, the most important of which is the absence of shared responsibility of public actors. The number of collapses multiplied which became a source for the creation of large office buildings with modernist tendencies, but without any architectural identity. The real estate park in downtown Annaba brings together urban entities according to various principles and logics of composition, structuring the urban image of the city of Annaba. The objective of this study is to build a complete catalogue summarizing the structures and fundamental characteristics of old buildings. Initially, this study defines all the notions linked to urban morphology and the typologies of housing. Secondly, an architectural study will be carried out on the “income house”, which represents the basic unit for the development of this historic nucleus. The typological analysis was applied to 44 buildings from the 19th and early 20th centuries located on the boulevard named “Revolution Square” in order to identify a set of common and specific criteria for the classification of “house income”.

**Key words:** revenue house, historical, urban fabric, typological analysis, architectural type

## 1 Introduction

The construction of buildings during the 19th and 20th centuries made a major contribution to the structuring of spaces and the enrichment of architectural typologies, distinguished by their forms, styles, and the organization of their window networks and by the architectural elements and decorations that dressed their façades. Just as much as the medina, the colonial (19<sup>th</sup> and 20<sup>th</sup> centuries) city constitutes one of the characteristics of the historic town centres of Algerian cities. The juxtaposition of the Arab-Muslim entity and the colonial entity makes the Algerian or Maghreb city certainly a dual city but rich in the field of architecture.

However, the colonial legacy, and more precisely that of colonial constructions, remains undervalued because it refers to the memory of the balance of power that the dominant European class maintained with the local population. Indeed, the collective memory has difficulty in recognizing the legacy of a civilization considered hostile and foreign. Therefore,

since independence, neglect, overexploitation, anarchic transformations, and a succession of natural disasters have seriously altered or partially destroyed this heritage [1]. Even more devastating was the lack of clearly expressed interest by the actors in charge of this heritage, which is still awaiting recognition and status.

Like other Algerian cities, the city of Annaba inherited from the colonial period a rich and varied but relatively degraded housing stock. The deterioration is the result of a combination of factors: its reappropriation by a population unable to maintain the buildings, its over-densification, the lack of interest shown by those in charge, and status of co-ownership of the buildings for which management mechanisms have not been put in place [2]. The advanced state of degradation has led to multiple collapses creating empty pockets within this core, coveted by private developers whose objective is the creation of large office buildings with curtain walls with so-called modernist tendencies but without any architectural identity. This study aims to provide a comprehensive catalogue based on the typological analysis of colonial buildings. It highlights the main structures and characteristics of these ancient buildings in the city of Annaba. By revealing the architectural and architectural richness of the colonial buildings, this catalogue could serve as a reference tool for architects and contractors to consult before deciding on any rehabilitation project; it would orient the pre-operative perspectives for the treatment of certain types of housing. To this end, the analysis focuses on the historical colonial core of Annaba in general and on a sample of buildings from the Revolution Square (formerly known as Cours Bertagna) for their historical, and architectural values.

The historical study represents a kind of prelude, a stage aimed at understanding the urban place before approaching its analysis with a view to better knowing, understanding, and transforming it. The historical approach contributes to deciphering the modalities of its workforce productivity and transformation, to unveil and understand the strategies implemented for the manufacture of this space.

## **2 Elaboration of the architectural typology of the colonial urban building of Annaba, Algeria**

### **2.1 Spatial criterion**

The analysis focuses on the historical centre of Annaba and is carried out on the scale of the built-up area, a level of analysis that makes it possible to grasp initially the relationship of the building with the segment of the urban territory which includes it. Consequently, the building constitutes the basic unit of the building under study. It is therefore agreed that the building is made up of all the built volumes, superimposed and served by the same doorway-stairway sequence; this whole being coherent in terms of the constructive structure and the land division [3]. The buildings are part of the urban fabric of Islet 1 of *Revolution Square* in the figures (Figure 1). To determine their structure and typology, the built-up areas are divided into plots made up of strips perpendicular to the street axis. The boundaries of the building coincided with three of the boundaries of the plot: in contact with the street and contact with the plots, the building participates in a continuous row of buildings, a row which directly

constitutes the space of the street, the urban collective space [4]. However, it is a question of going beyond a simple cadastral interpretation, of examining the thickness of the building and determining how the colonial urban fabric is constituted.



Figure 1: Location of the colonial city centre

## 2.2 Historical criterion

The historical criterion is important because each historical period is marked by a specific architectural style and urban forms that reveal the society in place at a given historical period. Indeed, the period of construction of the buildings studied corresponds to the neo-classical period in France, a style reproduced in colonised countries such as Algeria in the figures (Figure 2).

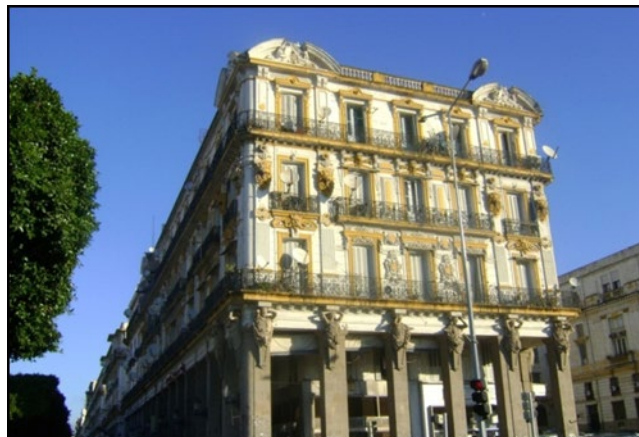


Figure 2: Example of a neoclassical building « Palais Calvin »

## 2.3 Morphological and architectural criteria

Since every typology is the result of classification, the definition of the corpus, the division and the level of interpretation become relevant questions. The present study aims at the elaboration of an architectural typology of the colonial urban buildings of Annaba, using

geographical, historical, morphological, and architectural criteria. For each building named as a study sample, surveys (plans and façades) are carried out, and descriptive technical data sheets are drawn up, each of which includes a presentation of the block, specifying its position in the town centre, but also explains each sample, i.e., the building, its occupation of the plot, its survey (plans and façades) and its location in the figures (Figure 3). The typology first required an inventory resulting from careful observation of the objects, and then by a description of the properties that distinguish them and allow criteria of differentiation or similarity to be established. Next, the type had to be defined by bringing together the common properties of the objects of the same family. Hence, we were able to identify the association with common organisational structures. There is a constant link related to the shape of the land, the way it is occupied, the way the flats are distributed, superimposed, illuminated, and used, and the principle of the organisation of the façades. These constants contribute to the elaboration of a canonical model within which the variants and languages specific to each singular building, such as ornamentation and materials, develop. The passage between the building typological categories was then carried out based on the essentially morphological criteria: a type historically based on its appearance as a typological category is characterised in this second stage by its relationship to the urban training in which it is involved, but also by its programme, several flats, surface areas [5]. The physical characteristics of the type are then described by noting distributive, functional, dimensional, and stylistic indices which are always interpreted [6].

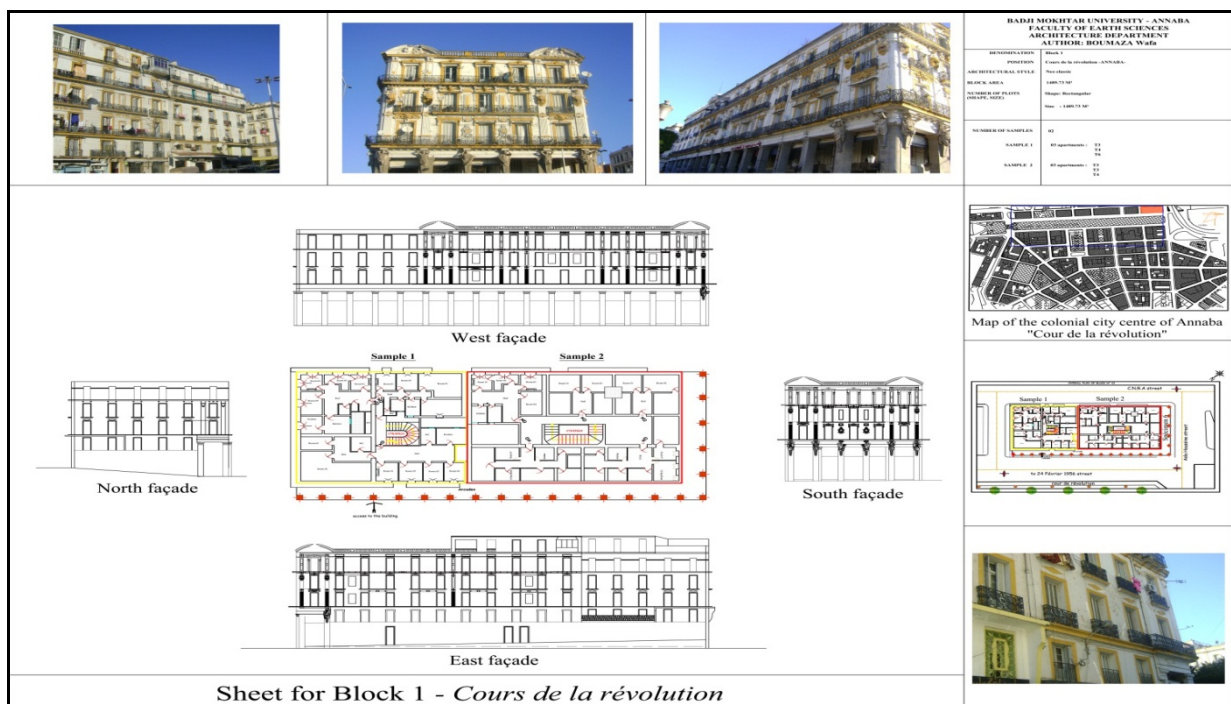


Figure 3: Example of a data sheet for Block 1 on the *Revolution Square* in Annaba

### 3 Results and discussion

#### 3.1 Delimitation of the sector of study and choice of the corpus of investigation

The study area corresponds to a small fraction of the city centre of Annaba, a city in the extreme north-east of Algeria known for its rich historical heritage. The city's historical designations Hippone, Hippo-Regius, Bouna, Bône and finally Annaba bear witness to the historical depth of this city [2]. This sector of colonial creation (between 1865 and 1905) located near the medina differs radically from the typo-morphological points of view and the logic of urban manufacture. This sector of Annaba town centre is delimited to the east by the medina, to the south by the port, to the north-west by the Rondon Column and the GasometerCity, and to the south-west by the *Champ de Mars* (formerly known as *Champ de Manœuvre*) in the figures (Figure 4).

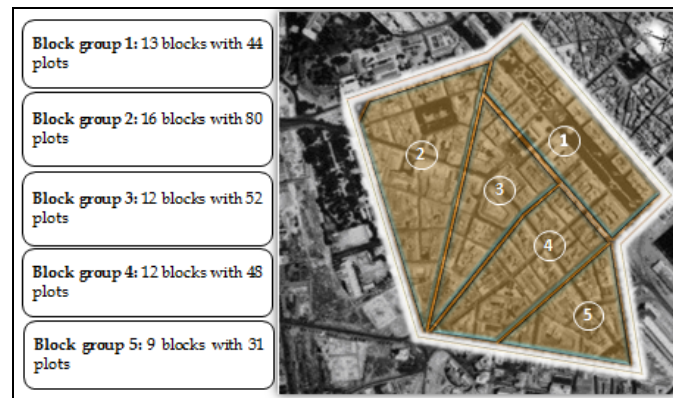


Figure 4: Overview of the boundary of the study site.

The historical colonial centre of Annaba (4<sup>th</sup> Algerian city) is characterised by a real homogeneity in terms of building typology and is delimited by the first French wall in Bône built between 1850-1888 [2]. It groups buildings built since the 19<sup>th</sup> century on a plot of land in a characteristic form: a façade on a narrow street, a deep building with adjoining walls with contiguous buildings which are sufficiently homogeneous for the present case study.

A representative analysis based on a sample of 44 buildings [7] was carried out on either side of the *Revolution Square* and is considered to be fairly representative of colonial urban architecture. Thus, the knowledge of the city of Annaba and the more general "urban phenomena" helped to give consistency to the study specimens. The buildings were chosen for their representativeness (quantitative and typological) and the possibilities of access inside the buildings [8], initially with the modes of distribution of the common spaces (courtyards and staircases) and the possibilities of access to the flats in a second stage (agreement of the owners and tenants).

### 3.2 Morphological and architectural characteristics of the corpus of study

#### 3.2.1 Typological classification of buildings according to the general shape of the building

Among the permutations that could be identified, the delineated level structures are the most attested in the corpus in the figures (Figure 5). This phase of the analysis highlights the shape of the buildings, which may contain from one to four samples or flats. As a result, the most dominant shape in our corpus of flat buildings is the rectangular shape with a percentage of 41%, 23% square, 19% form L and 12% form U. This explains why the organisation of the plots is geometrically regular and aligned with the street.

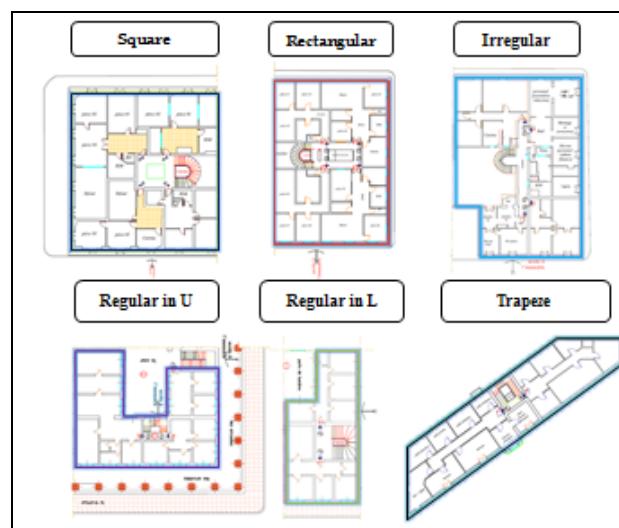


Figure 5: Summary of the building forms used in our corpus

#### 3.2.2 Typology of buildings by number of stories

The buildings included in the corpus of the study have a ground floor containing a 4.5 m high mezzanine floor, which differentiates it from the standard 2.40 m high floors of the building. They differ from each other in terms of their respective heights and number of floors. Four-storey buildings are the most dominant form, accounting for 50% of the corpus. This result could justify the choice of the typology of the revenue house which, a priori, consists of housing the most allochthonous population during the colonial settlement in Annaba.

#### 3.2.3 Typology according to the distribution of the interior spaces of the building

The main distribution space of the building is the staircase that gives access to the different floors. The flats can be served either directly, with the entrance door of the flat leading to a storey in the stairwell, or indirectly, via a corridor allowing the distribution of flats far from the staircase. The corridor, deprived of natural light, is not necessarily repeated on each floor. Its presence depends on the distribution level by level. It can also be served indirectly, via a corridor. The passageway appears to link two buildings separated by an inner courtyard on

which it emerges. The different positions occupied by the staircase constitute a determining characteristic of the morphology of the building. It can be located at the back of the building, opposite the street, and be in daylight on a courtyard or passageway, and/or in a median position (central staircase) it can then be in daylight on an inner courtyard or be totally in darkness.

- **Physical and spatial characteristics of the stairs and stairwell**

The staircase can be characterised by its structure, construction material and dimensions. The common feature of all these staircases is that they are built into a shaft made up of walls that can be either slit or specific shaft walls. The steps are recessed in the wall for the stairs, for the wooden stairs, the false stringers and the storey beams are recessed. Four types of staircases can be distinguished: core wall staircase, or with daylight, and spiral or has a straight flight (single, double, or triple flight staircase) [9]. This distinction is based on technical and spatial requirements. The most commonly used materials are stone and wood. The stones used in the realization of the staircase are intended to reinforce the load-bearing elements of the stairs. Regarding wood, it was used in the realization of the stairs but with caution because the study site is in a very humid area. The typologies according to stairwells are summarised in the table (Table 1).

Table 1: Typology of stairwells accessible to in situ surveys

Type of staircase	Samples
Hollow stone core	10 samples
Hollow wood core	6 samples
Solid stone core	15 samples
Solid wood core	7 samples

It emerges that the most frequent type of stairwell in our study of buildings remains the stairwell with a solid stone core, followed by stairwells with hollow stone cores and with a central position; this could mean that wooden stairwells would be the rarest prototype in the Annabi colonial city centre. The different positions occupied by the staircase are a determining feature of the building's morphology. It can be located at the back of the building, opposite the street, and can emerge from a courtyard or passageway. Or, it can be in a median position (central staircase), it can then take daylight on an inner courtyard or be in complete darkness. Both cases can even be found in the same building. Table 2 presented the Stairwells also differ in their positioning.

Table 2: Differentiated positioning of stairwells

Stairwell position	Samples
Central	38 samples
Lateral	6 samples
Central and lateral	8 samples

- **Inner courtyards**

The courtyard is an empty, uncovered space inside the building. It produces an exterior that provides lighting, ventilation, and the relationship to the atmospheric conditions of the rooms opening onto it. Situated in the middle of the building, it creates a partition between living



areas, divided into both sides, which make up two of its façades (courtyard façades). The other façades are made up of a blind partition wall and a stairwell (or a corridor system). The surfaces of the inner courtyards vary greatly but can be grouped into three main classes in the tables (Table 3).

The small courtyard category (less than 50 m<sup>2</sup>) predominates; but the other categories of inner courtyards are certainly less important in quantitative terms, but they provide more favourable conditions of comfort, particularly those of lighting in the absence of sunshine. The threshold  $L = H / 2$  ( $L$  = length of the courtyard,  $H$  = height of the building) can be used as a reference point. The corpus of the study presents a prospect that varies from 0.5 to 3.10, which explains why this typology of buildings perfectly meets the standards of hygiene and comfort.

Table 3: Classification of the courtyards of the buildings according to the surface area

Size of courtyards	Samples	
	No. of samples	%
Small size (0 to 50 m <sup>2</sup> )	19	43%
Medium size (50 to 100 m <sup>2</sup> )	12	27%
Large size (100 to 200 m <sup>2</sup> )	09	21%
With very large size (< 200 m <sup>2</sup> )	04	9%

### 3.2.4 Typology according to the morphology of living spaces

The study of the morphology of the building's living spaces takes into consideration two types of characteristics: dimensional characteristics (lengths, widths, areas, and proportions) and their arrangement in relation to each other. The aim here is to characterise the model of room distribution based on the opposition between representation rooms (living room, main bedrooms) on the street and service rooms on the courtyard on either side of an antechamber. The reference floor chosen for the analysis will be the first floor, which generally presents the most regular morphology. For all the flats in the buildings in the sector studied, we have established a grid of the basic surface areas of the standards of the flat blocks (Figure 5) and compared them with the one built in Paris during the same period. This is a way of comparing the morphological characteristics of the flats built in Annaba with those in Paris, for which the minimum surface areas in the rental sector were at least:  $T1 = 16 \text{ m}^2$  to  $28 \text{ m}^2$ ,  $T2 = 46 \text{ m}^2$ ;  $T3 = 60 \text{ m}^2$ ,  $T4 = 73 \text{ m}^2$ ). Out of a total of 65 flats distributed in 44 of the corpus of the study, the F4 flats are the most represented in the tables (Table 6) with surfaces ranging from  $52.36 \text{ m}^2$  to  $207.24 \text{ m}^2$ .

The comparison between the surface areas of the flats surveyed in the Annabi colonial core and the surface areas of the buildings built in Paris during the same period shows a huge difference in dimensions. This result proves that the construction logic of this type of building spatially speaking is very different from the buildings built in Paris during the same period because even if it is the same period, it is not the same context. These buildings were intended for a Maltese and Spanish population, the logic of the colonist to give Algeria an image of a French continent.

### 3.2.5 Typology according to the organization of the façades

The architectural language of the façades is described in terms of the division into horizontal registers and vertical spans, the composition, and the rhythm of the openings. These clues are related to the constructive aspects which are revealed through the composition of the façade and the visible materials. The decorative clues, stylistic references, richness, or absence of decoration and the relationship between it and the construction systems are indicative of the status of the building. The fenestrated network presents general discontinuities which organise its elements into a distinct sub-set. These are the obvious discontinuities that allow the analysed entity to be divided down into parts, and thus to build a structural model. As a result, we observe that the organization of our façade corpus is regulated in levels and spans; two storeys constitute the segmentations of our windowed network. This segmentation consists of "selecting segments deemed significant among all the discernible segments" [10]. This includes sections or well-delimited parts. The façades are generally organized according to a fenestrated network characterized by a regulated distribution of bays forming a reticular structure; they are grouped into sub-assemblies by various discontinuity processes known as lyses. The results of the application of morphological analysis led to four underlying typologies of the corpus, which themselves present subtypes that constitute only a basic model for the organization of colonial neo-classical façade systems, as they can vary according to decorations [7]. These models reflect a very particular positioning logic on the blocks located on either side of the study site: Type 1 and Type 2 present a horizontal organization according to a simple or double level of composition and a vertical organization obeying a central symmetry. These two types represent 30% of the main façades of the *Revolution Square* in the figures (Figure 6). Types 3 and 4 are structured with a single or double level of composition and a regular vertical organisation with the same type of decoration on the entire façade; 35% of them are located on the rear façades of the blocks overlooking the tertiary roads in the figures (Figure 6).

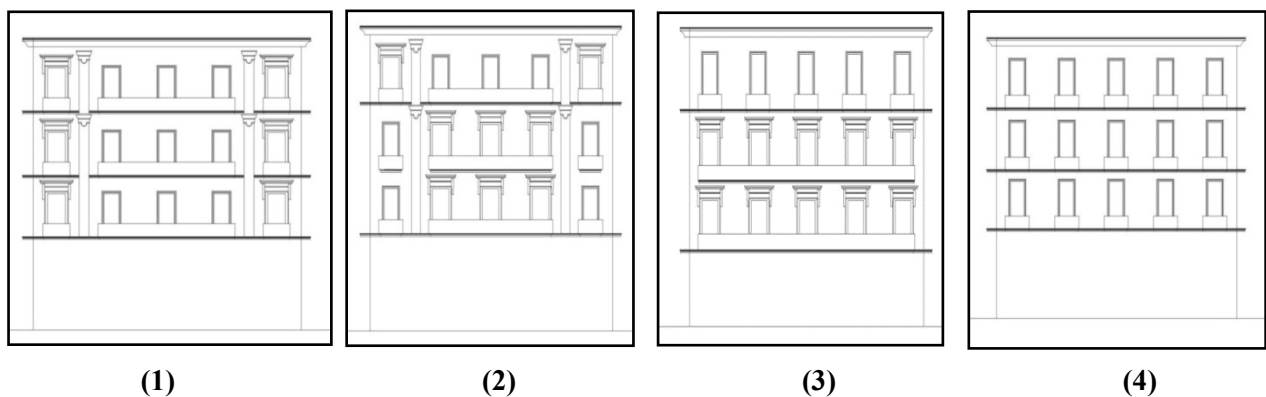


Figure 6: Type 1, 2, 3 and 4 of the selected façades

### 3.3 Typology according to the combination of morphological and architectural characteristics

This phase is the most important step in the typological analysis. Therefore, first, all the criteria explained above have been reported in a general summary table including the 44 samples proposed for analysis. Through a general interpretation of the whole corpus and according to the composition of each sample, we will extract the typologies according to each criterion to demonstrate the relevance of the latter.

A combination of these typologies will be carried out to identify the types of rental buildings that characterised the *Annabi* town centre and which, a priori, remains the main result of our investigation.

The results of this analysis carried out on the scale of the building composition, provide information on the intrinsic qualities of the *Annabi* colonial urban fabric, both from the point of view of urban morphology and the characteristics of the built elements. It emerges that two typologies characterise the revenue house according to the combination of the different typologies retained by the classification criteria in the figures (Figure 7). The typologies of the revenue house in the 44 samples are listed in Tables (Table 4).

Table 4: Summary of architectural characteristics of Type 1 and Type 2

Architectural feature	Type 1	Type 2
Shape of the building	Rectangular shape with street alignment	A square shape with street alignment
Stairwell (Type-Position)	A stone solid core stairwell with a central position that serves all the flats on the storey.	A stone hollow-core stairwell with a central position that serves all the flats on the storey and another lateral stairwell.
Courtyard and passageway	A courtyard in the middle of the building with average dimensions that vary between (0 to 50 m <sup>2</sup> ); it establishes a partition between habitable premises, distributed on either side and which make up two of its façades (courtyard façades).	A courtyard in the middle of the building with average dimensions that vary between (50 to 100 m <sup>2</sup> ); it establishes a partition between habitable premises, distributed on either side, and which constitute two of its façades (courtyard façades).
Number of flats per storey	A common floor with two flats per floor, type F4 with surfaces ranging from 52.36 m <sup>2</sup> to 207.24 m <sup>2</sup> .	A common floor with three flats per floor, type F3 with surfaces ranging from 51.36 m <sup>2</sup> -129.2 m <sup>2</sup> .
Spatial configuration	A basic distribution scheme with a room layout based on the opposition between representation rooms (living room, master bedrooms) on the street and service rooms on the courtyard on either side of an antechamber.	
Organisation of the façade	A horizontal organisation is according to a simple level of composition and a vertical organisation obeying a central symmetry and a rear façade obeying a regular structuring with a simple level of composition and with a regular vertical organisation according to the same type of decoration on the whole façade.	A horizontal organisation with a double level of composition and a vertical organisation is obeying a central symmetry and a rear façade obeying a regular structuring with a double level of composition and with a regular vertical organisation following the same type of decoration on the whole façade.

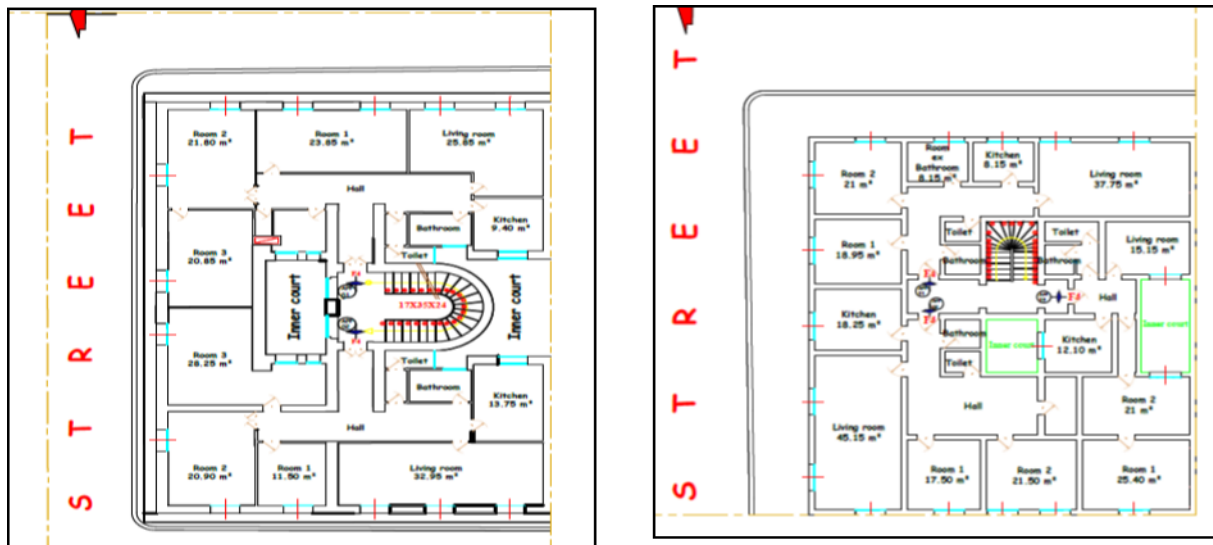


Figure 7: Diagram of type 1 and type 2 of investment buildings selected

#### 4 Conclusion

This study was carried out following a report about colonial buildings from the 19th and early 20th centuries in the historic centre of the city of Annaba. The effect of time, the unconsciousness of society and the negligence of the State have contributed to the degradation of this heritage. However, the colonial city, just like Medina, is an architectural and urban entity that deserves the recognition of its rich heritage by society and support by the State insofar as it represents a part of Algerian urban history, is endowed with an architectural identity and is the bearer of a specific culture. It is in this wake that this study was undertaken to demonstrate some of its specific characteristics and to support the idea that we should work for its preservation and therefore its sustainability.

Furthermore, this paper did not aim to provide an exhaustive document that would reflect the diversity of old housing and more specifically the "revenue house", but rather a comprehensive catalogue that highlights the basic structures and characteristics of old buildings and defines the typical structures of the different categories of buildings. The richness of the colonial-built heritage was highlighted by the identification, in situ, of the architectural and architectural typologies of the historic colonial core of Annaba.

The definition of the type of building in this research was considered a relevant approach to reveal the diversity and richness of this built heritage. It has made it possible to classify the multiform objects that constitute it; to identify categories that make it possible to order the confused mass of reality by identifying the formal and structural regularities that establish typical correspondences between homologous elements. The typological category classification of 19th and early 20th century flat blocks, to which this research has led, has shown the different architectural and architectural characteristics of each typological category in continuity of filiation through a "canonical" distribution of the flats in the building. The catalogue produced could serve as a reference and guidance tool for architects and contractors

who would be involved in urban planning operations such as refurbishment, rehabilitation, and restoration.

More generally, it is important to point out that the type of building is determined by the type of construction. This construction by rational abstraction can be done in two stages. First, in each given family, we will explain the properties of the objects that compose it, then we will gather the common properties of the objects of a family to define the type; the set of non-common properties marks the different variations on the type.

The typology leads to an understanding of architecture in a fabric. Built types appear to be doubly determined by culture and by a location, but this determination is not deterministic: in each place for a given time, several solutions are possible; the history of the project is part of this openness. In this kind of exercise, the historical study is a kind of prelude, a stage aimed at understanding the urban place before approaching its analysis to transform it.

## References

- [1] Abdel Tawab A. G. (2013), Evaluating the authenticity of earthen heritage: The case of Ramses WissaWassef art centre in Egypt,Alexandria Engineering Journal 52(3):489-498.
- [2] LAOUAR D. (2018),L'accessibilitéspatialecommeindice de fragmentation urbainedans les villescoloniales. Le cas de la villed' Annaba,BadjiMoukhtar University Algeria, 2018.
- [3] Ahmed H. A. A. H. (2012), Jordan: Guidelines for Urban and Architectural Heritage Conservation: Umm Qais case study,International Journal of Architectural Heritage 6(1): 62-85
- [4] Andrés M. A. N., Pozuelo F. B. (2009), Evolution of the architectural and heritage representation,Landscape and Urban planning 91(2): 105- 112.
- [5] Vecco M. (2010), A definition of cultural heritage:From the tangible to the intangible, Journal of Cultural Heritage 11(3): 321-324.
- [6] Souami M. A., Zerouala M. S., Ait-Meziane Y. (2016), The impact of building proportions in the preservation of Algiers architectural • Urbanism. Arhitectură. Construcții • Vol. 8 • Nr. 3 • 2017
- [7] BOUMAZA O. (2018), Morphogénèse des typologies architecturales et urbainesdu centre- ville colonial de Annaba, tesis . BadjiMoukhtar University Algeria, 2018
- [8] Viñas S. M. (2002), *Contemporary theory of conservation*, Studies in Conservation47(3): 25-34.
- [9] Ghomari F. (2007), The medina of Tlemcen: The legacyof *history*[in French], Web Journal onCultural Patrimony 2(1): 11-28.
- [10] Kioussi A., Karoglou M., Labropoulos K., BakolasA., Moropoulou A. (2013), *Integrateddocumentation protocolsenablingdecisionmaking in cultural heritage protection*, Journalof Cultural Heritage 14(3): 141-146.

## Project Info Water

**Mária Hlinková, Martina Zeleňáková**

Technical University of Košice, Slovakia  
Faculty of Civil Engineering, Department of Environmental Engineering  
e-mail: maria.hlinkova@tuke.sk

### Abstract

The main goal of Project Info Water is to raise awareness about water management and water resources in the Slovak republic. The target groups of the project are kindergarten students, primary school students, citizens of the affected area, and the government. The project contains four groups of activities – informal, media, online, and presentation activities. Informal activities include thematic brochures with a brief description of the topics Water of Eastern Slovakia, Household water, Flood, Flood protection, Water structures of Eastern Slovakia, Water in the landscape. The presentation activities include the description of webinars, the media, and social activities include print advertisement and access to social media fun pages.

**Key words:** environmental education, water management, water project, water sustainability

## 1 Introduction

Society is currently feeling the negative consequences of past decisions that have resulted in current environmental problems. The ongoing climate change is only the beginning of a new era in which the current, but especially the next generation will live. The global consequences of climate change can already be seen in rising ocean levels [1], increasing hydrological drought [2], or the heating of glaciers [3].

With the growing climatic problems, the need for education of the inhabitants of the affected area is also growing. Environmental education appears to be a reliable tool for supporting education and obtaining solutions for adaptation to climate change. In Slovakia, direct environmental education is provided mainly at universities, but more and more emphasis is placed on the support of education at lower levels. It is not necessary to provide environmental education only in educational institutions, but it is necessary to be aware of the consequences of one's own decisions in relation to the environment [4,5]. Institutionalized environmental education aims to offer students an overview of the current state of the environment and teach them to implement practical principles in life [6]. Environmental education as part of the cross-cutting themes of school subjects should be a matter of course.

The environment is a whole from which it is not possible to exclude a certain part of society. In addition, the current situation associated with the Covid-19 pandemic has set up a mirror for society, reflecting major shortcomings in critical infrastructure. One of the most affected areas was the education and educational system. Students remained tethered at home, unable to attend school fully. Educational materials had to be moved to the online space so that students could access them from the comfort of their homes. The main advantage we can consider keeping educational materials online for a long time, as well as easy access with literally one click. Even in this difficult situation, which is slowly stabilizing, it is possible to find small benefits.

The need for education in environmental-related topics is based on several surveys conducted among the population. The study of the area of interest is based on general knowledge. If we want to examine the living conditions of the inhabitants of a given area, it is necessary to obtain their opinions and gather their knowledge. It is, therefore, appropriate to use available methods to raise citizens' awareness of environmental issues affecting their lives.

Given the emerging climate change and its expected negative impact on the environment (including water) it is essential that we protect, maintain, and save water resources as a rare and irreplaceable raw material that already has strategic value today. Drinking water is one of the world's greatest problems for the future of mankind. Although it is one of the most abundant substances on earth, it is the first of the five basic problems of civilization (water, nutrition, health, ecology, and energy). We use water for various purposes, and it often happens that we do not save water, either because of convenience, ignorance, or the economic complexity of alternative options. For example, it is not necessary to use drinking water sources for technological processes, but it is possible to use service water. However, such a system requires ecological thinking, but first and foremost informing people about this issue. The first step on this long journey is to raise people's awareness of the possibilities of dealing with water resources.

Universities currently have the greatest potential to support environmental education [7]. The Technical University of Košice, mainly Faculty of Civil Engineering, participates in the support of environmental education. Thanks to the financial support from the Operational program Quality of the Environment, the project InfoWater NFP310010R074 is an ongoing project aimed at raising awareness about water management and water resources in the Slovak republic. The project is designed for the public, the description in detail is provided below.

## **2 Project Info Water**

The target groups of the mentioned project are kindergarten students, primary school students, citizens of the affected area, and the government. The project is primarily settled for citizens of eastern Slovakia. Activities outgoing from the Water project are divided into 4 groups – informal activities, medial activities, online activities, and presentation activities. The submitted paper describes informational, media, online, and presentation activities in detail.

### **2.1 Informal activities**

The first group of the project activities are informal activities. Those also include 4 sub-groups – the thematic brochures, audio records, video records, and pamphlets. There are three

types of thematic brochures, and each of them contains two topics: Water of Eastern Slovakia, Household water, Flood, Flood protection, Water structures of Eastern Slovakia, Water in the landscape. For the sake of simplification, the information brochures are named Information brochure no. 1, Information brochure no. 2, and Information brochure no. 3. The content of the mentioned brochures is adapted to the target groups. The brochure is a single-purpose, paperback, and simply a small-scale publication. Thematic brochures consist of professional text supplemented by appropriate illustrations to address the reader appropriately and engagingly and provide him with important information in the field of environmental protection and water management. In such case, that one brochure is designed for a wide range of readers, it is necessary to know how to inform every member of the group. You can't write complicated and difficult to understand full text for kindergarten children, on the other hand, you should not use picture diagrams for government to explain flood.

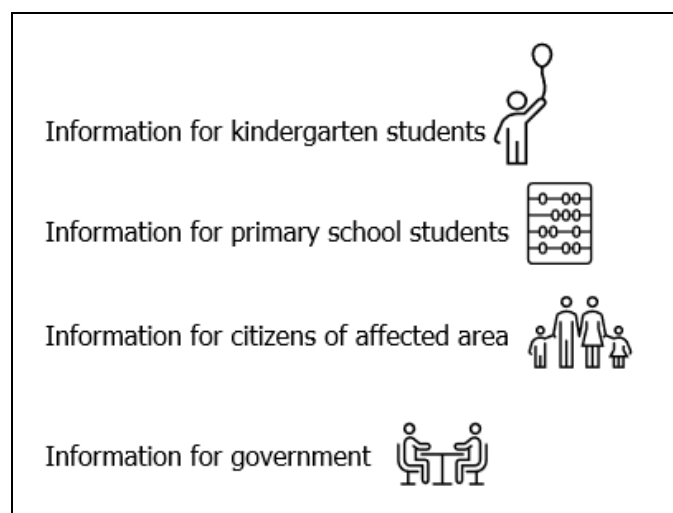


Figure 1: Labeling of the target groups in Information brochures

Figure 1 shows four icons, which are used to label the content of the information brochures. Elaborated topics are individually adapted for each mentioned group. When creating the content page of brochures, it was important that the content was tailored to the target group. Therefore, icons are used in the brochures to indicate to which group the page is intended. The Information brochure no. 1 contains topics Water of Eastern Slovakia and Household water. Information about the first topic, Water of Eastern Slovakia addressed for kindergarten children is very easily described. Children can find pictures of precipitation, rivers, snowman, or ice cubes with an explanation of how water gets to the ground (Figure 2).



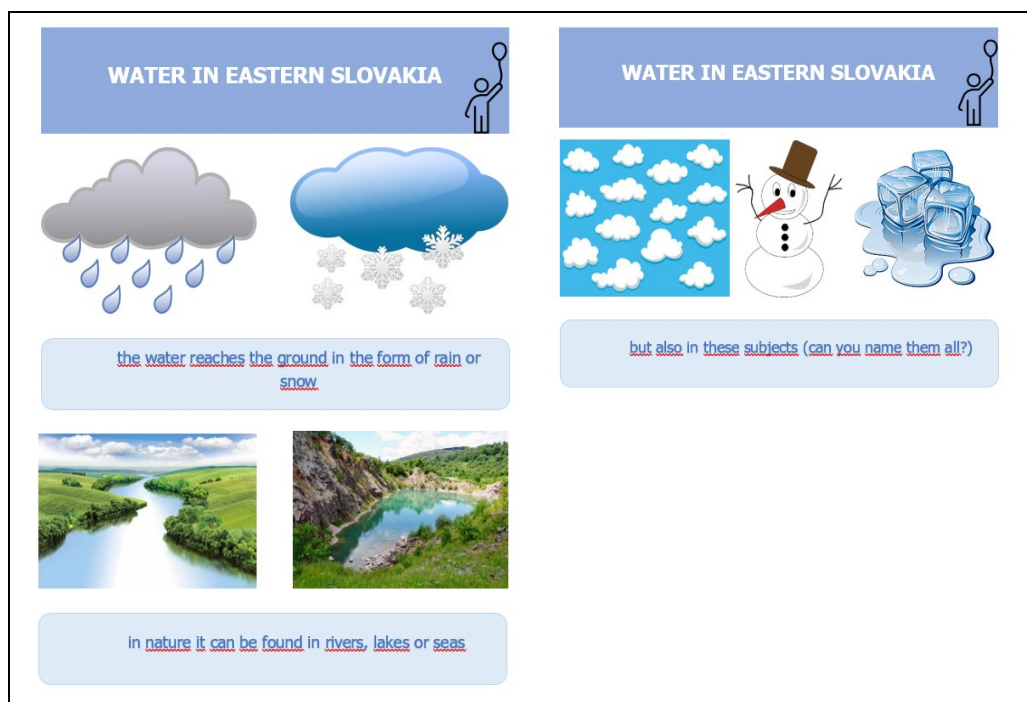


Figure 2: Pictures of the water for kindergarten children (originally in the Slovak language)

The following topic Household water also contains some easy pictures for kindergarten children. In this section, the pictures are aimed at how can kids save water in their households. For example, using a shower instead of a bath, stopping the water while brushing teeth, and using the rainwater to water the flowers (Figure 3).



Figure 3: Pictures for kindergarten students in the section Household water

More complex information contains sections primarily designed for primary school students. There are some questions about rivers in Slovakia, a blind map, and a crossword (Figure 4).

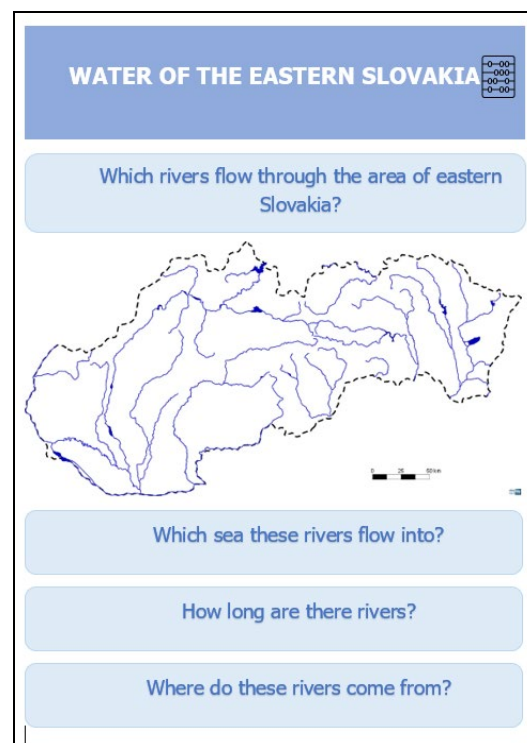


Figure 4: Example of blind map and questions tailored for primary school students

The most complex information can be found in the section tailored for citizens in the affected area and government. In the Information brochure, no. 1, are described some information about drink water in Eastern Slovakia, basic data about the main drink water source Starina and a brief description about water quality according to Decree 247/2017. Citizens and government should read the Information brochure no. 1 because of the availability and simplicity of the data about average daily household water consumption, how and why to use grey water, what about the price of the water and finally there is described a current state of drinking water supply and development of public sewers in conditions of Slovak republic. Information brochure no. 2 contains topics Flood protection and Water structures of Eastern Slovakia. The content is also divided into four groups, and the icons label suitability of the readers (Figure 1). The topic Flood protection in the kindergarten children section includes some pictures of floods with a couple of questions to enhance the critical thinking of the children (Figure 5).

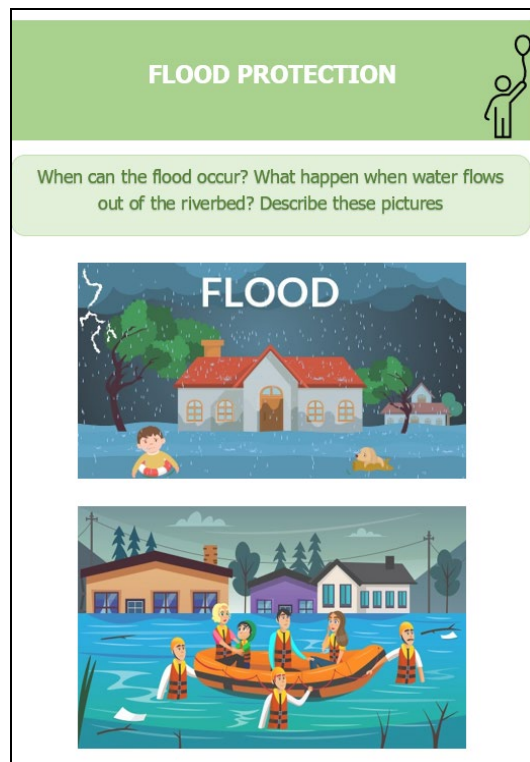


Figure 5: Example of kindergarten children´s sections - description these picture help children to think about occurrence of flood

Primary school students can exam themselves in the test questions related to flood and flood protection, and citizens and government can read about the review of the flood situation in Slovakia in recent years.

In the year 2018, the questionnaire survey was conducted. The survey focused on the state of preparedness of the municipalities of Eastern Slovakia in case of a flood. Results of the survey were shown in the bachelor thesis, and part of the results are available in the Information brochure no. 2, as a brief description of the current state of the affected area. Representatives of municipalities from eastern Slovakia took part in the questionnaire survey.

The Project Info Water is mainly designed for the area of eastern Slovakia, so the target groups are informed about the current situation.

The last Information brochure no. 3 presents topics Water in landscape and Water retention measures. Kindergarten children can color a picture of the water cycle in nature and talk about the water cycle processes. Mentioned activity should also help to increase and support critical thinking. Section designed for primary school students contains a problem to determine the amount of rainwater in the city. To solve the problem, students should use the Model hectare method. The calculation procedure of the mentioned problem is described in detail to help primary school students solve it. In the section designed for citizens and government, readers can find a brief description of water retention measures, for example:

The water retention measures are multifunctional measures aimed at protecting water resources and addressing water-related problems or the maintenance of aquatic ecosystems, as well as the characteristics of water bodies using natural resources and processes.

The water retention measures:

- retain water (outflow) beyond the existing capacity of the systems, discharge it at a controlled rate or ensure its penetration/infiltration into groundwater,
- they make it possible to use the retention capacity of soils and aquatic ecosystems to ensure further improvements in the environment and well-being, such as water quality, biodiversity, value, resilience, and adaptation to the effects of climate change, they are usually used on a relatively small scale; compared to the size of the river basin or territory in which they are carried out,
- they imitate a natural process.

Urbanization and how to mitigate the adverse impact of urbanization are described in the government's section. As a sample, there are adduced infiltration ditches, soaking, and filter belts. All three Information brochures are designed in the same style. Mentioned icons (Figure 1) show content suitable for the target groups (kindergarten children, primary school students, citizens in the affected area, and the government). There are 3 types of brochures with 6 topics above mentioned. All three brochures are also color-coded.

## 2.2 Media activities

Within Project InfoWater, the media activity includes a print advertisement. An advertisement is a targeted report for a specific group of people, published mostly for a fee in a newspaper or magazine. The advertisement contains a brief text; resp. also pictures and is stylized to address a selected target population. This project, focus on addressing the broad to the public to provide information on the sustainability of water resources.

## 2.3 Online activities

Online activities contained in the InfoWater project includes web page, social networks, and online competitions. The webpage is available online [8]. As social networks are used webpage YouTube, Facebook, and Instagram. YouTube channel Info Voda contains videos with topics Physical properties of liquids, Water and the water structures, Watercourse treatment, Longitudinal and transverse profile and bank modification, Revitalization of the water courses, Weirs, Water reservoirs, and dams (Figure 6).

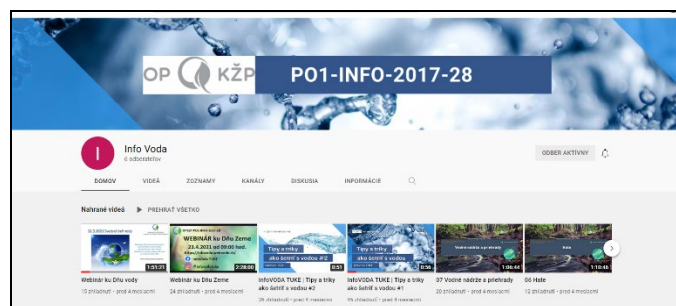


Figure 6: YouTube channel of the Info Water project

There took place also two webinars – the first webinar named Water Day webinar has been held on the International Day of the Water 22.3.2021. The record from the webinar is available online (<https://www.youtube.com/watch?v=IRmIgcI4RJk>).

The second Earth Day webinar have been held a few weeks ago, and the record is also available online (<https://www.youtube.com/watch?v=n0Eu5dMSp4g>). Both webinars were attended by experts from the Faculty of Civil Engineering and experts from the professional public.

To join the webinar, the invitation letters were sent to the mayors of municipalities of Eastern Slovakia through their email addresses. Together there were sent 1 063 invitations. Because of the technical failure, 33.04% of the emails were not delivered.

Among online activities belong active social networks – Facebook and Instagram. Administrators of the mentioned social networks publish posts related to the main theme of the project – water management and water resources in Slovakia.

Social media activities are also aimed at the target groups, especially the kindergarten, and primary school students. The students can join the challenges and competitions and get valuable prizes. The competitions have a great success, and a lot of students are involved. Facebook fan page of the project shows especially pictures of students' creations. Followers of the fan page can vote for the best picture by "like" to the post. The most "liked" post is the winner. On the wall on the Facebook webpage, InfoVoda TUKE is available online (<https://www.facebook.com/infovoda.svftuke>) can be seen the list of all competitors' winners. The most involved competitors were kindergarten students. Their contributions are shared on the mentioned website, and there can be seen also the list of the winners. The indicator for the winner was the quantification of likes. Facebook competitions were several times extended because of the big interest in participating.

## 2.4 Presentation activities

At the time of the project's presentation activities, the pandemic situation did not allow them to participate in these activities in person. Therefore, presentation activities took place online. As mentioned above, among online activities were included presentation activities, also webinars.

Water Day webinar was focused on the review of the current water situation. The lectures were presented by prof. Martina Zeleňáková, and the lecturers were experts from the professional public. The topic of the Water Day webinar was The climate conditions of Eastern Slovakia, Safety of water mains in buildings during a pandemic of the COVID-19, An overview of the municipality providing the construction of public water supply and public sewerage with the support of funds from the environmental fund, Water retention measures in municipalities – the possibility of drawing funds from the Operational Program Environmental Quality, The impact of water erosion on the clogging of small reservoirs within the scope of the Bodrog River Basin District, Trebišov and Water and greenery in architecture.

The Earth Day webinar was also held online due to the COVID-19 pandemic situation. Invitation letters for both webinars were sent online to governments of Eastern Slovakia email address. Webinars were primarily designed for the government target group, but online access to the YouTube channel is open for public. Lectures at the second webinar describe topics Self-government: Together for a better environment; How to retain water in the country; Soil moisture regime monitoring; Soil erosion as a significant water management problem of municipalities and river basins; Use of preparation and auxiliary preparations for plant protection in public greenery on the market in the Slovak Republic; Building Act – procedures for issuing building permits; Expert institute in construction.

Webinars records and lectures records are available online on the YouTube channel Info Voda [9].

The Project Info Water is still ongoing. Due to the pandemic situation of COVID-19, present activities had to be prepared in the online form, and the deadlines had to be moved to a later date.

## 3 Conclusion

The submitted paper briefly presents the project Raising the awareness of residents, especially Košice and Prešov county in the field of sustainability of water resources with emphasis on the involvement of students. The main goal of the mentioned project is to provide target groups with basic information about water sources and water management in the Slovak republic in a very simple and playful form. The mentioned project includes informal, online, media, and presentation activity. The submitted paper provides a brief overview of all project activities. Nowadays, the project is very successful, and the activities are still ongoing. The main goal of the project is to address as many schools as possible. The first output of the project is the list of schools in Eastern Slovakia with a statistical review of involvement in the project. Measurable project indicators include a count of thematic brochures distributed to the schools, audio and video record, and pamphlets in print.

Online activities contained in the InfoWater project includes web page, social networks, and online competitions. The active social profile provides photos and posts related to mentioned competitions and the winners. Also, on the social network's readers can find the records of lecturers that took place

on Water and Earth Day.

Available online websites, fan pages, and YouTube channel provide an open access to the public. Most of the project activities are in an electric form, which contributes to sustainability. Thanks to the electronic form of the activities, the content is available not only to address target groups (Figure 1) but also to the general public and the content still can be used after the end of the project.

Each activity is monitored, and the results of the project will be processed statistically. To achieve the measurable indicator of project results is needed: 3 types of thematic information brochures, 1 audio record, 10 thematically different video records, 3 thematically different pamphlets, 10 add-in regional newspapers, 20 actualizations of the webpage, 30 social network posts, 3 online competitions, and 5 lectures. All information about Project Info Water is now available online [8].

## Acknowledgments

This work has been supported by the project Raising the awareness of the population, especially the Košice and Prešov self-governing regions in the field of sustainability water resources with an emphasis on the involvement of school students NFP310010R074.

## References

- [1] Brown S, Wadey M. P., Nicholls R. J., Shareef A., Khaleel Z., Hinkel J., Lincke D. & McCabe M. V. (2020). Land raising as a solution to sea-level rise: An analysis of coastal flooding on an artificial island in the Maldives. *Flood Risk Management*, 3-18.
- [2] Wang F, Wang Z, Yang H, Di D, Zhao Y, Liang Q. & Hussain Z. (2020). Comprehensive evaluation of hydrological drought and its relationship with meteorological drought in the Yellow River basin, China. *Journal of Hydrology* (584).
- [3] Thompson L. G. (2010). The evidence and our options. *Behav Analyst* (33), 153-170.
- [4] Huttmanová E. (2013). *Možnosti environmentálneho vzdelávania na Slovensku*. Prešovská univerzita v Prešove.
- [5] Kováčová L. (2014). Vzdelávanie ako nástroj riešenia environmentálnych problémov. *Košická bezpečnostná revue* (4(1)), 82-90.
- [6] Adamišín P. & Chovancová J. (2013). *Stav a perspektívy environmentálneho vzdelávania na vysokých školách*. Prešovská univerzita v Prešove.
- [7] Chovancová J. & Harausová H. (2013). Environmentálne povedomie a potreba environmentálneho vzdelávania budúcich manažérov na Slovensku a v Čechách. *Stav a perspektívy environmentálneho vzdelávania*, 78-91.
- [8] OPKZP-PO1-INFO-2017-28. *Raising the awareness of the inhabitants of the Košice and Prešov self-governing regions in the field of sustainability of water resources with emphasis on the involvement of school students*. 6.12.2021 from <https://infovoda.webnode.sk/>
- [9] YouTube. *Info Water*. 6.12.2021 from <https://www.youtube.com/channel/UCrdHI9V0k77V-TxCugjxzNQ>

## Treatment of clay soil with paper ash

**Berdi Inas, Messast Salah, Benzaid Riad, Idoui Imane**

University of Jijel, Algeria  
Faculty of Natural and Life Sciences, Geological Engineering Laboratory  
e-mail: inas.berdi@univ-jijel.dz

### Abstract

The mineralogy of fine soils such as clays has always posed problems and remains an uncontrollable phenomenon in the presence of water and causes destructible damage throughout the world. In order to minimize the cost of implementation, it is necessary to find practical and less expensive solutions to ensure the stabilization of these soils by the valorisation of local waste available in nature. This article concerns an experimental study on the treatment of reconstituted soil by the addition of paper ash of different proportions on a set of standardized tests, the preliminary results show that the paper ash to the clay soil improves its swelling potential, its plasticity, its compaction characteristics, and its shear strength parameters.

**Key words:** recovery, industrial waste, stabilization, paper waste ash

## 1 Introduction

Paper ash is an inorganic waste product from the burning of paper and has a cementitious and pozzolanic appearance due to the presence of lime (CaO). The increasing accumulation of waste in nature requires rapid action to minimise the high cost of implementation on the one hand and to protect the environment on the other. The use of waste paper as an additive in the stabilisation of clay soils has shown satisfactory values. Following the results obtained by [1] used Nanostructured Waste-Paper Ash (NWPA) as adjuvants to improve the geotechnical properties of lateritic soil with different percentages from 3% to 15% by weight on a set of standardized tests. The best results are obtained at 12% a decrease in the plasticity index, good compactness, an increase in the CBR index. The compressive strength increases with the 28 day cure time.

The work [2] determined the optimum percentage concentration of Waste-Paper Sludge Ash (WPSA) as an additive for best performance of clay soil with variants from 2% to 14% by total weight with a curing time of 14 to 28 days. A proportional increase between the addition and the compressive strength and CBR value up to 12% and then it starts to decrease. The durability of the addition is ensured by the curing time of 28 days.



The authors [3] repeated the experiment on soft sandy clay soil to show the effect of wastepaper sludge ash (WPSA) on the mechanical behaviour and microstructures of the soil. A mixture of soil and additions from 2% to 16% by weight. The highest values of shear strength, compression are obtained at 10% of the addition. Without forgetting the change of the microstructure due to the appearance of new minerals.

The authors in [4] presented two investigations which were carried out to stabilize the soil, the first in the laboratory by compression testing and the second in situ by compaction testing using percentages ranging from 3% to 6% by weight. The mixture of calcined paper sludge and cement promotes an improvement in the bearing capacity of the soil.

The authors in [5] used paper ash as an alternative lime stabilizer. The experimental study showed the effectiveness of the addition on soil behavior and this was proved by improving soil workability and increasing compressive strength with curing periods of 7-14 days.

The same authors [6] have succeeded in showing that ash sludge is a good additive and modifies the geotechnical properties of soil better than lime and cement.

Other authors [7] treated clay soil with sludge from paper ash with a percentage of 2% to 10% by weight over a set of geotechnical tests. The results show a decrease in maximum dry density from 18.2% to 24.2% and an increase in water content from 16.71 (kN/m<sup>3</sup>) to 14.97 (kN/m<sup>3</sup>) and an increase in compressive strength up to optimum mixing. The saturation threshold is found at 6% of the addition.

The results are similar to the work [8], which confirmed the adhesion between paper ash and clay soil and that the best values are obtained with 5% of the addition.

Because of the enormous amount of paper used for waste in the various departments of the faculties of our university, we wanted to conduct an experiment to exploit and reuse it in the context of soil stabilization and to know its impact in the long- and short-term impact.

## 2 Materials used

### 2.1 Reference soil

- **The kaolin** of the Tamazert deposit is extracted by the Soalka company, it is located 17 km north of El-Milia in Jijel City (North-East of Algeria), it contains only the clay fraction. It is a treated kaolin 2 (KT2).
- **Bentonite** originates from the clay deposits of M'Zila (City of Mostaganem). It is a commercial clay. The proprieties of components are in Tables 1 and 2.



Figure 1: The reference soil components

Table 1: Properties of the reference soil components

Proprieties	Bentonite	Kaolin
pH	7.86	4.94
Water content(%)	9.20	20.00
Gravity specific	2.60	1.87
Free swelling index (%)	83.33	7
Particle size analysis ( $\leq 0,08\text{mm}$ )	73	80
Methylene blue	19	2.66
Specific surface area ( $\text{m}^2/\text{g}$ )	399	55.86
liquidity Limite (%)	123	37
Plasticity Limite (%)	40	15
Plasticity Index (%)	83	22

Table 2: Chemical analysis of soils used by XRF (x-ray fluorescence)

Oxides	Kaolin	Bentonite
$\text{SiO}_2$	54.3	65.8
$\text{Al}_2\text{O}_3$	29.2	14.5
$\text{CaO}$	0.863	6.39
$\text{Fe}_2\text{O}_3$	7.83	3.50
$\text{K}_2\text{O}$	4.56	2.65
$\text{MgO}$	0.630	2.87
$\text{TiO}_2$	0.294	0.349
$\text{Na}_2\text{O}$	0.156	3.04
$\text{SO}_3$	0.356	0.479
$\text{P}_2\text{O}_5$	0.421	0.0818

## 2.2 Industrial waste

Paper is considered an industrial waste available in all Algerian administrations. The first phase is focused on the collection of paper and then combustion to obtain ash prepared for use as a stabilizing addition. The proprieties of the paper ash are in Tables 3 and 4.



Figure 2: The stages of preparation of industrial waste

Table 3: Physical properties of paper ash

Proprieties	paper ash
pH	12.33
Gravity specific	3.42

Table 4: Chemical analysis of paper ash by XRF

Oxides	SiO <sub>2</sub>	Al <sub>2</sub> O <sub>3</sub>	CaO	Fe <sub>2</sub> O <sub>3</sub>	K <sub>2</sub> O	MgO	TiO <sub>2</sub>	Na <sub>2</sub> O	SO <sub>3</sub>	Cl
Paper ash	4.58	1.74	86.3	2.07	0.256	0.977	0.162	1,14	4.58	0.592

### 3 Properties of reference soil

We used it as feedstock for the preparation of reconstituted soil which is composed of 80% Kaolin KT2 and 20% Bentonite. This option of using reconstituted soil allows us experimentally to have a swelling reference soil with the identical properties for the different test samples.

#### 3.1 Physical-mechanical properties

The identification is based on the physical-mechanical parameters during the preliminary tests. The characteristics are in Table 5.

Table 5: Geotechnical Properties of reference soil

		Properties	Values
Physical Properties	pH		9.81
	Specific gravity		1.78
	Free swelling index (%)		61.5
	Liquidity limits (%)		70
	Plasticity limits (%)		35
	Plasticity index (%)		35
	Methylene blue		6.66
Mechanical proprieties	Compaction	Optimum water content (%)	20.20
		Maximum dry density (t/m <sup>2</sup> )	1.55
	Shear test	Cohesion (Bar)	0.02
		Internal friction angle (°)	3
	Compressibility	Compression index (%)	19.4
		Swelling index (%)	9.8

Atterberg limits allows to know the type of soil and the state of soil from the index of plasticity according to [9], it is a plastic clayey soil. According to the same classification, the results show that the soil is swelling, medium compressibility. The cohesion value found shows the weak liaison between the particles and also the shape of the narrow Proctor curve shows the sensitivity of the soil, all these properties favour the swelling of the soil.

### 3.2. Chemical analysis of soil mixture

The chemical analyses performed at the University of Farhat Abbas 1's Unit of Research on Emerging Materials are summarized in the Table 6.

The results of chemical studies indicate that the major constituents of the studied soil are oxides  $\text{SiO}_2$  (56.2%),  $\text{Al}_2\text{O}_3$  (27.3%), and  $\text{Fe}_2\text{O}_3$  (7.19%), with  $\text{K}_2\text{O}$  (4.23%) coming in second, followed by traces of  $\text{MgO}$ ,  $\text{TiO}_2$ ,  $\text{Na}_2\text{O}$ ,  $\text{SO}_3$  and  $\text{P}_2\text{O}_5$ . The soil is relatively rich in silica, aluminium. The presence of silica with aluminium favours the appearance of kaolinite. The presence of potassium is attributed to the existence of illite and muscovite.

Table 6: Chemical analysis of soils used by XRF (x-ray fluorescence)

Oxides	$\text{SiO}_2$	$\text{Al}_2\text{O}_3$	$\text{CaO}$	$\text{Fe}_2\text{O}_3$	$\text{K}_2\text{O}$	$\text{MgO}$	$\text{TiO}_2$	$\text{Na}_2\text{O}$	$\text{SO}_3$	$\text{P}_2\text{O}_5$
80%K+20%B	56.2	27.3	1.51	7.19	4.23	0.872	0.299	0.465	0.339	0.381

The information in Table 3 shows that the  $\text{CaO}$  content is very high and the most abundant (85%). Due to the nature of the waste, which contains only celluloses, the triangular table  $\text{SiO}_2$ -  $\text{CaO}$ -  $\text{Al}_2\text{O}_3$  allowed us to classify this waste in class C according to the American Society for Testing and Materials (ASTM) standards, which favours the chemical reaction between the paper ash and the soil components and the growth of the cementitious products C-S-H, C-A-S-H, which play a role in soil improvement.

### 3.3 Mineralogical analysis of soil mixture

Mineralogical analysis of the natural soil is performed by X-ray diffraction (XRD) on a sample  $< 63 \mu\text{m}$  air-dried sample. The objective was to determine the main mineralogical phases. The appearance of an intense peak corresponding to Quartz ( $\text{SiO}_2$ ) ( $2\theta = 26.26$ ,  $d = 3.34$ ) then kaolin ( $\text{Al}_2\text{Si}_2\text{O}_5(\text{OH})_4$ ) ( $2\theta = 12.3$ ,  $d = 7.16$ ), muscovite ( $2\theta = 8.2$ ,  $d = 9.9$ ), Biotite, also the appearance of illite ( $(\text{KH}_3\text{O})\text{Al}_2\text{Si}_3\text{AlO}_{10}(\text{OH})$ ) ( $2\theta = 26.26$ ,  $d = 9.99$ ) (Figure 3).

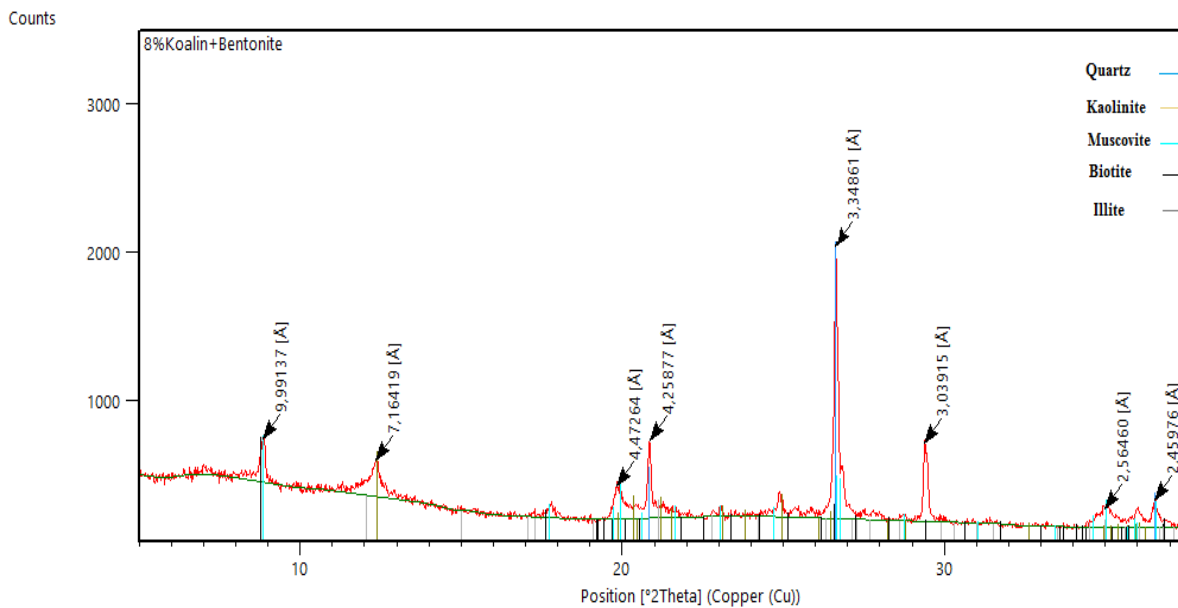


Figure 3: X-ray diffraction of reference soil

## 4 Methods

In order to ensure the stability of reference soil, paper ash was used as an additive to improve the geotechnical properties of this soil, several percentages have been proposed 2 %by weight, 4%, 6%, 8% on a series of standardized tests:

a) pH according to standard NF ISO 10390:1994 [10]

The determination of the pH is necessary to quantify the contribution of acidity, the alkalinity of a solution can be expressed by the concentration of  $H^+$ . The reading is made directly on a pH meter.

b) Specific gravity according to standard NF P 94-054

The standard (NF P 94-054) [11] applies to any sample of intact or reworked soil whose largest elements are smaller than 2 mm. The purpose of the test is to determine the average density of a sample composed of particles.

c) Free swelling index according to standard IS-2720-PART-40-1970 [12]

Soil passing through a 425-micron sieve is used in this test. 10 g are soaked in two test tubes for 24 hours (one with distilled water and the other with kerosene)

$$\text{Percent} = ((Vd - Vk) / Vk) * 100$$

Or:

$Vd$  = The volume of the soil sample read in the graduated cylinder containing distilled water.

$Vk$  = The volume of the soil sample read in the graduated cylinder containing kerosene.

d) Atterberg limits According to standard NF P 94-051 [13]

It is a property characterizing a coherent soil, resulting in a variation of the mechanical behaviour of this soil according to its water content. The three distinguished limits ( $W_L$ ,  $W_p$ ,  $I_p$ ) make it possible to classify the soil (very plastic, plastic, less plastic).

e) Compaction test according to standard NF P94-093 [14]

The test consists in damming a soil sample in a defined and repetitive way by varying its water content. The regular measurement of the water content and the dry density of the material once plotted on a graph, gives a bell-shaped curve. The optimum is then determined by the maximum point of the curve which gives the optimum water content for a maximum density.

f) Direct shear test. According to standard NF P 94-071-1 [15]

The test comprises the shearing of three specimens of the same dimensions prepared under conditions sheared at the same speed but subjected to different vertical forces. The principle of the test consists in determining the intrinsic characteristics of soil  $C$  and  $\phi$ .

g) Compressibility test according to the standard (XP P 94-090-1) [16]

The compressibility test according to the standard XP P 94-090-1 is a fundamental and slow test because it is necessary to wait for the end of the consolidation for each stage on fine soils and fine coherent materials. The oedometer compressibility curve can be characterized by several parameters: the swelling index and the compressibility index.

## 5 Results and discussions

The results of the effect of paper ash on soil behaviour are summarized in the following figures:

### 5.1 Effect of paper ash on the pH

Figure 4 shows that the treated soil has a higher pH than the untreated one and this is for all the proportions of addition used. It is a basic medium, which is reflected by a better dissolution of silicates and aluminates of the clayey proportion of the soil stabilized by the paper ash and improved mobility of ions during ionic interactions.

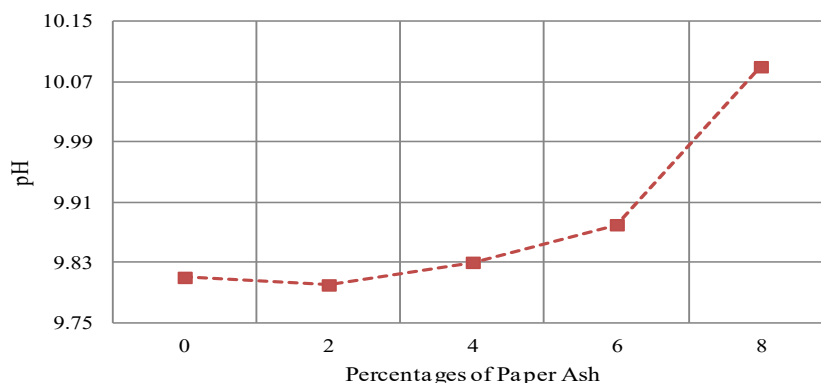


Figure 4: Effect of paper ash on the pH

### 5.2 Effect of paper ash on specific gravity

Figure 5 shows the change in specific gravity of the soil mixed with a varying percentage of the paper ash. The addition of the admixture increases the specific gravity of the soil. This increase may be due to the higher value of the ash (3.42) than that of reference soil (1.78) which makes the soil denser.

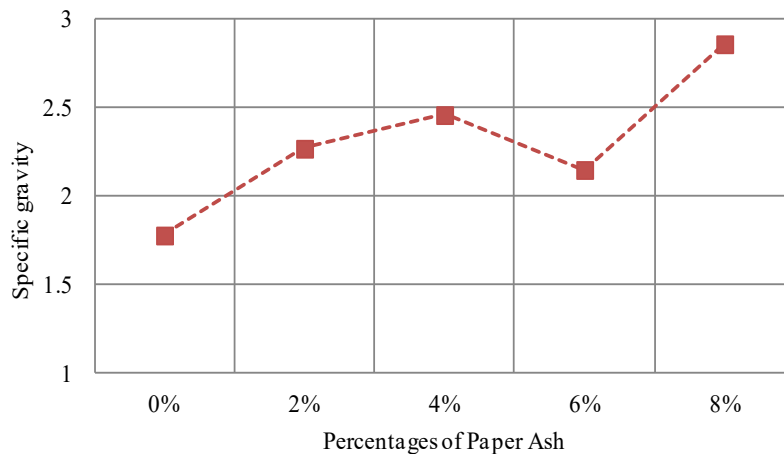


Figure 5: Effect of paper ash on specific gravity

### 5.3 Effect of paper ash on the free swelling index

Figure 6 shows a noticeable decrease of the free swelling index with the increase of the percentage of paper ash. It decreases to 2%, then it increases to 4% and then it starts to decrease progressively until it reaches the value of 11%.The improvement exceeds almost 80% of the reference soil.

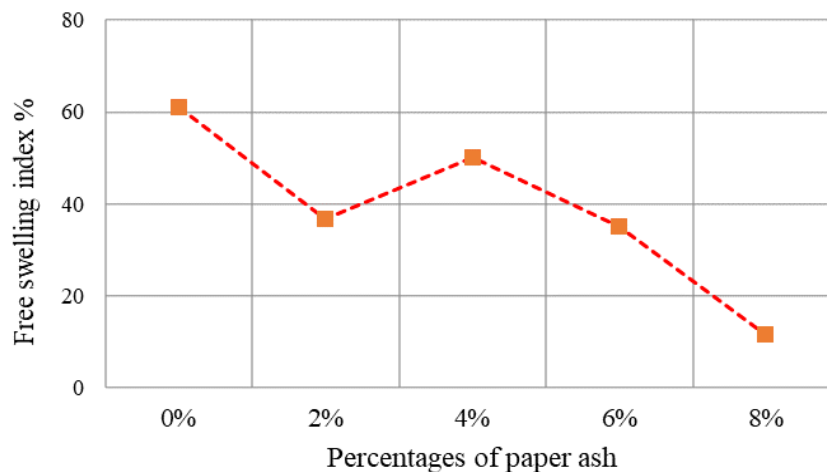


Figure 6: Effect of paper ash on the free swelling index

### 5.4 Effect of paper ash on the Atterberg limits

The Atterberg limit is considered as an indicator qualifying the plasticity. The results obtained from reference soil show that the plasticity index is 35%, the liquidity limit is 70% and a plastic limit of 35%, which indicates that the clay is of high plasticity.

A considerable increase in the plasticity limit of the soil compared to the liquidity limit which increases slightly with the increase of the percentage of ash. So, the effect of paper ash is approved when the plasticity index gradually decreases from 35% for untreated soil to 28% for treated soil with 8% addition, which makes the soil less plastic with better soil workability (Figure 7).

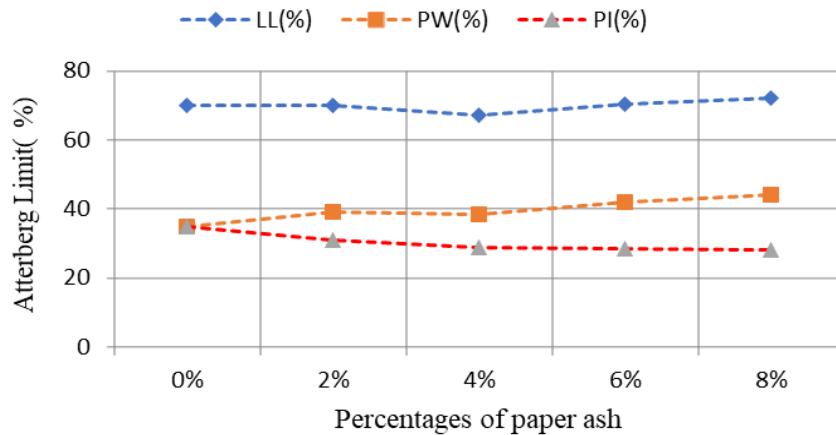


Figure 7: Effect of paper ash on the Atterberg limits

### 5.5 Effect of paper ash on compaction

Figure 8 demonstrated the effect of paper ash on soil compaction. A notable decrease in the dry density compared to the reference soil. After the percentage of 2% the density remains almost constant (1.42-1.40-1.39) is justified by the need for low compaction energy. The same figure shows that the optimum water content decreases linearly with the evolution of the ash up to 6%, this is due to the cementitious effect of paper and necessitates water for its hydration.

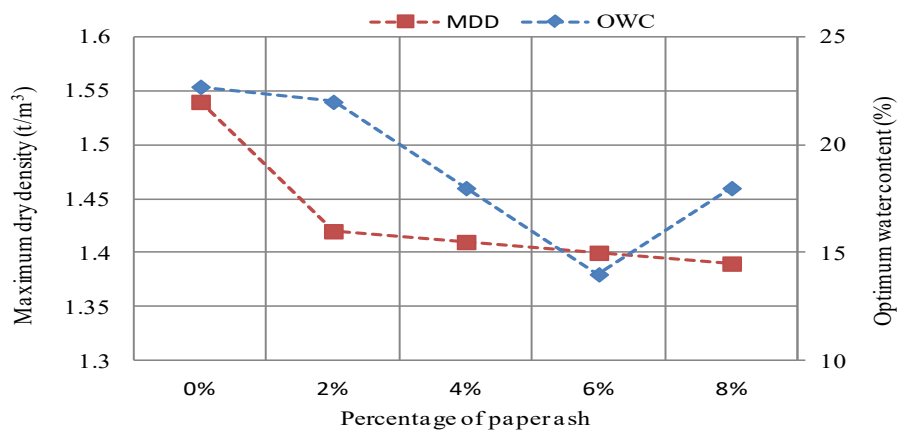


Figure 8: Effect of paper ash on compaction



## 5.6 Effect of paper ash on shear strength

Shear strength is one of the most significant soil properties and is required whenever a structure depends on the shear strength of the soil. The mechanical characteristics determined in direct shear (Figure 9) show that the reconstituted soil has varying angles of friction. A well-developed cohesion is comparable to the reference soil. The increase in cohesion from 0.02 bar to 0.64 bar, after the percentage of 4% the curve begins to decrease until 0.39 bar then it increases by 0.54 bar. While the angle of friction increases gradually from 4.5° for 0% to 13° for 4%. Then it increases from 11° for the percentage of 6% to 15° for the percentage of 8%. Cohesion and friction angle promote the increase in shear strength. The best results are provided by the combination of cohesion = 0.5 bar and friction angle = 15°.

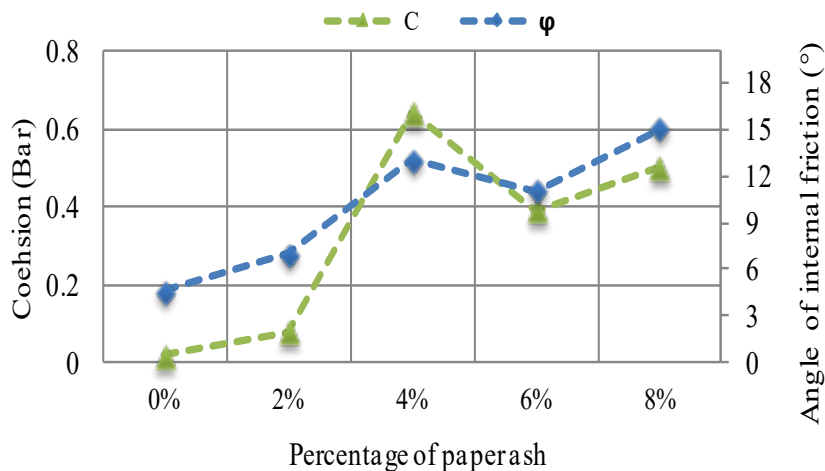


Figure 9: Effect of paper ash on shear strength

## 5.7 Effect of paper ash on the oedometer compressibility test

The effect of paper ash on compressibility is shown in Figure 10. The increase in addition gradually decreases the swelling index from 9.8% = 10% for a reference soil to 5.5% for 8% paper ash, and also a reduction in compression index from 31% for the untreated soil to 5% for 8% addition, so there is a decreasing linear variation for the soil to go from swelling to less swelling and from less compressible to non-compressible soil. The reason for the decrease in swelling is justified by the additive which has modified the mineralogy of the reference soil by the formation of new minerals interacting with the cementitious-looking paper ash components.

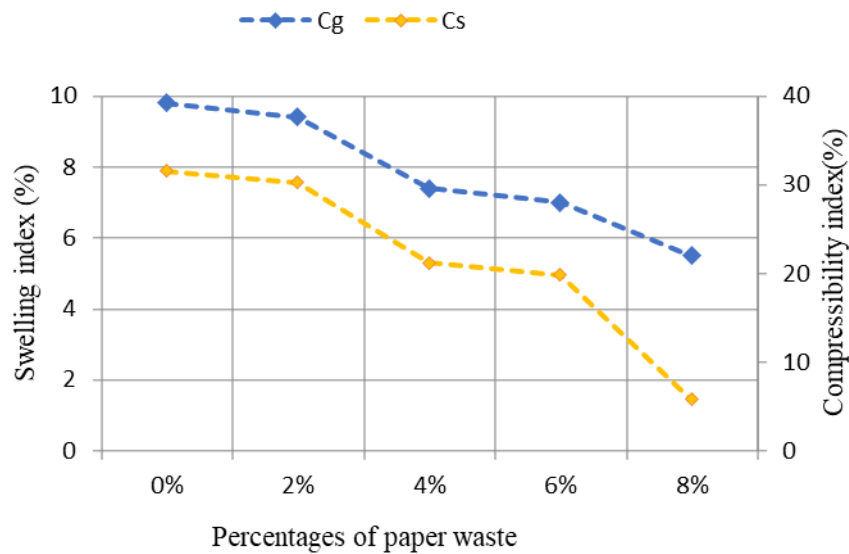


Figure 10: Effect of paper ash on soil compressibility

## 6 Conclusion

Soil treatment is a technique that has developed very rapidly in recent years and is still set to undergo significant development. Easy to implement, economical and efficient, soil stabilization by paper ash promotes the improvement of geotechnical properties in the short term on the various tests carried out:

- An improvement in soil plasticity decreases by almost 20% compared to the reference soil.
- A decrease of 80% in the free swelling index compared to the untreated soil.
- An increase of 43% in the angle of friction and 60% in the cohesion compared to the reference soil.
- A decrease of 81% in the swelling index and 40% in the compressibility index compared to the reference soil.

Our objective is also to choose the right percentage that gives us the best improvement results and confirms the saturation threshold.

For future work it is also necessary to know the microstructure of the soil by SEM to confirm the observed macrostructure, also to confirm the durability of this addition in the long term.

## References

- [1] Onyelowe, K.C. (2017). Nanostructured waste paper ash stabilization of lateritic soils for pavement base construction purposes. *Electronic Journal of Geotechnical Engineering*.vol 22, no 09, p. 3633-3647.
- [2] Khalid, N., Mukri, M., Kamarudin, F, et al. (2012).Clay soil stabilized using waste paper sludge ash (WPSA) mixtures. *Electronic Journal of Geotechnical Engineering*.vol.17, p.1215-1225.
- [3] Khalid, N., Mukri, M., Kamarudin, F., et al. (2014).Soft soil subgrade stabilization using waste paper sludge ash (WPSA) mixtures. In: *InCIEC*. Springer, Singapore, 2015. p. 439-446.
- [4] Lisbona,A., Vegas,I.,Ainchil,J, et al. (2012). Soil stabilization with calcined paper sludge: laboratory and field tests. *Journal of Materials in civil engineering*.vol. 24, no 6, p. 666-673.

- [5] Mavroulidou, M., Ziniatis,A., Gray,C. (2017).Alternative calcium-based chemical stabilisers for ground improvement: Paper Sludge Ash treatment of London Clay. In: *15th International Conference on Environmental Science and Technology (CEST2017)*.
- [6] Mavroulidou, M.(2018).Use of waste paper sludge ash as a calcium-based stabiliser for clay soils. *Waste Management & Research* .vol. 36, no 11, p 1066-1072.
- [7] Kumar,A et Gupta,S.S.(2016).Strength Development of Soil using Waste Paper Sludge (WPS). *Int. Res. J. Eng. Technol.* vol. 3, no 6, p. 2144-2147.
- [8] Bawa,A., Bawa,N.(2017).Development of strength in soft soil stabilized with waste paper sludge.
- [9] Costet,J., Sanglerat,G.,Biarez, J., *et al.* (1969).*Cours pratique de mécanique des sols*. Dunod.
- [10] ISO, N., 10390 (1994).Qualité du sol. *Détermination du pH*. AFNOR, Paris.
- [11] NF,P. 94-054 (1991) .reconnaitances et essais, Détermination de la masse volumique des particules solides des sols, Méthode du pycnomètre à eau. *Association Française de Normalisation, France (in French)*.
- [12] IS-2720-PART-40 (1970). Free swell index test of soil.
- [13] NF,P. 94-051 (1994). Détermination des limites d'Atterberg la limite à la coupelle – limite de plasticité au rouleau.
- [14] NF, P. 94-093 (1999). Détermination des références de compactage d'un matériau: essai Proctor normal-Essai Proctor modifié. Association Française de Normalisation (AFNOR).
- [15] NF, P. 94-071-1. (Août 1994). Essai de cisaillement rectiligne à la boîte-Partie 1: Cisaillement direct. Association Française de Normalisation (AFNOR).
- [16] XP P94-091(décembre 1995).Sols .reconnaitance et essais - Essai de gonflement à l'oedomètre - Détermination des déformations par chargement de plusieurs éprouvette. (AFNOR).

## An attempt to apply the kinematic method of rigid solids in the study of bearing capacity of shallow foundations

Messaouda Boutahir Born Bencheikh<sup>1,2</sup>, Assia Aidoud<sup>1,2</sup>, Benamara Fatima Zohra<sup>1,2</sup>, Belabed Lazhar<sup>1,2</sup>, and Dorbani Meriem<sup>1,2</sup>

<sup>1</sup>University 8 May 1945, Laboratory of Civil Engineering and Hydraulic (LGCH), Guelma, Algeria.

<sup>2</sup>Faculty of science and technology, Department of civil Engineering and Hydraulics  
e-mail: Bencheikh2005@yahoo.fr

### Abstract

In the geotechnical engineering field, shallow foundations are frequently needed to ensure good fieldwork stability. They are also intended to permanently and uniformly transmit all load pressure on the seating floor. However, numerous mechanical constraints, such as bearing capacity of foundations, durability, stability, design of shallow foundations, lead, unfortunately, to a serious realization challenge. Finding an adequate solution presents the main goal and effort of both scholars and professionals. Indeed, the corresponding drawback is observed through the high number of reported damages that occurred in the structure of foundations and the punching failure.

The failure mechanisms of shallow foundations, verified in full size or on scale models, show "sliding surfaces" and rigid (solid) blocks, which can be described with the kinematic method of rigid solids.

The main objective of this study is the application of the kinematic method of rigid solids in the study of the stability of shallow foundations with respect to punching, the purpose of which is to determine the bearing capacity factors  $N_c$ ,  $N_\gamma$ , and the passive earth pressure coefficient  $K_p$  of foundations. In this context, two mechanical models have been proposed with 5 and 7 rigid solids, and a program developed via the MathCAD environment is applied to check the validity of the two previous models. The kinematic method of rigid solids gives results very close and comparable with that of Caquot/Kerisel for the factors of the bearing capacity and passive earth pressure coefficient - the ratio  $K_p$  - according to the five- and seven-solid model.

**Key words:** bearing capacity, kinematic method of rigid solids, shallow foundations, sliding surface

## 1 Introduction

The problem of determining the bearing capacity of foundations, resting on a layer of soil of given resistance, constitutes one of the oldest and fundamental questions of geotechnical engineering [1]. This implies the objective of the rational sizing and designing of a footing, which safely transfers the static loads from the structure to the foundation soil.

The formulation of the load-bearing capacity problem, as well as the techniques applied for its resolution, have evolved, and continue to evolve in two directions [2,3]: (1) from a practical

point of view, following the current needs of the construction industry and the growing demand for more effective foundations and, (2) from a theoretical point of view, by enriching the known solutions, relevant for the mathematical modeling of the problem, by the adoption and the implementation of new analytical and numerical tools.

The two aspects of the problem are strongly linked, i.e., all the empirical knowledge of the construction sector and the experimental results constituted to date must be interpreted through analytical methods or reproduced through numerical models.

The problem posed is to find a new method for the evaluation of the bearing capacity of superficial foundations. Therefore, this article mainly focuses on the application of the kinematic method of rigid solids, which has been used for a long time for the stability of slopes.

In most applications of geotechnical engineering, the analysis of the stability of a slope is often a very complex issue due to the wide diversity of the sites and their heterogeneity. The kinematic method of rigid fracture solids is a very powerful tool commonly used in the limit analysis, which was described by [1]. Moreover, this method allows computing the potentialities of the system's resistance in the given geometry. This can be done by applying the principle of compatibility between the balance of this system and the resistance of its constituent material. This goal can be achieved by means of two mechanical models of possible rupture of the shallow foundations by punching, which is proposed in the following subsection, where we determine the bearing capacity factor  $N_c$  and passive earth pressure coefficient  $K_p$  of foundations. The program is developed via the MathCAD environment and applied to check the validity of the two previous models. We suppose that:

- The foundation rests on a homogeneous horizontal massif; whose behavior is characterized by cohesion and an internal friction angle.
- The effect of shear stresses at soil-foundation contact is neglected.
- No water table is present.
- The problem is modeled in two dimensions.
- The soil located above the horizontal of the base of the foundation acts as a constant vertical overload of intensity  $\gamma D_f$ ; with  $\gamma$  self-weight of the soil,  $D_f$  the depth or the embedding of the foundation (in this case we took  $D_f = 0$ ).

### 1.1 Kinematic method of rigid fracture solids and principle of minimum safety

The type of the plastic limit state that a soil mass system reaches after sufficiently large deformations depends on the static and kinematic boundary conditions. The experience has shown that, in most cases, shallow foundations tend to break along sliding surfaces.

Therefore, the computation of the failure limit state can be carried out through the kinematic method. Compared to conventional stability checks, the rigid solid kinematic method reflects the actual mechanisms. By considering shear resistance and possible cohesion forces along secondary slip surface the system's safety reserves are properly and fully exploited [4]. It is assumed that in the state of rupture of the shallow foundations, plastic shear deformations concentrate in the slip surfaces while the rest of the soil mass does not deform (is intact). It is only under these conditions that the kinematic method of rigid failure solids can be applied [5,6].

The kinematic method of rigid break solids is based on two principles [3,7,8].

#### A. Principle of kinematic compatibility of potential rupture mechanisms

- Breaking mechanisms consisting of rigid solids must generally have only one degree of kinematic freedom.
- Rigid solids undergo small reciprocal movements along the slip surfaces. Solid movements are represented by a sliding plane called Hodograph.

#### B. Principle of minimum safety through variation in the geometry of the slip surface

All possible system-breaking mechanisms need to be studied to find the most critical mechanism with the most dangerous slip surface. Therefore, for each breaking mechanism, one must vary the inclinations of the slip surfaces as much as possible until one obtains the most critical mechanism that gives the minimum of safety [8].

The search for the mechanism of failure with minimum security, i.e., the most decisive mechanism, is systematically done in four phases [1,9]:

- (1) Grouping all types of rigid solid breaking mechanisms.
- (2) Formulating the boundary state equations for each mechanism.
- (3) Variation of the inclinations of slip surfaces to find the geometry of the most unstable slip surfaces for each mechanism.
- (4) Search for the most unstable fracture mechanism.

In the following, we will study two potential models of the rigid solid break with flat sliding surfaces. The punching of the shooting foundation in the ground is studied and subjected to a vertical load.

## 2 The mechanical model, including five separated rigid solids (Model I)

In this section, the study of the total equilibrium of Model I is established according to Figure 1. Accordingly, it includes five separated rigid solids, illustrated as follows. To study the total balance of Model I the five solids are separated.

The results of the  $Q_i$  ( $Q_{12}$ ,  $Q_{23}$ ,  $Q_{34}$ ) friction forces are tilted from the angle-relative to normal on the Figure 2 slip surfaces so that their components are parallel to the slip.

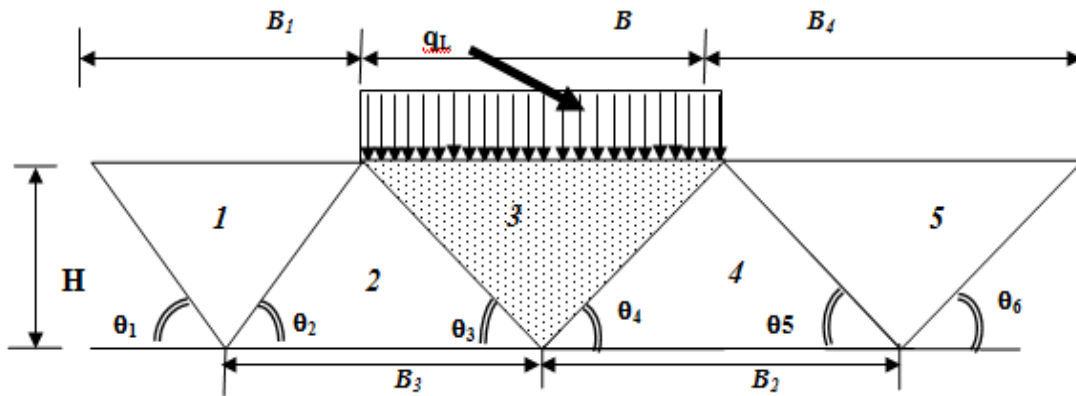


Figure 1: Failure's model including five separated rigid solids

As depicted in Figure 2, the cohesion forces  $C_i$  that are uniformly supplied over the sliding surfaces are computed by [3]:

$$C_i = c \cdot l_i \quad (1)$$

where  $C_i$  the cohesion forces,  $c$  is the soil cohesion,  $l_i$  denotes the length of the corresponding sliding surface.

Moreover, Figure 2 shows that the previous cohesion forces also act in the opposite direction to the movement of rigid solids [10].

The position of the point of application of the forces plays no role in these models because the balance of moments is neglected [11,12,13]. The location of the friction forces  $Q_i$  on the side of the solid has no influence because we are not working with the moments.

For different types of soils and the diverse slip angles  $\theta_1$ ,  $\theta_2$ ,  $\theta_3$ ,  $\theta_4$ ,  $\theta_5$  and  $\theta_6$ , the two load-bearing capacity factors  $N_\gamma$  and  $N_c$  can be computed for a sliding footing case. This can be done by isolating each separated body and applying the kinematic method on each one afterward. Finally, due to the complex numerical computations performed when applying the kinematic method, it is possible to reduce the number of the unknown angles  $(\theta_i) = 1, \dots, 6$  using the following variable change [10,12]:

$$\theta_3 = \theta_4 = (\pi/4) + (\phi/2) \quad (2)$$

where  $\phi$  denotes the internal friction angle.

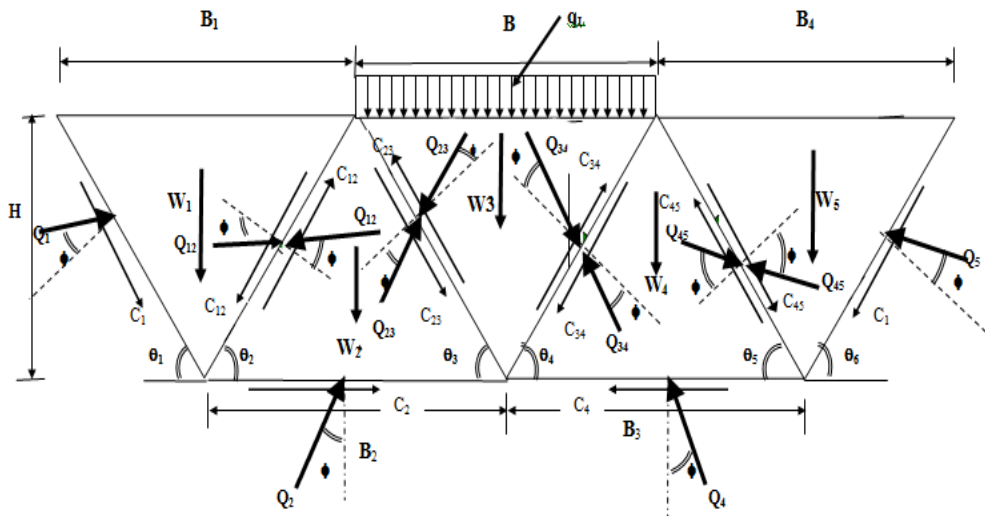


Figure 2: Presentation of deferent's strengths acting on the failure of the model with five rigid solids

To study the total equilibrium of the model (Figure 2), each solid is separated. The resultants of the friction forces  $Q_i$  are inclined by the angle  $\phi$  with respect to the normal on the sliding surfaces so that their components parallel to the sliding surfaces act against the movement of the fracture solids. For example, the forces insulated on the solid 1 are the following: own weight  $w_1$ ,  $Q_{12}$  as the force generated because of the separation of solid 2 on the solid 1 - inter-solid force, and the cohesion force  $C_{12}$ , between the two solids 1 and 2.

Therefore, the remaining angles such as  $\theta_1$ ,  $\theta_2$ ,  $\theta_5$ , and  $\theta_6$  can easily be deduced according to both angles  $\theta_3$  and  $\theta_4$  [1, 12]. It yields also the two expressions (Equations A, B in the Appendix).

### 3 The mechanical model, including seven separated rigid solids (Model II)

The study of the total equilibrium of Model II is similarly established as the one mentioned above. Furthermore, the proposed Model II includes seven separated rigid solids (see Figure 3):

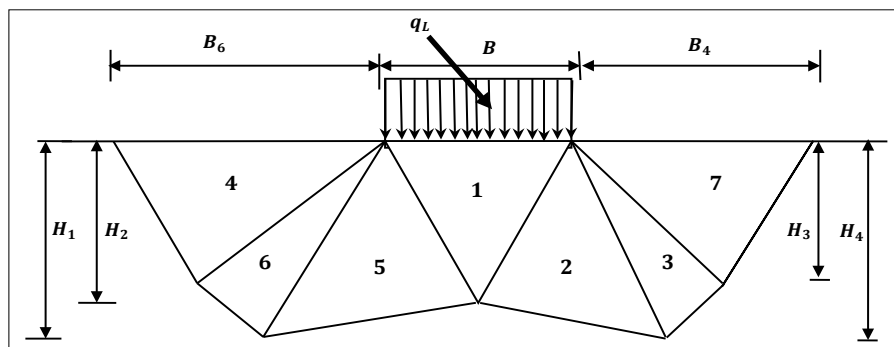


Figure 3: Failure's model including seven separated rigid solids



The same procedures are used to develop the balance equations of each solid. Finally, after the development of the equations, the general equation of the bearing capacity is obtained. The bearing capacity factors for the case of a strip footing, by applying the kinematic method of rigid fracture solids are given by Equations 3 and 4 [14]:

$$N_C = N_{C1} + N_{C2} \quad (3)$$

and

$$A = \frac{\cos(\theta_{12} - \phi)}{\sin(\theta_1 + \theta_{12} - 2\phi)}, \quad B = \frac{\cos(\theta_{15} - \phi)}{\sin(\theta_4 + \theta_{15} - 2\phi)} \quad \text{and} \quad C = 2 \frac{\sin \theta_{15} \sin \theta_{12}}{\sin(\theta_{15} + \theta_{12})} \quad (4)$$

The Equations are further elaborated in the Appendix (C, D).

#### 4 Parametric study

The parametric study is conducted to validate the equations found after the development of the models with five and seven rigid solids. In the next step, a program developed via the MathCAD environment is applied to check the validity of the two previous models. This test is performed only on the first model including five rigid solids, because the same results would be obtained for the seven rigid solids model. Accordingly, the given numerical results are compared with those provided by the common Caquot/Kérisel model, available in the literature. Consequently, Table 1 compares the coefficient ratios  $K_{p\gamma}$  and  $K_{pc}$ , obtained with the first proposed model, and the corresponding  $K_{p\gamma}$  and  $K_{pc}$ , provided by the Caquot/Kérisel model. Moreover, Table 2 compares the bearing capacity factors  $N_\gamma$  and  $N_c$ , given by the first proposed model, and the corresponding  $N_{\gamma K}$  and  $N_{CK}$ , provided by the Caquot/Kérisel model. The comparison study is performed when the internal friction angle  $\phi \in [10^\circ, 40^\circ]$  is gradually increased by  $5^\circ$  [6,14,15].

According to the calculation of bearing capacity factors  $N_c$  and  $N_g$  for the five- and seven-solid model and the model of Caquot/ Kerisel, and concerning the passive earth pressure coefficient  $K_p$ , we note a good agreement between the two models (kinematic and conventional). The kinematic model with five rigid solids gives slightly smaller limit pressures compared to the conventional model in most cases of  $N_g$  and  $N_c$ , as well as the abutment coefficients  $K_p$  limiting pressure  $q_L$ , and the bearing capacity factors.

Table 1\*: Passive Earth pressure coefficient - the ratio  $K_p$  according to the five-solid model and the Caquot / Kérisel model

$\phi$ [°]	$\theta_1$ [°]	$\theta_2$ [°]	$\theta_3$ [°]	$\theta_6$ [°]	$\lambda$ [°]	$K_{p\gamma cal}$	$K_{pccal}$	$K_{p\gamma K}$	$K_{pck}$
10	50	50	50	50	-40	1.39	2.28	.143	1.27
15	52.5	52.5	52.5	52.5	-37.5	1.69	1.52	1.75	1.58
20	55	55	55	55	-35	2.20	1.12	2.19	1.19
25	57.5	57.5	57.5	57.5	-32.5	2.82	2.54	2.84	2.57
30	60	60	60	60	-30	3.32	3.42	3.39	3.46
35	62.5	62.5	62.5	62.5	-27.5	5.69	4.97	5.75	5.01
40	65	65	65	65	25	9.75	8.31	9.71	8.18

The limit load  $q_L$  is calculated by applying the general equation of a strip footing subjected to a centered vertical load [16,17]:

$$q_L = \frac{1}{2} \gamma B N \gamma + c N c \quad (5)$$

(Conventional model), and by applying our general equation deduced based on the kinematic method of rigid solids (Model I kinematic) for the tilt angles of the fracture surfaces [17, 18]:

$$\theta_3 = \theta_4 = \left( \frac{\pi}{4} + \frac{\phi}{2} \right) \quad (6)$$

The results are grouped in Tables 2-5:

Table 2\*: Bearing capacity factors  $N_c$  and  $N_\gamma$  according to the five-solid model and the model of Caquot/ Kerisel

$\phi$ [°]	$\theta_1$ [°]	$\theta_2$ [°]	$\theta_3$ [°]	$\theta_6$ [°]	$\lambda$ [°]	$N_{\gamma cal}$	$N_{ccal}$	$N_{\gamma K}$	$N_{cK}$
10	50	50	50	50	-40	0.98	8.22	1.00	8.30
15	52.5	52.5	52.5	52.5	-37.5	2.22	10.65	2.30	11.00
20	55	55	55	55	-35	4.80	14.38	5.00	14.80
25	57.5	57.5	57.5	57.5	-32.5	9.89	20.64	10.4	20.70
30	60	60	60	60	-30	21.64	30.68	21.8	30.10
35	62.5	62.5	62.5	62.5	-27.5	47.85	46.08	47.9	46.10
40	65	65	65	65	25	113.18	75.23	113	75.30

The values  $q_L$  in Table 3 are calculated using the Equation (7):

$$\theta_3 = \theta_4 = \frac{\pi}{4} + \frac{\phi}{2} \quad (7)$$

Table 3\*: Calculated  $q_L$  values

$\phi$ [°] / c [kN/m <sup>2</sup> ] $q_L$ [kN/ml]	40/0	35/5	30/10	25/20	20/35
Model I Kinematic	2037.24	1091.70	696.32	590.82	593.30
Model Conventional	2034.00	1092.70	693.40	601.20	604.40

Table 4\*: Passive Earth pressure coefficient  $K_p$  according to the seven-solid model and the Caquot / Kérisel model

$\phi$ [°]	$\theta_1$ [°]	$\theta_2$ [°]	$\theta_3$ [°]	$\theta_4$ [°]	$\lambda$ [°]	$K_{p_{cal}}$	$K_{p_{ccal}}$	$K_{p_{JK}}$	$K_{p_{cK}}$
10	50	50	50	50	-40	1.36	2.28	.143	1.27
15	52.5	52.5	52.5	52.5	-37.5	1.59	1.52	1.75	1.58
20	55	55	55	55	-35	2.12	1.12	2.19	1.19
25	57.5	57.5	57.5	57.5	-32.5	2.72	2.54	2.84	2.57
30	60	60	60	60	-30	3.22	3.42	3.39	3.46
35	62.5	62.5	62.5	62.5	-27.5	5.54	4.97	5.75	5.01
40	65	65	65	65	25	9.81	8.31	9.71	8.18

Table 5\*: Bearing capacity factors  $N_c$  and  $N_\gamma$  according to the seven-solid model and the model of Caquot/ Kerisel

$\phi$ [°]	$\theta_1$ [°]	$\theta_2$ [°]	$\theta_3$ [°]	$\theta_4$ [°]	$\lambda$ [°]	$N_{\gamma_{cal}}$	$N_{ccal}$	$N_{JK}$	$N_{cK}$
10	50	50	50	50	-40	1.36	2.28	.143	1.27
15	52.5	52.5	52.5	52.5	-37.5	1.59	1.52	1.75	1.58
20	55	55	55	55	-35	2.12	1.12	2.19	1.19
25	57.5	57.5	57.5	57.5	-32.5	2.72	2.54	2.84	2.57
30	60	60	60	60	-30	3.22	3.42	3.39	3.46
35	62.5	62.5	62.5	62.5	-27.5	5.54	4.97	5.75	5.01
40	65	65	65	65	25	9.81	8.31	9.71	8.18

\* The abbreviations are explained in the Appendix.

## 5 Conclusion

The objective of this work is to contribute to the study of the mechanical behaviour of shallow foundations with respect to punching, i.e., the study of their bearing capacity. Our contributions focused on the fundamental aspect of the problem which is the development of new mechanical models of puncture failure of shallow foundations, hence a new formulation of the bearing capacity using the kinematic approach of rigid solids. This leads to offer new tools for the treatment of relevant problems, oriented towards the new design philosophy of aesthetic, economical and reliable structures through the performance-based design.

In this paper, the stability of the shallow foundations is discussed, in which two mechanical models are proposed. The first one includes five separated rigid solids wherein the second model is characterized by seven separated rigid solids. These models allow computing the coefficient ratios as well as the bearing capacity factors for several internal friction angles. The results obtained through the five-solid model are compared with those provided by the commonly used model of Caquot/Kerisel. This comparison leads to some significant conclusions summarized as follows:

- (1) Failure always occurs when the failure angle  $\theta$  is greater than the internal friction angle  $\phi$  ( $\phi > \theta$ ). This result is well justified physically (there is a movement of the ground).
- (2) The limit load increases with increasing internal friction angle  $\phi$  and decreasing cohesion  $C$ .
- (3) Following the results obtained from  $K_{P\gamma}$  and  $K_{Pc}$ , we note a good agreement between the two models (kinematic and conventional). The kinematic model with 5 rigid solids gives slightly smaller limit pressures compared to the conventional model in most cases  $N_\gamma$  and  $N_c$ , as well as the abutment coefficients  $K_{P\gamma}$  limiting pressure  $q_L$  and the bearing capacity factors.
- (4) The modeling accuracy of the fracture mechanisms is ensured only by the kinematic method compared to other classical methods. This allows to accurately use the resistance against shearing of the soil in the sliding surfaces as well as against the cohesion forces developed in the same areas.
- (5) The choice of the kinematic method in the mechanical modeling of the stability of shallow foundations problem depends on (a) the good description of observed fracture modes and (2) it's the proper exploitation of the resistance reserves to the shear.
- (6) When the inclinations of the extreme solids (dimensions) are well fixed in accordance with the active thrust theory, the corresponding inclination of the stop force is also fixed in its critical state with the same theory.
- (7) The theory of the kinematic method of rigid solids reflects well the nature of ruptures of surface foundations by punching and gives realistic results.

The main drawback of the kinematic method, applied to rigid solids, is the introduction of different functions whose complexity increases with the increase in the number of rigid solids (to be considered). It depends also on the shapes of previous functions such as triangular form, curve form and so on. Further research could usefully explore the study of the stability of shallow foundations using the kinematic approach in the cases: heterogeneous soils, presence of water, or the three-dimensional analysis.

## References

- [1] Salençon, J 1974. *Théorie de la plasticité pour les applications à la mécanique des sols*. Eyrolles: Paris.
- [2] Belabed, L 1996. *Zuverlässigkeitsuntersuchung des Tragsystems, mehrfach verankerte Stützwände "mit probabilistischen Methoden"*, PhD thesis, University of Weimar, Allemagne .
- [3] Belabed, L 1995. *Standsicherheitsuntersuchung zweifach verankerter Stützwände mit der kinematischen Starrkörpermethode*. *Geotechnik* 19, 171-174.
- [4] Breitschaft, G. And Hanisch, J 1978. Neues Sicherheitskonzept im Bauwesen aufgrund wahrscheinlichkeitstheoretischer Überlegungen – Folgerungen für den Grundbau unter Einbeziehung der Probenahme und der Versuchsauswertung. Vorträge der Baugrundtagung in Berlin. *Herausgegeben von der Deutschen Gesellschaft für- und Grundbau e.v. DGEG, Essen*,659-694.
- [5] Chatzigogos, C 2007. *Seismic behaviour of superficial foundations, Towards the consideration of a performance criterion in the design*. PhD thesis, Solid Mechanics Laboratory. École Polytechnique, Paris.
- [6] Benamara, F.Z 2005. *Stability of walls in nail floors*. Magister's memoir, Department of Civil Engineering and Hadraulic, University of Guelma, Algérie.
- [7] Zhou, X. Gu, X. Yu, M. et al 2016. Seismic bearing capacity of shallow foundations resting on rock masses subjected to seismic loads. *KSCE J Civ Engineering Geology* 20,216–228  
<https://doi.org/10.1007/s12205-015-0283-6>.
- [8] Belabed, L 1999. Application of the probabilistic safety concept on the verification of the overall stability of anchored retaining walls with the kinematics of rigid solids, *French Journal of Geotechnics* 89, 49-54.
- [9] Belabed, L. and Bencheikh, M 2008. Analyse semi-probabiliste de la capacité portante des fondations superficielles. *Revue Française de Géotechnique* 124 (3), 61-75.
- [10] Belabed, L 1995. *Standsicherheitsuntersuchung zweifach verankerter Stützwände mit der kinematischen Starrkörpermethode*. *Geotechnik* 19, 171-174.
- [11] Zhou, XP And Cheng, H 2014. Stability analysis of three-dimensional seismic landslides using the rigorous limit equilibrium method. *Engineering Geology* 174,87-102.  
<https://doi.org/10.1016/j.enggeo.2014.03.009>.
- [12] Meyerhof, G.G 1963. some recent research on the bearing capacity of foundations. *Canadian Geotechnical Journal* 1, 16-26.
- [13] Salençon, J 1983. *Calculation at Break and Limit Analysis*, Paris, ENPC Press.
- [14] Bencheikh, M 2010. *Analyse de la stabilité des fondations superficielles avec les méthodes probabilistes*. PhD thesis, Department of Civil Engineering and Hadraulic, University of Guelma, Algérie.
- [15] Bencheikh, M 2005. *Probabilistic analysis of the stability of shallow foundations*. Magister's memoir, Department of Civil Engineering and Hadraulic, University of Guelma, Algérie.
- [16] Meyerhof, G.G 1953. The bearing capacity of foundations under eccentric and inclined loads. *Proceedings, 3<sup>rd</sup> International Conference on Soil Mechanics and Foundation Engineering* 3, 193 Paris.
- [17] Costet, J. Sanglerat, G 1969. *Practical Course in Soil Mechanics*, Volume 2, Dunod Edition. Paris.
- [18] Fakhim,i A. Villegas, T 2007. Application of dimensional analysis in calibration of a discrete element model for rock deformation and fracture. *Rock Mech Rock Eng* 40:193–211.  
<https://doi.org/10.1007/s00603-006-0095-6>.

## Appendix

### \*Abbreviations used in the Tables

$N_\gamma$  calculated:  $N_{\gamma cal}$ ,

$N_c$  calculated:  $N_{c cal}$ ,

$K_{Pc}$  calculated:  $K_{Pc cal}$ ,

$K_{P\gamma}$  calculated:  $K_{P\gamma cal}$ ,

$N_\gamma$  from coulomb and Caquot/Kerisel:  $N_{\gamma K}$ ,

$N_c$  from coulomb and Caquot/Kerisel:  $N_{cK}$ ,

$K_{P\gamma}$  from coulomb and Caquot/Kerisel:  $K_{P\gamma K}$ ,

$K_{Pc}$  from coulomb and Caquot/Kerisel:  $K_{PcK}$ ,

For our case  $\beta n = 0$  (horizontal ground surface),

$\delta p = -\phi$  (since it is about the friction of the earth on itself, i.e., in the case of a stop, the passive force of the stop is inclined by the angle  $\delta p = -\phi$  ( $\phi$  is the internal friction angle of the soil))

### Equations

(A)

$$N_C = \frac{\sin \theta_4 \left[ \frac{2 \cos \varphi \sin \theta_1 \sin(\theta_2 + \theta_3) \sin(\theta_1 + \theta_2 - 2\varphi) + \sin \theta_2 \sin \theta_3 [\cos(2\theta_1 - \varphi) \sin(\theta_1 - 2\varphi) - \sin \theta_1 \cos(\theta_2 - \theta_1 + \varphi)]}{\sin(\theta_3 + \theta_4) \sin(\theta_1 + \theta_2 - 2\varphi) \sin(\theta_3 - 2\varphi) \sin \theta_1 \sin \theta_2} \right] + \frac{\sin \theta_3 \left[ \frac{2 \cos \varphi \sin \theta_6 \sin(\theta_4 + \theta_5) \sin(\theta_5 + \theta_6 - 2\varphi) + \sin \theta_2 \sin \theta_3 [\cos(2\theta_1 - \varphi) \sin(\theta_1 - 2\varphi) - \sin \theta_6 \cos(\theta_5 - \theta_6 + \varphi)]}{\sin(\theta_3 + \theta_4) \sin(\theta_5 + \theta_6 - 2\varphi) \sin(\theta_4 - 2\varphi) \sin \theta_6 \sin \theta_5} \right] + 2 \frac{\sin \theta_3 \sin \theta_4}{\sin(\theta_3 + \theta_4)}}{2}$$

(B)

$$N_\gamma = - \frac{\sin(\theta_1 + \theta_2) \sin^2 \theta_3 \sin^2 \theta_4 \sin(\theta_1 - \varphi) \cos(\theta_2 - \varphi) \sin \theta_1 \cos(\theta_2 - 2\varphi)}{\sin \theta_2 \sin \theta_1 \sin(\theta_3 - 2\varphi) \sin(\theta_1 + \theta_2 - 2\varphi) \sin^2(\theta_3 + \theta_4)} - \frac{\sin \theta_3 \sin \theta_4}{\sin(\theta_3 + \theta_4)} + \frac{\sin(\theta_1 + \theta_2) \cos(\theta_3 - \varphi) \sin \varphi \sin^2 \theta_4 \sin \theta_3}{\sin \theta_2 \sin(\theta_3 - 2\varphi) \sin^2(\theta_3 + \theta_4)} + \frac{\sin(\theta_4 + \theta_5) \cos(\theta_4 - \varphi) \sin \varphi \sin^2 \theta_3 \sin \varphi}{\sin \theta_5 \sin(\theta_4 - 2\varphi) \sin^2(\theta_3 + \theta_4)} \times \sin \varphi - \frac{\sin(\theta_5 + \theta_6) \cos(\theta_4 - \varphi) \sin(\theta_6 - \varphi) \sin^2 \theta_3 \sin^2 \theta_4 \sin(\theta_5 - 2\varphi) \cos(\theta_4 - \varphi)}{\sin \theta_5 \sin \theta_6 \sin(\theta_4 - 2\varphi) \sin(\theta_5 + \theta_6 - 2\varphi) \sin^2(\theta_3 + \theta_4)}$$

where:  $N\gamma$  and  $Nc$  are the bearing capacity factors,  $\theta_1, \theta_2, \theta_3, \theta_4, \theta_5$  and  $\theta_6$  are the slip angles, and  $\phi$  is the internal friction angle.

(C)

$$N_C = \left[ \begin{aligned} & \left( \frac{\sin(\theta_{23} + \theta_{12}) \sin \theta_{12}}{\sin(\theta_{15} + \theta_{12}) \sin(\theta_{23} - \theta_1)} \cos(2\theta_1 - \phi) \right. \\ & \left. + \frac{\sin \theta_{15} \sin \theta_{12}}{\sin(\theta_{15} + \theta_{12}) \sin \theta_{34}} \left[ \frac{\cos(\theta_{34} - \theta_2 + \phi) \sin(\theta_1 + \theta_{23} - 2\phi)}{\sin(\theta_{23} - \theta_2)} + \right. \right. \\ & \left. \left. - \frac{\cos(\theta_{34} - \theta_3 + \phi) \sin(\theta_{34} + \theta_2 - 2\phi)}{\sin(\theta_{34} + \theta_3 - 2\phi) \sin(\theta_{23} - \theta_2)} \right] \times \right. \\ & \left. + \frac{\sin \theta_1 \sin \theta_{15} \sin(\theta_{23} + \theta_{12}) \cos(2\theta_2 - \phi)}{\sin(\theta_{15} + \theta_{12}) \sin \theta_2 \sin(\theta_{23} - \theta_2)} - \frac{\sin \theta_{15}}{\sin(\theta_{15} + \theta_{12})} \sin(\theta_{12} - \theta_1 + \phi) \right. \\ & \left. - \frac{\sin \theta_1 \sin \theta_{15} \sin(\theta_1 - \theta_{23}) \cos(2\theta_3 - \phi) \sin(\theta_{34} + \theta_2 - 2\phi)}{\sin \theta_3 \sin(\theta_{15} + \theta_{12}) \sin(\theta_{34} + \theta_3 - 2\phi) \sin(\theta_{23} - \theta_2)} \right. \\ & \left. - \frac{\sin \theta_{12} \sin \theta_{15} \sin(\theta_1 + \theta_{12})}{\sin(\theta_{15} + \theta_{12}) \sin(\theta_{23} - \theta_1)} \left[ \frac{\sin(\theta_{23} - \theta_1) \cos(\theta_{23} + \theta_2 - \phi)}{\sin(\theta_{23} - \theta_2)} + \right. \right. \\ & \left. \left. + \cos(\theta_{23} - \theta_1 + \phi) \right] \right) \\ & + B \left( \frac{\sin(\theta_{65} + \theta_{15}) \sin \theta_{12}}{\sin(\theta_{65} - \theta_4) \sin(\theta_{15} + \theta_{12})} \cos(2\theta_4 - \phi) \right. \\ & \left. + \frac{\sin \theta_{12} \sin \theta_{15}}{\sin \theta_{67} \sin(\theta_{15} + \theta_{12})} \left[ \frac{\cos(\theta_{67} - \theta_5 + \phi) \sin(\theta_4 + \theta_{56} - 2\phi)}{\sin(\theta_{56} - \theta_5)} + \right. \right. \\ & \left. \left. - \frac{\cos(\theta_{67} - \theta_6 + \phi) \sin(\theta_{67} + \theta_5 - 2\phi)}{\sin(\theta_{67} + \theta_6 - 2\phi) \sin(\theta_{56} - \theta_5)} \right] \times \right. \\ & \left. + \frac{\sin \theta_{12}}{\sin(\theta_{15} + \theta_{12})} \frac{\sin \theta_4 \sin(\theta_{65} + \theta_{15}) \cos(2\theta_5 - \phi)}{\sin \theta_5 \sin(\theta_{56} - \theta_5)} + 2 \frac{\sin \theta_{15} \sin \theta_{12}}{\sin(\theta_{15} + \theta_{12})} \right. \\ & \left. - \frac{\sin \theta_{12} \sin \theta_{15}}{\sin \theta_{15} \sin(\theta_{15} + \theta_{12})} \sin(\theta_{15} - \theta_4 + \phi) \right. \\ & \left. - \frac{\sin \theta_{12} \sin \theta_{15} \sin(\theta_4 - \theta_{56}) \cos(2\theta_6 - \phi) \sin(\theta_{67} + \theta_5 - 2\phi)}{\sin \theta_6 \sin(\theta_{15} + \theta_{12}) \sin(\theta_{67} + \theta_6 - 2\phi) \sin(\theta_{56} - \theta_5)} \right. \\ & \left. - \frac{\sin(\theta_4 + \theta_{15}) \sin \theta_{12}}{\sin(\theta_{65} - \theta_4) \sin(\theta_{15} + \theta_{12})} \left[ \frac{\sin(\theta_{56} - \theta_4) \cos(\theta_{56} + \theta_5 - \phi)}{\sin(\theta_{56} - \theta_5)} + \right. \right. \\ & \left. \left. + \cos(\theta_{56} - \theta_4 + \phi) \right] \right) \end{aligned} \right]$$

(D)

$$N_{\gamma} = \left[ \begin{array}{l} \left( \frac{1}{2} \gamma B - \frac{\sin \theta_{12} \sin (\theta_{65} + \theta_4) \sin (\theta_4 + \theta_{15}) \sin (\theta_{65} + \theta_{15})}{\sin (\theta_{12} + \theta_{15})^2 \sin^2 (\theta_{65} - \theta_4)} \sin (\theta_4 - \phi) + \right. \\ \left. - \frac{\sin^2 \theta_{12} \sin^2 \theta_{15} \sin (\theta_5 + \theta_{67}) \sin (\theta_{65} - \theta_{67})}{\sin^2 (\theta_{12} + \theta_{15}) \sin \theta_{67} \sin (\theta_5 + \theta_{65})} \frac{\sin (\theta_5 - \phi) \sin (\theta_{56} - \phi)}{\sin (\theta_{56} - \theta_5)} \right) \frac{\cos (\theta_{15} - \phi)}{\sin (\theta_4 + \theta_{15} - 2\phi)} \\ \left. - \frac{\sin^2 \theta_{12} \sin^2 \theta_{15} \sin (\theta_6 + \theta_{67})}{\sin^2 (\theta_{12} + \theta_{15}) \sin \theta_6 \sin \theta_{67}} \frac{\sin (\theta_{67} + \theta_5 - 2\phi) \sin (\theta_6 - \phi) \sin (\theta_{56} - \theta_4)}{\sin (\theta_{67} + \theta_6 - 2\phi) \sin (\theta_{56} - \theta_5)} \right) \\ \left( \frac{\sin^2 \theta_{15} \sin (\theta_{23} + \theta_1) \sin (\theta_1 + \theta_{12}) \sin (\theta_{23} + \theta_{12})}{\sin^2 (\theta_{12} + \theta_{15}) \sin^2 (\theta_{23} - \theta_1)} \sin (\theta_1 - \phi) + \right. \\ \left. - \frac{\sin^2 \theta_{12} \sin^2 \theta_{15} \sin (\theta_2 + \theta_{34}) \sin (\theta_{23} - \theta_{34})}{\sin^2 (\theta_{12} + \theta_{15}) \sin \theta_{34} \sin (\theta_2 + \theta_{23}) \sin (\theta_1 + \theta_{12} - 2\phi)} \frac{\sin (\theta_2 - \phi) \sin (\theta_{23} - \phi)}{\sin (\theta_{23} - \theta_2)} \right) \frac{\cos (\theta_{12} - \phi)}{\sin (\theta_1 + \theta_{12} - 2\phi)} \\ \left. - \frac{\sin^2 \theta_{12} \sin^2 \theta_{15} \sin (\theta_{34} + \theta_3)}{\sin^2 (\theta_{12} + \theta_{15}) \sin \theta_{34} \sin \theta_3} \frac{\sin (\theta_{34} + \theta_2 - 2\phi) \sin (\theta_3 - \phi) \sin (\theta_{23} - \theta_1)}{\sin (\theta_{34} + \theta_3 - 2\phi) \sin (\theta_{23} - \theta_2)} \right) \\ \left. - \frac{\sin \theta_{12} \sin \theta_{15}}{\sin (\theta_{12} + \theta_{15})} \right]
 \end{array} \right]$$

where:  $N_{\gamma}$  and  $N_c$  are the bearing capacity factors,  $\theta_1$ ,  $\theta_2$ ,  $\theta_3$ ,  $\theta_4$ ,  $\theta_5$  and  $\theta_6$  are the slip angles, and  $\phi$  is the internal friction angle.



## Influence of NaOH treatment of rubber aggregates on the durability properties of rubberized mortars

Kechkar Chiraz<sup>1</sup>, Benamara F.Zohra<sup>1</sup>, Nigri Ghania<sup>1</sup>, Hebhoub Houria<sup>2</sup>, Cherait Yacine<sup>1</sup>, Mouloud Belachia<sup>1</sup>

<sup>1</sup> University 08 May 1945, P.B N°401, Guelma, 24000 Algeria  
Faculty of science and technology, Laboratory of civil Engineering and Hydraulics  
<sup>2</sup>LMGHU Laboratory, University of 20 August 1955, Skikda, 21000 Algeria  
e-mail: chiraz\_kechkar@yahoo.fr

### Abstract

The work presented in this paper aims to study the durability of mortars, in which part of the sand has been replaced with rubber aggregates from used tires and have undergone a surface treatment with a sodium hydroxide solution (NaOH). The substitution rates studied are 10%, 17.5%, and 25%. The results are compared with ordinary mortar and mortars with untreated rubber aggregates while samples with the same substitution rates were used. To do this, the following properties have been studied: compressive strength, flexural tensile strength, water absorption by capillarity, water absorption by total immersion, water-accessible porosity, water permeability, and resistance to the chemical degradation by sulfuric acid  $H_2SO_4$ .

The results obtained show that the treatment of rubber aggregates by the solution method (NaOH) presented a considerable improvement in mechanical performance (increase in compressive strength and flexural tensile strength) and better durability compared to reference mortar and mortar with untreated rubber granulate.

**Key words:** mortar, aggregate, rubber, tires, durability, surface treatment, sodium hydroxide solution (NaOH)

## 1 Introduction

The massive use of concrete exerts considerable pressure on natural resources, leading to intensive exploitation of quarry aggregates, with the consequences of risk of depletion of these resources and environmental problems (destruction of fauna and flora, pollution of groundwater, etc.). Thus and in order to remedy this problem, the Algerian authorities have tightened the conditions for opening new quarries, as well as the promulgation of increasingly drastic laws for the protection of the environment. Therefore, it is necessary to look for new sources of aggregate supply. Moreover, the accumulation of waste such as used tires becomes more and more uncontrollable and occupies a significant public space. According to their compositions, tires are classified as non-dangerous and non-degradable waste (approximately 400 years), but due to the risk of uncontrollable fires in landfills because of toxic fumes given

off, the stagnation of water in these places, as well as insects, their valorization seems to be an obligation rather than a choice [1,2].

Anterior studies on the incorporation of rubber aggregates from used tires into cementitious materials have shown better toughness, better impact resistance [3,4], and also better thermal and sound insulation properties than ordinary cementitious materials [5]. On the other hand, they observed drops in the mechanical resistances [6,7].

Among the causes of this decreased resistance is low adhesion between the rubber aggregate and cement paste. For this, much research has been carried out to improve the performance of cementitious materials incorporating rubber aggregates by a surface treatment. Among the surface treatment methods used for rubber aggregates, there is the treatment method with the alkaline solution of sodium hydroxide (NaOH).

Several studies on the influence of this treatment method on the performance of cementitious materials were already carried out. Marques et al. [8] in their study on the Influence of the surface treatment with NaOH solution of rubber aggregates on the properties of mortars found that this method of treatment did not show a significant improvement. Compared to mortars with untreated aggregates, mortars with treated rubber aggregates showed a slight decrease in workability and water absorption. On the other hand, the mechanical properties (compressive strength, tensile strength, and modulus of elasticity) of mortars with untreated rubber granulate showed better results than those treated.

In addition, Iman Mohammadi et al. [9] studied the influence of the treatment of rubber aggregates on the mechanical properties of concrete. They noticed that using this treatment method resulted in notable improvement for the compressive strength, and moderate enhancement in the flexural strength. Qingwen and Jinchao [10] observed the same remark. They used different kinds of rubber aggregate (rubber powder 28 meshes, colloidal particle 0.1-5mm and colloidal particle 2-8mm). They found that the compressive strength and bending strength of rubber concrete improved after soaking in NaOH solution, and the growth rate was related to particle size (the growth rate increases with the decrease in the size of particles).

Ruizhe et al. [11] studied the effect of the treatment of rubber aggregates with NaOH on the properties of self-compacting concrete (fresh state and in the hardened state). They noticed that this method of treatment slightly decreased the workability, expansion, drying shrinkage and improved the compressive and the splitting tensile strength compared to self-compacting concrete with untreated rubber aggregates.

Most of these studies are focused on the influence of treatment with NaOH solution on the improvement of mechanical characteristics and only several studies on the influence of this method on the durability of cementitious materials.

The purpose of this work is to study the effect of incorporating rubber aggregates treated with the alkaline solution of sodium hydroxide (NaOH) on the durability of the mortar. We were interested in the mechanical aspect (compressive strength and flexural tensile strength) as well as the most decisive indicators of durability, namely: absorption by capillarity, water

absorption by total immersion, porosity, permeability to water, and resistance to chemical attack by sulfuric acid  $H_2SO_4$ .

## 2 Materials and experimental procedures

### 2.1 Materials

**Cement:** a CEM II-A with strength class 42.5 was used, manufactured according to the Algerian standard NA 442-2008 [12]. The absolute density and apparent density of the cement were  $3.11 \text{ g/cm}^3$  and  $1.09 \text{ g/cm}^3$  respectively. A specific surface area was  $3371 \text{ cm}^2/\text{g}$  and with the chemical composition as presented in Table 1.

**Sand:** the class 0/3 of natural sand from the Tebessa region (Algeria) was used, the absolute density and apparent density of the sand were  $2.56 \text{ g/cm}^3$  and  $1.6 \text{ g/cm}^3$  respectively, and the fineness modulus was 2.26.

**Rubber granulate:** comes from the mechanical grinding of used tires, the maximum dimension of which was 2 mm (Figure 1), and the absolute density and apparent density were  $0.87 \text{ g/cm}^3$  and  $0.47 \text{ g/cm}^3$  respectively.

**Superplasticizer:** The superplasticizer used in the mortar mixtures is an Algerian superplasticizer based on Ether Polycarboxylate, commercially named POLYFLOW SR 3600.

**Sodium hydroxide:** Also called caustic soda, Chemical Formula: NaOH of U.E origin and packaged by the Algerian company PROCHIMA-SIGMA. In the form of white pearls. Melting point:  $318.4 \text{ }^\circ\text{C}$  and-Boiling point:  $1393 \text{ }^\circ\text{C}$ . PH: 13-14 (0.5% solenoid).

**Sulfuric acid ( $H_2SO_4$ ):** the sulfuric acid used is from Sigma-Aldrich Chemie GmbH Company – Germany. In liquid form, colorless, odorless, pH 0.3 at  $49 \text{ g/l}$  at  $25 \text{ }^\circ\text{C}$  and their density was  $1,84 \text{ g/cm}^3$ .

Table 1: Chemical composition of the cement CPJ-CEM II/A

Compounds	CaO	SiO <sub>2</sub>	Al <sub>2</sub> O <sub>3</sub>	Fe <sub>2</sub> O <sub>3</sub>	MgO	K <sub>2</sub> O	Na <sub>2</sub> O	SO <sub>3</sub>	PAF	MnO
(%)	58.6	24.9	6.6	3.6	1.2	0.8	0.08	2.2	1.7	--

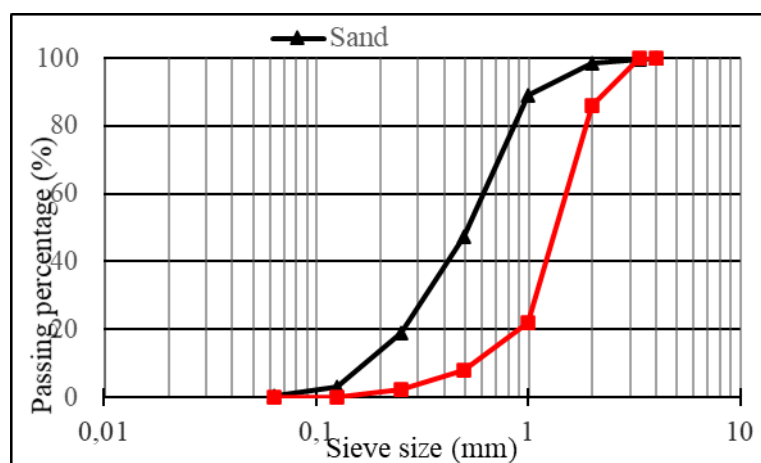


Figure 1: Sieve analysis for sand and rubber used.



Figure 2: Rubber aggregate used

## 2.2 Experimental program

### 2.2.1 Mix design

Test specimens of mortar were prepared according to the standard EN196-1 [13]. The same W/C ratio of 0.5 was fixed for all mixes. The superplasticizer dosage is 1.5% of the cement weight.

We are prepared two series of mortars. The first series with untreated rubber aggregate and the substitution percentages of 10%, 17.5% and 25% (RM10%, RM17.5%, and RM25% successively) by volume of sand, the second series with treated rubber aggregate and with the same percentage of substitution (RMT10%, RMT17.5%, and RMT25% successively) and reference mortar (M) (0% rubber aggregate) was used as a reference.

The different compositions of the mortars are grouped in Table 3.

Table 3: Mortars mix constituents

	M	RM10%	RM17.5%	RM25%	RMT10%	RMT17.5%	RMT25%
<i>Cement (kg/m<sup>3</sup>)</i>	500.0	500.0	500.0	500.0	500.0	500.0	500.0
<i>Sand (kg/m<sup>3</sup>)</i>	1500.0	1350.0	1237.5	1125.0	1350.0	1237.50	1125.0
<i>Rubber (kg/m<sup>3</sup>)</i>	--	52.2	91.4	130.5	52.2	91.4	130.5
<i>Water (kg/m<sup>3</sup>)</i>	250.0	250.0	250.0	250.0	250.0	250.0	250.0
<i>Superplasticizer (%)</i>	1.5	1.5	1.5	1.5	1.5	1.5	1.5

For the treatment of rubber aggregates with NaOH:

- The rubber aggregate is immersed in NaOH solution (prepared from the dissolution of 10 g of sodium hydroxide NaOH in 90 cm<sup>3</sup> of distilled water) for 30 minutes.
- After 30 min of immersion, rinsing with distilled water follows to remove all the soda adsorbed on the surface of the rubber aggregates. To ensure that all the soda has been removed from the rubber aggregates, the pH of the solution is tested until this pH is equal to 7.
- The rubber aggregates are dried in the open air before use [14].

## 2.2.2 Testing methods

The tests carried out on the different formulations are:

- Compressive strength and flexural tensile strength on specimens of size (40x40x160) mm<sup>3</sup> in accordance with standard EN 196-1 [13]. These tests were studied at the age of 14 and 28 days.
- Capillary water absorption test, water absorption test by total immersion, and porosity test were carried out on specimens of size (40x40x160) mm<sup>3</sup> in accordance with standard NF EN 480-5 [15], standard NBN B15-215 [16], and standard EN18-459 [17] respectively.
- Water permeability tests (based on the depth of penetration of water under pressure), were carried out on specimens of size (150×150×150) mm<sup>3</sup> in accordance with standard NF EN 12390-8 [18]. To determine diffusion depth into specimens after water penetration, the specimens were crushed, and water diffusion depth was measured.
- Attack acid: after a 28-day water cure (zero time), the (40×40×160) mm<sup>3</sup> mortars specimens were weighed to determine the mass (M<sub>0</sub>) before being subjected to immersion for 14, 28, and 90 days in acid sulfuric solution H<sub>2</sub>SO<sub>4</sub> concentrated at 5%. They were used to estimate the loss in mass according to the standard ASTM C 267-96 [19]. The attack solution was renewed every 15 days.

## 3 Results and discussion

### 3.1 Compressive strength

The variation of compressive strength as a function of time is presented in Figure 3. We note that the substitution of part of the sand by rubber aggregates is accompanied by a decrease in compressive strength and that for the different ages studied. This decrease increases with the increase in the substitution rate. The drop in compressive strength is explained by the fragile adhesion between the cement matrix and the rubber aggregate, as well as the low rigidity of rubber aggregates compared to that of natural aggregates [20,21].

For example, at the age of 28 days, the compressive strength was 41.05MPa for the reference mortar (M) against compressive strengths of 21.43 MPa and 25.57 MPa for the RM25% and RMT25% mortars respectively, decreases of 47.80% and 37.71% respectively. Therefore, for RMT25%, there is an improvement in compressive strength of 19.3% compared to RM25%. The same for RMT10% and RMT17.5% mortars, there is an improvement in compressive strength but with different speeds. Improvement of 15.02% for the RMT10% and of 20.46% for the RMT17.5% compared to RM10% and RM17.5% respectively.

The treatment of rubber aggregates with the NaOH solution contributed to an increase in the compressive strength of the mortars studied (improvement of more than 15%). This increase is justified by the fact that the treated rubber aggregates have undergone considerable modifications in the roughness of their outer surfaces, which has improved their adhesion to the cement matrix. In addition, the treatment of rubber aggregates with the NaOH solution improved hydrophilicity and homogeneity of these particles, thus increasing the rate of water

transfer around the particles, which can also ensure the completion of hydration of cement around particles [11]. Similar results have been observed by Naji Hilal [22].

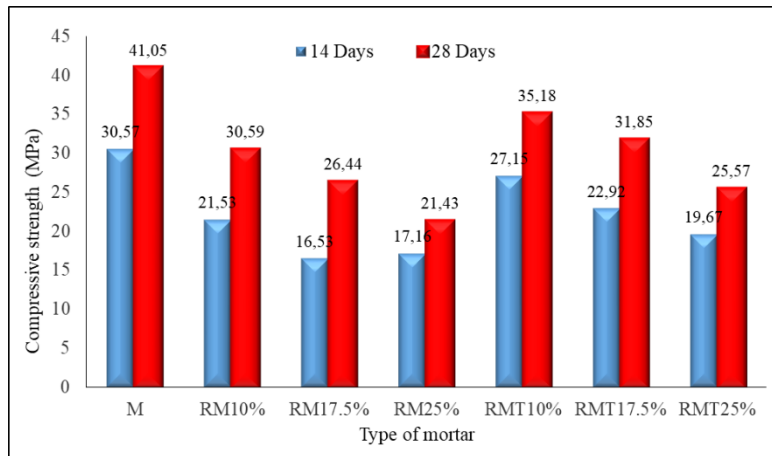


Figure 3: Compressive strength of the mixtures as a function of curing time

### 3.2 Flexural Tensile Strength

The results of the flexural tensile strength at the age of 14 and 28 days are shown in Figure 4. For the flexural tensile strength, the observation is the same as for the compressive strength, a decrease in the flexural tensile strength of rubber mortars compared to the reference mortar. This drop increase with increasing dosage of rubber. The treatment of rubber aggregates with NaOH solution improved the flexural tensile strength of rubber mortars. For example, at the age of 28 days, the RM25% mortar gave a flexural tensile strength of 4.4 MPa, therefore, a decrease of 46.24% compared to the reference mortar (8.18 MPa); against a flexural tensile strength of 5.76 MPa for MCT25%, so a decrease of 29.69% compared to the reference mortar (M). Therefore, NaOH treatment of rubber aggregate showed an improvement of 30.78% compared to MC25%.

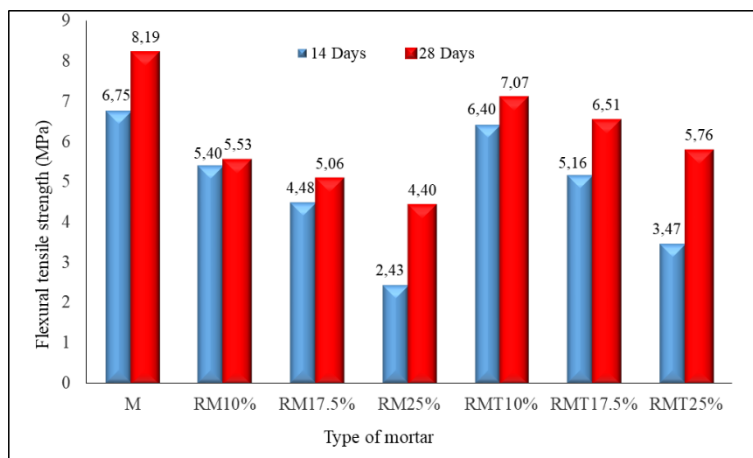


Figure 4: Flexural tensile strength of the mixtures as a function of curing time.

### 3.3 Absorption by capillarity

From Figure 5, we notice that the rubber aggregates decrease the amount of water absorbed gradually as the rate of rubber aggregates increases. After 48 hours, the quantity of water absorbed by the mortars RM10%, RM17.5%, RM25%, RMT10%, RMT17.5%, RMT25% was respectively reduced by 3.48% ; 7.68% ; 22.78% ; 5.39% ; 17.25% and 30.43% compared to that of the reference mortar (M). The incorporation of rubber aggregates in the cement matrix tends to limit the water absorption of the composite. The addition of rubber particles decreases the amount of water absorbed, because the rubber particles are hydrophobic, do not absorb the water [23]. Similar results have been found by [23,24].

We also note that the quantities of water absorbed by mortars with treated rubber are lower than the quantities of water absorbed by mortars with untreated rubber. This decrease varies between 1.98% and 10.36%. The decrease in water absorption is justified by the improvement in the adhesion between the cement paste and the rubber aggregates. Similar results have been found by [25].

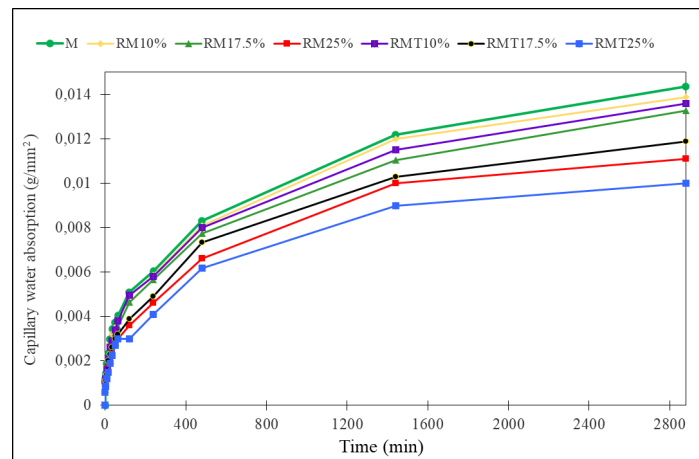


Figure 5: Absorption by capillarity of different types of mortars mixtures

### 3.4 Water absorption by total immersion

From Figure 6, it may be noted that the water absorption by total immersion of untreated rubber mortars is greater than that of reference mortar, and it increases with the increase in the substitution rate. Compared to reference mortar (M), there is an increase of 12.22% for RM10% against an increase of 24.44% for mortar RM25%. This result could be linked to the pores generated by the rubber aggregates due to their non-polar nature and their tendency to trap air on the surface. Air trapped in the mortar containing rubber aggregates makes the mortar more porous, thus becoming more permeable and thus allowing increased water [26].

For mortars with treated rubber, there was a remarkable reduction in the amount of water absorbed by total immersion of these mortars compared to mortars with untreated rubber aggregates and compared to reference mortar (M). It goes from 7.20% for (M) to 7.03% for RMT10%, 6.19% for RMT17.5% and 4.96% for RMT25%. So a decrease of 2.36%, 14.03%,

and 31.11% respectively compared to (M). This reduction in water absorption is justified by the improvement in the adhesion between the cement paste and the rubber aggregates which has made it possible to reduce the voids through which water can infiltrate. This same trend was observed by [27].

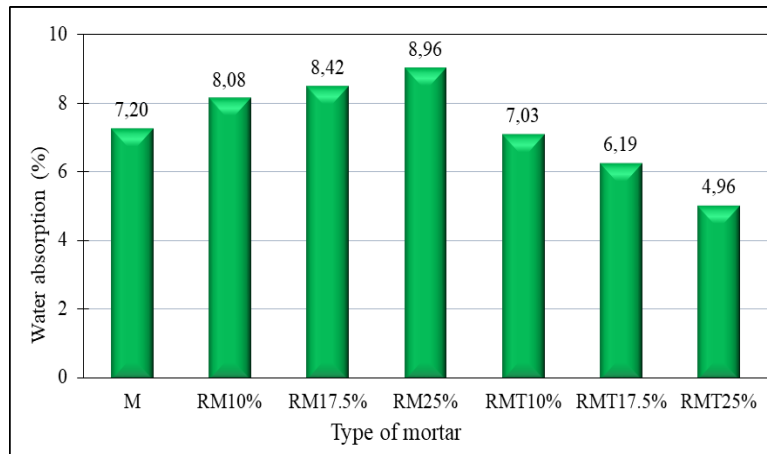


Figure 6: Water absorption of different types of mortars mixtures

### 3.5 Water-accessible porosity

In Figure 7, we have assembled the results of the measurements of the Water-accessible porosity of the different study mortars. We note that the porosity of rubber mortars is slightly lower than that of reference mortar, and that it decreases with an increasing substitution rate. For example, the porosity of the reference mortar (M) is 14.77% against a porosity of 13.38% for the rubber mortar RM25%, therefore a decrease of 9.41%. This decrease can be justified by the fact that rubber is a hydrophobic material that does not absorb water.

For mortars with treated rubber granulate, there is a considerable reduction compared to reference mortar (M) as well as compared to mortars with untreated rubber granulate. Compared to reference mortar (M), there are decreases of 20.65%; 24.78%, and 36.63% for mortars (RMT10%); (RMT17.5%) and (RMT25%) respectively. This reduction in porosity is always justified by the treatment of the rubber aggregates with the NaOH solution which has improved the adhesion between the cement paste and the rubber aggregates and has reduced the voids through which water can infiltrate.



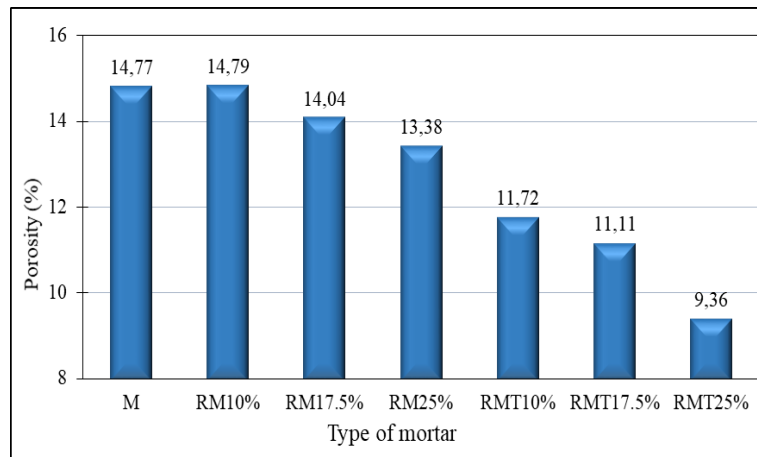


Figure 7: Porosity of different types of mortars mixtures

### 3.6 Water permeability depth

From Figure 8, we notice that the depth of water penetration of mortars containing rubber aggregates is greater than that of reference mortar, and that it increases with the increase in the substitution rate. It goes from 2.1cm for reference mortar to 3.4cm; 4.2cm; 5.7cm; 2.9cm; 3.1cm and 4.8cm for rubber mortars RM10%; RM17.5%; RM25%; RMT10%; RMT17.5% and RMT25% respectively. Expressed as a percentage, 36%; 68%; 128%; 16%; 24% and 92% respectively.

Moreover, we note that the water penetration depths for mortars with treated rubber are lower than the water penetration depths for mortars with untreated rubber. This decrease is the order of 55.56%; 64.71% and 28.13% for RMT10%; RMT17.5% and RMT25% respectively. The decrease in permeability is always justified by the fact that the treatment with the NaOH solution improved the adhesion between the cement paste and the rubber aggregates which made it possible to reduce the voids through which water can infiltrate.

Although the porosity and water absorption of mortars with treated rubber aggregates is lower than that of reference mortar (M), the permeability increases. The reason for this behavior is the lack of good bonding between the rubber aggregates and the cement paste, where the interface surface between the cement paste and the rubber aggregates acts as the bedding for pressurized water to flow in the mortar containing rubber [28]. Similar results have been observed by Ganjian et al. [28].

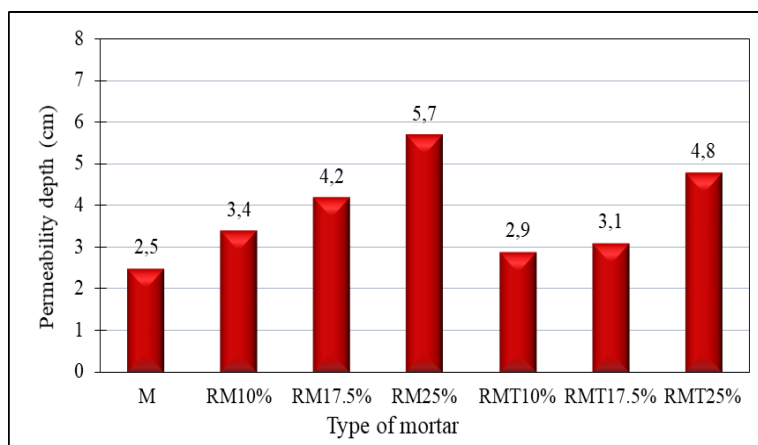


Figure 8: Water permeability depth results

### 3.7 Attack with sulfuric acid $H_2SO_4$ (loss in mass)

The values of the loss in mass test observed after 14, 28, and 90 days for the mortars studied are presented in Figure 9. The substitution of part of the sand by rubber aggregates is accompanied by a loss in mass, and that for the different ages studied. This loss in mass decreases with the increase in the substitution rate of sand by rubber aggregates. This same tendency has been observed by Kechkar et al. [29]. For example, at the age of 90 days, we notice a loss in mass of 22.98% for reference mortar (M) against losses in mass of 20.18% ; 17.93% ; 12.76% ; 15.43% ; 13.12% and 9,38% for rubber mortars RM10% ; RM17,5% ; RM25% ; RMT10% ; RMT17,5% and RMT25% respectively. This reduction of loss in mass for mortars containing rubber aggregates is justified by the nature of being chemically resistant to the penetration of acid of these particles.

We also note that the mortars with treated rubber showed a lower loss in mass than that of the mortars with untreated rubber. Mortars with treated rubber granulate showed a decrease in mass loss of 23.54%; 26.83% and 26.49% compared to RM10%; RM17.5% and RM25% respectively. This reduction in mass loss is justified by the improvement in the adhesion between the cement paste and the rubber aggregates, which has made it possible to reduce the voids through which the acid can infiltrate.

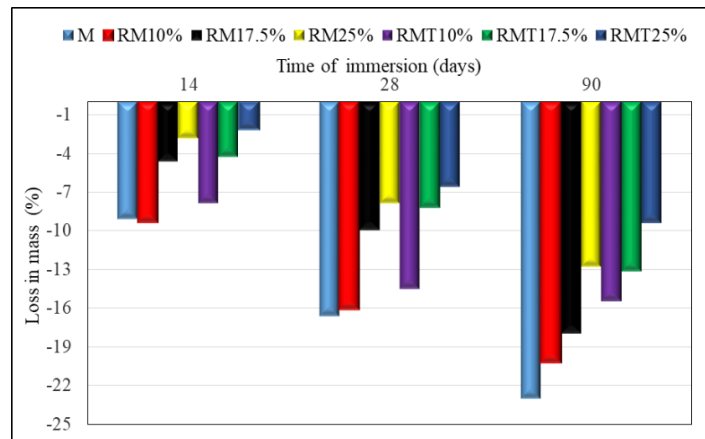


Figure 9: Variation of the mass of mortar according to the immersion time in  $H_2SO_4$

## 4 Conclusions

This experimental study was carried out to evaluate the influence of the treatment of rubber aggregates with the solution (NaOH) on the durability of mortars based on rubber aggregates as a partial replacement for ordinary sand. Rubber aggregate partially replaced sand at 0%, 10%, 17.5%, and 25% by volume. From the results, we can draw the following main conclusions:

- Generally, the incorporation of rubber aggregates to mortars reduces the mechanical characteristics of the mortars. However, the treatment of rubber aggregates with NaOH can decrease this negative point or at least reduce their effects to acceptable limits.
- The use of rubber aggregates lowers the amount of absorption by capillarity and porosity. This decrease is more significant in the case of rubber aggregates treated with the solution (NaOH) compared to untreated rubber aggregates.
- The water absorption by total immersion of mortars containing rubber aggregates is greater than that of reference mortar. However, the treatment of these aggregates with the NaOH solution improved this property. Mortars with treated rubber aggregates gave a lower water absorption than ordinary mortar.
- The water permeability of mortars containing rubber aggregates is higher than the reference mortar. The rubber granulate treatment with NaOH solution has improved this property, mortars with treated rubber aggregates have lower water permeability than mortars with untreated rubber aggregates.
- Treatment of rubber aggregates with NaOH improved resistance to chemical attack by  $H_2SO_4$ . A reduction in the mass loss of mortars with treated rubber aggregates compared to reference mortar and mortars with untreated rubber aggregates.

Therefore, the treatment of rubber aggregates with the NaOH solution has improved the mechanical performance and durability of rubberized mortars by improving the adhesion between the rubber aggregates and the cement matrix.

## References

- [1] Sukontasukkul P & Tiamlom K (2012). Expansion under water and drying shrinkage of rubberized concrete mixed with crumb rubber with different sizes. *Construction and Building Materials*. 29, 520–526. DOI:10.1016/j.conbuildmat.2011.07.032.
- [2] Qiao D, Baoshan H & Xiang S (2013). Rubber modified concrete improved by chemically active coating and silane coupling agent. *Construction and Building Materials*. 48, 116–123. <https://doi.org/10.1016/j.conbuildmat.2013.06.072>
- [3] Roychand R, Gravina RJ, Zhuge Y, Ma X, Youssf O & Mills JE (2020). A comprehensive review on the mechanical properties of waste tire rubber concrete. *Construction and Building Materials*. 237,117651. <https://doi.org/10.1016/j.conbuildmat.2019.117651>
- [4] Reda Taha MM, El-Dieb A, Abd El-Wahab M & Abdel-Hameed M (2018). Mechanical, fracture, and microstructural investigations of rubber concrete. *Journal of Materials in Civil Engineering*. 20 (10), 640–649. DOI: 10.1061/(ASCE)0899-1561(2008)20:10(640).
- [5] Svoboda J, Dvorský T, Václavík V, Charvát J, Mácalová K, Heviánková S & Janurová E (2021). Sound-Absorbing and Thermal-Insulating Properties of Cement Composite Based on Recycled Rubber from Waste Tires. *Construction and Building Materials*. 23(2),1084-1092. DOI: 10.1016/j.conbuildmat.2008.05.021
- [6] Bhaskar M A, Ravichandran P T, Annadurai R & Kannan Rajkumar P R (2018). Studies on Properties of Concrete Using Crumb Rubber as Fine Aggregate. *International Conference on Intelligent Computing and Applications*. Advances in Intelligent Systems and Computing 846, Proceedings of ICICA. Springer Nature Singapore. [https://doi.org/10.1007/978-981-13-2182-5\\_2](https://doi.org/10.1007/978-981-13-2182-5_2)
- [7] Ben Nakhai A & Alhumoud JM (2020). Properties of Concrete Containing Scrap (Recycled) Tire-Rubber. *Journal of Engineering and Applied Sciences*. 15 (2), 653-658. DOI: 10.36478/jeasci.2020.653.658
- [8] Marques AC, Akasaki JL, Trigo APM & Marques ML (2008). Influence of the surface treatment of tire rubber residues added in mortars. *IBRACON Structures and Materials Journal*. 1, 113-120. DOI: 10.1590/S1983-41952008000200001
- [9] Mohammadi I, Khabbaz H & Vessalas K (2015). Enhancing mechanical performance of rubberised concrete pavements with sodium hydroxide treatment. *Materials and Structures*. DOI: 10.1617/s11527-015-0540-7
- [10] Qingwen M & Jinchao Y (2013). Effect on Mechanical Properties of Rubberized Concrete due to Pretreatment of Waste Tire Rubber with NaOH. *Applied Mechanics and Materials*. 897-904. DOI: 10.4028/www.scientific.net/AMM.357-360.897
- [11] Ruizhe S, Jiaqing W, Shuaicheng G, Qingli D & Song H (2018). Evaluation of laboratory performance of self-consolidating concrete. *Journal of Cleaner Production*. 180, 823-831. <https://doi.org/10.1016/j.jclepro.2018.01.180>
- [12] NA 442. (2000). Algerian standard. Hydraulic binders, current cements: composition, specification and conformity criteria. 2nd edition. IANOR. Algeria
- [13] NF EN 196-1 (2006). Methods of testing cement – Part 1: Determination of strength
- [14] Al-Khuzai MG, Al-Humeidawi, BH & Abbas Al-Sa'idi RF (2020). Assessment of the mechanical properties of concrete pavement containing crumb rubber of tires. *IOP Conference Series Materials Science and Engineering* 737:012141. DOI: 10.1088/1757-899X/737/1/012141.
- [15] EN 480-5. (2006). Admixtures for concrete, mortar and grout - Test methods - Part 5: determination of capillary absorption.
- [16] NBN B15215. (2018). Testing hardened concrete - Absorption of water by immersion.
- [17] EN 18-459. (2010). Concrete - Testing hardened concrete - Testing porosity and density
- [18] NF EN 12390-8. (2019). Testing hardened concrete - Part 8 : depth of penetration of water under pressure
- [19] ASTM C 267-96 (1996). Standard Test Methods for Chemical Resistance of Mortars, Grouts, and Monolithic Surfacing and Polymer Concretes.
- [20] Lia G, Stubblefield MA, Garrick, G, Eggers J, Abadie C & Huang B (2004). Development of waste tire modified concrete. *Cement and Concrete Research*. 34, (12), 2283-2289. <https://doi.org/10.1016/j.cemconres.2004.04.013>

- [21] Najim KB & Hall MR (2010). A review of the fresh/hardened properties and applications for plain- (PRC) and self-compacting rubberized concrete (SCRC). *Construction and Building Materials*. 24, 2043–2051. DOI:10.1016/j.conbuildmat.2010.04.056.
- [22] Naji Hilal N (2017). Hardened properties of self-compacting concrete with different crumb rubber size and content. *International Journal of Sustainable Built Environment*. 6, 191-206. <https://doi.org/10.1016/j.ijbsbe.2017.03.001>
- [23] Boukour, S & Benmalek, ML (2016). Performance evaluation of a resinous cement mortar modified with crushed clay brick and tire rubber aggregate. *Construction and Building Materials*. 120, 473–481. <https://doi.org/10.1016/j.conbuildmat.2016.05.119>.
- [24] Benazzouk A, Douzane O, Langlet T, Mezreb K, Roucoult JM & Quéneudec M. (2007). Physico-mechanical properties and water absorption of cement composite containing shredded rubber wastes. *Cement and Concrete Composite*. 29, 732–740. DOI:10.1016/j.cemconcomp.2007.07.001.
- [25] Segre N & Joeke I (2000). Use of tire rubber particles as addition to cement paste, *Cement and Concrete Research*. 30, 1421–1425. DOI: 10.1016/S0008-8846(00)00373-2.
- [26] Adamu M & Uche OAU (2014). Durability properties of concrete containing scrap tyre as fine and coarse aggregate in Concrete. *International Journal of Scientific and Engineering Research*. 5(11), 628-634. DOI
- [27] Ruizhe S, Shuaicheng G & Qingli D (2017). Durability performance of rubberized mortar and concrete with NaOH-Solution treated rubber particles. *Construction and Building Materials*. 153, 496–505. <http://dx.doi.org/10.1016/j.conbuildmat.2017.07.085>
- [28] Ganjian E, Khorami M & Maghsoudi AA (2009). Scrap-tyre-rubber replacement for aggregate and filler in concrete. *Construction and Building Materials*. 23, 1828-1836. <https://doi.org/10.1016/j.conbuildmat.2008.09.020>
- [29] Kechkar C, Belachia M & Cherait Y (2020). Contribution to the study of the durability of rubberized concrete in aggressive environments. *Civil and Environmental Engineering Reports*. 28 (2), 111-129. DOI: 10.2478/ceer-2020-0009.

## Effects of different processes of tunneling on displacements soil using 3D Finite Element Method

**Nawel Bousbia**

University of 20 Août 1955 - Skikda, Algeria  
Faculty of technology, Department of Civil Engineering  
Laboratory LMGHU  
e-mail: bousbia1101@yahoo.com

### Abstract

The excavation process of tunnels induces stresses and deformation in the surrounding soil. The method of excavation is one of the major problems related to the safety of the operators and the ground stability during the construction of underground works. So, it is necessary to choose an ideal method to minimize the displacements and stresses induced by tunneling.

The main aim of this study is to simulate numerically the effect of different processes of tunneling on ground displacements, the settlements at surface soil and the internal efforts induced in the lining tunnel; in order to select the best process of excavation, which gives us a less effects on displacements generated by tunneling, thus, ensuring the stability and the solidity of the underground constructions. In addition, this study allows us to control and to predict the diverse movements generated by tunneling (displacements, settlements, efforts internes) exclusively for the shallow tunnel nearby to the underground constructions in the urban site. This modeling will be done by employing five different processes for tunnel excavation using the NATM (New Austrian Tunneling Method) method.

The first process, the modeling of the excavation tunnel, is done almost in the same way as in reality; the partial face excavation, with seven slices, made by the excavation. The second process, by partial face excavation, is divided into eleven slices, next, we used the partial face excavation by nine slices, and then in thirteen slices. Finally, the dig is made by full-face excavation.

The paper contributes to the prediction of the response of the soil environment to tunnel excavation using the NATM method and to minimize the diverse movements generated by tunneling. The appropriately chosen methodology confirms that displacements and subsidence are strongly influenced by the tunneling method. The three-dimensional Finite Elements Method using Plaxis3D program has been applied in the numerical simulation. The study resulted in the recommendation of a process that minimizes the effect of excavation on subsidence and ground displacement for a particular Setiha tunnel.

**Key words:** tunnel, excavation, process, finite element analyses, Plaxis3D

## 1 Introduction

The nature of the excavation work being undertaken will affect the selection of an excavation method and safe system for this work. Deep excavations are usually employed in urban development projects and the works are carried to construct underground infrastructures such as deep basements, subways, and service tunnels. The execution of underground structures has always been of major risk concern, as intense ground movements and displacements of the settlement at surface soil are induced during the excavation process [1, 2, 3, 4, 5]. Also, they cause severe damage to the neighboring structures. The performance of excavation is affected by various factors, including the local ground conditions, the structural support systems, the construction processes, and the technique of excavation. The finite element analysis is generally used to model deep excavation construction processes. In urban areas, there are many situations where the tunnels facilities are proposed to be constructed adjacent to an old building. There are many types of execution techniques and methods developed for the construction of tunnels, and there are different processes of the excavation tunnel, where the researchers and engineers have given significant attention to the responses of soils due to the tunnel excavation method. Inadequate tunnel method construction or inadequate scenario can cause damage to the adjacent structure, more or less significant, depending on the process of drilling adopted. The tunneling operations lead to changes in the stresses, movements, and displacements of the surrounding soil. The study of the crossing tunnel under the mount of Setiha (tunnel zone) (Figure 1) appears in the setting of the modernization of the National Road n° 43. For the realization of this study, where the geotechnical stability and the soil/structure interaction dress a fundamental role, we chose the PLAXIS 3D software.

## 2 Tunnel project characteristics

The location of the object of the study is located in the region of Mount Atlas, in the middle of the summits of Koudiet Es Sous and Koudiet Bous En Nar (Figure 1). It is situated at about 20 km in the Southwest of Skikda city and at about 50 km to the Northeast of Constantine town. The total length of the tunnel at about 935 meters, it constitutes a single gallery, which will fit two ways.



Figure 1: Trace of the tunnel retrieved from Google Earth

### 3 Tunnel model calculation

The transversal section type (Figure 2) expected will guarantee the insertion of a road platform with a total width of about 7.60 m and will assure a 5.0 m height along this width. In the central zone, an additional area above this height permits the installation of the ventilation system inside the tunnel.

The top of the tunnel is 24.50 m below the surface of the soil. The tunnel has a height of 7.5 m and a width of 10.20 m; the tunnel lining with a thickness lining of 25 cm consists of a cement B 25 layer, which includes the steel reticulate HEB160 /0.75.

Figure 3 presents the geometry of elements following with the calculation model representative in the road kilometer point [KP 0+400], using the PLAXIS3D program. This model aims to value the geotechnical and structural tunnel behavior in the zone where the cover is reducing and where the tunnel crown crosses a clayey layer that seems to correspond to a faille (fragment of rocks).

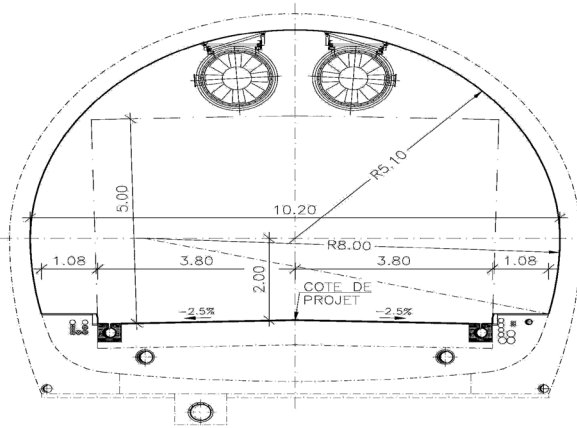


Figure 2: Transverse section type of tunnel

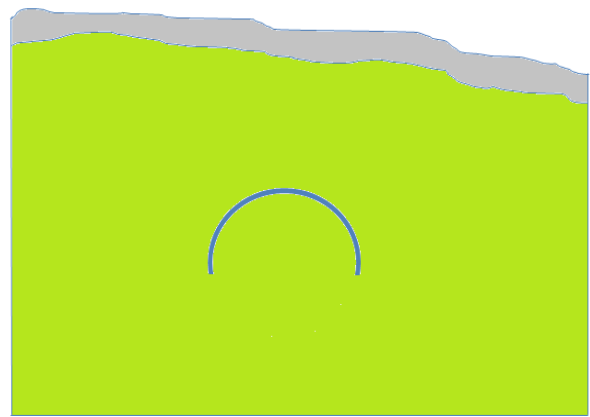


Figure 3: Geometry of model at KP 0+400

#### 3.1 Soil horizons

Concerning the soil horizons (rubble, clay) these were simulated using the constituent model of Mohr-Coulomb. The parameters associated with these horizons were defined carefully with regards to the results of SPR tests (Standard Penetration Test) or the nature of the horizons. Besides, the clayey layer associated with a possible faille (fragment) close to the portal is also simulated with this constituent model. The parameters are given in Table 1.

Table 1: Mechanical and geotechnical characteristics of soils in the PLAXIS3D program for the Mohr-Coulomb Model.

Soil	Unit weight (kN/m <sup>3</sup> )	Friction angle $\Phi$	Cohesion (MPa)	Elastic modulus (MPa)	Poisson ratio $\nu$
rubble	18	35	10	50	0,3
Faille (clay)	22	35	30	50	0,3

The tunnel is constructed in a homogeneous soil, with a linear elastic model for the tunnel

SSP



lining. The Mohr Coulomb model is adopted for simulating the plastic behavior of soil under static conditions.

NOTE: No hydrostatic pressure has been considered because we planned the installation of the drainage devices during the excavation. Therefore, the phreatic level does not have any influence on tunnel behavior.

### 3.2 Properties of the tunnel lining

Table 2 presents the properties of tunnel lining "Plate" considered for the calculation of the excavation phase, simulating the lining support (incorporating or not of the metallic hangers) through a linear elastic behavior.

Table 2: Tunnel lining parameters as inputted in the PLAXIS3D program

	Description	$EA$ ( $\times 10^3$ ) kN/m	$EI$ kN/m <sup>2</sup>	$\nu$
Lining tunnel	Shotcrete 25 cm+ Steel	6520	35380	0.15

## 4 Numerical simulation of the tunnel (ATM Method)

All calculations are founded on the choice of the triangular elements to a 15-node triangle. An elastic-plastic law governs the behavior of soil and the tunnel where the criteria of Mohr-Coulomb has been adopted. For the tunnel, an elastic linear behavior has been adopted. The boundary conditions are taken into account while blocking the horizontal displacement and the two displacements - horizontal and vertical - for the lower limit of the model. The mesh is refined to the region of the tunnel. The Setiha tunnel will be constructed according to the ATM method. All works will be performed in the same technique as the installation of the components of the support system. The excavation is made in stages for the Crown, Bench, and Invert [6].

In this analysis, the cross-section of the tunnel type is selected (NAT Method) (Figure 4). The top of the tunnel is 24, and 50 m below the surface of the soil. The surrounding ground tunnel constitutes two different layers. The modeled domain was 80 m in length, 40 m in width, and 50 m in depth.

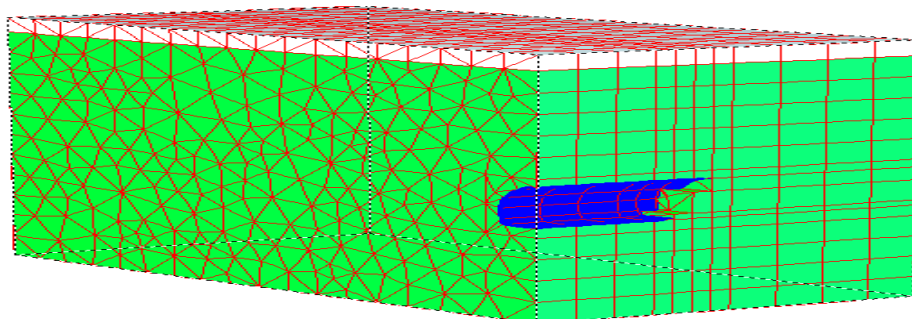


Figure 4: 3D Finite element mesh of NATM Tunnel project (symmetrical model)

## 5 Numerical simulation procedure of the tunnel

The effect of different processes of tunneling on movements of the soil is assessed in terms of the global displacements and the internal forces that build up in the lining during tunnel excavation. The three-dimensional Finite Element Method using the Plaxis3D program has been applied in the numerical simulation. The soil is described through Mohr-Coulomb behavior. i:

- The partial face excavation
- The full-face excavation

Five processes are tested: Each process includes several slices. Every slice is 2m (excavation step).

### 5.1 Partial face excavation (Processes n°: 1, 2, 3, 4)

The modeling of the calculation phases is done almost in the same manner as in reality, the excavation is made by partial face excavation, and it is performed according to the first, second, third, and fourth process, as shown in the following Figures (5, 6, 7, and 8).

Part excavated (10 m)		Part to excavate				Part excavated (10 m)		Part to excavate						
Slice 1		Slice 2	Slice 3	Slice 4	Slice 1		Slice 2	Slice 3	Slice 4	Slice 1		Slice 2	Slice 3	Slice 4
10 m	2 m	01	02	03	Top heading (crown)		10 m	2 m	01	03	04	Top heading (crown)		
	2 m	04	05	bench		2 m		02	05	bench				
	2 m	06	invert		2 m	06		invert						
Fig.5 Excavation phases from the First process						Fig.6 Excavation phases from the Second process								
Part excavated (10 m)		Part to excavate				Part excavated (10 m)		Part to excavate						
Slice 1		Slice 2	Slice 3	Slice 4	Slice 1		Slice 2	Slice 3	Slice 4	Slice 1		Slice 2	Slice 3	Slice 4
10 m	2 m	01	02	05	Top heading (crown)		10 m	2 m	01	04	06	Top heading (crown)		
	2 m	03	04	bench		2 m		02	05	bench				
	2 m	06	invert		2 m	03		invert						
Fig.7 Excavation phases from the Third process						Fig.8 Excavation phases from the Fourth process								

### 5.2 Full section excavation (Fifth process)

The modeling of the calculation phases is made through full-face excavation, by total section, and it is performed according to the fifth process, as shown in Figure 9.

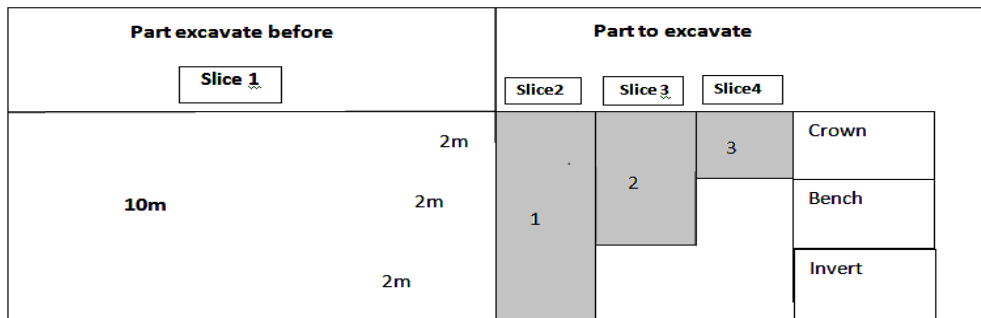


Figure 9: Excavation phases from the Fifth process

## 6 Results and discussion

The study reveals a significant effect of the order of the tunnel cutting sections on the subsidence on the free soil surface, accepting five different processes.

The aim is to simulate numerically the effects of different processes of tunneling on movements/displacements, and settlement of surface soil, also the convergence and the internal efforts induced in the tunnel lining. The excavation is made through slices for the calotte, stross (crown), and invert, the step of advancement is equal to 2 m. It has been modeled in two phases for each component (excavation - shotcrete).

### 6.1 Prediction of the vertical displacement of the soil /settlement

Loganathan et al. [7, 8] studied the analytical predictions of tunneling-induced ground movements. The vertical and the horizontal displacements, and the settlement induced by the tunnel excavation following the five distinguished processes are displayed in Figure 10.

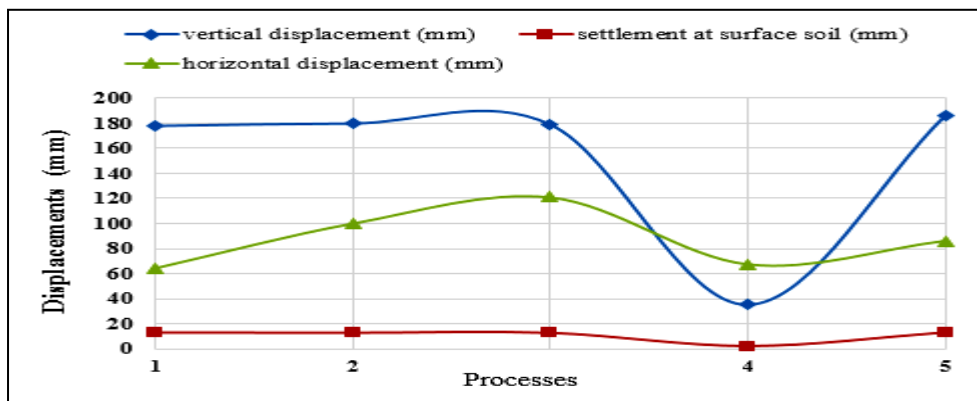


Figure 10: Displacements following the different processes

Figure 10 presents the settlement profiles at the free soil surface, also the vertical and horizontal displacements of soil, due to the excavation of the tunnel, using different processes of tunneling. It is registered that the excavation of the tunnel by the partial face section according to the fourth process gives lower results in terms of displacements (vertical /horizontal) and the settlement at surface soil. The first process offers a minimum value for the horizontal displacement compared to the vertical displacement.

According to these profiles, we can conclude that displacements and subsidence are strongly influenced by the tunneling excavation method (process).

The comparison of the results shows that the process n°4 minimizes the effect of excavation on settlement and ground displacement.

## 6.2 Effects of different processes on the vertical displacement of the frontal section

In this part, the vertical displacements (subsidence) of the first plan (frontal section of tunnel excavation) are analyzed for different processes of excavation.

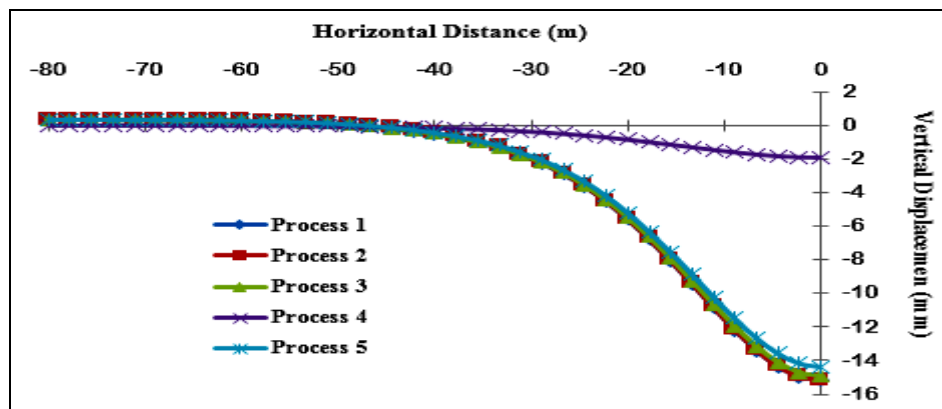


Figure 11: Vertical displacement following the different processes in the tunnel's front section

Figure 11 presents the vertical displacements at the front section of the tunnel corresponding to each excavation process without considering the displacements of the previous phases. Figure 11 shows that each method of excavation (process) generates a vertical displacement relative to the horizontal distance from the starting profile. The settlements engendered in this profile by the fourth process are lower compared to the other processes, therefore this process is selected (n°4), leading to the reduction of the settlement in the front section.

## 6.3 Effect of the elevation of different parts of the tunnel on the ground movement and settlement

Thayanan [9] and Dong et al. [10] investigated the effects of the construction sequence and the cover depth on the crossing-tunnel interaction. The tunnel is excavated in different parts (for example, crown, bench, and invert), where successive parts are executed at a certain distance after the previous part. After the excavation of the separated parts, the tunnel contour is secured by the temporary lining of the tunnel. The effect of elevation of each part of the tunnel's excavation on the settlement of the surface soil and the ground displacements is investigated and the influence of each excavated part (crown, bench, and invert) on the

response of the soil is observed. The stability of the soil was investigated in four variants. The full tunnel height was 7.5m. (1) The first variant: The elevation of each part to be excavated (crown, bench, and invert) is equal to  $H/3$  (2.5m, 2.5m, 2.5m) respectively, as shown in Figure 12.

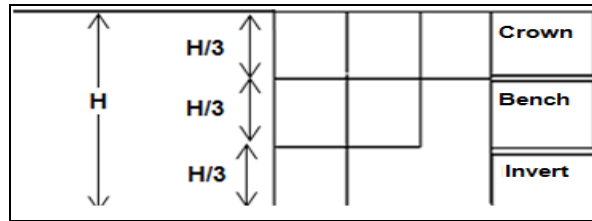


Figure 12: The first variant of the tunnel excavation

(2) Second variant: The elevation of each tunnel part (crown, bench, and invert) is equal to  $H/4$ ,  $H/4$ , and  $H/2$  respectively, as shown in Figure 13.

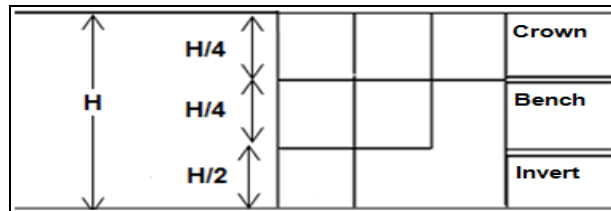


Figure 13: The second variant of the tunnel excavation

(3) The third variant: The elevation of each tunnel part (crown, bench, and invert) is equal to  $H/2$ ,  $H/4$ , and  $H/4$  respectively, as shown in Figure 14.

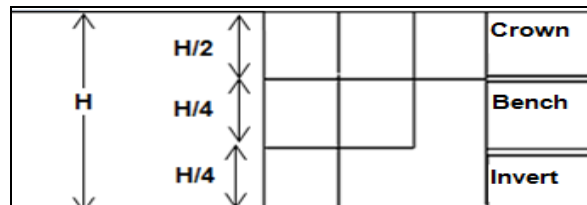


Figure 14: The third variant of the tunnel excavation

(4) The fourth variant: The elevation of each tunnel part (crown, bench, and invert) is equal to  $H/4$ ,  $H/2$ , and  $H/4$  respectively, as shown in Figure 15.

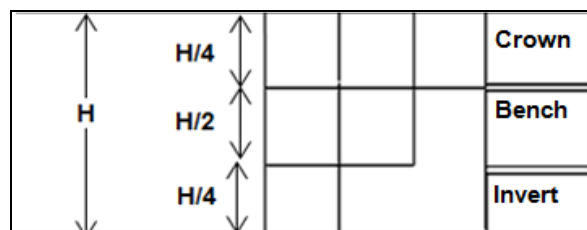


Figure 15: The fourth variant of the tunnel excavation

The effects of the elevation of the different parts (crown, bench, and invert) of the tunnel to be excavated on subsidence and ground displacement, according to different variants are displayed in Figure 16.

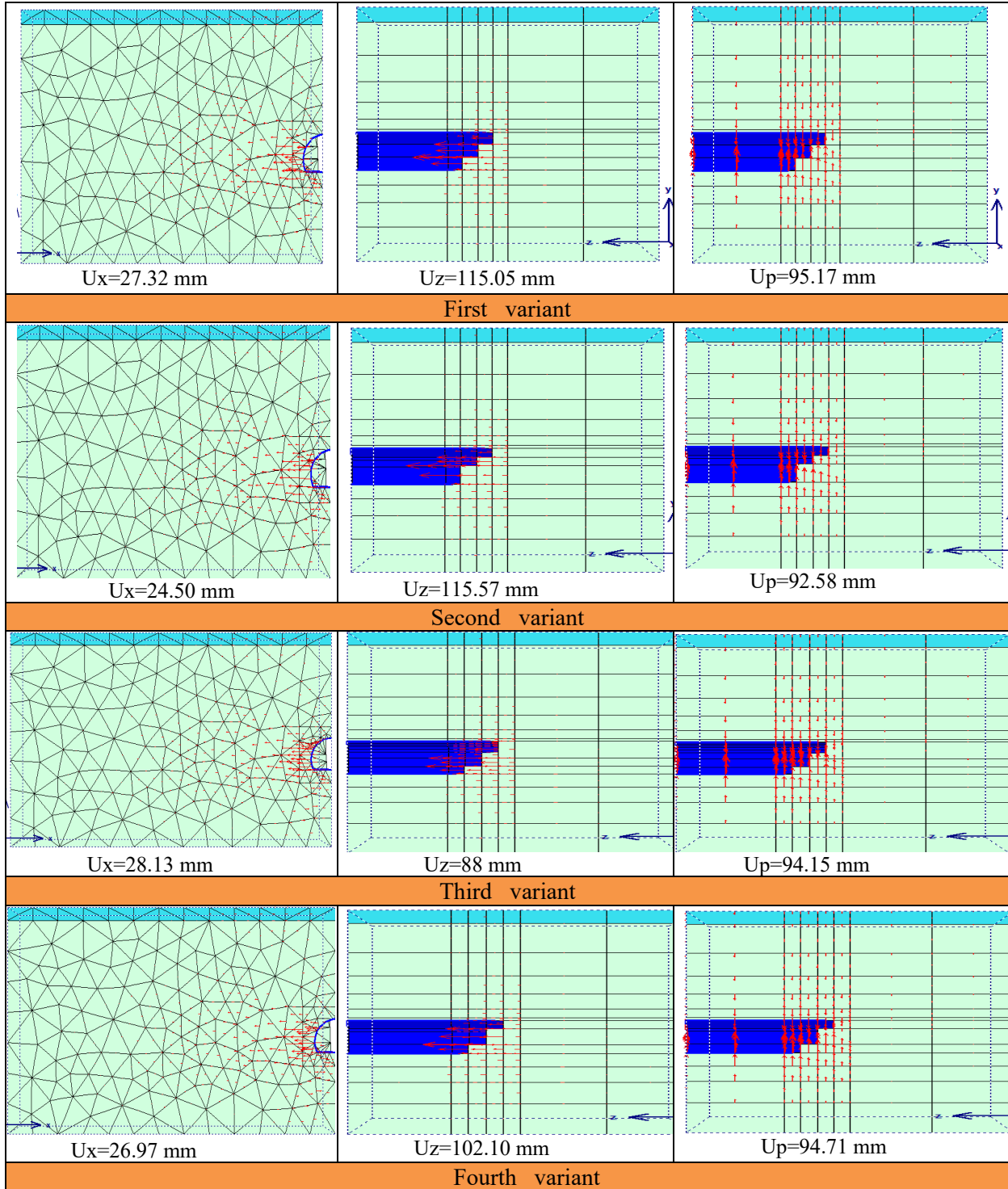


Figure 16: Results obtained for different variants

Figure 17 shows the settlement profiles relative to the horizontal distance for each variant.

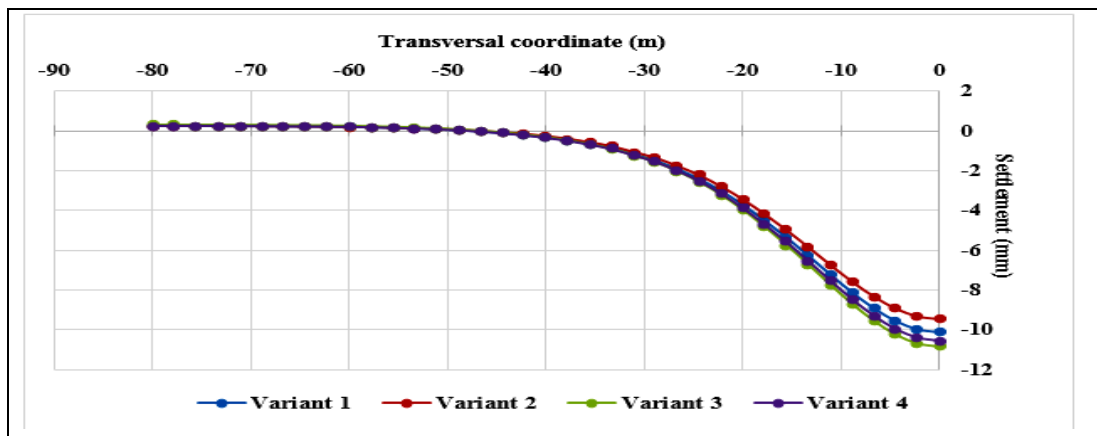


Figure 17: Settlements values at soil surface following the different variants

The results show that the maximum value of the settlement appears on the level of the vertical axis of the tunnel for each variant and then decreases to zero.

It can be seen from Figure 17 that the numerically calculated settlement values at the soil surface in the transverse section for diverse variants (considering only the vertical displacement of the last phase) are almost similar; where the maximum values are between 9.5 mm and 10.8 mm but slightly decreasing for the second variant (-9.5 mm).

So, the excavation by adopting the second variant gives lower results compared to other variants.

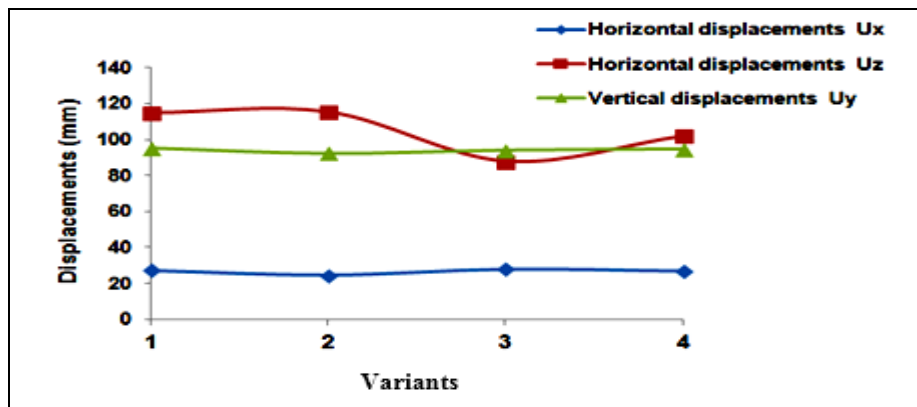


Figure 18: Soil displacement values according to different variants

Figure 18 presents the displacements (horizontal  $U_x$ , horizontal  $U_z$ , and vertical  $U_p$ ) relative to each variant. The results illustrate that the minimum horizontal displacement  $U_x$ , and the vertical displacements  $U_p$  emerge for the second variant. On the other hand, it can be noticed that the minimum horizontal displacement  $U_z$  (in the longitudinal direction) appears for the third variant.

Hence, the movements of the soil occur due to the change of the soil rigidity because of the

SSS

weakening of the excavation surroundings. This is an important factor in the movement of the ground.

Therefore, for the lower effect on the settlement and displacement of the soil, we propose, in this case, excavating the tunnel in accordance with the second variant. This case is explained per the quantities of excavation soil. The excavation of the tunnel shall be done in little quantities so to the soil is not destabilized (crown =  $H/4$ ; bench =  $H/4$ , then invert  $H/2$ ).

### 6.4 Effect of the order of parts of tunnel excavation on the settlement and movements of the soil

To analyze the effect of the order of the excavation of tunnel parts (typical construction stage procedure) on the settlement of the surface soil, we use several configurations of excavation. The tunnel is simulated numerically using the section-divided method. In this case, it is required to use a three-dimensional model (3D).

Eight (8) configurations of the construction sequence are tested and shown in Figure 19.

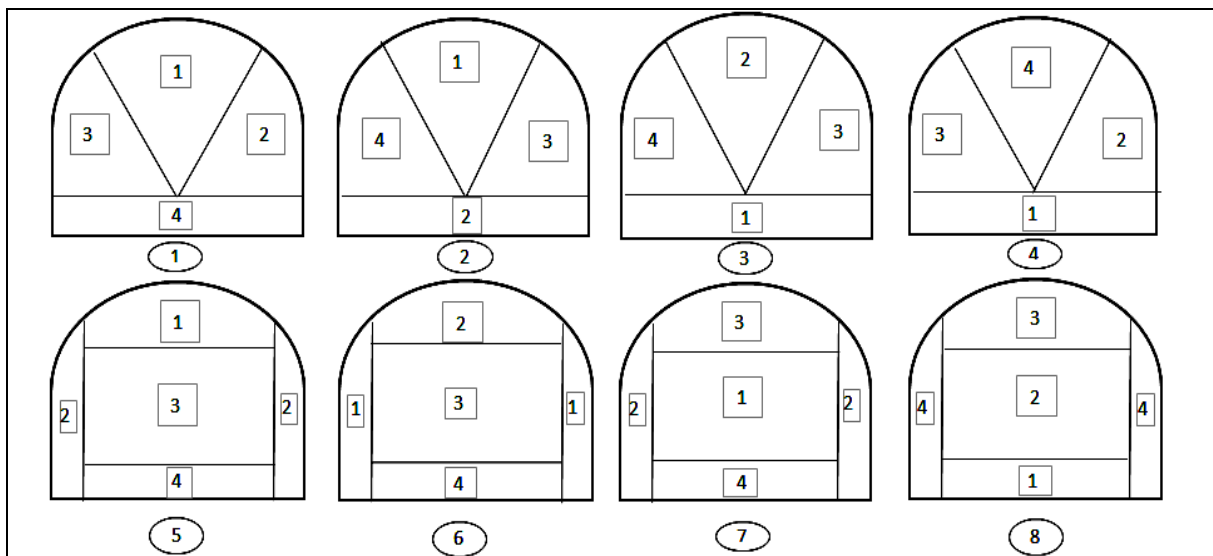
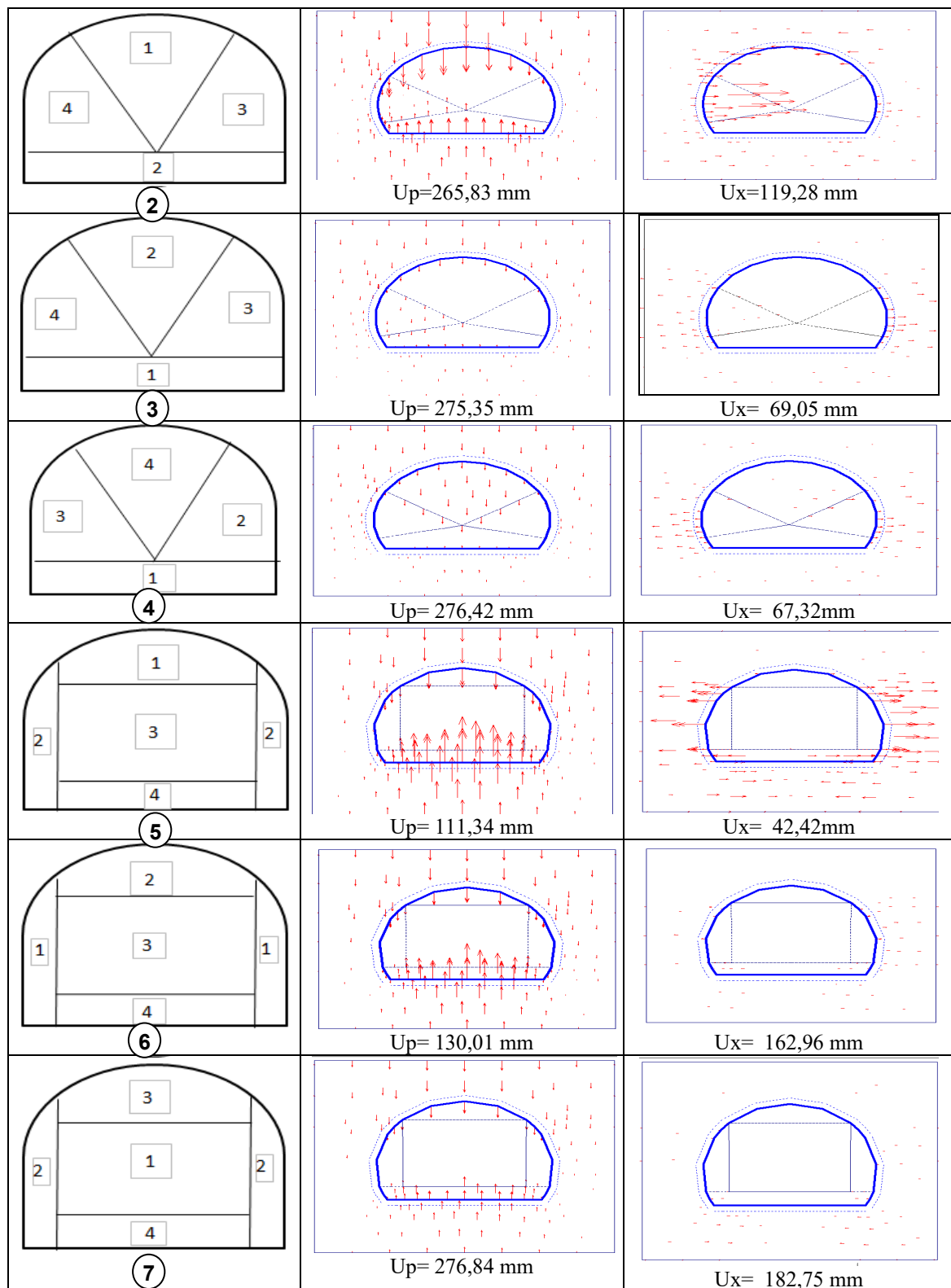


Figure 19: Eight configurations in the cross-section view (typical construction stage procedure)

The results obtained through this numerical study for the eight configurations of the construction sequence are summarized in Figure 20.

Scenario number	Vertical displacement (mm)	Horizontal displacement(mm)
<p>①</p>	<p><math>U_p=204,81</math> mm</p>	<p><math>x=109,38</math> mm</p>





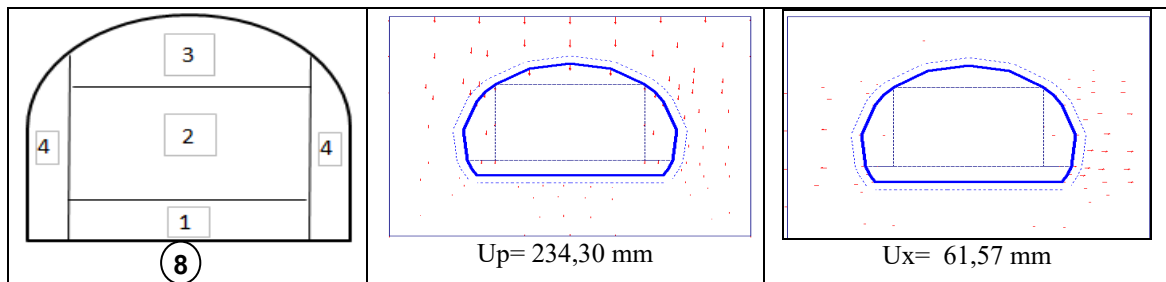


Figure 20: Results of the analysis for different construction sequences

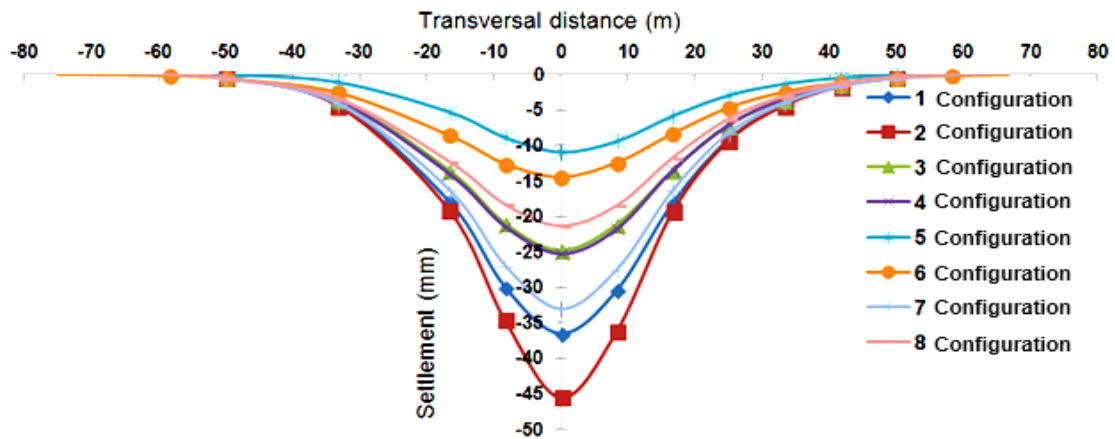


Figure 21: The settlement of the soil surface relative to the horizontal distance for different configurations

Figure 21 shows the distribution of settlement at the soil surface relative to the horizontal distance for different configurations of the construction sequence.

As illustrated in this Figure, the minimum settlement value mainly occurs at the fifth configuration. Maximum settlements occur at the second configuration. Due to the destabilization of the soil at the zone of influence differentiated by the lines that project 45° from the tunnel spring line (tunnel crown), the stability of the surroundings will be weakened. This is an important factor in the settlement of the soil surface.

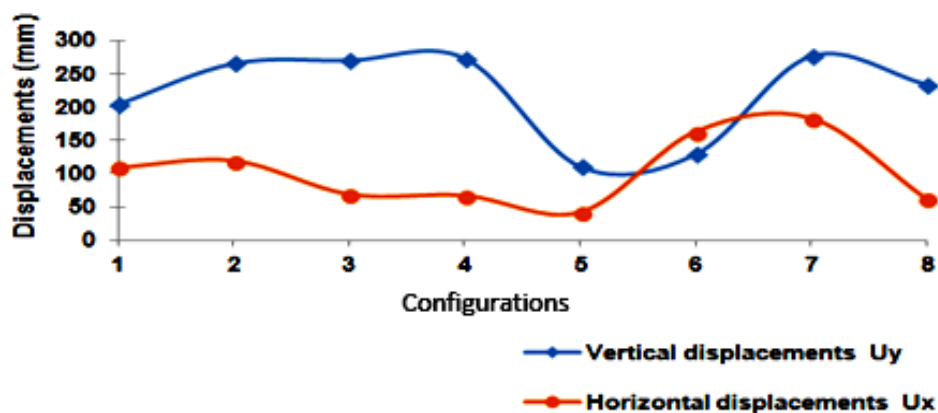


Figure 22: Soil displacement values according to the different configurations of the construction sequences

Figure 22 presents the values of different displacements (horizontal  $U_x$ , and vertical  $U_p$ ) relative to the construction sequence.

Analysis results demonstrate that the minimum horizontal displacements and the vertical displacements appear at the fifth construction sequence.

The same goes for the settlement, where the minimum value appears at the fifth construction sequence.

Regarding different configurations of the construction sequences, we propose to excavate our tunnel in accordance with the fifth construction sequence and to minimize the effects (fewer impact) of tunneling on displacements and subsidence.

## 7 Conclusion

In this research, numerical modeling of the effect of different tunneling processes on movements and displacements of soil was presented, based on the three-dimensional Finite Element Method using the Plaxis3D program.

The modelling of the effects of the different tunneling processes was performed using the NRTM method on ground displacements and settlements of the soil surface. The modeling has been applied to a specific tunnel in Setiha to propose how to minimize the diverse movements generated by tunneling.

The following conclusions can be drawn from this numerical study:

- The procedures of construction affect the settlement, displacement, and internal efforts in the tunnel lining.
- The displacements and settlements engendered by tunneling using the partial-face excavation method are less important than the displacements and settlements obtained using the full-face excavation method. The difference between the results obtained using the two methods is mainly due to an augmentation of the number of open segments in the tunnel front. Therefore, the drilling using the partial-face excavation minimizes the effect on subsidence and ground displacement, thus we sufficiently ensure the stability of the tunnel front.
- This study reveals a significant effect of the order of the tunnel cutting sections on the subsidence of the free soil surface, accepting five different processes.
- Regarding the process of the excavation, there are five processes tested, four (4) with partial-face excavation, and one (1) with full-face excavation. The effect of the process of the excavation on the settlement and displacements shows that the fourth process is the best, with minimum values regarding the displacements and settlement predicting more stability of the ground.
- Regarding the effect of elevation of different parts of the tunnel (crown, bench, and invert) on the movement and settlement, there are four variants established. The effect of elevation of different parts of the tunnel shows that the second variant is the best (has less impact).
- Regarding the effect of the order of the tunnel excavation parts on the settlement and the movement of the soil illustrates that the fifth configuration of the construction sequence is the best of the eight configurations tested (less effect).
- The study resulted in the recommendation of a process/variant of excavation that minimizes the effect of excavation on subsidence and ground displacement. The conclusions are applicable to the practice of underground structures.

## References

- [1] Bousbia Nawel, Messast Salah (2015). Numerical modeling of two parallel tunnels interactions using three- dimensional finite element. *Geomechanics & Engineering*. 9(6), 775-791
- [2] Moorak Son, Edward J. Cording (2008). Numerical model tests of building response to excavation-induced ground movements. *Canadian Geotechnical Journal*. 45(11), 1611-1621
- [3] Alan Graham Bloodworth (2002). Three-dimensional analysis of tunneling effects on structures to develop design methods. Ph.D. Thesis, University of Oxford, UK
- [4] C.W.W. Ng, H. Lu (2014). Effects of the construction sequence of twin tunnels at different depths on an existing pile. *Canadian Geotechnical Journal*. 51(2), 173-183
- [5] Messast. S, Hazem. M, Bousbial N, Mokhbi H (2014). Numerical modeling of the face reinforcement of Djebel El-Kantour tunnel face (highway east-west). *J. Appl. Eng. Sci. Techno*. 1(1) 23-29.
- [6] Shinji. (2009). Three-dimensional numerical modeling of a NATM tunnel. *International Journal of the Japanese Committee for Rock Mechanics* 5.33-38.
- [7] Loganathan N and Poulos H G. (1998). Analytical Predictions of Tunnelling Induced Ground Movements. *Geotechnical Engineering Journal*.124 (9).
- [8] Loganathan, N, Poulos, HG, Bustos-Ramirez, A (2000). Estimation of ground loss during tunnel excavation. *Geo.Eng.* Australia, November
- [9] Thayanan Boonyarak, Charles W.W. Ng (2015). Effects of construction sequence and cover depth on Crossing-tunnel interaction. *Canadian Geotechnical Journal*.52(7) 851- 867
- [10] Dong, Y, Burd, H.J, Houlsby,G,T (2016). Finite element analysis of a deep excavation case history”, *Geotechnique* ,66 (1), 1-15
- [11] Giovanni Barla. (2016). Full face excavation of large tunnels in difficult conditions. *Journal of rock mechanics and geotechnical engineering*. 8, 294-303
- [12] Guo-Hua Zhang, Yu-Yong Jiao, Li-Biao Chen, Hao Wang, Shu-Cai Li. (2016). Analytical model for assessing collapse risk during mountain tunnel construction. *Canadian Geotechnical Journal*.53(2), 326-342
- [13] Guo-Hua Zhang, Yu-Yong Jiao, Hao Wang (2014). Outstanding issues in excavation of deep and long rock tunnels: a case study. *Canadian Geotechnical Journal*. 51(9), 984- 994
- [14] J Y Ruwanpura, S M AbouRizk, M Allouche (2004). Analytical methods to reduce uncertainty in tunnel construction projects. *Canadian Geotechnical Journal*.31(2), 345-360
- [15] Kaveh Ahangari, Sayed Rahim Moeinossadat, Danial Behnia (2015). Estimation of tunneling-induced settlement by modern intelligent methods. *Soils and foundations* 55(4), 737-748
- [16] R. K. Rowe, K. Y. Lo, G. J. Kack (1983). A method of estimating surface settlement above tunnels constructed in soft ground. *Canadian Geotechnical Journal* 20(1) 1-22
- [17] Rolf Zumsteg, Lars Langmaac (2017). Mechanized tunneling in soft soils: Choice of excavation mode and application of soil conditioning additives glacial deposits. *Engineering* 3, 863-870
- [18] Wang Ran (2017). *Effects of the existing tunnel shape on three-dimensional crossing tunnels interaction in sand: Centrifuge and numerical modeling*. PhD thesis. University of Hong Kong, China
- [19] Yu Wang, Jiangwei Shi, Charles W.W. Ng (2011). Numerical modeling of tunneling effect on buried pipelines. *Canadian Geotechnical Journal*. 48(7) 1125-1137
- [20] Zdravkovic, L, Potts, D, M, St. John H, D (2005). Modeling of a 3D excavation in finite element analysis. *Geotechnique*. 55(7) 497-513